

**Aus dem Institut für Anatomie und Zellbiologie
der Justus-Liebig-Universität Gießen**

Leiter: Prof. Dr. Eveline Baumgart-Vogt

**Peroxisomal functions in the lung and their role in the pathogenesis of lung
diseases**

**Habilitationsschrift
zur Erlangung der Venia legendi
des Fachbereichs Medizin
der Justus-Liebig-Universität Gießen**

vorgelegt von Srikanth Karnati

Gießen 2018

Die nachfolgende Arbeit nimmt Bezug auf folgende Originalarbeiten:

1. **Karnati S***, Graulich T, Oruqaj G, Pfreimer S, Seimetz M, Stamme C, Mariani TJ, Weissmann N, Mühlfeld C, Baumgart-Vogt E (2016). Postnatal development of the secretory cells of the distal airways, the bronchiolar club cells in the mouse lung: stereological and molecular biological studies. *Cell and Tissue Research*. Jun;364(3):543-57.
2. **Karnati S**, Baumgart-Vogt E (2009) Peroxisomes in airway epithelia and future prospects of these organelles for pulmonary cell biology. *Histochem Cell Biol*. Apr: 131(4):447-54.
3. **Karnati S**, Lüers G, Pfreimer S and Baumgart-Vogt E (2013) Manganese Superoxide dismutase 2 (MnSOD) is localized to mitochondria but not in peroxisomes. *Histochemistry and Cell Biology*, Aug:140(2):105-17
4. **Karnati S**, Palaniswamy S, Alam MR, Oruqaj G, Stamme C, Baumgart-Vogt E (2015) C22-bronchial and T7-alveolar epithelial cell lines of the immortomouse are excellent murine cell culture model systems to study pulmonary peroxisome biology and metabolism. *Histochemistry and Cell Biology* Mar;145(3):287-304.
5. Oruqaj G[§], **Karnati S[§]**, Vijayan V, Kotarkonda LK, Boateng E, Zhang W, Ruppert C, Günther A, Shi W, Baumgart-Vogt E (2015) Compromised peroxisomes in idiopathic pulmonary fibrosis, a vicious cycle inducing a higher fibrotic response via TGF- β signaling. *Proc Natl Acad Sci*. 112(16):E2048-57. [§] Both authors contributed equally to the study.
6. Vijayan V, Tumpara S, **Karnati S**, Garikapati V, Linke M, Kamalyan L, Mali SR, Sudan K, Kollas A, Schmid T, Schulz S, Spengler B, Weichhart T, Immenschuh S, Baumgart-Vogt E (2017) A new immunomodulatory role for peroxisomes in macrophages activated by the TLR-4 ligand LPS. *Journal of Immunology* Mar 15;198(6):2414-2425. doi: 10.4049/jimmunol.1601596

Übersichtsarbeiten

7. Boateng E, El-Merhie N, Trompak O, Tumpara S, Seimetz M, Pilatz A, Baumgart-Vogt E, **Karnati S*** (2016) Targeting PPAR γ in Lung fibroblasts: Prospects of therapeutic treatment for IPF. *PVRI Chronicle* vol 3, issue 2, p33-37

Tables and contents

1 INTRODUCTION	1
1.1 ANATOMY OF THE LUNG	1
1.2 RESPIRATORY TRACT	1
1.3 TERMINAL BRONCHIOLES AND RESPIRATORY BRONCHIOLES	3
1.4 WHY ARE CLUB CELLS AND CLUB CELL STEREOLOGY IMPORTANT?	4
1.5 LUNG PARENCHYMA	5
1.6 IDIOPATHIC PULMONARY FIBROSIS	6
1.7 THE PATHOGENESIS OF IDIOPATHIC PULMONARY FIBROSIS	7
1.8 ROLE OF TGF β 1 AND ROS GENERATION IN THE PATHOGENESIS OF IPF	8
1.9 ROLE OF PEROXISOMAL METABOLISM AND PPAR-MEDIATED PEROXISOME PROLIFERATION IN PULMONARY FIBROSIS	11
1.10 DISCOVERY OF PEROXISOMES AND PEROXISOMAL ENZYMES	14
1.11 PEROXISOMAL BIOGENESIS AND METABOLIC FUNCTIONS	15
1.12 PEROXISOMAL FUNCTIONS IN SCAVENGING ROS AND RNS	17
1.13 DO PEROXISOMES CONTAIN SOD2?	18
1.14 PEROXISOMES IN THE LUNG: WHERE WE STAND	19
1.15 PULMONARY PEROXISOMES AND THEIR IMPORTANCE IN THE LUNG METABOLISM	22
2 AIMS OF THE WORK	24
3 APPLIED METHODOLOGY FOR THE ANALYSIS OF AIMS OF THE WORK	26
4 RESULTS AND DISCUSSION	28
4.1 CLUB CELL DIFFERENTIATION IS A POSTNATAL PHENOMENON	28
4.2 ABUNDANCE OF PEROXISOMES IN THE BRONCHIOLAR AND ALVEOLAR EPITHELIAL CELLS OF THE DEVELOPING LUNG	32
4.3 SOD2 IS NOT LOCALIZED IN PEROXISOMES	37
4.4 C22 AND T7 ARE THE BEST CELL LINES TO STUDY THE FUNCTIONS OF PEROXISOMES IN THE CLUB AND AECII CELLS	42
4.5 PPAR-DEPENDENT PEROXISOME SIGNALING AS A TREATMENT STRATEGY FOR IPF	49
4.6 PPARs AND THEIR ROLE IN PREVENTING THE IDIOPATHIC PULMONARY FIBROSIS	56
4.7 PPAR-INDEPENDENT PEROXISOME SIGNALING IN CHRONIC INFLAMMATORY LUNG DISORDERS	58
5 SUMMARY	60
6 ZUSAMMENFASSUNG	62
7 OUTLOOK	64
COMPARTMENTALIZATION OF PEROXISOMAL MEMBRANE PROTEINS BY SUPER- RESOLUTION MICROSCOPY	64
8 REFERENCES	67
9 ACKNOWLEDGMENTS	84

1 Introduction

Fresh air entering the mouth and nose is brought to the blood-gas barrier in the lungs by a repetitively branching network of airways. This airway tree achieves an enormous amplification in cross-sectional area from the trachea to the terminal bronchioles.

1.1 Anatomy of the lung

The lung is a very complex heterogeneous air-filled organ specially adapted for gas exchange. The lung parenchyma is divided into lobes and segments. Each lobe having its own blood supply originating from the bronchial arteries. The lungs are positioned in the pleural cavity within the thoracic cavity and are surrounded by the visceral pleural membrane which is directly adherent to the lung surface tissue, and the parietal pleural membrane which lines the chest wall. In between these pleural membranes, approximately 100–300 ml of serous fluid acting as a lubricating agent was observed in interpleural space (Noppen et al., 2000). Contraction of the intercostal muscles, movement of the ribs and the diaphragm increases the intrathoracic volume. In consequence, during inspiration, the intrapleural pressure decreases to approximately -6mm Hg, and the lungs expand, causing the pressure in the airways to become slightly negative and leading to air flow into the lungs. During expiration, the diaphragm and intercostales external muscles relax causing the thorax and lungs to recoil. The air pressure within the lungs increases to above the pressure of the atmosphere, causing air to be forced out of the lungs.

1.2 Respiratory tract

The two functionally and structurally distinct regions of the respiratory system are the upper and lower respiratory tracts. The upper respiratory tract consists of nasal cavity, pharynx, and larynx (collectively called as nasopharyngeal region), while the lower respiratory tract consists of trachea, bronchi, bronchioles until terminal bronchioles and alveolar region. The

respiratory system includes two zones: the proximal conducting zone and the distal respiratory zone. In the proximal conducting zone (nose, pharynx, larynx, trachea, bronchi, bronchioles, and terminal bronchioles), the inhaled air is filtered, warmed, and humidified in the conducting airways, thus protecting the distinct lining epithelia of the lower tract from damage, while in the distal respiratory zone (respiratory bronchioles, alveolar ducts, and alveoli), the gas exchange occurs (Duncker, 2008).

In the human, the dichotomous bifurcation of the branching morphogenesis of the trachea gives rise to two daughter bronchi with a similar smaller diameter than the mother branch. In the human lung, these proximal airways undergo divisions 23 times (13 times in the mouse) to generate distal airways down to the respiratory bronchioles and alveolar region (Duncker, 2008; Herriges and Morrissey, 2014; Iber and Menshykau, 2013). The first 16 airway generations form the conducting zone functioning to conduct air to the deeper parts of the lungs, while the last 7 airway generations form the respiratory zone participating in the gas exchange (Rodney, 2013).

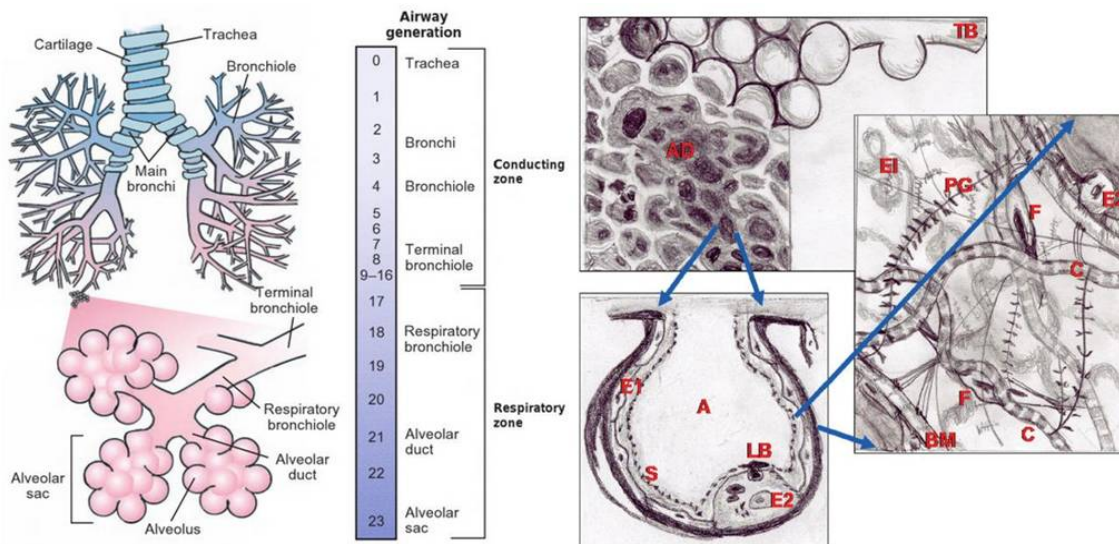


Fig. 1 Divisions of airway tree. The left picture depicts the division of the trachea and the main bronchi. The airway tree possesses conducting and respiratory zones (Rodney, 2013). The right picture illustrates the complex structure of the parenchyme in the alveolar region (Suki et al., 2011). The top panel shows a terminal bronchiole (TB) leading via respiratory bronchiole to an alveolar duct (AD). The bottom left is a zoom into a single air-filled alveolus

(A) with alveolar epithelial type I cells (AECI) (E1) and alveolar epithelial type II (AECII) (E2) cells covered by the surfactant (S) film at the air-liquid interface. Secretion of lamellar body (LB) containing surfactant phospholipids by the AECII cell is shown. The right panel shows the extracellular matrix (ECM) of the alveolar septal wall with various components, including amorphous elastin (E), wavy collagen fibers (C), complex proteoglycans (PG), basement membrane (BM), and fibroblasts (F).

1.3 Terminal bronchioles and respiratory bronchioles

The terminal bronchioles are the smallest distal airways of the conducting zone that undergo continuous cellular maturation characterized by possessing sets of specialized cells, serving different functions in the respiratory system (Gail and Lenfant, 1983). In adult mice (C57BL/6J), the majority (64% of the volume) of bronchiolar epithelial cells lining the distal airways are club cells (Karnati et al., 2016a). In addition, the terminal bronchioles, which comprise ciliated cells (Plopper et al., 1983), serous cells, and endocrine cells (Peake et al., 2000; Sorokin, 1988), are the narrowest airways of the lung and transitional region connecting the terminal bronchioles leading to respiratory bronchioles via alveolar duct to alveolar regions in which gas exchange occurs. Although relatively little has been published about the structure of the mouse lung compared to other species, it is important to mention that the mouse lung is considerably different from the human lung. The right mouse lung has four lobes, whereas left lung is non-lobatedung, and the mouse pleura is thin. The mouse lung parenchyma occupies a smaller fraction of the total lung (18%), which is more than that of human lungs (12%). Furthermore, the alveoli of the mouse lung are smaller (80 μm mean linear intercept [MLI]) than those of the human (MLI 210 μm) as well as the blood-gas barrier thickness (mouse: 0.32 μm ; human: 0.62 μm), which might play an important role in the gas exchange and parenchymal lung mechanics.

Mouse lungs instead of respiratory bronchioles fewer transient bronchioles and airway generations (13–17 generations), exhibiting domain branching, planar bifurcation and orthogonal bifurcation branching pattern (Crapo et al., 1982b), than human lungs (17–21 generations) in which the airways undergo a regular dichotomous branching pattern. Further,

large pulmonary veins of the mouse contain heart muscles inside of the lung whereas these were absent in human pulmonary veins (Karnati and Baumgart-Vogt 2008). In addition, an important functional difference is that mouse distal airways exhibit a complete absence of submucosal glands and with a high number of club cells, whereas the human distal airways predominantly have ciliated cells and less club cells (McBride, 1992). Multiple studies describe a discrete junction between conductive and respiratory epithelial compartments termed the bronchoalveolar duct junction (BADJ), a sudden transition in cell type and morphology (Bal and Ghoshal, 1988; Haefeli-Bleuer and Weibel, 1988; Karnati et al., 2016a; Weibel, 2009). This region acts as the niche for bronchoalveolar stem cells (BASCs), a regional stem cell population potentially important and responsible for certain types of lung repair and lung cancer (Giangreco et al., 2002; Kim et al., 2005). The functional integrity of the airway and alveolar epithelia is essential for respiration (Plopper and Pinkerton, 1991).

1.4 Why are club cells and club cell stereology important?

The pulmonary airway tree is a system of structural complexity that functions in the dynamic environment imposed by respiration and ongoing environmental pollution of the inspired air. Indeed, there might be an embedded link between terminal bronchiole structure and function per se. These structural changes of the terminal bronchioles can be nicely evaluated in mice with design-based stereology, especially club cells, since they constitute most of the bronchiolar epithelium in mice in which continuous cellular maturation occurs (Plopper et al., 1983). Furthermore, it is very important to understand the postnatal differentiation of club cells since they are involved in the metabolism of xenobiotic materials and exhibit anti-inflammatory and cytokine-decreasing properties as well as synthesize the club cell proteins, CC10, and surfactant proteins (SP) A, B, and D (Karnati et al., 2016a). In fact, previous studies reported that club cell secretory proteins are strongly reduced in chronic lung disease, such as asthma, chronic obstructive pulmonary disease (COPD), and posttransplant

obliterative bronchiolitis (Bernard et al., 1992; Hermans et al., 1999; Jorens et al., 1995; Van Vyve et al., 1995). It has also been suggested that CC10 protein levels could act as a biomarker for club cell damage (Hermans et al., 1999). Indeed, the small conducting airways of the lung are the most important targets of early dysfunction in the pathogenesis of chronic bronchitis and emphysema in studies where mice are used (Cosio et al., 1978; Cudmore et al., 1962). Consequently, information on the postnatal development of club cells is necessary in both functional and comparative point of view. Thus, the club cell differentiation of the distal airways during postnatal development (newborn, P15, and adult) of the mouse lung based on design-based stereology addressing their morphological and functional changes is essential. Indeed, no detailed morphometric reports existed on club cell differentiation in the mouse lung prior to our study (Karnati et al., 2016a).

1.5 Lung parenchyma

The many thin-walled alveoli of the lung parenchyma form an enormous surface area, which maintains proper gas exchange. The alveolar surface is lined by a single layer of cells, the alveolar epithelium, which is covered by a thin surfactant liquid film. The alveolar epithelium is composed predominantly of terminally differentiated alveolar epithelial type-I (AECI) cells (constituting 93% of the alveolar epithelial surface area and 33% of alveolar epithelial cells by number) and the surfactant-producing cuboidal alveolar epithelial type-II (AECII) cell (comprising the remaining 7% by surface area and 67% by epithelial cell number) (Crapo et al., 1982a). AECII cells are positioned frequently in the corners of the alveolus and are involved in secreting, synthesizing, clearing, and recycling pulmonary surfactant. Moreover, AECII cells serve as progenitor cells for regeneration of AECI cells (Uhal, 1997).

The alveolar septal walls are composed of AECI cells on the surface of septa, interstitial cells (fibroblasts, endothelial cells, and alveolar macrophages) and extracellular matrix (ECM). Alveolar macrophages are important in modulating acute and chronic inflammatory responses

and are capable of phagocytosing bacteria and apoptotic cells (Rahman and Adcock, 2006). Most importantly, macrophages are the main source of cytokines, chemokines, and other inflammatory mediators that propagate or suppress the immune response. Following an insult, alveolar macrophages and lung epithelial cells secrete chemokines and cytokines, promoting neutrophil accumulation and local inflammation (Rahman and Adcock, 2006; Rahman et al., 2006).

Fibroblasts are important in the synthesis and maintenance of ECM. The common structural components of ECM are fibrillar collagens, elastic fibers, laminin, entactin, and proteoglycans (Dunsmore and Rannels, 1996). Changes in the synthesis or turnover of interstitial ECM components leading to the progression of diseases, such as emphysema and fibrosis, may be caused either by cellular remodeling or injury (Suki et al., 2011). In addition, differentiation of fibroblasts to myofibroblasts and abnormal excessive deposition of collagen in the lung accompanied by the stiffening of the lung tissue is the hallmark of idiopathic pulmonary fibrosis (IPF) (Cui et al., 2011; Katzenstein and Myers, 1998; Oruqaj et al., 2015).

1.6 Idiopathic pulmonary fibrosis

Idiopathic pulmonary fibrosis (IPF), the most common form of idiopathic interstitial pneumonias, is a chronic, devastating, and lethal fibrotic disorder in human lung (Noble and Homer, 2005). Former assumptions described IPF as a chronic inflammatory disease resulting from a response to an unknown stimulus, which later progresses to lung injury and fibrosis (Callahan et al., 1952; Noble and Homer, 2005). The reported median survival rate of patients diagnosed with IPF is from 2.5 to 3.5 years, and most available treatment compounds have not proved effective (Bourke, 2006), including the antioxidant N-acetylcysteine, which is only known to slow lung function decline and has no impact on mortality (Demedts et al., 2005). IPF is characterized by a worsening of pulmonary function and remodeling of the lung parenchyma due to fibrotic foci formation by activated fibroblasts and myofibroblasts as well

as excessive production and deposition of ECM components (ECM) (Cui et al., 2011; Katzenstein and Myers, 1998; Kuhn and McDonald, 1991; Pardo and Selman, 2002).

1.7 The pathogenesis of idiopathic pulmonary fibrosis

The pathogenesis of IPF is a very complex process and still not completely understood. So far, there is no unifying mechanism known that explains the pathogenesis of lung fibrogenesis. Based on the etiology, the pathogenesis of IPF is most likely a multifactorial process (Coward et al., 2010). The two proposed theories for the development of IPF are the inflammatory pathway (older) and the alveolar epithelial cell injury and ineffective wound repair model (more recent) (Sisson et al., 2010; Williams et al., 2004). As a key process is suggested, that an initial lung injury disrupts the alveolar-capillary basement membrane, leading to a deterioration of reepithelialization and reendothelialization and a strong cytokine-mediated fibroblast proliferation (Strieter and Mehrad, 2009). Transforming growth factor $\beta 1$ (TGF $\beta 1$), an ubiquitously expressed multifunctional cytokine that functions in numerous biological pathways in vitro and in vivo, is the major cytokine involved in this process (Sheppard, 2006), (Border and Noble, 1994; Lawrence, 1996). TGF $\beta 1$ is known to 1) mediate the recruitment and activation of fibroblasts during lung injury (Sureshbabu et al., 2011), 2) to stimulate connective tissue synthesis and deposition, and 3) inhibit connective tissue degradation (Gharaee-Kermani et al., 2009). Additionally, it transdifferentiates fibroblast into aggressive myofibroblast phenotypes, which are responsible for the production and secretion of the ECM components in the interstitial tissue of the alveolar region (Leask and Abraham, 2004; Moore and Herzog, 2013; Phan, 2002; Vaughan et al., 2000).

In addition, several factors, such as free radicals, smoking, pollution, and unknown genetic factors, influence and initiate this lung disease, leading to the ultimate death of patients. Indeed, chronic inflammation and TNF α are important in inducing IPF with inflammatory mediators, such as chemokines, cytokines, growth factors, and reactive oxygen species key

players in the progression of this disease (Dempsey, 2006; Oruqaj et al., 2015). So far, not a single factor solely causing this devastating disease could be identified, although it is well accepted that TGF β 1 signaling plays a key role in the pathogenesis of IPF. However, the mechanisms by which TGF β 1 and TNF α promote the fibrotic response in IPF are insufficiently understood. Nevertheless, much of the literature on IPF is derived from TGF β 1 signaling in which it was inhibited by blocking its downstream Smad3 gene expression in bleomycin-induced fibrosis in mouse models (Warburton et al., 2013; Zhao et al., 2002). Indeed, these results show that Smad3 knockout mice, deficient in a downstream mediator of TGF β 1 signaling, are protected from bleomycin-induced pulmonary fibrosis, indicating that Smad3 may serve as a novel target for potential therapeutic treatment of lung fibrosis (Zhao et al., 2002).

1.8 Role of TGF β 1 and ROS generation in the pathogenesis of IPF

The anatomy, location, and function of the lungs make them highly susceptible to oxidative damage in comparison to other organs. Therefore, airways and alveolar epithelial cells are more prone to oxidative injury. Reactive oxygen species (ROS), superoxide ($O_2^{\cdot-}$), hydrogen peroxide (H_2O_2), hydroxyl radicals (HO^{\cdot}), peroxy radicals (RO_2^{\cdot}), alkoxy radicals (RO^{\cdot}), and hydroperoxy radicals (HO_2^{\cdot}) as well as reactive nitrogen species (RNS), nitric oxide (NO^{\cdot}), nitrogen dioxide (NO_2), and peroxynitrite ($ONOO^{\cdot}$) regulate cell signaling in physiological conditions. However, an excess of these ROS/RNS is implicated in organ injury and oxidative-induced damage (Kinnula et al., 2005; Waghray et al., 2005). It is widely accepted that the imbalance between oxidants and antioxidants could play a major role in the pathogenesis of the IPF (Bargagli et al., 2009; Kinnula et al., 2005). Several studies suggest that TGF β 1 triggers secretion of H_2O_2 in human lung fibroblasts by activating NADH:flavin:O₂ oxidoreductase (Thannickal et al., 2000), in which ROS-induced TGF β 1 signaling increases collagen-I synthesis and fibrogenesis in pulmonary fibrosis (Kliment and

Oury, 2010; Kondrikov et al., 2011). Additionally, animal studies using bleomycin-induced pulmonary fibrosis revealed that ROS are important in the development of the fibrotic process. Moreover, superoxide dismutases (SODs), such as SOD1 (CuZnSOD), SOD2 (MnSOD), and SOD3 (ECSOD), are known to reduce oxidative stress by catalyzing the dismutation of superoxide into oxygen and hydrogen peroxide (Kinnula et al., 2005). Deletion of ECSOD in mice aggravates the pulmonary damage after exposure to bleomycin or asbestos (Fattman et al., 2003). Furthermore, deficiency of the p47^{phox} subunit of NADPH oxidase (Nox) protected the mice against bleomycin-induced lung fibrosis (Kinnula et al., 2005; Kliment and Oury, 2010; Kondrikov et al., 2011; Manoury et al., 2005). In addition, Hecker and colleagues suggested that NOX4-dependent generation of H₂O₂ plays a crucial role in TGFβ1-induced myofibroblast differentiation and ECM production (Hecker et al., 2009). The myofibroblasts secrete excessive TGFβ1, which stimulates AECII to undergo cell apoptosis, thereby inhibiting the wound healing process (Cutroneo et al., 2007; Fernandez and Eickelberg, 2012). Lung fibroblasts are key cells for synthesizing collagen and generation of ECM, while TGFβ1 is the “master switch” for the pulmonary fibrosis (Cui et al., 2011; Verrecchia et al., 2001). Collagen type I is the major collagen type synthesized by both normal and myofibroblasts, whereas TGFβ induces the synthesis of different collagen types, such as I, III, and V, in fibroblasts and myofibroblasts (Eickelberg et al., 1999; Raghu et al., 1989). TGFβ1-induced Smad signaling enhances the transcriptional activation of collagens and as consequence myofibroblasts secrete high levels of ECM proteins, especially collagens and fibronectin, contributing to the deposition of collagens and fibrosis (Cutroneo et al., 2007; Fernandez and Eickelberg, 2012).

Direct injury to the alveolar epithelium and the inflammation in the alveolar and bronchiolar regions could activate different cell signaling pathways leading to the elevated expression of pro-inflammatory genes in fibroblasts and release of profibrotic cytokines (TGFβ1, TNFα, IL-1, IL-6, IL-8), growth factors, platelet-derived growth factors, and chemokines (Kinnula

et al., 2005; Kinnula and Myllarniemi, 2008). Furthermore, cytokine-mediated ROS release can trigger the apoptosis of AECI cells, leading to the activation of alveolar macrophages (Bargagli et al., 2009). Thereby, release of ROS production by activating immune cells, such as macrophages and neutrophils, through NADPH oxidase activation was noted in IPF patients (Kinnula and Myllarniemi, 2008). In this context, it is important that transcription factor activator protein 1 (AP1) family members are implicated in different stress signals and control subsequent processes, including proliferation, apoptosis, wound healing, inflammation, and tumorigenesis (McKeown et al., 2009; Palumbo et al., 2011). Interestingly, inhibition of AP1 abolished the profibrotic effects of TGF β 1 signaling and prevented skin fibrosis development (Avouac et al., 2012) as well as ECM production, and TGF β 1 signaling activation was also noted in Swiss 3T3 fibroblasts treated with TNF α , suggesting AP1 as a potential candidate for antifibrotic therapy (Palumbo et al., 2011; Sullivan et al., 2009).

Released cytokines play an important role in the fibrogenesis observed in the bleomycin-induced lung fibrosis mouse model. In particular, TNF α plays a crucial role in the BLM-induced lung injury development, partially through upregulation of TGF β 1 (Ortiz et al., 1998; Verjee et al., 2013). Interestingly, α SMA and COL1 protein expression was increased when fibroblasts were treated with recombinant human TNF α (Verjee et al., 2013). In addition, TNF α increases TGF β 1 expression and enhances ECM synthesis in Swiss 3T3 fibroblasts (Sullivan et al., 2009). Strikingly, bleomycin-induced mice treated with TNF α antagonists abrogated lung fibrosis development, suggesting TNF α as a potential candidate for antifibrotic therapy (Piguet and Vesin, 1994).

In addition to other cytokines, IL-6 is also secreted by several pulmonary cell types, including fibroblasts, and it has been suggested that it mediates inflammatory processes in the lung in a variety of diseases, including interstitial lung diseases (Moodley et al., 2003). Interestingly, IL-6-deficient mice challenged with bleomycin showed decreased levels of

IPF markers, such as collagen, suggesting a potential therapeutic approach in treating pulmonary fibrosis (Moodley et al., 2003; Saito et al., 2008).

Interestingly, to date no comprehensive study has been performed on the function of different organelles in IPF and also the functional role of peroxisomes and its alterations in IPF patients has not been investigated. However, we could show that alterations in peroxisomal metabolism and enzyme content exert a strong impact on the pathogenic mechanisms in IPF (Oruqaj et al., 2015).

1.9 Role of peroxisomal metabolism and PPAR-mediated peroxisome proliferation in pulmonary fibrosis

Peroxisome proliferator-activated receptors (PPAR- α , - β , - γ) are members of the ligand-activated nuclear hormone receptor superfamily. The term PPAR was derived from the fact that the activation of the first molecule of this family found PPAR α resulted in peroxisomes proliferation in rodent hepatocytes (Issemann and Green, 1990). The biological roles of PPAR α and PPAR γ are considerably better defined compared to PPAR β , because, they are targets for drugs used in the treatment of dyslipidemias and type 2 diabetes, respectively (Moraes et al., 2006; Ward and Tan, 2007). In recent years, several hundreds of publications on these PPAR receptors were published, suggesting their importance in controlling complex cellular mechanisms by regulating the transcription of genes (transactivation) involved in lipid and glucose metabolism, metabolic homeostasis, differentiation, proliferation, adipogenesis as well as inflammation (Lakatos et al., 2007). PPARs can also inhibit gene transcription through transrepression mechanisms that involve interactions with other transcription factors and their coactivators to prevent effective DNA binding (Nolte et al., 1998).

PPAR exerts their function depending on the cell type (Karnati, 2014). PPAR α is activated by a variety of fatty acids e.g. eicosanoids, polyunsaturated fatty acids and synthetic fibrates and

is implicated in the regulation of lipid metabolism, lipoprotein synthesis and metabolism, and inflammatory response in liver and other tissues (Kersten et al., 2000; Kim et al.; Schoonjans et al., 1996). It is highly expressed in tissues with high fatty acid oxidation (such as liver, kidney, and heart muscle), where it controls a comprehensive set of genes that regulate most aspects of lipid catabolism. Moreover, it is also expressed at high levels in the lung vascular endothelial cells, airway smooth muscle cells, monocyte/macrophages, T-lymphocytes, and eosinophils (Patel et al., 2003; Reynders et al., 2006; Trifilieff et al., 2003; Woerly et al., 2003). Activation of PPAR α in selected cellular systems increases high-density lipoprotein (HDL) cholesterol synthesis, stimulates “reverse” cholesterol transport, and reduces triglycerides and the risk for cardiovascular disease development (Fruchart and Duriez, 2006; Hansen and Connolly, 2008; Konstandi et al.; Robillard et al., 2005).

PPAR β is activated by synthetic agonists and endogenous fatty acid ligands (Michalik et al., 2006; Molnar et al., 2005), and its functions are associated with inflammatory response (Kilgore and Billin, 2008; Kostadinova et al., 2005), glucose, energy, and lipid metabolism (Desvergne et al., 2006; Muller et al., 2008). The PPAR β protein is expressed in lung epithelial cells, lymphocytes, macrophages, neutrophils, and mast cells (Patel et al., 2003; Reynders et al., 2006; Sugiyama et al., 2000; Trifilieff et al., 2003; Woerly et al., 2003). Indeed we recently showed that PPAR β regulates the numerical abundance and metabolic function of peroxisomes and enhances osteoblast differentiation (Qian et al., 2015).

PPAR γ was originally characterized as a regulator of adipose tissue differentiation but also plays key roles in glucose and lipid metabolism. Activation of PPAR γ also occurs in response to a wide variety of potential endogenous ligands as well as synthetic agonists, such as the thiazolidinedione (TZD), and naturally occurring PPAR γ ligands including polyunsaturated fatty acids (PUFAs), such as linoleic acid, arachidonic acid, eicosapentanoic acid, and oxidized lipids (Ward and Tan, 2007; Willson et al., 2000). PPAR γ is present in a wide variety of cell types, namely eosinophils (Woerly et al., 2003), dendritic cells (Gosset et al.,

2001), AECII (Michael et al., 1997), bronchial smooth muscle cells (Benayoun et al., 2001; Patel et al., 2003), fibroblasts (Huang et al., 2005), and airway epithelium (Benayoun et al., 2001; Wang et al., 2001). PPAR γ agonists exert strong antiatherogenic, anti-inflammatory (Huang et al., 2005; Huang and Glass, 2010; Pascual et al., 2005; Wahli and Michalik, 2012), and antioxidant effects by inhibiting several inflammatory mediators (TNF α , IL-1, IL-6, and iNOS), transcription factors (nuclear factor- κ B [NF- κ B], Nrf2, FOXO, Egr1, AP1) and other pro-inflammatory transcription factors via multiple mechanisms (Barish, 2006; Cabrero et al., 2002; Polvani et al., 2012; Staels, 2005).

Interestingly, the interaction among AECII, fibroblasts, and macrophages at injury sites of the alveolar and bronchiolar regions could activate the fibroblasts to release profibrotic cytokines and appears to be central to the pathogenesis of IPF (Kendall and Feghali-Bostwick; Oruqaj et al., 2015). In this respect, it is important that peroxisome dysfunction leads to a profibrotic phenotype and treatment of rats with a peroxisome proliferator-activated receptor alpha (PPAR α)-specific agonist significantly attenuated tubulointerstitial renal fibrosis (Boor et al., 2011). Even though several studies have shown beneficial effects of PPARs in fibrosis development in different organ systems, nobody has studied whether this beneficial effect is mediated by peroxisomal proliferation or their metabolic activation until we reported recently (Oruqaj et al., 2015). In this respect, it is important to mention that PPAR α was known to mediate the action of some drugs, mostly hypolipidemic agents that proliferate peroxisomes in rodent liver (Baumgart, 1997; Fahimi et al., 1996), and activates different peroxisomal and mitochondrial β -oxidation enzymes, such as peroxisomal acyl-CoA oxidase and peroxisomal 3-ketoacyl-CoA thiolase as described previously (Baumgart, 1997; Fahimi et al., 1996). Interestingly, several peroxisomal genes contain a PPAR response element in their promoter region by which their transcription can be altered (Shimizu et al., 2004).

1.10 Discovery of peroxisomes and peroxisomal enzymes

Rhodin (1954) first described peroxisomes in the proximal tubule of the mouse kidneys as small, single membrane-bound organelles, which were initially called microbodies. Christian de Duve was the first to isolate peroxisomes from rat liver and identify them as a new class of cell organelles distinct from lysosomes and gave them the name peroxisomes because of their involvement in the metabolism of hydrogen peroxide (H₂O₂) (De Duve, 1965; De Duve and Baudhuin, 1966). Later, peroxisomes were located in tissue sections at light and electron microscopic levels by using the alkaline 3, 3'-diaminobenzidine (DAB) method to visualize the peroxidatic activity of catalase (Fahimi, 1968, 1969; Novikoff and Goldfischer, 1969). Almost at the same time, peroxisomal β -oxidation was discovered in plants (Cooper and Beevers, 1969) and subsequently also found in animals (rat liver) (Lazarow, 1977; Lazarow and De Duve, 1976). Furthermore, ether lipid and cholesterol-synthesizing enzymes, such as glycerone-phosphate O-acyltransferase (GNPAT) (Hajra et al., 1979; Keller et al., 1985) and 3-hydroxy-3-methylglutaryl-coenzyme A reductase (HMGCR), were discovered in rat liver peroxisomes (Keller et al., 1985). Profiling of peroxisomes by proteomic analysis showed that these organelles contain over 130 different proteins involved in various metabolic pathways, including degradation of various toxic, bioactive pro-inflammatory and signaling lipid derivatives and metabolism of ROS and reactive nitrogen species (RNS) (Islinger et al., 2006; Wiese et al., 2007). In addition to the various oxidases producing H₂O₂, peroxisomes harbour antioxidative enzymes, such as Cu, Zn-SOD, glutathione peroxidase, and peroxiredoxins I and V (Heijnen et al., 2006; Immenschuh and Baumgart-Vogt, 2005; Schrader and Fahimi, 2004).

Peroxisomes are found in almost all eukaryotic cells except spermatozoa and mature red blood cells (Karnati and Baumgart-Vogt, 2009). They are dynamic organelles with distinct protein composition and abundance in different organs or cell types (Chang et al., 1999; Fahimi et al., 1996; Karnati and Baumgart-Vogt, 2008; Nenicu et al., 2007). Peroxisomes can

be rapidly induced to proliferate in response to metabolic or pharmacological stimulation (Baumgart, 1997; Fahimi et al., 1996).

1.11 Peroxisomal biogenesis and metabolic functions

Peroxisome biogenesis, a complex biological process comprises three crucial steps:

(a) formation of the peroxisomal membrane, (b) import of peroxisomal matrix proteins, and (c) proliferation of peroxisomes. It is mediated by a set of proteins termed “peroxins” with the acronym of corresponding genes (PEX) or proteins (*Pex*) and numbered according to their date of discovery (Distel et al., 1996). The peroxisomal proteins are synthesized on free ribosomes and posttranslationally imported into the organelle as shown in Fig. 2. The import of peroxisomal matrix and membrane proteins that are synthesized on free ribosomes into the organelle requires peroxisomal targeting signal (PTS) sequences (Subramani, 1998; Terlecky and Fransen, 2000). The PTS1 is a major peroxisomal targeting signal at the C-terminus of peroxisomal matrix proteins and is recognized and bound by the cytoplasmic receptor protein PEX5p, whereas the PTS2-carrying peroxisomal matrix proteins (with the PTS2 at the N-terminal region) are bound by the cytoplasmic receptor PEX7p (Eckert and Erdmann, 2003; Lazarow and Fujiki, 1985; Purdue and Lazarow, 2001). Upon binding, these receptors carry the nascent peroxisomal matrix proteins to the translocation machinery of the docking complex, containing PEX13p and PEX14p, on the peroxisomal membrane. Cargo-complex translocation is achieved by docking the receptor-cargo complexes to the peroxisomal membrane. The receptors will then dissociate from the cargo either prior to the transport process or after the translocation step in the peroxisomal lumen and recycle back into the cytosol to repeat the same process.

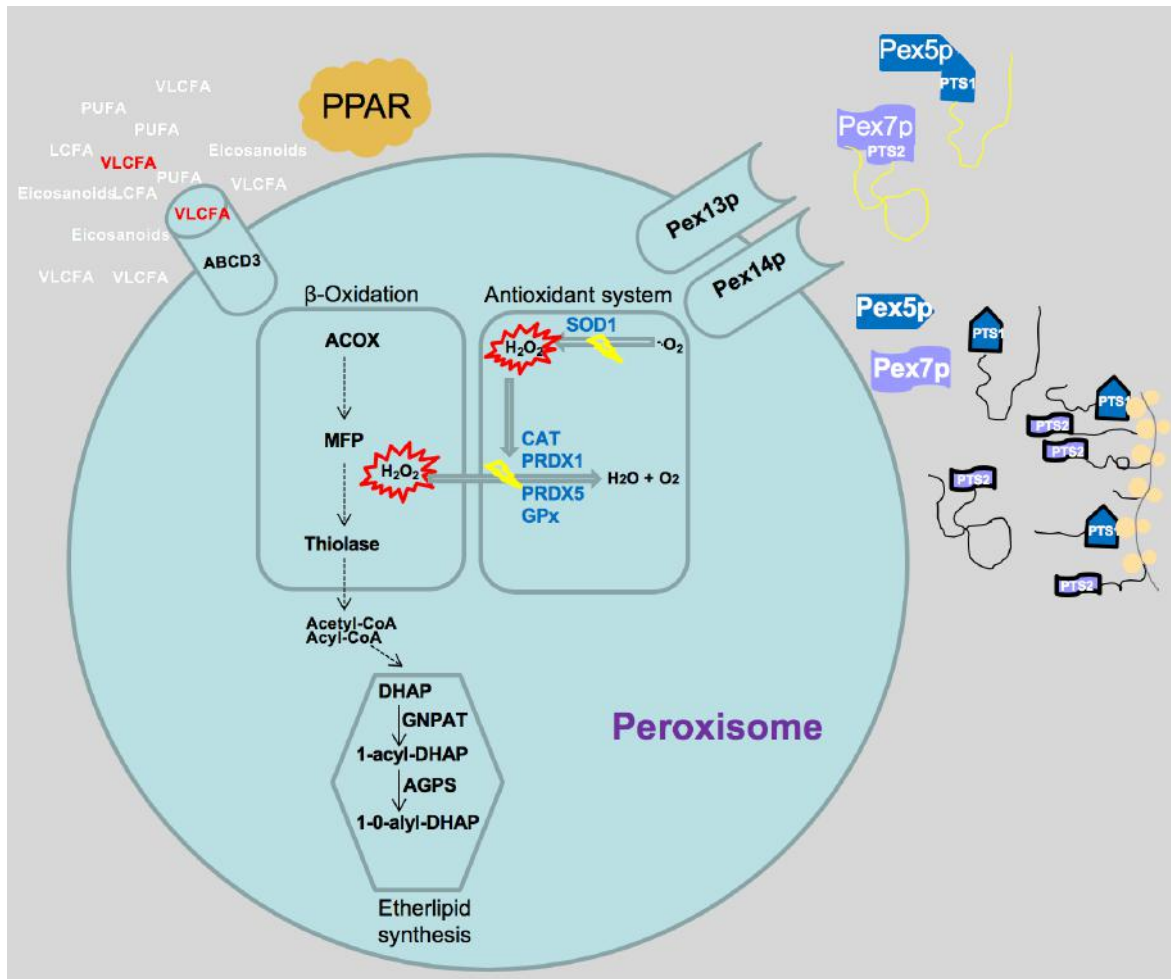


Fig. 2 Biogenesis and metabolic functions of the peroxisomes (Karnati et al., unpublished data).

Peroxisomes play an important role in the lipid metabolism by catalyzing (a) fatty acid α -oxidation, (b) fatty acid β -oxidation, (c) polyunsaturated fatty acid biosynthesis, (d) ether phospholipid synthesis, and (e) cholesterol precursor synthesis as well as synthesis of other isoprenoids (Moser, 1999). Long-chain fatty acids (LCFA), very-long-chain fatty acids (VLCFA), polyunsaturated fatty acids (PUFAs), branched chain fatty acids and eicosanoids are transported by ABC family member D3 (ABCD3) into the peroxisomal matrix, where they are oxidized by the peroxisomal lipid β -oxidation enzymes. The acetyl-CoA units produced by the β -oxidation systems serve as substrates for the biosynthesis of ether glycerolipids and cholesterol precursors. Lipid derivatives oxidized by the peroxisomal β -oxidation pathways are poor substrates for mitochondrial β -oxidation (e.g., very-long-chain

fatty acids [\geq C24; VLCFA], branched chain fatty acids, dicarboxylic acids, eicosanoids [prostaglandins, leukotrienes], [n-3] and [n-6] polyunsaturated fatty acids, and bile acid precursors (Moser, 1999).

Peroxisomes degrade a large amount of LCFA when the mitochondrial carnitine palmitoyl transferase 1 (CPT1) system is overloaded or mitochondria are dysfunctional (Colasante et al., 2015; Moser, 1999). These fatty acids are degraded in peroxisomes and thereafter transferred to the mitochondria for complete oxidation (Beier and Fahimi, 1991; Moser, 1999). In addition, several peroxisomal oxidases are involved in the degradation of polyamines, D-amino acids, and uric acid (in nonprimates) as well as in the detoxification of glyoxylate and xenobiotics via several H_2O_2 -producing oxidases and (Colasante et al., 2015).

1.12 Peroxisomal functions in scavenging ROS and RNS

H_2O_2 is produced by acyl-CoA oxidases during the peroxisomal β -oxidation process and by the activity of other peroxisomal oxidases. The toxic H_2O_2 is decomposed by the antioxidant machinery of the peroxisomal matrix characterized by a set of antioxidative enzymes, such as catalase,

peroxiredoxin 1, 5, and glutathione peroxidase (Immenschuh and Baumgart-Vogt, 2005; Schrader and Fahimi, 2006). In addition, the free superoxide anion radical is decomposed to H_2O_2 by superoxide dismutase 1 in peroxisomes (Fig. 2). Interestingly, when cells were exposed to oxidative stress or ultraviolet irradiation, a significant increase in the biogenesis of peroxisomal compartment, and upregulation of PEX genes was observed (Schrader et al., 2015). However, a significant reduction of catalase was observed in inflammatory processes, including asthma bronchialis, infections, and allograft rejection (Ghosh et al., 2006). This reduction of catalase was explained by the suppressive effect of $TNF\alpha$ on peroxisome function and $PPAR\alpha$ (Rahman, 2006). Moreover, the deficiency of peroxisomes in PEX5

knockout mice with Zellweger syndrome induces mitochondrial defects and leads to impaired mitochondrial respiratory chain functions, thereby inducing high generation of ROS release in these animals (Baumgart et al., 2001). It is well-known that pro- and antioxidative enzymes are localized in specific subcompartments, such as the plasma membrane, the endoplasmic reticulum, peroxisomes, or mitochondria, and the cytoplasm [128]. Interestingly, peroxisomes contain the largest amount of prooxidative (peroxisomal oxidases and iNOS) as well as antioxidative enzymes (catalase, SOD 1, Prdx I and Prdx V, and glutathione peroxidase) in their matrix [128, 136]. In this context, it is important that peroxisomal enzymes are involved in scavenging ROS, and RNS, and are mediating the decomposition of various toxic, bioactive and pro-inflammatory lipid mediators (Karnati and Baumgart-Vogt, 2008; Schrader and Fahimi, 2004; Wiese et al., 2007). In line with these functions and peroxisomes harboring a variety of antioxidative enzymes, many researchers believed that SOD2 is also localized in peroxisomes (Singh et al., 1999).

1.13 Do peroxisomes contain SOD2?

Superoxide dismutases (SODs), essential antioxidative enzymes belonging to the group of metalloenzymes of all oxygen-respiring organisms, catalyze the dismutation of highly reactive superoxide radicals into hydrogen peroxide and molecular oxygen (Miao and St Clair, 2009). While SOD1 has been localized to different subcellular compartments, such as the cytoplasm, nucleus, microsomes, mitochondrial matrix space, and also peroxisomes (McCord and Fridovich, 1969; Okado-Matsumoto and Fridovich, 2001), SOD2 is localized in the mitochondrial matrix (Da Cruz et al., 2003; Shimoda-Matsubayashi et al., 1996; Slot et al., 1986; Weisiger and Fridovich, 1973a, b). In contrast, SOD3 is localized in the extracellular matrix of mammalian tissues (Nozik-Grayck et al., 2005). Interestingly, in addition to SOD1, based on the immunostaining and on biochemical evidence, several researchers believed that SOD2 is also localized in the peroxisomes (Singh et al., 1999),

suggesting a dual localization of SOD2 in mitochondria and peroxisomes. Because of this claim, scientists in the peroxisomal and mitochondrial field continued to believe and cite this article without having any additional proof from the literature (Abdelraheim et al., 2003; Antonenkov et al., 2009; Antonenkov and Hiltunen, 2006; Dansen and Wirtz, 2001; Moldovan and Moldovan, 2004; Schrader and Fahimi, 2006).

Singh and colleagues described the localization of SOD2 in the peroxisomal membrane and peroxisomal core, whereas in the matrix of the organelle, no SOD2 was present (Singh et al., 1999). In fact, SOD2 has no peroxisomal targeting signal but a rather clear mitochondrial signal (Miao and St Clair, 2009; Shimoda-Matsubayashi et al., 1996). Indeed, the subcellular localization of SOD2 in immunofluorescence analyses of diverse mammalian tissues suggested a specific and exclusive mitochondrial staining pattern. Therefore, the true peroxisomal localization of SOD2 and its correct subcellular localization were doubted very often in the peroxisome community.

1.14 Peroxisomes in the lung: where we stand

Information on peroxisomes in the lung is derived from old (45 years old) purely descriptive electron microscopic studies by using the alkaline DAB method for the localization of catalase activity in man, mouse, rat, hamster, guinea pig, rabbit, cat, pig, and monkey (Eguchi et al., 1980; Hirai et al., 1977; Petrik, 1971; Schneeberger, 1972a, b). In these studies, peroxisomes were visualized *only* in bronchiolar club cells and alveolar AECII cells and were not detected in AECI cells or the macrophages, even though macrophages are intimately involved in ROS and lipid metabolism (Hirai et al., 1983; Moriguchi et al., 1984). The significance of peroxisomal function in the mouse and human lung became possible only after the establishment of sensitive morphological and biochemical techniques to visualize different proteins in the peroxisomal compartment of *all* pulmonary cell types, however, with distinct labeling intensities (Karnati and Baumgart-Vogt, 2008, 2009). Furthermore, peroxisomes

exhibited a strong heterogeneity in their numerical abundance, size, and protein composition in a variety of pulmonary cell types of the mouse and human lung, suggesting functional differences of this organelle in the distinct cell types (Karnati and Baumgart-Vogt, 2008, 2009). In the ciliated cells of the mouse lung, peroxisomes were less numerous and smaller in size in comparison to larger peroxisomes in club cells (Karnati and Baumgart-Vogt, 2009). Moreover, the peroxisomes of the club and AECII cells of the mice contain a distinct subset of enzymes with high levels of catalase, ABCD3, and ACAA1 in comparison with the ciliated cells of the bronchiolar epithelium.

Interestingly, β -oxidation enzymes are highly abundant in the peroxisomes of AECI cells, which are smaller and possess low levels of catalase. In contrast to the alveolar region, the presence of larger peroxisomes with high catalase activity in club cells distinguishes them clearly from the ciliated cells of the bronchiolar epithelium (Karnati and Baumgart-Vogt, 2008). Previous studies considered catalase as a sole and typically strong marker protein of peroxisomes; however, with the optimization of sensitive labeling techniques, “PEX14p” is considered as a new marker for the detection of pulmonary peroxisomes (Karnati and Baumgart-Vogt, 2008). PEX14p labeling in mouse and human lungs suggested the presence of similar PEX14p protein levels on individual peroxisomes in distinct pulmonary cell types (Karnati and Baumgart-Vogt, 2008, 2009). In contrast to catalase, PEX14p is now considered as the optimal marker for peroxisomes at the light microscopic level as it is abundant in nearly similar amounts in all peroxisomes in a ubiquitous way in *all* cell types of a large variety of mouse and human tissues (Grant et al., 2013).

After the establishment of optimal marker proteins to detect peroxisomes in mouse and human lung tissue, the role of peroxisomes in the peroxisome rich club and AECII cells was investigated. To dissect the intracellular signaling pathways regulating peroxisomal metabolism and biogenesis and to shed more light on the possible peroxisomal functions in club and AECII cells, primary cell cultures are required. In fact, several groups (including

ours) tried to isolate and establish primary club cell cultures but did not succeed because of the contamination with ciliated cells (Belinsky et al., 1995). Although several good protocols were established in recent years to isolate AECII from the mouse lung (Karnati et al., unpublished data) with highest purity up to 95% (Rice et al., 2002), it is difficult to maintain the AECII cell phenotype in the primary culture as they dedifferentiate into AECI cells (Rice et al., 2002; Shannon et al., 1992; Sugahara et al., 1995). Thereby, AECII cells change their phenotype by losing their microvilli (Diglio and Kikkawa, 1977), lamellar bodies (Shannon et al., 1992), and synthesis of surfactant (Shannon et al., 1992) in primary cell culture conditions. Many new approaches to culture primary cells were developed, however, these cells all reach senescence within two to four weeks. Also, several club and AECII cell lines were developed in recent years from mouse and human tissues, but generally, these have originated from tumors, and most of them do not secrete surfactant proteins. None of these cell lines are phenotypically close to club or AECII cells and do not accurately reflect the cell biology and physiology of club and AECII (Karnati et al., 2016b; Mallampalli et al., 1992; Smith, 1977). To overcome these problems and to understand the biology of AECII and club cells, DeMello and colleagues generated C22-club and T7-AECII cell lines by isolating primary club and AECII cells from the immortal mouse containing the ts SV40 large T antigen (deMello et al., 2000; Demello et al., 2002).

The H-2k^b-tsA58 immortal mouse (Jat et al., 1991) was used to produce the T7 (AECII) and C22 (club cell) cell lines containing a temperature-sensitive (ts) simian virus 40 (SV40) T antigen. The expression of this T antigen induced by γ -interferon (γ -INF) and the stability of this protein is decreased by the cell culture temperature. The C22 and T7 cell lines are non-tumor-derived immortalized cell lines that proliferate at 33°C in the presence of γ -INF and the *first cell lines* used in pulmonary biology that show comparable features of club and AECII cells of the lung. Furthermore, the secretory granules in the C22 cell line are morphologically similar to the ones in the club cells (Ryerse et al., 2001). Moreover, they are able to produce

surfactant proteins SP-A, SP-B, and SP-D and the 10-kDa club cell secretory protein (CC10), whose function is not yet completely understood (Demello et al., 2002; Karnati et al., 2016b). Similarly to C22 cells, T7 cell lines secrete and synthesize all surfactant lipids and phosphatidyl choline, which is a major lipid component of the surfactant that reduces intra-alveolar surface tension at end-expiration as well as AECII cell-specific marker proteins (Demello et al., 2002; Karnati et al., 2016b). Therefore, by using the immortomouse-derived C22 and T7 cell lines, functional aspects of club and AECII cells in the lung can be well studied (deMello et al., 2000; Demello et al., 2002; Karnati et al., 2016b). Though peroxisomes are ubiquitous and highly abundant in club cells and AECII, the enzyme composition and peroxisome number in these cell lines might vary. Therefore, it was important to characterize the distribution of peroxisomal enzymes and profiling of peroxisomal proteins in C22 and T7 cell lines. The characterization of the peroxisomal compartment in these cell lines revealed that they are fully suitable and excellent models allowing us in the future to study the regulation and metabolic role of peroxisomes in club and AECII cells by paracrine or external growth factors or inflammatory cytokines (Karnati et al., 2016).

1.15 Pulmonary peroxisomes and their importance in the lung metabolism

The lung is in a high-oxygen environment, and in addition contains a large epithelial surface area and blood supply. Thus, pulmonary airways are exposed to high concentrations of oxidants, eventually leading to oxidation of proteins, DNA, and lipids, which may cause direct lung injury or induce a variety of cellular responses through the generation of secondary metabolic reactive species (Rahman and MacNee, 1996; Rahman et al., 1996). To encounter the oxidant-induced oxidative stress, the lung is equipped with a set of antioxidants. If the balance between the oxidants and antioxidants is severely disturbed, it will lead to inflammation, lung injury associated with tissue remodeling, and risk of developing diseases,

such as asthma, COPD, and IPF. In this aspect, peroxisomes might perform important functions in the lung.

In the following these possible roles are summarized:

- 1) Peroxisomes synthesize nonenzymatic antioxidants, such as plasmalogens, that will trap the ROS in the plasma membranes of lung epithelial cells or in the surfactant film secreted by AECII.
- 2) Peroxisomes degrade the deleterious ROS and play an important role in maintaining cellular redox homeostasis by harboring antioxidative enzymes, such as SOD1, catalase, glutathione peroxidase, and peroxiredoxins, which are localized in the peroxisomal matrix of various pulmonary cell types.
- 3) Peroxisomes metabolize leukotrienes and prostaglandins via β -oxidation, which are crucial modulators of inflammation in inflammatory lung diseases.
- 4) Peroxisomes are the primary intracellular site to produce docosahexaenoic acid (DHA) and eicosapentaenoic acid (EPA), which form the backbone for a series of resolution mediators.
- 5) Peroxisomes degrade bioactive toxic substances and lipid derivatives via their β -oxidation system and prevent lipotoxicity in case mitochondria are over-flooded with long-chain fatty acids.

2 Aims of the work

The well-studied pulmonary cells of the lung are club cells, AECII, fibroblasts, and alveolar macrophages. The structure, function, and differentiation capacity of the club cells change with respect to the lung milieu and its development stage. Understanding the club cell differentiation is very important since this cell has the capacity to enter the cell cycle in response to lung injury. However, no knowledge was available in the international literature on morphological and functional postnatal differentiation of club cells in distinct mouse lung developmental stages.

Moreover, these pulmonary cells in the bronchial and alveolar epithelium and stroma are exposed continuously to higher concentrations of environmental oxidants. Indeed, peroxisomes with their antioxidative enzymes might protect the pulmonary epithelium by metabolizing ROS. However, the distribution and enzymatic composition of peroxisomal proteins in epithelial cells of the lung postnatal developmental stages were not known. Furthermore, several anti-oxidative enzymes (SOD1, glutathione peroxidase, and peroxiredoxin 1) of the lung might be localized in several different intracellular compartments, including peroxisomes. In this context, SOD2 has been suggested to be present in peroxisomes along with its mitochondrial localization. Apparently, this dual localization of SOD2 has been well accepted in the peroxisome field, and the citation on its peroxisome localization continued, even though no positive experimental controls were provided.

Much of the knowledge on the functional importance of peroxisomes and their involvement in the metabolism was derived from the experiments based on culturing or treating peroxisome-deficient fibroblasts of patients with peroxisomal biogenesis disorders, children develop fibrotic liver disease and die from liver cirrhosis. This fact suggests that peroxisomes play an important anti-fibrotic role, however, its molecular

pathogenesis is not known. Also the role of peroxisomes in the onset and progression of idiopathic pulmonary fibrosis (IPF) was not known. In contrast to fibroblasts, club cells and AECII are very difficult to isolate and maintain in primary culture. To understand the peroxisomal functions in both cell types and to dissect the molecular mechanisms by distinct intracellular signaling pathways, an optimal experimental cell culture model system of both cell types was needed.

The goals of this research work (Habilitationsschrift) were to address the various open questions as follows:

- 1) Do club cells differentiate postnatally? How many club cells and club cell granules are present in the terminal bronchioles during the postnatal lung development?
- 2) In which cell types (club cells vs. AECII) are peroxisomal proteins abundant during lung development? Are these organelles important for pulmonary cell biology?
- 3) Pulmonary peroxisomes harbor a large variety of various antioxidative enzymes, including SOD1. Do lung peroxisomes also contain SOD2?
- 4) What are the best cell culture model systems to study pulmonary epithelial cell peroxisomes?
- 5) Is modulation of the peroxisomal compartment via PPARs a new strategy to treat lung diseases, e.g. idiopathic pulmonary fibrosis?

3 Applied methodology for the analysis of aims of the work

The following list of methods was applied in this habilitation thesis.

Number	Article	Methods used
1	Karnati S* , Graulich T, Oruqaj G, Pfreimer S, Seimetz M, Stamme C, Mariani TJ, Weissmann N, Mühlfeld C, Baumgart-Vogt E (2016). Postnatal development of the secretory cells of the distal airways, the bronchiolar club cells in the mouse lung: stereological and molecular biological studies. <i>Cell and Tissue Research</i> . Jun;364(3):543-57.	Immunofluorescence, stereology, light microscopy, postembedding immunoelectron microscopy, transmission electron microscopy (TEM), Scanning electron microscopy (SEM), laser captured microdissection, RNA isolation and cDNA synthesis, RT-PCR, Western blotting, statistics
2	Karnati S , Baumgart-Vogt E (2009) Peroxisomes in airway epithelia and future prospects of these organelles for pulmonary cell biology. <i>Histochem Cell Biol</i> . Apr: 131(4):447-54.	Immunohistochemistry, immunofluorescence, in situ hybridization
3	Karnati S , Lüers G, Pfreimer S and Baumgart-Vogt E (2013) Manganese Superoxide dismutase 2 (MnSOD) is localized to mitochondria but not in peroxisomes. <i>Histochemistry and Cell Biology</i> , Aug:140(2):105-17	Immunofluorescence, postembedding immunoelectron microscopy, immunolabelling of ultrathin cryosections, immunocytochemistry, transmission electron microscopy, RNA isolation and cDNA synthesis, RT-PCR, Western blotting, statistics
4	Karnati S , Palaniswamy S, Alam MR, Oruqaj G, Stamme C, Baumgart-Vogt E (2015) C22-bronchial and T7-alveolar epithelial cell lines of the immortomouse are excellent murine cell culture model systems to study pulmonary peroxisome biology and metabolism. <i>Histochemistry and Cell Biology</i> Mar;145(3):287-304.	Immunofluorescence, immunocytochemistry, postembedding immunoelectron microscopy, transmission electron microscopy (TEM), qRT-PCR, Western blotting, statistics
5	Oruqaj G [§] , Karnati S[§] , Vijayan V, Kotarkonda LK, Boateng E, Zhang W, Ruppert C, Günther A, Shi W, Baumgart-Vogt E (2015) Compromised peroxisomes in idiopathic pulmonary	Immunofluorescence, siRNA, transfection, RNA isolation, cDNA synthesis, RT-PCR, qRT-PCR, ELISA, luciferase-reporter gene assays, cytokine (IL6, TNF- α) measurements, Western

	fibrosis, a vicious cycle inducing a higher fibrotic response via TGF- β signaling. <i>Proc Natl Acad Sci.</i> 112(16):E2048-57. § both authors contributed equally to the study.	blotting TGF- β inhibitor, PPAR α agonist (ciprofibrate, WY14643) and PPAR β antagonist (GW6471) treatments, poly-L-lysine coating, transfection and Dual luciferase assay, ROS measurements and Sircol collagen assay, statistics
6	Vijayan V, Tumpara S, Karnati S , Garikapati V, Linke M, Kamalyan L, Mali SR, Sudan K, Kollas A, Schmid T, Schulz S, Spengler B, Weichhart T, Immenschuh S, Baumgart-Vogt E (2017) A new immunomodulatory role for peroxisomes in macrophages activated by the TLR-4 ligand LPS. <i>Journal of Immunology</i> Mar 15;198(6):2414-2425.	Immunofluorescence, mitotracker and thioflavin T stainings, siRNA, transfection, qRT-PCR, Western blotting, ELISA, flow cytometry, liquid chromatography–tandem mass spectrometry, statistics

Overview of the techniques and methods used in this habilitation thesis

Cell culture: Isolation and culture of primary human control and idiopathic pulmonary fibroblasts, mouse alveolar macrophages, peritoneal macrophages, bone marrow-derived macrophages, mouse embryonic fibroblasts, HepG2, Hepa 1-6, C22 and T7 cell lines.

Morphology: Perfusion fixation, tissue freezing or embedding into paraffin or resins (Epon, LR White) for light or electron microscopy of mouse lung tissue

Light microscopy: Wide-field and phase-contrast microscopy

Fluorescence microscopy: Immunofluorescence, confocal laser scanning microscopy (CLSM), laser capture microdissection (LCM), structured illumination microscopy (SIM) and stimulated emission depletion (STED) microscopy

Image analysis and quantification software: ImageJ, FIJI, Icy, GraphPad Prism, Photoshop

Electron microscopy: Transmission electron microscopy (TEM), scanning electron microscopy (SEM), post-embedding immunoelectron microscopy, immunocytochemistry and cytochemical alkaline 3, 3'-diaminobenzidine procedure for catalase activity

Molecular biology: RNA isolation, cDNA synthesis, RT-PCR, qRT-PCR, agarose gel electrophoresis, siRNA and plasmid transfection, dual-luciferase reporter assays

Biochemistry: Homogenization of lung tissue, subcellular fractionation of organelles, SDS-PAGE, Western blotting, enzyme activity assays, liquid chromatography-tandem mass spectrometry (LC-MS), ELISAs and Sircol collagen assay

4 Results and Discussion

4.1 Club cell differentiation is a postnatal phenomenon

Prior to understanding the important roles of peroxisomes in the pulmonary cell types and club cells, their secretory proteins were characterized during the postnatal development of the mouse lung. In fact, this study is the first comprehensive research work on the club cell differentiation by combining light- and fluorescence microscopic techniques, as well as scanning and transmission electron microscopic approaches, together with design-based stereology of the three developmental stages (newborn, 15-day-old, and adult) of the mouse lung. Also, this study was conducted keeping in the mind that club cells were also detected in intra- and extrapulmonary airways of rabbits (Plopper et al., 1993). Therefore, we explored *only* the club cells of distal airways and their morphological and functional alterations (Karnati et al., 2016a).

Before investigating the number of club cells and the abundance of the CC10 protein during the development of the lung, a club cell marker protein CC10 antibody was characterized for its quality and specificity in wild type (CC10^{+/+}) and CC10 knockout (CC10^{-/-}) animals as well as post-embedding immune TEM. Indeed, CC10 was exclusively detected in club cells of the wild type mice, whereas it was completely absent in CC10 knockout animals. Post-embedding immunoelectron microscopy of CC10 revealed that CC10 was exclusively localized to the secretory granules of the club cells (Karnati et al., 2016a). In addition to CC10, club cells secretory proteins, such as SP-A, B, and D, were increased in the microdissected bronchiolar epithelial cells during the postnatal lung development, suggesting that club cell maturation occurs postnatally (Karnati et al., 2016a). Interestingly, more club cell secretory granules containing CC10 were detected both in P15 and adult club cells, which is in agreement with rat club cells (Bedetti et al., 1987; Karnati et al., 2016a). Jeffery (Jeffery, 1977) proposed that distal airways reorganize constantly according to the maturation of the

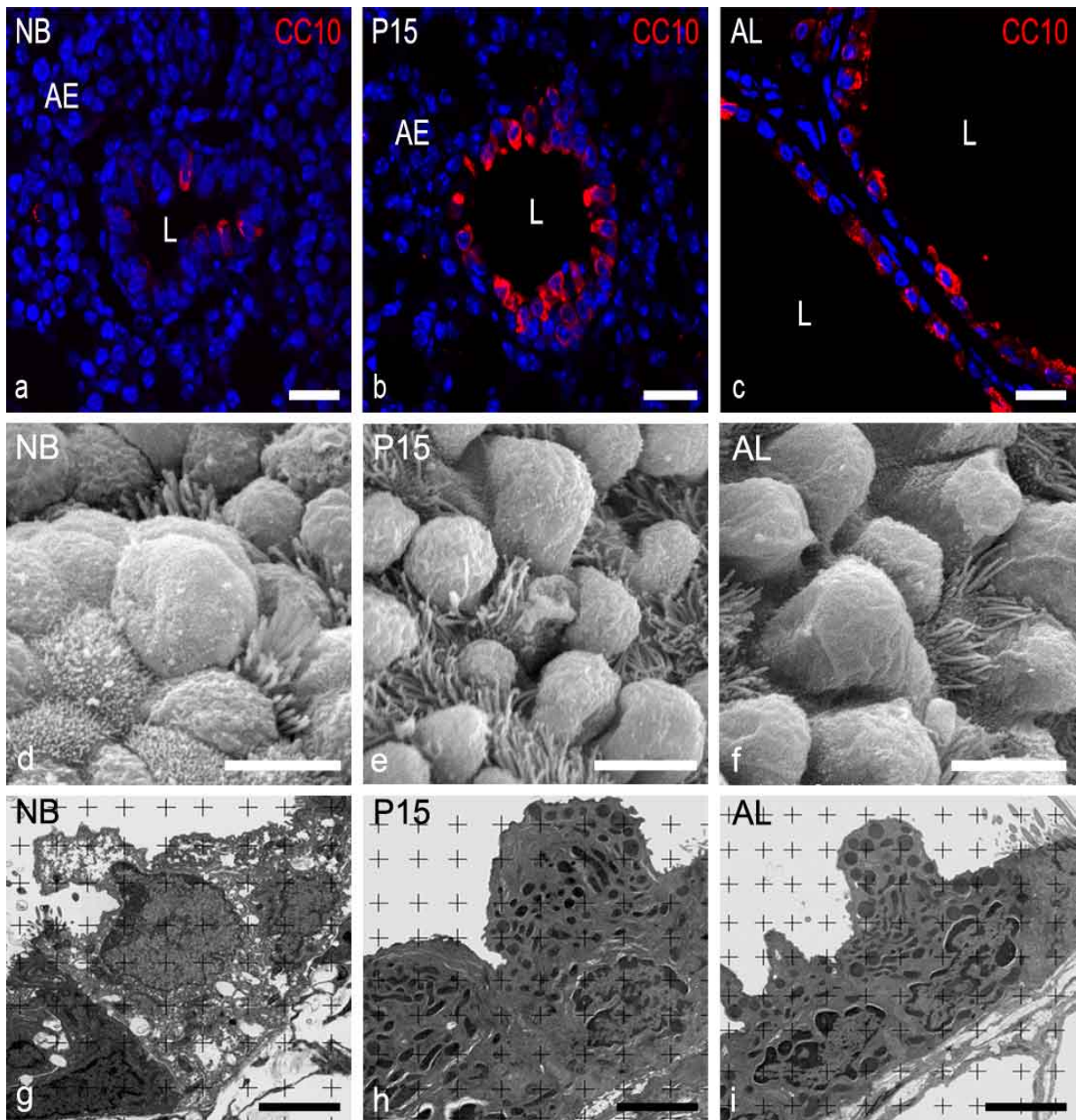


Fig. 3 Various morphological techniques such as immunofluorescence (a–c), scanning electron microscopy (d–f), and transmission electron microscopy (–h) combined with design-based stereology on ultrathin sections of the terminal bronchioles of the mouse three lung developmental stages (newborn, 15-day-old, and adult) suggested that club cells and club cell secretory protein abundances were increased during the postnatal development of the lung (Karnati et al., 2016a). Bars represent a–c: 25 μm ; d–i: 5 μm .

lung. To overcome this problem, we used large sampling procedure with design-based stereology at light- and electron microscopic (EM) level of three postnatal lung development stages as previously suggested (Hill, 1979; Lowrie, 1973). Based on these criteria, we achieved a quantitative description of the postnatal club cells and club cell secretory granules

during the postnatal lung development. Our results showed 64% of the volume of bronchiolar epithelial cells from adult mice of the C57BL/6J strain lining the distal airways were club cells as compared to the club cells of the Swiss-Webster mice (77% of the volume) (Fanucchi et al., 1997a; Karnati et al., 2016a). This strain-specific difference in the number of club cells of the bronchiolar epithelium could also be influenced by the environmental conditions of the animals used (Cardoso et al., 1993; Karnati et al., 2016a; Plopper et al., 1993). Interestingly, stereologic analysis demonstrates that the total lung volume increased 9.2x from newborn to P15 animals and increased 1.8x from P15 to adult mice. Further, bronchiole volume increased 7.2x from newborn to P15 animals, and the club cell volume increased 6.6x from newborn to P15 animals (Karnati et al CTR). Moreover, the volume of intracellular club cell secretory granules in the lung significantly increased within 15 days after birth, suggesting that the club cell is not mature or fully differentiated cell at birth and that maturation occurs postnatally (Fig. 3) (Karnati et al., 2016a). In fact, this observation was also in agreement with other species, such as rabbit, pig, and humans (Baskerville, 1970; Plopper et al., 1983; Rosan and Lauweryns, 1972). Furthermore, the club cell distribution depends on the age and anatomic location of the airway since CC10 protein was detected only in the proximal airways of the canalicular stage and distal airways of the saccular stage, whereas it was not expressed in the pseudoglandular stage of all airways (Fanucchi et al., 1997b).

Indeed, CC10, SP-A, and SP-D proteins are not only involved in the modulation of inflammation but also act as host defense to the pulmonary infections (Reynolds and Malkinson, 2010; Singh and Katyal, 1984; Wright, 2005). This notion is supported by the studies with CC10 or SP-A or SP-D-deficient mice that are highly susceptible to bacterial or viral challenge (Wright, 2005). In this context, it is important to mention that CC10-deficient mice are susceptible to pulmonary fibrosis by preventing T_H2 -mediated inflammation and the release of pro-fibrotic T_H2 cytokines, such as IL-4, IL-5, and IL-13 (Van Vyve et al., 1995). Interestingly, CC10-deficient mice that were treated with bleomycin markedly increased the

level of TGF β -mRNA in the lungs, suggesting that CC10 may have a therapeutic potential for the treatment of pulmonary fibrosis (Van Vyve et al., 1995). Although literature is available on the anti-inflammatory role of CC10 in various lung diseases, the precise molecular mechanism by which CC10 controls lung inflammation is not clearly understood. Furthermore, also the synthesis pathway of secretory surfactant proteins in club cells and their turnover in the bronchiolar lumen are not known (Auten et al., 1990; Endo and Oka, 1991; Karnati et al., 2016a; Savov et al., 2000). To shed more light on this aspect, structural modifications of club cell surface dynamics during the postnatal development of the lung were explored. Interestingly, club cell extrusions into the lumen of bronchioles (mainly in adult terminal bronchioles) were detected, which could be necessary features for exerting the functional physiological role of club cells (Karnati et al., 2016a) (Figure 3).

Further progressive ciliation was detected during the postnatal development of mouse lung, which is supported by Toskala and colleagues (Karnati et al., 2016a; Toskala et al., 2005). The postnatal maturation of club cells was further manifested by the absence of large glycogen fields in the P15, and adult club cells in comparison to the newborn club cells suggested that glycogenolysis might be an important indicator for the maturation of club cells (Cutz and Conen, 1971; Karnati et al., 2016a). In this context, it is important to mention that glycogenolysis provides energy for the division of club cells when the airway epithelium is injured since club cells are stem/progenitor cells for club and AECII cells (Reynolds and Malkinson, 2010; Sorokin, 1961; Wang et al., 2012). Moreover, recent evidence suggests that club cells differentiate into AECII cells during the repair of the alveolar epithelium following severe pulmonary injury (Reynolds and Malkinson, 2010; Sorokin, 1988; Wang et al., 2012; Zheng et al., 2013). Interestingly, CC10 protein expression was increased in bronchoalveolar stem cells (BASCs) during the postnatal development of the mouse lung, suggesting that BASCs are required for club cell differentiation and might proliferate during the restoration of

the pulmonary epithelium upon injury or damage (Karnati et al., 2016a; Kim et al., 2005; Lawson et al., 2002; Plopper et al., 1992a; Plopper et al., 1992b; Zheng et al., 2013).

A clear significant association between the expressions of club cell secretory protein abundance and the decrease in glycogen content during the postnatal developmental stages indicate that mice can be used as an excellent animal model to study the factors controlling club cell differentiation and its functional role in the pathogenesis of pulmonary diseases.

4.2 Abundance of peroxisomes in the bronchiolar and alveolar epithelial cells of the developing lung

As species-specific differences were already detected in the number of club cells in the bronchiolar epithelium of two different strains of mice (swiss-Webster and C57BL/6J, Fanucchi et al 1997, Karnati et al 2016), differences were also detected for marker proteins of the peroxisomal compartment of man and mice. The highest protein abundance of classical peroxisomal marker “catalase” was detected in the distal conducting airways and AECII cells of the E18.5 mouse lung (Karnati and Baumgart-Vogt, 2009). In agreement to the catalase localization, immunofluorescence analysis for the novel peroxisomal marker “peroxisome biogenesis protein 14 - PEX14p” showed a similar distribution and higher abundance in club cells as well as in alveolar regions containing AECII or in the early phase of transdifferentiation into AECI of the E18.5 lungs, suggesting that peroxisomes are important in the differentiation process of the lung (Karnati and Baumgart-Vogt, 2009). In contrast to E18.5 lungs in rats, and in man, it was suggested that peroxisomes disappear parallel to the differentiation of AECII to AECI (Moriguchi et al., 1984; Schneeberger, 1972b). In fact, Hirai et al. could not detect mouse AECI peroxisomes (Hirai et al., 1983; Hirai et al., 1977) and Moriguchi and colleagues did not find peroxisomes in fully differentiated human AECI (Moriguchi et al., 1984). Therefore, our group established sensitive methods to detect

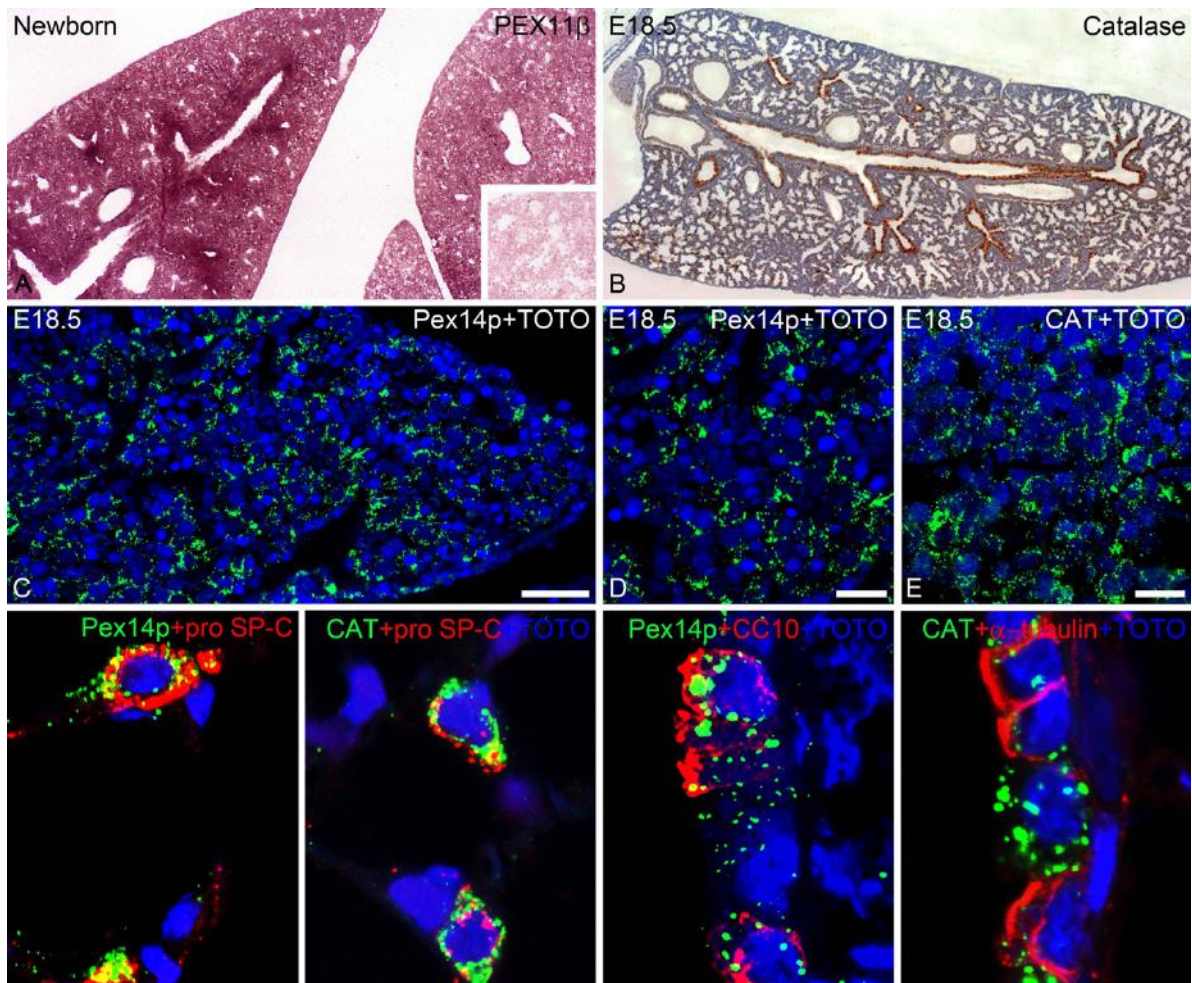


Fig. 4 *Pex11β* mRNA and peroxisomal marker proteins are shown in different mouse lung developmental stages (E18.5, newborn, and adult). The catalase and PEX14p were labeled strongest in the club and undifferentiated alveolar regions in E18.5 lungs (B–E). In situ hybridization (ISH) for the *Pex11β* mRNA in the newborn mouse lung (A). The catalase and PEX14p were also strongly labeled in the AECII and club cells of the adult mouse lung (F–I) (Karnati & Baumgart-Vogt, 2009). Bars represent c: 50 μ m; d, e: 25 μ m; e: 25 μ m; f-i: 20 μ m.

peroxisomes in distinct pulmonary cell types in which peroxisomes are less numerous, such as in AECI or endothelial cells (Karnati and Baumgart-Vogt, 2008, 2009).

With these sensitive methods, high numerical abundance of large peroxisomes was observed in club cells, AECII, and macrophages of the adult mouse lung, whereas small and less numerous peroxisomes were detected in AECI, endothelial cells, and ciliated cells of the mouse lung (Karnati and Baumgart-Vogt, 2008) (Table 1). In contrast, a higher abundance of peroxisomal proteins, such as catalase, PEX14, and ABCD3, was detected easily in ciliated

cells, club cells, AECII, and macrophages of the human lung. However, peroxisomal β -oxidation enzymes (ACOX1, ACAA1) were very weakly labelled (Karnati and Baumgart-Vogt, 2008, 2009) (Table 2). Interestingly, in the mouse lung, these enzymes (ACOX1, ACAA1) were strongly abundant in the few AECI cell peroxisomes revealing cell type-specific functional differences of peroxisomes in AECI in comparison to AECII cells (Karnati, 2008, 2009) (Table 1). These results summarize at least some of the species-specific differences of pulmonary peroxisomes in the mouse and human lung.

Tab. 1 Distribution and abundance of peroxisomal proteins in the **bronchiolar epithelial cells and macrophages** of the lungs of man and mice

PO proteins	Mouse			human		
	Club	Ciliated	Macrophages	Club	Ciliated	Macrophages
Catalase	++++	++	+++	++	++++	++++
PEX14p	++++	++	++	+++	++++	++++
ABCD3	++++	++	++	++++	++++	+
ACOX1	++++	++	+++	+++	+	++++
ACAA1	++++	++	+++	++	+	++

++++ very strong, +++ strong, ++ weak, + very weak, n.t.:not tested; n.d.: not detected

Tab. 2 Distribution and abundance of peroxisomal proteins in the **alveolar epithelial cells and macrophages** of the lungs of man and mice

PO proteins	Mouse			Human		
	AECII	AECI	Macrophages	AECII	AECI	Macrophages
Catalase	++++	+	++++	++++	+	++++
PEX14p	++++	++	++++	++++	+	++++
ABCD3	++++	+	++	+++	+	++++
ACOX1	++++	+++	+++	+++	++	++++
ACAA1	++++	+++	+++	++	n.d.	n.d.

++++ very strong, +++ strong, ++ weak, + very weak, n.t.:not tested; n.d.: not detected

The distribution pattern of majority of peroxisomal proteins is highly similar in bronchiolar (club) and alveolar cells (AECII) of the mouse lung. Similarly, the same pattern was also

observed in bronchiolar and alveolar macrophages. In the human lungs, the majority of peroxisomal proteins were also similar in the bronchiolar region (ciliated cell peroxisomes more being abundant in number than club peroxisomes) and alveolar region (AECII cell peroxisomes being more abundant in number than AECI cell peroxisomes). The high numerical abundance of peroxisomes in the bronchiolar and alveolar region (AECII) suggests that these organelles play an important protective role in lung epithelia against high oxygen concentration and oxidative stress (Karnati and Baumgart-Vogt, 2009).

In addition, the presence of peroxisomal β -oxidation enzymes and lipid transporter suggests that peroxisomes are involved in the pulmonary lipid metabolism and alterations in reduced ether lipid synthesis or reduced peroxisomal β -oxidation of eicosanoids, which are important inflammatory mediators for lipid signaling, eventually might lead to inflammation.

In this context, it is important to mention that several studies have already reported an association between reduced plasmalogens and bronchopulmonary dysplasia (BPD), a leading cause of morbidity in prematurely born infants (Brites et al., 2004). In fact, premature infants increase their risk of developing BPD when plasmalogen levels in the tracheal aspirants were low (Koch et al., 2003; Rüdiger et al., 1998). This notion is supported by the fact that premature infants who received higher plasmalogen content in the surfactant as a therapy experienced a better life, suggesting an important role of peroxisomes in the developing lung (Vijayan et al., 2017). Interestingly, Berry and colleagues used MALDI-MS imaging to investigate the anatomical distribution of pulmonary lipids in lung sections. They reported that plasmalogens were highly abundant in the large and small airways as well as in the pulmonary epithelial cell membranes (Terlecky et al., 2006). Indeed, ciliated, club and AECII cells contain a high number of peroxisomes and show an increased metabolic activity that is essential for a continuous supply of plasmalogens in these cell types. Furthermore, plasmalogens trap ROS and act as an antioxidant that protects against ROS-induced respiratory diseases (Brites et al., 2004; Karnati and Baumgart-Vogt, 2008, 2009). Lung

plasmalogens are enriched with arachidonic acid (AA), which plays an important role in immune defense of the lung. In this respect, it is noteworthy that activation of PPARs, which regulate peroxisome proliferation, alleviates the inflammatory reaction in pulmonary airways (Karnati and Baumgart-Vogt, 2009; Kulkarni, 2012). Recent evidence suggests that PPAR γ plays an important role in the transcriptional activity of several antioxidative enzymes, including the ones localized in the peroxisomal compartment (Polvani et al., 2012). The classical peroxisome proliferators, such as clofibrate, which was extensively studied, proliferated the peroxisomes by activating the PPAR α in parallel to a significant increase in the lamellar bodies, suggesting that these compounds increased the surfactant synthesis (Fringes et al., 1988a, b; Fringes and Reith, 1988).

In this context, it is important to mention another peroxisomal protein, PEX11 β , which is deeply embedded into the peroxisomal membrane and involved in controlling the proliferation (Schrader et al., 1998) and numerical abundance of peroxisomes (Koch et al., 2003). Because of its membrane localization, there are still no sensitive correct specific antibodies to localize endogeneous protein levels of PEX11 β . Therefore, the in situ hybridization (ISH) technique, which was previously established (Grabenbauer et al., 2001), was subjected to visualize *Pex11 β* mRNA in the newborn lung. Indeed, the strongest expression of the *Pex11 β* mRNA was detected in distal airway epithelial cells and AECII in agreement to the other peroxisomal proteins in the lung (Karnati and Baumgart-Vogt, 2009). In fact, *Pex11 β* mRNA expression was higher in the lung in comparison to hepatocytes of the liver, revealing that PEX11 β p might play an important role in the lung development, especially in the developing airways and alveolarization. Indeed, the important functions of the PEX11 β p was revealed by generating PEX11 β -deficient mice (Li et al., 2002). These animals die shortly after birth and are severely growth-retarded, exhibiting the similar phenotype of patients with Zellweger syndrome (Baumgart et al., 2003; Gärtner, 2003). PEX11 β -deficiency effects lung morphogenesis and maturation as well as severely alters the

alveolarization process by altering the specific genes, targeting the signal transduction pathways of distal morphogenesis (Wnt5a) and differentiation of pulmonary cell types (PPARs) (Karnati, 2009). PEX11 β -deficient animals die shortly after birth because the lungs are not developed, and drastic dysregulation of lipid signaling induced the early death of these animals (Li et al., 2002). Furthermore, PEX11 β -deficiency induced an imbalance of antioxidative enzymes and severe alterations of proinflammatory proteins, suggesting that peroxisomal metabolism is essential in maintaining lung homeostasis via PPARs (Karnati, 2009). In this context, mitochondrial SOD2 was strongly increased in PEX11 β -deficient club and AECII cells, suggesting an increase in oxidative stress, which was also observed in Pex5 knockout mice (Baumgart et al., 2001). Indeed, the defect in mitochondrial respiratory complexes I and III exerts more superoxide radicals. In consequence, mitochondrial SOD2 is upregulated to convert this radical into less toxic H₂O₂, which is further decomposed by mitochondrial glutathione peroxidase or peroxisomal antioxidative enzymes (Karnati, 2009). Interestingly, peroxisomes contain the largest amount of prooxidative (peroxisomal oxidases and iNOS) as well as antioxidative (catalase, SOD1, PrdxI and PrdxV, and glutathione peroxidase) enzymes in their matrix. In line with these functions and peroxisomes harboring a large variety of antioxidative enzymes, many researchers believed that SOD2 was also localized in the peroxisomes (Singh et al., 1999).

4.3 SOD2 is not localized in peroxisomes

SOD2 has been proposed to have multi-subcellular localization, such as in the mitochondria (Da Cruz et al., 2003; McCord and Fridovich, 1969; Shimoda-Matsubayashi et al., 1996; Weisiger and Fridovich, 1973a), the peroxisomal matrix, and the peroxisomal membrane (Rickett and Kelly, 1990; Singh et al., 1999). In fact, SOD2 localization in peroxisomes was always questionable due to the sole usage of biochemical fractionation and Western blotting for proving the peroxisomal localization of SOD2. Therefore, correct SOD2 subcellular

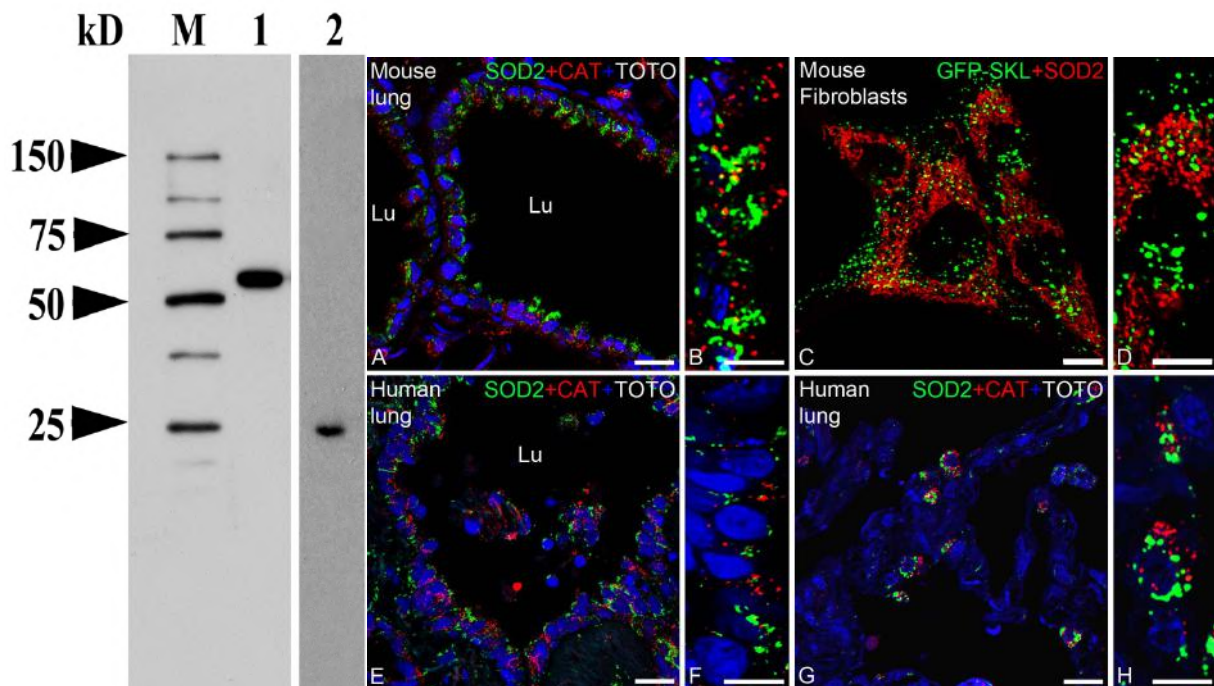


Fig. 5 Western blot for catalase (lane 1) and SOD2 (lane 2) in adult mouse liver homogenates. The characterized antibodies were used for double-IF staining of the mouse bronchiolar epithelium (A–B), GFP-labeled mouse fibroblasts (C–D), and the human bronchiolar epithelium (E–F) as well as the human alveolar epithelium (G–H), depicting the clearly distinct subcellular distribution in individual subcellular compartments (Karnati et al., 2013). Bars represent a, c, f, g: 25 μm ; b, d, f, h: 10 μm .

localization by using highly sensitive morphological methods in distinct pulmonary cell types was analysed. In this respect, sensitive and specific antibodies that can recognize SOD2 and catalase are particularly useful to confirm their subcellular localization for qualitative and quantitative analysis of distinct organs and cell types, in particular, the lung that contains more than 40 different cell types (Karnati et al., 2013; Sorokin, 1988). To test the antibody quality, Western blot analysis with the anti-SOD2 and anti-catalase antibodies were performed in mouse liver homogenates (Fig. 5), revealing a single band with correct molecular weight, suggesting a high specificity of the antibody reaction (Karnati et al., 2013). Mouse club cells and AECII as well as human bronchiolar, alveolar epithelial cells, and fibroblasts were analysed in comparison to liver hepatocytes for a correct subcellular

localization of SOD2 together with the catalase in double IF stainings to address whether SOD2 is localized in peroxisomes. The liver samples were used for a relative comparison since SOD2 is 10 times higher abundant in hepatocytes than in other tissues (Marklund, 1984). Moreover, in the newborn liver sections, peroxisomes are smaller and contain less catalase (Baumgart et al., 2003). Apparently, SOD2 was not colocalized with catalase, and SOD2 labeling was detected mainly in mitochondria (Fig. 5).

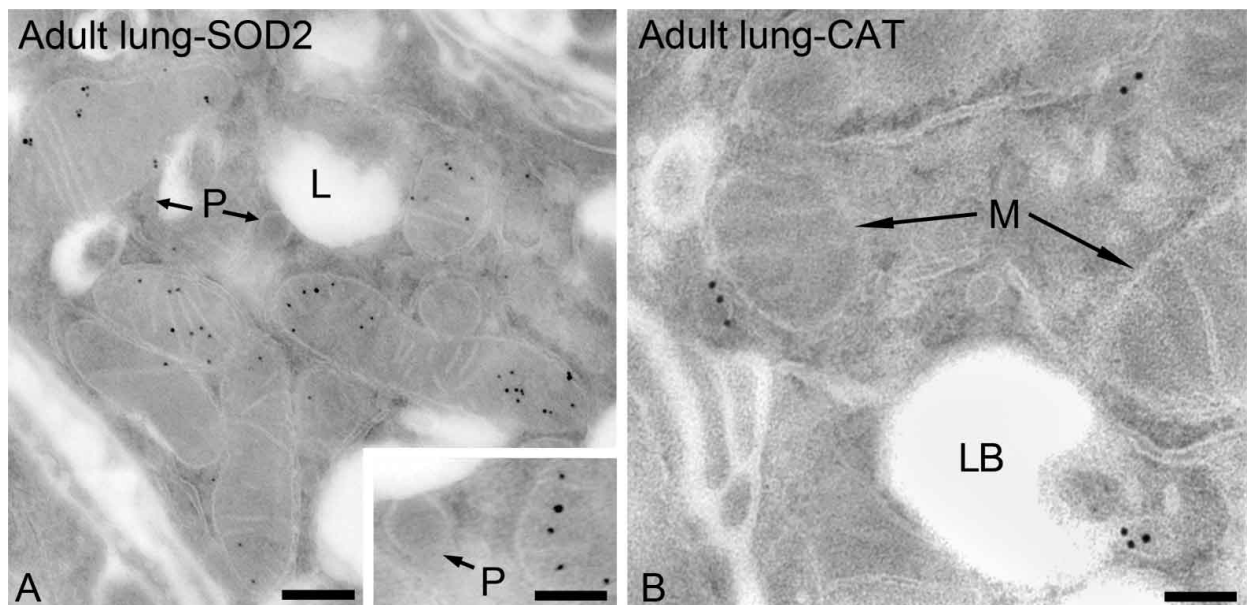


Fig. 6 Ultrastructural immunocytochemical localization of SOD2 in LR white sections of adult mouse lung with the ultrasmall gold silver intensification method (A) and peroxisomes were labeled for catalase with the protein A gold method (PAG) (B). SOD2 labeled mitochondria only but not peroxisomes (inset A) whereas catalase labeled peroxisomes but not mitochondria. Bars represent a: 0.25 μm ; b: 1 μm .

However, occasionally in some regions, both protein signals (SOD2 and catalase) were superimposed, which is explained by the fact that (1) mitochondria and peroxisomes are in very close contact to each other (see above in the electron micrograph, Fig. 6), possibly near or less than 200 nm that will come under the diffraction limit of a CLSM (Abbe's law: resolution is limited by the diffraction of light). This means that CLSM was not able to resolve the two organelles in this frame, but these images were obtained by 2-D settings. Since they might lie underneath each other, only 3-D imaging might possibly resolve these

structures. In order to illustrate the correct subcellular localization of SOD2 and to overcome the above-mentioned problems, the suitable best method “immunocytochemistry” on ultrathin lung sections was used. At ultrastructural level, LR white sections of lung and liver were immunolabelled for SOD2 in parallel to catalase revealing a highly specific mitochondrial labeling for SOD2, whereas catalase labeled solely peroxisomes and no other organelles were stained (Karnati et al., 2013). Indeed, electron micrographs of lung epithelial cell types showed a close association of mitochondria and peroxisomes (Fig. 6) confirming the above observations (Karnati et al., 2013). Since negative controls with PAG techniques on LR white sections showed several gold particles, therefore to obtain highest sensitive labeling for SOD2, ultrathin cryosections using ultrasmall gold-labeled Fab fragments and silver intensification as secondary method was used. Indeed, mitochondria were clearly labeled with SOD2 and peroxisomes were devoid of SOD2 labeling. Moreover, biochemical analysis of isolated peroxisomal fractions suggested that SOD2 and catalase were localized to the corresponding enriched fractions of mitochondria and peroxisomes suggesting that SOD2 is a mitochondrial protein (Karnati et al., 2013).

Antioxidative enzymes are highly expressed in the lung and SOD2 activity is higher in the lung than liver, but, we did not observe any peroxisomal localization of SOD2 as previously reported by the Singh group (Karnati et al., 2013; Rickett and Kelly, 1990; Singh et al., 1999). In contrast to the false-positive localization of SOD2 in peroxisomes, SOD1 has been described in the peroxisomes by several groups in different species (rat, mouse and human) (Dhaunsi et al., 1992; Islinger et al., 2009; Keller et al., 1991; Kira et al., 2002; Wanders and Denis, 1992). Interestingly, SOD1 is induced by ciprofibrate treatment in which peroxisomes were also proliferated (Dhaunsi et al., 1992). Keller group first proposed SOD1 to be also in peroxisomes in addition to cytoplasm, however, their abundances were independent to each other (Keller et al., 1991; Moreno et al., 1997). Indeed, the subcellular localization of proteins was depending upon the specific targeting signals that direct the proteins into the specific

subcellular compartment (Schatz, 1987). Most of the peroxisomal proteins contain a typical peroxisomal targeting signal 1 or 2 (PTS1 or 2) by which peroxisomal proteins are transported into the organelle. Despite the fact that, SOD1 is a peroxisomal protein but this protein does not contain any PTS signal, therefore the importing process is still not clear, until Islinger and colleagues proposed a “piggyback import mechanism” of SOD1 binding to its chaperon CCS into peroxisomes (Islinger et al., 2009). In contrast, SOD2 possesses a clear mitochondrial targeting signal and no chaperons were detected, therefore SOD2 is targeted into the mitochondria (Karnati et al., 2013; Miao and St Clair, 2009; Shimoda-Matsubayashi et al., 1996).

Overall, SOD2 labeling was mainly observed in the bronchiolar and alveolar epithelial cells in agreement to the previous studies (Chang et al., 1995). Further, macrophages were also strongly labeled as these cell types are also rich in mitochondria (Crapo and Stamler, 1994; Kinnula et al., 1994; Pietarinen-Runtti et al., 2000). The thin portions of the alveolar septa containing the long cytoplasmic extensions of AECI showed minimal labeling for SOD2 as AECI cells have few mitochondria (Harris et al., 1991). Immunohistochemical studies have shown that SOD2 is moderately expressed in interstitial fibroblasts, and visceral pleura of hyperoxia-exposed rats (Coursin et al., 1992). Further, *in situ* hybridization studies showed that *Sod2* mRNA distributed mainly in the airways, septal tips of alveolar ducts and arterioles near the airways (Clyde et al., 1993; Gilks et al., 1998). *Sod2* mRNA, protein and/or activity are increased in lung homogenates and in cultured pulmonary epithelial cells, fibroblasts, alveolar macrophages, and in malignant lung cells by oxidants, cigarette smoke, TNF α , IFN γ , IL-1 and IL-6 (Akashi et al., 1996; Shull et al., 1991; Weller et al., 1997; Wong and Goeddel, 1988). TNF α , which is the most widely, investigated cytokine, increases SOD2 activity and mRNA expression in a dose- and time-dependent manner in malignant lung adenocarcinoma and pleural mesothelioma cell (Jarvinen et al., 2000; Warner et al., 1991).

Interestingly, the SOD2 promoter contains binding sites for several transcription factors, such as AP1, AP2, and NF- κ B (Wan et al., 1994; Zhang, 1996). Although the expression of SODs has been characterized relatively well in animal and human lung, the specific role of the antioxidant enzymes in the pathogenesis of most lung diseases remains unclear. In fact, there are numerous studies showing that the oxidant burden in the lungs of the patients with pulmonary fibrosis is increased and that inflammatory cells of these patients generate more radicals than the cells of healthy control subjects (Tarrier et al., 1978; Wallaert et al., 1990). SOD2 is upregulated in inflammatory areas of various lung diseases, but whether its induction offers any protection in these diseases with variability in individuals and various cell types also remains to be investigated. Taken together, SOD2 is most highly expressed in bronchiolar epithelial cells, AECII and alveolar macrophages, and cell types with relatively high metabolic capacity and plays a major role in protecting lung tissue against free radicals.

4.4 C22 and T7 are the best cell lines to study the functions of peroxisomes in the club and AECII cells

The club and AECII cells contain the highest numerical abundance of peroxisomes in the lung, though the peroxisomal enzyme content is significantly different and peroxisomes in these cell types might fulfill important cell-specific metabolic functions (Karnati and Baumgart-Vogt, 2008, 2009; Karnati et al., 2016b). To understand the functional role of peroxisomes in these cell types, the best cell culture model systems are necessary. Therefore, mouse C22 and T7 cell lines were characterized for the distribution of peroxisomal enzymes. Further, we have profiled the peroxisomal proteins to understand the regulation and metabolic role of peroxisomes in club and AECII cells by the increase of paracrine or external growth factors (Karnati et al., 2016b). Primary club cells are very difficult to isolate. Several cell lines for club cells were developed in recent years by using mouse and human tissues, but most of them were originated from tumors and do not secrete club cell-specific proteins. In contrast to club cells, several good protocols have been established in recent years to isolate

primary mouse AECII cells (Rice et al., 2002; Wang et al., 2012); however, it is difficult to maintain the AECII cell phenotype in the primary culture as they dedifferentiate into AECl cells (Rice et al., 2002; Shannon et al., 1992; Sugahara et al., 1995). Most importantly, no good tumor cell lines are available that will resemble the original AECII phenotype. None of these cell lines are phenotypically close to club or AECII cells, and these cell lines do not accurately reflect the cell biology and physiology of club and AECII (Karnati et al., 2016b; Mallampalli et al., 1992; Smith, 1977). Therefore, to understand the biology of club cells and AECII, DeMello and colleagues generated C22-club and T7-AECII cell lines by using the immortal mouse containing the ts SV40 large T antigen (deMello et al., 2000; Demello et al., 2002). Indeed, the “immortal mouse” was already extensively used to establish the cell lines that are difficult to isolate and maintain their phenotype, such as osteoclasts (Chambers et al., 1993), colonic and small bowel epithelial cells (Whitehead et al., 1993), or podocytes of the kidney (Mundel et al., 1997). In our study, C22 and T7 cells expressed the appropriate mRNAs and synthesized the corresponding lung cell type-specific markers, such as CC10, SP-A and SP-B for C22 cells, and pro SP-C, SP-A, and SP-B for T7 cells. In addition, these marker proteins were localized on the subcellular level in C22 and T7 cells by using highly sensitive post-embedding immunocytochemistry for club cell secretory granules (for CC10) and lamellar bodies (for pro SP-C), suggesting that C22 and T7 cell lines resemble and mimic the native club and AECII cells in situ (Karnati et al., 2016b). Taken together, C22 cells in the culture act as native club cells. Similarly, T7 cells resemble the original AECII phenotype since they are able to produce cell type-specific marker proteins (Demello et al., 2002; Karnati et al., 2016b).

In agreement to the distribution of peroxisomal proteins in mouse and human lung tissue, C22 and T7 cells were highly differentiated and contained a high number of peroxisomes. Indeed, proteins involved in the proliferation of peroxisomes, such as the ones of the PEX11 family, were highly abundant in C22 and T7 cells, suggesting that peroxisomes divide frequently and

peroxisomal machinery is active (Karnati et al., 2016b). In fact, several studies already supported the fact that PEX11 β is involved in the homeostasis regulation of peroxisomal numerical abundance, PEX11 α mainly induces the proliferation of peroxisomes, and PEX11 γ is involved in the cluster formation of peroxisomes (Li et al., 2002; Li and Gould, 2002; Schrader et al., 1998). Indeed, C22 and T7 cell peroxisomes were often clustered similar to club cell and AECII peroxisomes in situ (Fig. 4. F-I), which is explained by the high level of the mRNA expression for *Pex11 γ* in these cell types (Fig. 7). In this context, it is important to mention that *Pex11 β* mRNA is strongly expressed in the distal airway epithelial cells and AECII (Karnati and Baumgart-Vogt, 2009). Interestingly, C22 cells showed mostly large and

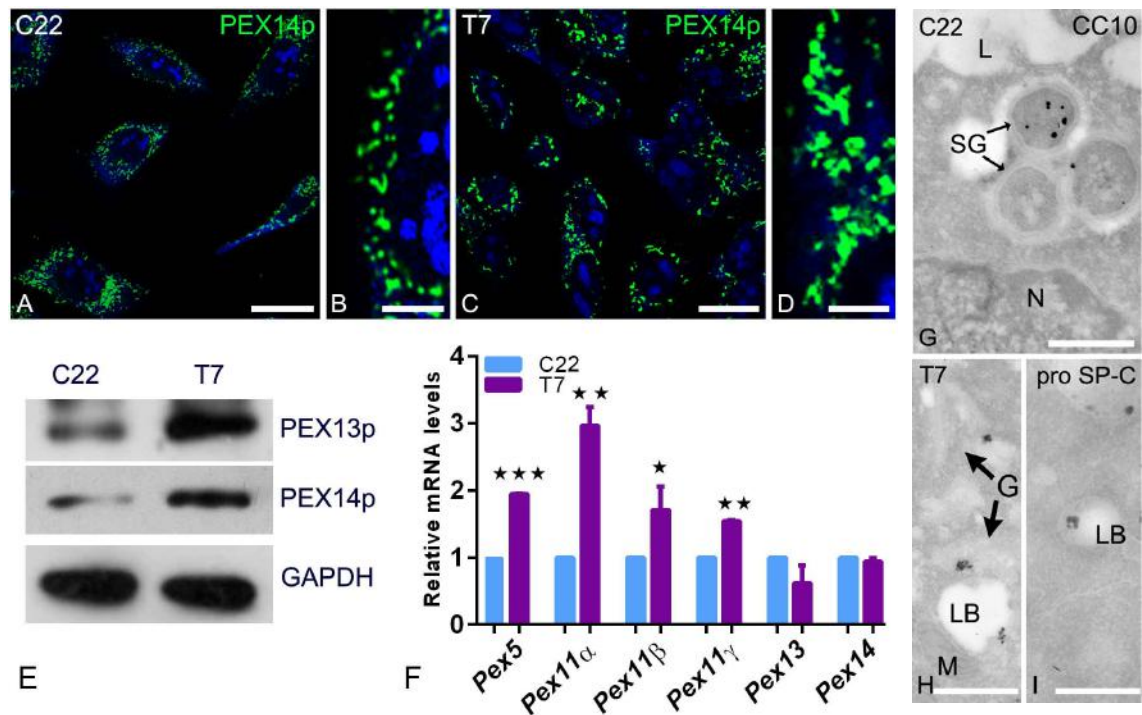


Fig. 7 Peroxisomal biogenesis protein 14 was more abundant in T7 cells than in C22 cells (A–D). The Western blot analysis of C22 and T7 cells probed with Pex13p and Pex14p (E) and qRT-PCR analyses of peroxisomal proteins involved in the proliferation of peroxisomes (F). Furthermore, the subcellular localization of club cell marker protein CC10 in secretory vesicles (G) and T7 cells marker protein, the pro SP-C protein localized to transport vesicles (H) and lamellar bodies (I) in C22 and T7 cells. Bars represent a and c: 20 μ m; b and d: 5 μ m; g, h, i: 0.3 μ m.

round peroxisomes, which also occur in the bronchiolar epithelial club cell peroxisomes, revealing that C22 peroxisomes resemble native club cell peroxisomes (Karnati and

Baumgart-Vogt, 2008; Karnati et al., 2016b). Moreover, T7 cells showed tubular peroxisomes (Fig. 7) similar to the tubular peroxisomes in AECII of the mouse lung tissue, suggesting that these cell lines resemble original AECII cells (Karnati and Baumgart-Vogt, 2008; Karnati et al., 2016b). Indeed, peroxisome shape, size, and number depend on the cell type and its metabolic activity (Baumgart et al., 2003; Issemann and Green, 1990).

In addition to the expression of peroxisomal biogenesis proteins in C22 and T7 cells, the peroxisomal proteins involved in the metabolic function were also characterized. Significant differences between the expression of peroxisomal β -oxidation enzymes in C22 and T7 cells exist. C22 cells possess the highest protein levels for ACOX1 and ACAA1 in comparison to T7 cells, whereas the lipid transporter ABCD3 involved in the transport of various lipid substrates across the peroxisomal membrane is highly expressed in T7 cells, which is in agreement with our previous observation in situ (Karnati and Baumgart-Vogt, 2008, 2009; Karnati et al., 2016b; Visser et al., 2007). The protein results were also corroborated by a significant higher mRNA expression of *Abcd3* in T7 cells, indicating that peroxisomes might play an important role in the synthesis and processing of surfactant lipids. In addition, high levels of the nonspecific lipid transfer protein/sterol carrier protein 2 (SCP2) were also described in the matrix of peroxisomes (Ossendorp et al., 1994), which shuttles the lipid intermediates within the multienzyme complex of the peroxisomal β -oxidation system (Wouters et al., 1998).

Furthermore, the mRNAs for peroxisomal β -oxidation pathway 1 enzymes, such as *Acox1* and *Acox2*, were strongly expressed in C22 cells in comparison to T7, suggesting that peroxisomes could protect the bronchiolar epithelium against pro-inflammatory eicosanoids that were secreted by activated macrophages in the bronchiolar epithelium. In this context, it is important to mention that peroxisomes are the primary intracellular site for the production of docosahexaenoic acid (DHA) and eicosapentaenoic acid (EPA), which are synthesized through the peroxisomal β -oxidation system forming the backbone for several resolution

mediators of inflammation, including resolvins, protectins, and maresins (Terlecky et al., 2012). Most importantly, patients with peroxisomal biogenesis disorders (Zellweger) showed a profound deficiency of DHA (<30% of normal levels) (Martinez, 1996; Spite and Serhan, 2010). In addition, in vitro studies suggested that peroxisomes metabolize leukotrienes (Jedlitschky et al., 1993) and prostaglandins (Diczfalusy et al., 1991) by their β -oxidation pathway, which are crucial modulators of inflammation.

Moreover, mounting evidence suggests that club cells and AECII metabolize arachidonic acid (AA) to biologically active eicosanoids (Van Scott et al., 1990), leukotrienes, and prostaglandins, which are involved in cellular signaling as lipid second messenger regulating several signaling enzymes (Sivarajah et al., 1983). Interestingly, PEX11 β -deficiency in the lung induced a high phospholipase activity, and the accumulation of AA, interfering with the feedback loop between PPAR γ and NF- κ B pathways involved in the activation of the antioxidant response and resolution of the pro-inflammatory response (Karnati et al., unpublished data). This suggests that peroxisomal metabolism might play an important role in the inflammatory diseases of the lung.

In addition to the peroxisomal β -oxidation, peroxisomes in C22 and T7 cells are also involved in the synthesis of cholesterol precursors. In fact, the early steps of cholesterol biosynthesis occur in the peroxisomes, and the later steps occur in the endoplasmic reticulum (Keller et al., 1985; Kovacs et al., 2007; Thompson and Krisans, 1990). Interestingly, the mRNAs for the early peroxisomal steps are highly abundant in C22 cells, whereas the later steps are highly expressed in T7 cells. Indeed, cholesterol is one of the important component in both alveolar and lamellar body surfactant and considered as an integral component of pulmonary surfactant (Orgeig and Daniels, 2001). Analysis of the limiting membrane of the AECII lamellar bodies (LB) revealed a high (76%) concentration of LB cholesterol (Orgeig and Daniels, 2001). Therefore, one can speculate on the involvement of peroxisomes in the alveolar cholesterol synthesis; however, so far, no experimental proof exists, and future

studies are needed to decipher the functional role of peroxisomes in the biology of alveolar cholesterol synthesis. In addition, peroxisomal ether lipid synthesizing enzymes GNPAT and AGPS revealed a clear localization in the peroxisomal compartment in both C22 and T7 cells; however, a higher abundance was observed in T7 cells. Indeed, the mRNA levels encoding these proteins were also significantly higher expressed in T7 cells (Karnati et al., 2016b), which is in agreement with the higher activity of GNPAT in total lung homogenates compared to liver (Van Veldhoven and Mannaerts, 1985). Interestingly, 40%–50% of the glycerophospholipids, which are components of the surfactant lipids, were synthesized through the peroxisomal enzymes via the acyl-DHAP pathway in 3T3 fibroblasts, suggesting that peroxisomes might play an important role in the surfactant synthesis. The peroxisomal β -oxidation system is capable of providing acetyl-CoA units for the synthesis of plasmalogens or cholesterol (Hayashi and Takahata, 1991) and is also used for the modification of polyunsaturated fatty acids, which are important components of the surfactant (Hiltunen et al., 1996).

Cholesterol and plasmalogens, minor components of the surfactant, might serve important functions in the lung. They regulate viscosity and function on surface tension (Rüdiger et al., 1998; Tölle et al., 2002), vesicle fusion, motion, and intracellular signaling (Brites et al., 2004; Gowdy and Fessler., 2012). Plasmalogens in the lung play an important role in the formation of hexagonal lipid structures that regulate the free movement of lipids out of the surface layer, whereas cholesterol stabilizes the surfactant layer. Furthermore, cholesterol is essential for the integrity of cellular membranes, maintaining membrane fluidity and membrane functions, including signal transduction. Plasmalogens generated in peroxisomes act as defensive agents by trapping the ROS under oxidative stress conditions. As mentioned in 4.3, pulmonary epithelial cells are well equipped with antioxidative enzymes that might help to protect against oxidative stress.

C22 and T7 cells harbor also a large set of antioxidative enzymes that are localized to different subcellular compartments such as perinuclear peroxisomal catalase, elongated tubular mitochondrial SOD2, and network of the endoplasmic reticulum HO-1. Interestingly, in comparison to T7 cells, C22 cells showed a higher abundance of peroxisomal antioxidative enzymes, such as PRDX1, GPX1, and SOD1, in addition to SOD2, SOD3, and TRX1, which are localized to other subcellular compartments (Karnati et al., 2016b). In contrast, T7 cells showed a higher protein abundance of the antioxidative enzymes that are localized to endoplasmic reticulum (TRX1 and HO-1), suggesting that these two enzymes might play an important role in protecting T7 cells. Redox-sensitive transcription factors, such as Nrf2, NF- κ B, and FOXO family members mediate the upregulation of antioxidative enzyme genes, such as the ones for HO-1, catalase, and SOD2 (Polvani et al., 2012). Moreover, PPAR γ , which proliferates peroxisomes, also functions as a transcription factor to upregulate various antioxidative enzymes (Polvani et al., 2012). Interestingly, PPAR γ is highly abundant in T7 cells similar to the murine AECII cells in which peroxisomes are also highly enriched as previously reported (Karnati et al., 2014; Simon et al., 2006), suggesting that activation of the PPAR γ leads to the activation of the peroxisomal compartment, which might play an important role as “protective organelles” against oxidative stress-induced lung diseases (Karnati and Baumgart-Vogt, 2008; Karnati et al., 2016b; Lakatos et al., 2007). In contrast, the PPAR γ activator 15-d-PGJ2, a prostaglandin that is degraded in peroxisomes, interferes with the redox-sensitive transcription factor pathway of NF- κ B independent of PPAR γ activation (Kim and Surh, 2006). In addition to PPAR γ , PPAR β is also higher expressed in T7 cells in comparison to C22 cells, suggesting that PPAR β might also play an important role in AECII lipid metabolism and epithelial differentiation as previously reported (Michael et al., 1997). The classic, well-known inducer of peroxisomes is PPAR α , which regulates the transcription of several peroxisomal genes, such as PEX11 α , ABCD3, and ACOX1, by binding to a PPAR-responsive element (PPRE) in their promoter regions, and is also

upregulated in T7 cells, suggesting that PPARs play an important role in the control of AECII lipid metabolism (Baumgart, 1997; Baumgart et al., 1996; Shimizu et al., 2004).

Taken together, C22 and T7 cells are excellent cell culture model systems to dissect the functional metabolic signaling of peroxisomes in club and AECII cells. Indeed, peroxisomes in club and AECII cells might play an important role as metabolic regulators in maintaining the ROS homeostasis and providing the lipid ligands for nuclear receptor activation.

4.5 PPAR-dependent peroxisome signaling as a treatment strategy for IPF

Oxidant and antioxidant imbalance in the lung leads to increased ROS levels, oxidative stress and lipid peroxidation, which is associated with various respiratory inflammatory diseases, such as asthma, IPF, adult respiratory distress syndrome, and COPD (Karnati and Baumgart-Vogt, 2008, 2009; Oruqaj et al., 2015). Recently, we showed that dysfunction of the peroxisomal compartment induced higher levels of oxidative stress in different organ systems, such as in the brain (Ahlemeyer et al., 2012) and in the lung (Karnati, 2009). Moreover, patients with Zellweger syndrome, the most severe phenotype of the peroxisomal biogenesis disorders, develop liver fibrosis and cirrhosis, leading to early death of patients during childhood (Gould and Valle, 2000; Li et al., 2002). In fact, also in milder forms of Zellweger syndrome, peroxisomal membrane ghosts or a reduced number of peroxisomes might be present, leading to the overall impairment of peroxisomal metabolic pathways and in consequence to the development of hepatic fibrosis (Steinberg et al., 2006). Due to the vast variety of antioxidative enzymes in the peroxisomal matrix and their capacity to synthesize ROS-trapping plasmalogens and PUFAs as well as their degradation potential of eicosanoids, peroxisomal alterations might contribute also to the molecular pathogenesis of IPF. Peroxisomes might play an important role in IPF, however, the functions of peroxisomes in the progression of IPF are unknown. We hypothesized that peroxisomal metabolism might be altered in the IPF patient lungs, and that peroxisome induction would attenuate the fibrotic

response, thus affecting the molecular pathogenesis of IPF. The typical markers for peroxisomes, the classical marker catalase, the most efficient anti-oxidative peroxisomal matrix enzyme and PEX14, an optimal marker for peroxisomes at the light microscopic level that stains *all* cell types of the human lung in a ubiquitous way, were used to analyze eventual differences of the peroxisomal compartment in different cell types in the lungs of IPF patients in comparison to human control lungs.

IPF patients showed a reduced number of peroxisomes in the bronchiolar region. Furthermore, catalase was strongly downregulated in fibrotic areas of IPF samples, suggesting an increase in ROS production due to impaired antioxidant response (Oruqaj et al., 2015). Similarly, isolated lung fibroblasts from these human IPF patients showed that PEX13p (binding partner of PEX14p), ACOX1, and ABCD3 (both involved in peroxisomal metabolism) were strongly reduced in IPF fibroblasts, suggesting that multiple peroxisomal functions were impaired. Furthermore, the mRNA levels of the pro-fibrotic markers (*TGF β* , *COL1A2*, and *IL-6*) were increased, and α -SMA protein abundance was increased in IPF fibroblasts in comparison to control cells. Also, the luciferase reporter assay studies using an SBE-luciferase reporter plasmid suggested that TGF β signaling was increased, confirming the pro-fibrotic phenotype of IPF cells (Oruqaj et al., 2015). In addition to catalase, other anti-oxidative enzymes of different subcellular compartments, such as SOD1, HO-1, and GR and their redox-sensitive transcription factor Nrf2 were decreased in IPF fibroblasts. Moreover, the luciferase activity for Nrf2 binding element (ARE) was significantly decreased in IPF fibroblasts, suggesting a disturbance in the antioxidant machinery of the IPF fibroblasts.

To understand the peroxisomal functions in the pathogenesis of IPF, *PEX13* was knocked down using a siRNA-mediated approach (Fig. 8). The *PEX13* deficiency in the fibroblasts triggered an increased production of the pro-fibrotic markers (*TGF β* , *COL1A2*, and *MMP2*) and proteins (COL3A1 and PDI) as well as pro-inflammatory cytokines (TNF α and IL-6) at

mRNA and protein level (Fig. 8). Furthermore, the peroxisome deficiency in the IPF fibroblasts increased TGF β 1 release into the culture medium, confirmed by increased SBE luciferase reporter activity, suggested that TGF β 1 signaling was activated. In parallel, increased collagen levels were also detected in the medium, and the *COL1A2* promoter activity was also increased in the fibroblasts with the *PEX13* deficiency. In addition, the knockdown of *PEX13* led to an increase in the production of ROS and increased ARE and AP1 promoter activity, which is in agreement with the previous studies in which dysfunction of peroxisomes in neurons led to an increased oxidative stress and elevated ROS species (Ahlemeyer et al., 2012; Baarine et al., 2012). In this respect, the protective role of peroxisomes in IPF could function in diminishing ROS, thus a possibility to prevent excessive ROS production and ROS-mediated inflammatory reactions (Cui et al., 2011; Karnati and Baumgart-Vogt, 2008; Rahman and MacNee, 2000). To counteract the increased oxidative stress, the abundance of the redox-sensitive transcription factor Nrf2 and its target antioxidant enzyme genes, such as HO1 and GR were upregulated in IPF fibroblasts. Since TGF β 1 was strongly expressed in the IPF fibroblasts in which peroxisome abundance was suppressed raised the question whether TGF β 1 signaling could regulate the metabolic functions of peroxisomes specifically by modulating the expression of the *PEX13* gene. Indeed, TGF β 1 treatment resulted in the downregulation of the *PEX13* mRNA and protein, and this effect was reversed when TGF β 1 signaling was specifically blocked using TGF β 1 receptor inhibitor (LY364947), suggesting that TGF β 1 influences peroxisomal biogenesis. The downregulation of peroxisomes in IPF, triggered by continuous biologically active TGF β 1 signaling, undermining peroxisomal matrix protein import due to the reduction of PEX13p. To translate and confirm the in vitro findings to the in vivo and in situ situation, lung mesenchyme-specific TGF β receptor II knockout mice (*Tgf β -RII KO*) were treated with bleomycin to induce fibrosis. Interestingly, bleomycin treatment in *Tgf β -RII KO* mice did not induce the downregulation of peroxisomes, in comparison to the reaction of wild type

mice, suggesting that TGF β -induced signaling *solely* drives the downregulation of peroxisomes. In addition, whereas bleomycin treatment of WT animals after 7 days showed the downregulation of peroxisomes, the abundances of peroxisomes on days 14 and 28 were recovered, indicating that the peroxisomal compartment is mainly downregulated in the

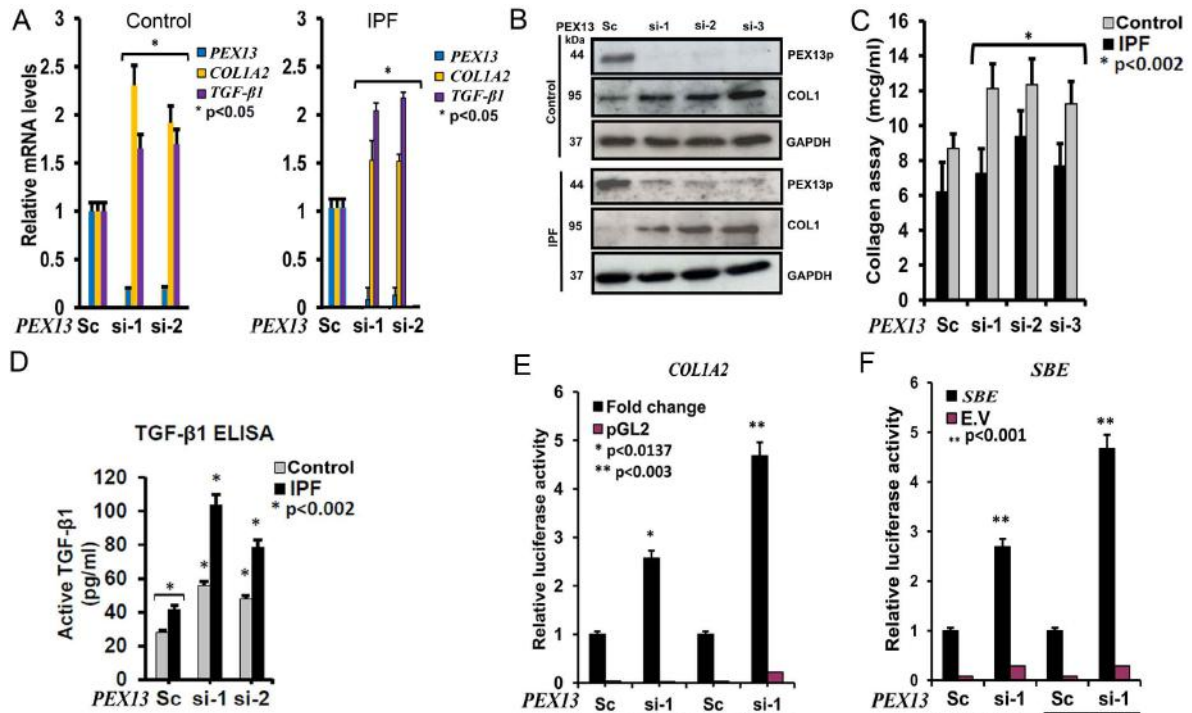


Fig. 8 *PEX13*-siRNA treated control and IPF fibroblasts exhibiting the activation of TGF β 1 signaling and its downstream genes *COL1A2* upregulation (A). Western blot analyses confirming the *PEX13* downregulation in parallel to an increase in COL1 protein abundance (B) and collagen Sircol assay confirming the collagen (C) as well as TGF β 1 (D) release in medium. SBE and *COL1A1* luciferase reporter activity in *PEX13*-siRNA treated control and IPF fibroblasts (E and F) (Oruqaj et al., 2015). Sc (scrambled siRNA control), si-1 (siRNA *PEX13*-1), si-2 (siRNA *PEX13*-2), si-3 (siRNA *PEX13* 1, 2).

inflammatory phase after bleomycin treatment and thereafter recovered again. Furthermore, TGF β -signaling via the Smad3 pathway was analyzed by using *PEX13* siRNA cell culture model. Interestingly, peroxisomal proteins were strongly upregulated in *Smad3* knockout mice, indicating a suppressive effect of TGF β signaling on peroxisomal metabolism (Orugaj, 2015). Consistent with these findings, *TgfbfRI* constitutively active mice (*TgfbfRI*^{CA}) inducing continuous TGF β signaling exhibited a reduced abundance of the

peroxisomes (Orugaj, 2015). In fact, this is the first study showing the direct role of TGF β 1 signaling in the regulation of peroxisomal genes possibly by interacting with downstream transcription factors of TGF β -signaling, such as Smad3 or Smad4 (Oruqaj et al., 2015).

Since, deletion of PEX13p increased pro-fibrotic and pro-inflammatory markers as well as induced AP1 and ARE promoter activities raises the question whether AP1 might be involved in the TGF β 1-mediated PEX13 downregulation. Indeed, TGF β 1 induced the activity of the AP1 reporter activity but not the ARE activity. Similarly, AP1-specific inhibitor SR11302 blocked the TGF β 1-mediated SBE activation and also the AP1 and the ARE-luciferase construct, indicating a role for AP1 in the TGF β 1-mediated, Smad-dependent pathway, which is in agreement with a study of Junn and colleagues in which AP1 triggered TGF β 1-signaling (Junn et al., 2000). However, Verrecchia and colleagues proposed that AP1 inhibits Smad-dependent signaling (Verrecchia et al., 2001). In fact, a cross talk exists in between TGF β 1 signaling and AP1 since the majority of research in this area is contradictory, AP1 is considered both profibrotic and antifibrotic (Rajasekaran et al., 2012; Roy et al., 2010). Therefore, further studies are necessary to illustrate the correct molecular mechanism. Finally, pretreatment with the AP-1 inhibitor SR11302 reversed the TGF β 1-mediated downregulation of the PEX13p protein, suggesting that the TGF β 1-induced downregulation of PEX13 is mediated through the transcription factor AP1.

The etiology of IPF is incompletely understood since multiple factors are associated in the pathogenesis of IPF. In addition to TGF β signaling, another cytokine TNF α , which has been widely shown in downregulating the peroxisomes, might also contribute to the downregulation of peroxisomes in IPF (Beier et al., 1997). Indeed, TNF α induced a significant downregulation of the *PEX13* mRNA and protein as well as increased AP1 luciferase activity. Indeed, *Tnfa*-knockout mice exhibited less liver fibrosis and reduced levels of fibrotic markers, suggesting that TNF α is crucial in initiation and progression of the

fibrosis (Gabele et al., 2009). In Swiss 3T3 fibroblasts, TNF α played an important role in the fibrogenesis together with AP1 signaling (Sullivan et al., 2009; Verjee et al., 2013). Furthermore, the AP1 inhibitor SR11302 reversed the TNF α -mediated downregulation of PEX13p, suggesting that downregulation of PEX13p is partially mediated through AP1 signalling. In addition to TNF α , another pro-inflammatory and pro-fibrotic cytokine IL-6 also induced the downregulation of PEX13p. In this respect, it is important to mention that IL-6 mediates pro-inflammatory processes and plays an important role in the pathogenesis of several respiratory disorders, including fibrosis (Pantelidis et al., 2001; Qiu et al., 2004).

In line with the notion, Saito and colleagues reported that IL-6 plays an important role in the pathogenesis of bleomycin-induced lung injury and subsequent fibrotic changes through the TGF β 1 signaling (Saito et al., 2008). The above-mentioned results summarize the fact that reduced peroxisome biogenesis is associated with an increased pro-fibrotic response via TGF β 1 signaling. Therefore, increasing peroxisome content and its metabolic functions in IPF could block the fibrotic effects, which would possibly be a good therapeutic strategy to treat the IPF patients. Therefore, the classical peroxisome proliferators, PPAR α agonists, such as ciprofibrate or WY14643, were used to treat IPF fibroblasts to check whether the peroxisome proliferation could block the TGF β 1-induced profibrotic signaling. However, PPAR α exerts multiple effects on cell fate is involved in different signaling pathways. To exclude other PPAR α effects that are not associated with peroxisome proliferation, thereby ascertaining the peroxisome-dependent, anti-fibrotic effects of PPAR α agonists, correct experimental strategies are required. Therefore, IPF cells were either first treated with PPAR α agonists for 48 hours to proliferate peroxisomes and thereafter with the PPAR α antagonist to block endogenous PPAR α activation or pretreatment with the PPAR α agonists only for 2 hours prior to TGF β 1 stimulation so that PPAR α is activated but peroxisomes are not proliferated. Interestingly, treatment with ciprofibrate or WY14643 for 48 hours showed a significant reduction in the TGF β 1-induced myofibroblast differentiation, whereas

pretreatment for 2 hours prior to TGFβ1 stimulation did not block the TGFβ1-induced myofibroblast differentiation, suggesting that peroxisome proliferation could inhibit the TGFβ1-induced profibrotic response and PPAR activity might interfere with this mechanism. In line with our notion, in fact, several other studies also support the properties of PPARα as a antifibrotic and anti-inflammatory agent since PPARα agonists (1) inhibited the cardiac fibrosis by inhibiting the proliferation of fibroblasts (Ogata et al., 2002), (2) reduced the bleomycin-induced lung injury (Genovese et al., 2005), and (3) inhibited TGFβ signaling in

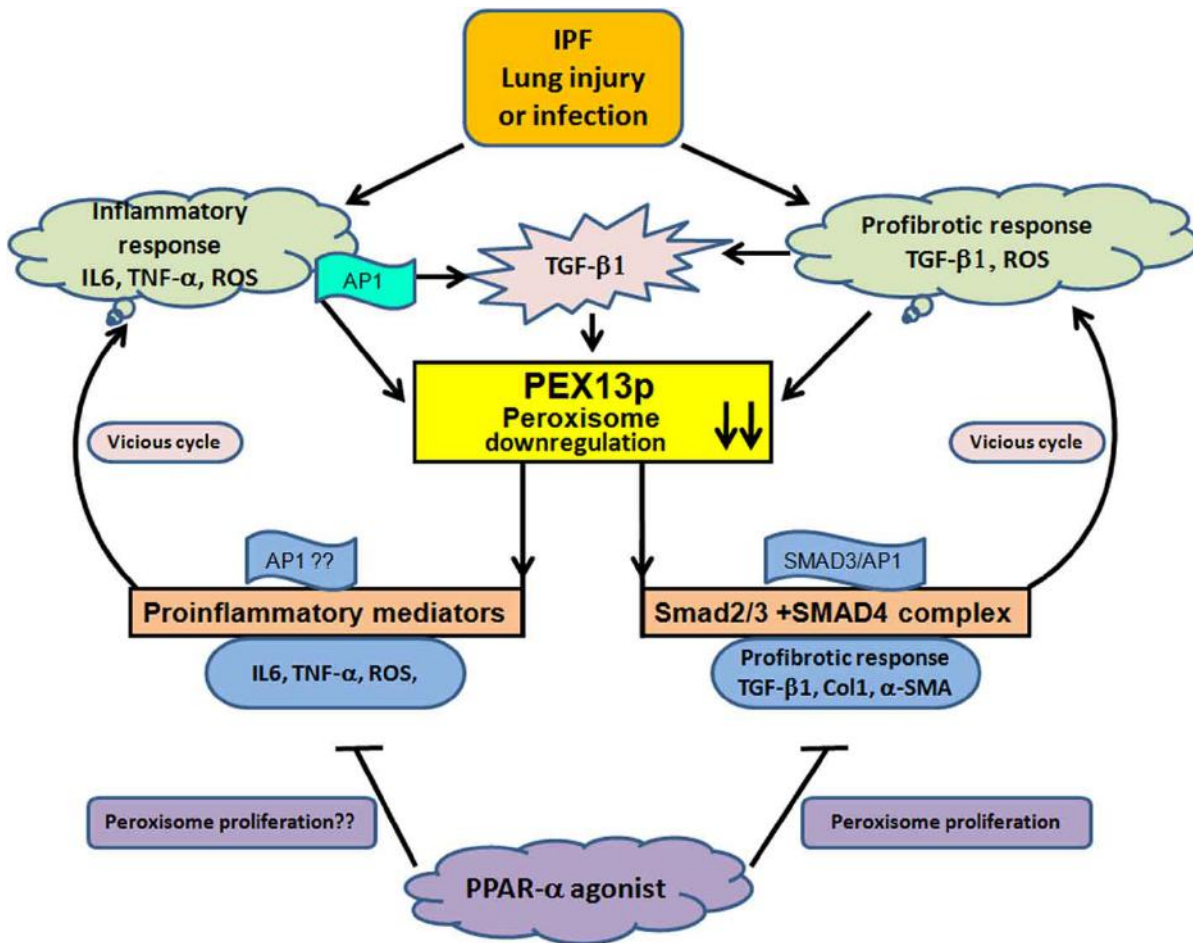


Fig. 9 Proposed model of TGFβ1-mediated signaling on peroxisome function in IPF (Oruqaj et al., 2015).

vascular smooth muscle cells (Kintscher et al., 2002). Although the results are promising, there is a technical limitation since PPAR agonists are classically used to induce peroxisome proliferation and exhibit pleotropic anti-inflammatory effects, such as inhibition of NF-kB

and AP1 signaling pathways, which leads to the suppression of various pro-inflammatory genes (Rigamonti et al., 2008).

The involvement of peroxisomes in the molecular pathogenesis of IPF is summarized in Fig. 9. Lung injury or infection triggers the release of pro-inflammatory mediators (TNF- α , ROS, and IL-6) in IPF, thereby activating pro-fibrogenic TGF β 1 and AP1 signaling. This leads to downregulation of peroxisomes, which, in turn, induces more ROS, promotes secretion of cytokines, such as IL-6, and triggers the activation of TGF β 1 and AP1 signaling in a vicious cycle, thus enabling the persistence of a fibrotic phenotype and inflammatory exacerbation phases in IPF patients. In addition, this vicious cycle also leads to increased production of collagen. In contrast, treatment with Ppar- α agonists induces the proliferation of peroxisomes, inhibiting the pro-fibrogenic mechanisms, such as myofibroblast differentiation and collagen release (Fig. 9). In summary, we identified a functionally relevant cellular mechanism in which modulating the peroxisomal compartment can offer a good possible therapeutic approach for IPF patients.

4.6 PPARs and their role in preventing the idiopathic pulmonary fibrosis

Indeed, bleomycin-treated PPAR α knockout mice showed a more severe inflammation and fibrosis development than wild-type mice (Crisafulli and Cuzzocrea, 2009). In addition, bleomycin-treated *PPAR α* knockout mice exhibited higher levels of TNF α , whereas treatment of mice with the PPAR α agonist WY-14643 significantly reduced inflammation and fibrosis progression, suggesting the importance of PPAR α role in the prevention of pulmonary fibrosis (Bowden, 1984; Crisafulli and Cuzzocrea, 2009).

In addition to PPAR α , PPAR γ plays also an important role in inflammation and wound healing processes and functions as an antifibrotic agent (Belvisi et al., 2004, 2006; Moras and Gronemeyer, 1998; Oruqaj et al., 2015). Several studies support the notion that PPAR γ promotes differentiation of lung fibroblasts into fat storing lipofibroblasts and inhibits the

critical differentiation of fibroblasts into myofibroblasts (Lakatos et al., 2007). Furthermore, PPAR γ agonists exhibited a reduced histological fibrosis with reduced α SMA expression, decreased inflammation, reduced collagen (Boateng et al., 2016; Lakatos et al., 2007), suppressed fibroblast profibrotic activities (Milam et al., 2008), and inhibited myofibroblast proliferation (Milam et al., 2008). Moreover, Burgess and colleagues suggested that PPAR γ agonists can control TGF β 1-mediated profibrotic effects and reverse primary human pulmonary myofibroblast differentiation and collagen production (Burgess et al., 2005). Another study by Milam and colleagues demonstrated that treatment of lung fibroblasts in culture with PPAR γ agonists, troglitazone and ciglitazone, and in vivo administration of troglitazone to bleomycin-treated mice inhibited TGF β 1-induced myofibroblast differentiation and collagen secretion in the lung (Boateng et al., 2016; Milam et al., 2008). In this respect, it is important to mention that rosiglitazone, a PPAR γ agonist, inhibits lung fibroblast migration and proliferation and myofibroblast transdifferentiation, confirmed by the downregulation of α SMA (Lin et al.). Moreover, upregulation of “phosphatase and tensin homologue deleted on chromosome 10” (PTEN) containing a PPRE element in its promoter, inhibited the fibroblast differentiation into myofibroblasts, and reduced the expression of α SMA in human and mouse fibroblasts (Barraya and Chauvin, 1971; Lakatos et al., 2007), suggesting that PPAR γ can be a therapeutic agent against the progression of IPF. Unfortunately, clinical trials of PPAR γ agonists as a therapeutic agent for fibrosis did not yield conclusive beneficial results, which might be explained by vastly diverse experimental approaches used to assess the efficacy of the treatment (Boateng et al., 2016; Kulkarni et al., 2012).

Much of the knowledge in understanding the pathogenesis of IPF is derived by PPAR α and PPAR γ . Many of these studies were often limited to analyse the inhibition of fibroblast to myofibroblast conversion using PPAR agonists. Indeed, histological analysis of fibrotic foci of IPF patients revealed a mixed population of fibroblasts and myofibroblasts (Scotton and

Chambers, 2007). However, the molecular effects of PPAR γ agonists on already differentiated myofibroblasts or TGF- β 1-stimulated fibroblasts were not addressed at all, which would best simulate the situation in IPF patients (Boateng et al., 2016). Furthermore, additional in vitro and in vivo experimental models are necessary to understand the role of PPAR γ ligands on ECM deposition and reversal of the progressive fibrotic phenotype after TGF β 1 stimulation, which might shed more light on the potentials of PPAR γ agonists as novel therapeutic agents for the treatment of fibrotic lung diseases. The best strategy to evaluate which PPAR-member is mediating antifibrotic effects would be to use the appropriate knockout models and challenge them with bleomycin-treatment as lung fibrosis model. An alternative approach for IPF treatment would also be to search for a PPAR-independent, specific inducer of peroxisomes to explore the complete potential of these organelles in protection against fibrotic or inflammatory lung diseases.

4.7 PPAR-independent peroxisome signaling in chronic inflammatory lung disorders

In addition to PPAR-agonists, 4-phenylbutyrate (4-PBA), a nonclassical peroxisome proliferator induces peroxisome proliferation, which is not mediated by PPAR α signaling (Li et al., 2002). This drug was used by our group to stimulate peroxisomes and thereby regulate the macrophage inflammatory response (e.g. in alveolar macrophages) (Vijayan et al., 2017). The induction of peroxisomes by 4-PBA in murine alveolar macrophages leads to a suppression of pro-inflammatory cytokines (TNF α , IL-6, and IL-12) after stimulation by LPS, which is independent of ER stress, suggesting that peroxisomes in alveolar macrophages play an important role in the inhibition of bacterial LPS-induced, pro-inflammatory response (Vijayan et al., 2017). Conversely, knockdown of 1) the *Pex14* gene encoding a peroxisome biogenesis protein in the membrane docking complex, or 2) the *Mfp2* gene, encoding the peroxisomal multifunctional enzyme in the β -oxidation pathway 2, in macrophages exerted an

induction of pro-inflammatory proteins, such as TNF α and COX2, indicating the existence of an intrinsic peroxisome-mediated regulation of pro-inflammatory effects in macrophages (Vijayan et al., 2017). In agreement to our observations, Kim and colleagues showed that 4-PBA treatment blocked the LPS-induced, pro-inflammatory cytokines TNF α and IL-6 in an in vivo mouse model of lung inflammation (Kim et al., 2013). Indeed, COX2 is an inducible form of the prostaglandin synthase, which is crucial for promoting inflammation via production of pro-inflammatory prostaglandins in LPS-induced lung inflammation (Seibert et al., 1997).

To dissect further peroxisome-mediated, anti-inflammatory regulatory mechanisms, LPS-activated, conditional medium of cell cultures of 4-PBA-treated macrophages was analyzed by LC-MS/MS. Strikingly, a dramatic increase of free arachidonic acid, PGJ2, and DHA was observed in the 4-PBA treated macrophages-conditioned medium (Vijayan et al., 2017). Interestingly, PGJ2 is anti-inflammatory (Hilliard et al., 2010) in nature and DHA, which is synthesized in the peroxisomes, is the precursor of many lipid resolution mediators, such as resolvins, maresins, and protectins. Moreover, treatment of macrophages with DHA showed a significant reduction of LPS-induced pro-inflammatory proteins (Kim et al., 2013). Taken together, induction of peroxisomes in macrophages provides an anti-inflammatory phenotype, and 4-PBA-mediated peroxisome proliferation might be a beneficial therapeutic intervention in chronic inflammatory disorders of the lung.

5 Summary

The well-studied pulmonary cell types of the lung are club cells, AECII, fibroblasts, and alveolar macrophages. Therefore, in this study, peroxisomal functions were mainly investigated in these cell types, and their possible functional roles in chronic lung diseases were summarized.

The morphological and functional postnatal differentiation of club cells in the mouse postnatal developmental stages (newborn, P15, and adult lung) by quantitative stereological analyses showed that 64% of the volume of bronchiolar epithelial cells from adult mice of C57BL/6J strain lining the distal airways were club cells (**Karnati et al., 2016a**). Furthermore, morphometric analysis demonstrated a significant increase in the number of club cells and volume of secretory granules within 15 days after birth, suggesting that the club cell is not a matured, rather fully differentiated cell, at birth, and maturation occurs postnatally (Karnati et al., 2016a). This investigation suggests that mice are excellent animal models to study the factors controlling club cell differentiation and the role of peroxisomes in the pathogenesis of pulmonary diseases (**Karnati et al., 2016a**).

The distribution and enzymatic composition of peroxisomal proteins in epithelial cells of the distinct lung developmental stages suggested that peroxisomal antioxidative enzymes might protect the pulmonary epithelium since higher abundance of peroxisomal proteins was detected in bronchiolar (ciliated cells, club cells), alveolar (AECII), and macrophages of the lung (**Karnati and Baumgart-Vogt., 2008, 2009**). Since peroxisomes harbor several antioxidative enzymes, therefore SOD2 was also considered to be a peroxisomal protein in addition to mitochondria (Singh et al., 1999). However, we showed that SOD2 was never present in peroxisomes and SOD2 is a pure mitochondrial protein (**Karnati et al., 2013**).

Indeed, club and AECII cells are very difficult to maintain in primary culture. Therefore, C22-club and T7-AECII cell cultures were established and we characterized the peroxisomal compartment and its associated metabolic signaling pathways therein (**Karnati et al., 2016b**). Peroxisomes in club cells and AECII play an important role in the regulation of ROS levels and nuclear receptors, suggesting that the C22- and T7-cell lines of the immortomouse lung are useful models to study the regulation and metabolic function of the peroxisomal

compartment and its alterations by paracrine factors in club cells and AECII (**Karnati et al., 2016b**).

IPF is a chronic, devastating disease, and its pathogenic mechanisms remain incompletely understood. By using human IPF and control fibroblast cultures as well as the bleomycin-induced mouse lung fibrosis model, we showed that the peroxisomal compartment is severely affected and compromised in IPF, mediated by TGF β 1 and AP1 signaling and the action of pro-inflammatory cytokines (TNF α and IL-6) (**Oruqaj et al., 2015**). Further, treatment of fibroblasts with ciprofibrate or WY14643, PPAR- α activators, induced peroxisome proliferation and reduced the TGF β -induced myofibroblast differentiation in IPF (**Oruqaj et al., 2015**). Furthermore, new experimental strategies were discussed to the role of PPAR γ ligands as novel therapeutic agents for the treatment of fibrotic lung diseases (**Boateng et al., 2016**).

We identified a new role of PPAR-independent signaling on peroxisomes in regulating the macrophage inflammatory response activated by the TLR-4 ligand LPS (**Vijayan et al., 2017**). 4-PBA, a PPAR-independent peroxisome proliferator, induced peroxisome proliferation in murine alveolar macrophages and suppressed pro-inflammatory cytokine release after stimulation by LPS, suggesting that peroxisomes in alveolar macrophages play an important role in the inhibition of LPS-induced pro-inflammatory response. Therefore, 4-PBA-mediated peroxisome proliferation might be a beneficial therapeutic intervention in chronic inflammatory disorders (**Vijayan et al., 2017**). In summary, this habilitation thesis suggests an important role of peroxisomes 1) in the differentiation process of the lung (**Karnati and Baumgart-Vogt., 2009**), (2) in the protective role against high oxygen concentration and oxidative stress by metabolizing ROS, and (3) in the pulmonary lipid metabolism with induction of the peroxisomal β -oxidation of eicosanoids and thus inhibition of the inflammatory cascade (**Vijayan et al., 2017**). Finally, the modulation of the peroxisome compartment might be a good future treatment option for patients with IPF or chronic inflammatory diseases.

6 Zusammenfassung

Die am besten untersuchten Zelltypen der Lunge sind Klubzellen, Pneumozyten Typ II, Fibroblasten und Alveolarmakrophagen. Daher untersuchte die vorliegende Studie hauptsächlich peroxisomale Funktionen in diesen Zelltypen und fasste ihre möglichen funktionellen Rollen bei chronischen Lungenerkrankungen zusammen. Die morphologische und funktionelle postnatale Differenzierung von Klubzellen in den postnatalen Entwicklungsstadien der Maus (Neugeborene, P15 und adulte Lunge) mittels quantitativer stereologischer Analyse ergab, dass 64% des Volumens der bronchiolären Epithelzellen, die die distalen Atemwege auskleideten, Klubzellen waren (**Karnati et al., 2016a**). Darüber hinaus zeigte die morphometrische Analyse innerhalb von 15 Tagen nach der Geburt einen signifikanten Anstieg der Anzahl der Zellen und des Volumens der sekretorischen Granula, was darauf hinweist, dass die Zellen bei der Geburt bereits ausdifferenziert sind und dass deren weitere Ausreifung jedoch postnatal stattfindet (**Karnati et al., 2016a**). Das Mausmodell erwies sich als hervorragend geeignet, um verschiedene Faktoren zu untersuchen, die die Differenzierung von Klubzellen und die Rolle von Peroxisomen bei der Pathogenese von verschiedenen Lungenerkrankungen betreffen (**Karnati et al., 2016a**).

Die Verteilung und enzymatische Zusammensetzung von peroxisomalen Proteinen in den Epithelzellen der verschiedenen Lungenentwicklungsstadien legt nahe, dass peroxisomale antioxidative Enzyme des Lungenepithels sowohl in Bronchiolarzellen (Zilien tragende Zellen, Klubzellen), Pneumozyten Typ II (AECII) und Makrophagen der Lunge vorkommen (**Karnati und Baumgart-Vogt., 2008, 2009**). Da Peroxisomen mehrere antioxidative Enzyme enthalten, wurde traditionell SOD2 neben dem typischen Vorkommen in Mitochondrien (Singh et al., 2002) auch als peroxisomales Protein postuliert. Wir haben jedoch gezeigt, dass SOD2 niemals in Peroxisomen vorhanden ist und somit ein reines mitochondriales Protein ist (**Karnati et al., 2013**). Allerdings sind Klub- und Pneumozyten Typ II in der Primärkultur sehr schwierig dauerhaft zu kultivieren. Daher wurden C22-Klub und T7-AECII-Zellkulturen etabliert und nachfolgend das peroxisomale Kompartiment und seine assoziierten metabolischen Signalwege charakterisiert (**Karnati et al., 2016b**). Peroxisomen in Klub- und Pneumozyten Typ II-Zellen spielen eine wichtige Rolle bei der Regulierung von ROS-Spiegeln und nukleären Rezeptoren der PPAR-Familie, was nahe legt, dass die C22- und T7-Zelllinien der Immortomouse-Lunge nützliche Modelle sind, um Regulation und metabolische Funktion des peroxisomalen Kompartiments und seine

Veränderungen durch parakrine Faktoren in Klubzellen und Pneumozyten Typ II zu untersuchen (**Karnati et al., 2016b**).

Die idiopathische pulmonale Fibrose (IPF) ist eine chronische, stark destruierende Lungenerkrankung. Dennoch sind die pathogenen Mechanismen weitgehend unverstanden. Unter Verwendung von menschlichen IPF- und Kontroll-Fibroblastenkulturen sowie dem Bleomycin-induzierten Maus-Lungenfibrose-Modell zeigten wir, dass das peroxisomale Kompartiment bei IPF stark beeinflusst und beeinträchtigt ist. Dies wird im Wesentlichen durch TGF β 1- und AP1-Signalwege und nachfolgende proinflammatorische Zytokinkaskaden (TNF α ; IL-6) vermittelt (**Oruqaj et al., 2015**). Weiterhin induzierte die Behandlung von Fibroblasten mit Ciprofibrat oder WY14643 die Peroxisomenproliferation und reduzierte die TGF β -induzierte Myofibroblasten-Differenzierung in IPF (**Oruqaj et al., 2015**). Darüber hinaus wurden neue experimentelle Strategien zur Rolle von PPAR γ -Liganden als innovative Therapeutika zur Behandlung von fibrotischen Lungenerkrankungen evaluiert (**Boateng et al., 2016**).

Weiterhin identifizierten wir eine neue Rolle der PPAR-unabhängigen Signaltransduktion auf Peroxisomen bei der Regulierung der Entzündungsreaktion in Makrophagen-, die durch den TLR-4-Liganden LPS aktiviert wird (**Vijayan et al., 2017**). 4-PBA, ein PPAR-unabhängiger Peroxisomproliferator, induzierte die Peroxisomenproliferation in murinen Alveolarmakrophagen und unterdrückte die proinflammatorische Zytokinfreisetzung nach Stimulation durch LPS, was darauf hindeutet, dass Peroxisomen in alveolären Makrophagen eine wichtige Rolle bei der Hemmung der LPS-induzierten proinflammatorischen Antwort spielen. Die 4-PBA-vermittelte Peroxisomenproliferation könnte eine sinnvolle therapeutische Intervention bei chronisch entzündlichen Lungenerkrankungen sein (**Vijayan et al., 2017**). Zusammenfassend legt diese Habilitationsschrift eine wichtige Rolle von Peroxisomen 1) im Differenzierungsprozess der Lunge (**Karnati und Baumgart-Vogt, 2009**), (2) in der protektiven Rolle gegenüber oxidativem Stress durch Metabolisierung reaktiver radikaler Sauerstoffspezies, und (3) im pulmonalen Lipidstoffwechsel mit Induktion der peroxisomalen β -Oxidation von Eicosanoiden und somit Inhibition der Inflammationskaskade (**Vijayan et al., 2017**), dar. Schließlich ergibt sich durch die Modulierung des Peroxisomenkompartiments eine vielversprechende zukünftige Behandlungsoption für Patienten mit IPF oder chronisch entzündlichen Erkrankungen.

7 Outlook

Compartmentalization of peroxisomal membrane proteins by super-resolution microscopy

PEX14 is an excellent marker protein for the localization of peroxisomes in stainings with excellent monospecific antibodies in large variety of different organs of various species at the light microscopic level (Grant et al., 2013). With our best anti-PEX14p-antibodies, we detected severe morphological alterations of peroxisomes under different pathological conditions (El-Merhie et al., 2017; Oruqaj et al., 2015). Moreover, we showed an excellent labelling and identification of peroxisomes in different cell types of mouse and human lung tissue sections (Karnati and Baumgart-Vogt, 2008, 2009). Likewise, the C22 (club)- and T7 (AECII)- cells in culture also exhibited a highly differentiated and abundant peroxisomal compartment, comparable to in situ results in the lung. Interestingly, PEX13p and PEX14p labelling in C22- and T7- cells often revealed elongated tubular peroxisomes with sometimes complex network-like structures specifically in the differentiation state of C22- and T7- cells (Karnati et al., manuscript under preparation). These network-elongated structures were quite difficult to resolve also by using electron microscopy since peroxisome membrane-specific antibodies, such as anti-PEX13p and anti-PEX14p, are integral membrane proteins with only few PEX14p few-positive antigens on the section surface in post-embedding electron microscopy. Therefore, to date no structural information and distribution patterns are available on these membrane proteins in individual peroxisomal profiles which are indeed complex challenging objects for microscopy. Moreover, the diameter of peroxisomes is close to the spatial resolution limit of conventional light microscopy; therefore, super-resolution microscopy for imaging of the subperoxisomal protein distribution is necessary. To

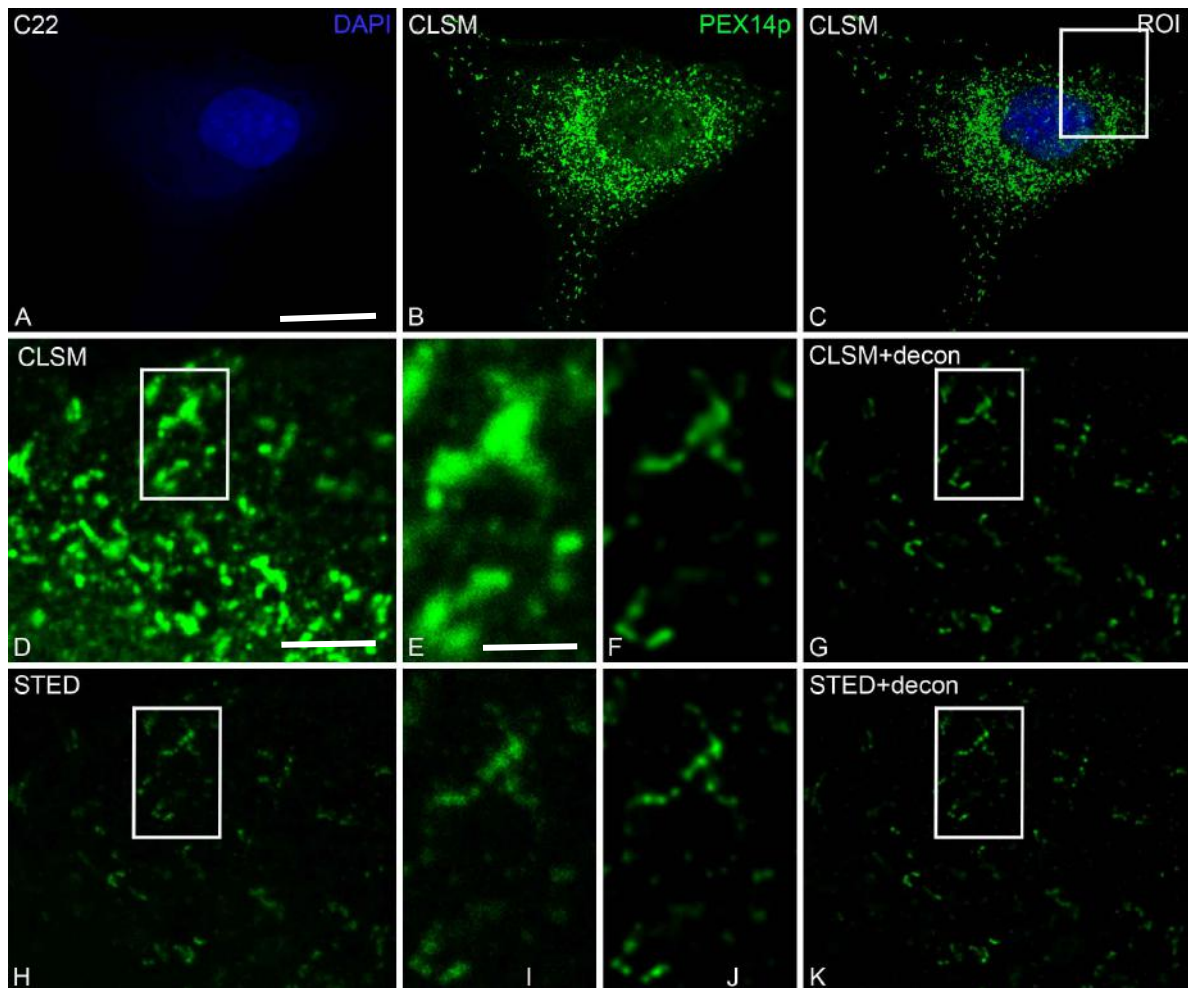


Fig.10 C22 cells were stained for PEX14p (b) and imaged with CLSM and STED followed by deconvolution. Regions of interest of CLSM image (C) are shown with low magnification (D), high magnification (E), deconvoluted CLSM low magnification (G) and high magnification (F). The same regions of interest were subjected to STED imaging with low magnification (H), high magnification (I), deconvoluted STED low magnification (K) and high magnification (J). Bars represent: a-c: 15 μm ; d, g, h, k: 5 μm ; e, f, i, j: 1 μm .

address the peroxisome-membrane dynamics and its organization, super-resolution microscopic techniques, such as SIM and STED followed by deconvolution, were applied to dissect peroxisomal biogenesis protein distribution in lung epithelial cells. ELYRA Zeiss (2-D and 3-D SIM, ZEN black, segmentation protocols designed for quantification) and Leica SP8 for CLSM, STED in collaboration with the University College of London (UCL), MRC-laboratory of London generated novel data aiming to quantify the number of PEX13p and PEX14p proteins on the peroxisomal membrane and to address whether the length, size, and

shape of the peroxisomes correlate the structural distribution patterns of PEX13p and PEX14p. Indeed, this is the first innovative report of structural organization and distribution of PEX13p and PEX14p on the membrane of lung peroxisomes providing a comparison of high-resolution laser-scanning confocal microscopy (CLSM), super-resolution structured illumination microscopy (SIM), and stimulated emission depletion microscopy (STED) to

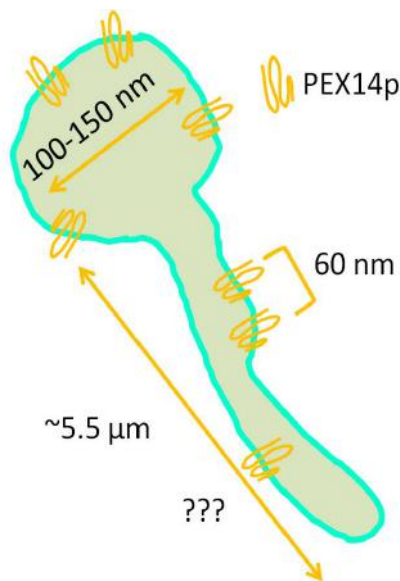


Fig.11 Proposed model of PEX14p distribution on the peroxisomal membrane.

obtain better insight into the structure of peroxisomes in C22 and T7 cells. Deconvoluted CLSM, STED, and SR-SIM images were analyzed using a segmentation and measurement workflow in Icy software. We conclude that with STED microscopy, we could achieve 60 nm resolutions in the focal plane, and our findings suggest that PEX13p and PEX14p are unevenly distributed exhibiting different labelling intensities on the peroxisomal membrane.

Srikanth **Karnati**¹, Kathrin M. Scherer², Eveline Baumgart-Vogt¹ Super resolution microscopy of peroxisomes (2019) *Scientific Reports* in preparation (IF: 4.122)

¹Institute for Anatomy and Cell Biology II, Division of Medical Cell Biology, Justus Liebig University, Giessen, Germany ²MRC Laboratory for Molecular Cell Biology, University College London, Gower Street London, WC1E 6BT, London, UK.

8 References

- Abdelraheim SR, Spiller DG, McLennan AG (2003) Mammalian NADH diphosphatases of the Nudix family: cloning and characterization of the human peroxisomal NUDT12 protein. *Biochem J* 374:329-335
- Ahlemeyer B, Gottwald M, Baumgart-Vogt E (2012) Deletion of a single allele of the Pex11beta gene is sufficient to cause oxidative stress, delayed differentiation and neuronal death in mouse brain. *Dis Model Mech* 5:125-140
- Akashi M, Takagi S, Hachiya M (1996) Anti-cancer agent OK432 induces manganese superoxide dismutase in human granulocytes. *Int J Cancer* 68:384-390
- Antonenkov VD, Grunau S, Ohlmeier S, Hiltunen JK (2009) Peroxisomes are oxidative organelles. *Antioxid Redox Signal* 13:525-537
- Antonenkov VD, Hiltunen JK (2006) Peroxisomal membrane permeability and solute transfer. *Biochim Biophys Acta* 1763:1697-1706
- Auten RL, Watkins RH, Shapiro DL, Horowitz S (1990) Surfactant apoprotein A (SP-A) is synthesized in airway cells. *Am J Respir Cell Mol Biol* 3:491-496
- Avouac J, Palumbo K, Tomcik M, Zerr P, Dees C, Horn A, Maurer B, Akhmetshina A, Beyer C, Sadowski A, Schneider H, Shiozawa S, Distler O, Schett G, Allanore Y, Distler JH (2012) Inhibition of activator protein 1 signaling abrogates transforming growth factor beta-mediated activation of fibroblasts and prevents experimental fibrosis. *Arthritis Rheum* 64:1642-1652
- Baarine M, Androletti P, Athias A, Nury T, Zarrouk A, Ragot K, Vejux A, Riedinger JM, Kattan Z, Bessede G, Trompier D, Savary S, Cherkaoui-Malki M, Lizard G (2012) Evidence of oxidative stress in very long chain fatty acid--treated oligodendrocytes and potentialization of ROS production using RNA interference-directed knockdown of ABCD1 and ACOX1 peroxisomal proteins. *Neuroscience* 213:1-18
- Bal HS, Ghoshal NG (1988) Morphology of the terminal bronchiolar region of common laboratory mammals. *Lab Anim* 22:76-82
- Bargagli E, Olivieri C, Bennett D, Prasse A, Muller-Quernheim J, Rottoli P (2009) Oxidative stress in the pathogenesis of diffuse lung diseases: a review. *Respir Med* 103:1245-1256
- Barish GD (2006) Peroxisome proliferator-activated receptors and liver X receptors in atherosclerosis and immunity. *J Nutr* 136:690-694
- Barraya L, Chauvin P (1971) [Cure of hiatal hernia with pillar suture in front of the esophagus. Renewal of interest in the abdominal approach]. *Ann Chir* 25:553-560
- Baskerville A (1970) Ultrastructural studies of the normal pulmonary tissue of the pig. *Res Vet Sci* 11:150-155
- Baumgart E (1997) Application of in situ hybridization, cytochemical and immunocytochemical techniques for the investigation of peroxisomes. A review including novel data. Robert Feulgen Prize Lecture 1997. *Histochem Cell Biol* 108:185-210
- Baumgart E, Fahimi HD, Steininger H, Grabenbauer M (2003) A review of morphological techniques for detection of peroxisomal (and mitochondrial) proteins and their corresponding mRNAs during ontogenesis in mice: application to the PEX5-knockout mouse with Zellweger syndrome. *Microsc Res Tech* 61:121-138
- Baumgart E, Vanhooren JC, Fransen M, Marynen P, Puype M, Vandekerckhove J, Leunissen JA, Fahimi HD, Mannaerts GP, van Veldhoven PP (1996) Molecular characterization of the

References

- human peroxisomal branched-chain acyl-CoA oxidase: cDNA cloning, chromosomal assignment, tissue distribution, and evidence for the absence of the protein in Zellweger syndrome. *Proc Natl Acad Sci U S A* 93:13748-13753
- Baumgart E, Vanhorebeek I, Grabenbauer M, Borgers M, Declercq PE, Fahimi HD, Baes M (2001) Mitochondrial alterations caused by defective peroxisomal biogenesis in a mouse model for Zellweger syndrome (PEX5 knockout mouse). *Am J Pathol* 159:1477-1494
- Bedetti CD, Singh J, Singh G, Katyal SL, Wong-Chong ML (1987) Ultrastructural localization of rat Clara cell 10 KD secretory protein by the immunogold technique using polyclonal and monoclonal antibodies. *J Histochem Cytochem* 35:789-794
- Beier K, Fahimi HD (1991) Environmental pollution by common chemicals and peroxisome proliferation: efficient detection by cytochemistry and automatic image analysis. *Prog Histochem Cytochem* 23:150-163
- Beier K, Volkl A, Fahimi HD (1997) TNF-alpha downregulates the peroxisome proliferator activated receptor-alpha and the mRNAs encoding peroxisomal proteins in rat liver. *FEBS Lett* 412:385-387
- Belinsky SA, Lechner JF, Johnson NF (1995) An improved method for the isolation of type II and Clara cells from mice. *In Vitro Cell Dev Biol Anim* 31:361-366
- Belvisi MG, Hele DJ, Birrell MA (2004) New advances and potential therapies for the treatment of asthma. *BioDrugs* 18:211-223
- Belvisi MG, Hele DJ, Birrell MA (2006) Peroxisome proliferator-activated receptor gamma agonists as therapy for chronic airway inflammation. *Eur J Pharmacol* 533:101-109
- Benayoun L, Letuve S, Druilhe A, Boczkowski J, Dombret MC, Mechighel P, Megret J, Leseche G, Aubier M, Pretolani M (2001) Regulation of peroxisome proliferator-activated receptor gamma expression in human asthmatic airways: relationship with proliferation, apoptosis, and airway remodeling. *Am J Respir Crit Care Med* 164:1487-1494
- Bernard A, Marchandise FX, Depelchin S, Lauwerys R, Sibille Y (1992) Clara cell protein in serum and bronchoalveolar lavage. *Eur Respir J* 5:1231-1238
- Boateng E, El-Merhie N, Trompak O, Tumpara S, Seimetz M, Pilatz A, Baumgart-Vogt E, Karnati S (2016) Targeting PPAR γ in Lung fibroblasts: Prospects of therapeutic treatment for IPF. *PVRI* 3:33-39
- Boor P, Celec P, Martin IV, Villa L, Hodosy J, Klenovicsova K, Esposito C, Schafer S, Albrecht-Kupper B, Ostendorf T, Heidland A, Sebekova K (2011) The peroxisome proliferator-activated receptor-alpha agonist, BAY PP1, attenuates renal fibrosis in rats. *Kidney Int* 80:1182-1197
- Border WA, Noble NA (1994) Transforming growth factor beta in tissue fibrosis. *N Engl J Med* 331:1286-1292
- Bourke SJ (2006) Interstitial lung disease: progress and problems. *Postgrad Med J* 82:494-499
- Bowden DH (1984) Unraveling pulmonary fibrosis: the bleomycin model. *Lab Invest* 50:487-488
- Brites P, Waterham HR, Wanders RJ (2004) Functions and biosynthesis of plasmalogens in health and disease. *Biochim Biophys Acta* 1636:219-231
- Burgess HA, Daugherty LE, Thatcher TH, Lakatos HF, Ray DM, Redonnet M, Phipps RP, Sime PJ (2005) PPARgamma agonists inhibit TGF-beta induced pulmonary myofibroblast differentiation and collagen production: implications for therapy of lung fibrosis. *Am J Physiol Lung Cell Mol Physiol* 288:L1146-1153
- Cabrero A, Alegret M, Sanchez RM, Adzet T, Laguna JC, Carrera MV (2002) Increased reactive oxygen species production down-regulates peroxisome proliferator-activated alpha pathway in C2C12 skeletal muscle cells. *J Biol Chem* 277:10100-10107

References

- Callahan WP, Jr., Sutherland JC, Fulton JK, Kline JR (1952) Acute diffuse interstitial fibrosis of the lungs. *AMA Arch Intern Med* 90:468-482
- Cardoso WV, Stewart LG, Pinkerton KE, Ji C, Hook GE, Singh G, Katyal SL, Thurlbeck WM, Plopper CG (1993) Secretory product expression during Clara cell differentiation in the rabbit and rat. *Am J Physiol* 264:L543-552
- Chambers TJ, Owens JM, Hattersley G, Jat PS, Noble MD (1993) Generation of osteoclast-inductive and osteoclastogenic cell lines from the H-2KbtsA58 transgenic mouse. *Proc Natl Acad Sci U S A* 90:5578-5582
- Chang CC, South S, Warren D, Jones J, Moser AB, Moser HW, Gould SJ (1999) Metabolic control of peroxisome abundance. *J Cell Sci* 112 (Pt 10):1579-1590
- Clyde BL, Chang LY, Auten RL, Ho YS, Crapo JD (1993) Distribution of manganese superoxide dismutase mRNA in normal and hyperoxic rat lung. *Am J Respir Cell Mol Biol* 8:530-537
- Colasante C, Chen J, Ahlemeyer B, Baumgart-Vogt E (2015) Peroxisomes in cardiomyocytes and the peroxisome / peroxisome proliferator-activated receptor-loop. *Thromb Haemost* 113:452-463
- Cooper TG, Beevers H (1969) Beta oxidation in glyoxysomes from castor bean endosperm. *J Biol Chem* 244:3514-3520
- Cosio M, Ghezzi H, Hogg JC, Corbin R, Loveland M, Dosman J, Macklem PT (1978) The relations between structural changes in small airways and pulmonary-function tests. *N Engl J Med* 298:1277-1281
- Coursin DB, Cihla HP, Oberley TD, Oberley LW (1992) Immunolocalization of antioxidant enzymes and isozymes of glutathione S-transferase in normal rat lung. *Am J Physiol* 263:L679-691
- Coward WR, Saini G, Jenkins G (2010) The pathogenesis of idiopathic pulmonary fibrosis. *Ther Adv Respir Dis* 4:367-388
- Crapo JD, Barry BE, Gehr P, Bachofen M, Weibel ER (1982a) Cell number and cell characteristics of the normal human lung. *Am Rev Respir Dis* 125:740-745
- Crapo JD, Barry BE, Gehr P, Bachofen M, Weibel ER (1982b) Cell number and cell characteristics of the normal human lung. *Am Rev Respir Dis* 126:332-337
- Crisafulli C, Cuzzocrea S (2009) The role of endogenous and exogenous ligands for the peroxisome proliferator-activated receptor alpha (PPAR-alpha) in the regulation of inflammation in macrophages. *Shock* 32:62-73
- Cudmore RE, Emery JL, Mithal A (1962) Postnatal growth of the bronchi and bronchioles. *Arch Dis Child* 37:481-484
- Cui Y, Robertson J, Maharaj S, Waldhauser L, Niu J, Wang J, Farkas L, Kolb M, Gaudie J (2011) Oxidative stress contributes to the induction and persistence of TGF-beta1 induced pulmonary fibrosis. *Int J Biochem Cell Biol* 43:1122-1133
- Cutroneo KR, White SL, Phan SH, Ehrlich HP (2007) Therapies for bleomycin induced lung fibrosis through regulation of TGF-beta1 induced collagen gene expression. *J Cell Physiol* 211:585-589
- Cutz E, Conen PE (1971) Ultrastructure and cytochemistry of Clara cells. *Am J Pathol* 62:127-141
- Da Cruz S, Xenarios I, Langridge J, Vilbois F, Parone PA, Martinou JC (2003) Proteomic analysis of the mouse liver mitochondrial inner membrane. *J Biol Chem* 278:41566-41571
- Dansen TB, Wirtz KW (2001) The peroxisome in oxidative stress. *IUBMB Life* 51:223-230
- De Duve C (1965) The separation and characterization of subcellular particles. *Harvey Lect* 59:49-87

References

- De Duve C, Baudhuin P (1966) Peroxisomes (microbodies and related particles). *Physiol Rev* 46:323-357
- Demedts M, Behr J, Buhl R, Costabel U, Dekhuijzen R, Jansen HM, MacNee W, Thomeer M, Wallaert B, Laurent F, Nicholson AG, Verbeken EK, Verschakelen J, Flower CD, Capron F, Petruzzelli S, De Vuyst P, van den Bosch JM, Rodriguez-Becerra E, Corvasce G, Lankhorst I, Sardina M, Montanari M (2005) High-dose acetylcysteine in idiopathic pulmonary fibrosis. *N Engl J Med* 353:2229-2242
- deMello DE, Mahmoud S, Padfield PJ, Hoffmann JW (2000) Generation of an immortal differentiated lung type-II epithelial cell line from the adult H-2K(b)tsA58 transgenic mouse. *In Vitro Cell Dev Biol Anim* 36:374-382
- Demello DE, Mahmoud S, Ryerse J, Hoffmann JW (2002) Generation and characterization of a conditionally immortalized lung clara cell line from the H-2Kb-tsA58 transgenic mouse. *In Vitro Cell Dev Biol Anim* 38:154-164
- Dempsey OJ (2006) Clinical review: idiopathic pulmonary fibrosis--past, present and future. *Respir Med* 100:1871-1885
- Desvergne B, Michalik L, Wahli W (2006) Transcriptional regulation of metabolism. *Physiol Rev* 86:465-514
- Dhaunsi GS, Gulati S, Singh AK, Orak JK, Asayama K, Singh I (1992) Demonstration of Cu-Zn superoxide dismutase in rat liver peroxisomes. Biochemical and immunochemical evidence. *J Biol Chem* 267:6870-6873
- Diczfalusy U, Kase BF, Alexson SE, Bjorkhem I (1991) Metabolism of prostaglandin F2 alpha in Zellweger syndrome. Peroxisomal beta-oxidation is a major importance for in vivo degradation of prostaglandins in humans. *J Clin Invest* 88:978-984
- Diglio CA, Kikkawa Y (1977) The type II epithelial cells of the lung. IV. Adaption and behavior of isolated type II cells in culture. *Lab Invest* 37:622-631
- Distel B, Erdmann R, Gould SJ, Blobel G, Crane DI, Cregg JM, Dodt G, Fujiki Y, Goodman JM, Just WW, Kiel JA, Kunau WH, Lazarow PB, Mannaerts GP, Moser HW, Osumi T, Rachubinski RA, Roscher A, Subramani S, Tabak HF, Tsukamoto T, Valle D, van der Klei I, van Veldhoven PP, Veenhuis M (1996) A unified nomenclature for peroxisome biogenesis factors. *J Cell Biol* 135:1-3
- Duncker H, Kummer, W. (2008) Atemsystem In: Makroskopische Anatomie, Histologie, Embryologie, Zellbiologie, Band 1 Hrsg: Benninghoff A; Drenckhahn D Urban & Fischer, München
- Dunsmore SE, Rannels DE (1996) Extracellular matrix biology in the lung. *Am J Physiol* 270:L3-27
- Eckert JH, Erdmann R (2003) Peroxisome biogenesis. *Rev Physiol Biochem Pharmacol* 147:75-121
- Eguchi M, Spicer SS, Mochizuki I (1980) Cytochemistry of type II pneumocytes in Chediak-Higashi syndrome of mice. *Exp Mol Pathol* 32:290-306
- Eickelberg O, Pansky A, Musmann R, Bihl M, Tamm M, Hildebrand P, Perruchoud AP, Roth M (1999) Transforming growth factor-beta1 induces interleukin-6 expression via activating protein-1 consisting of JunD homodimers in primary human lung fibroblasts. *J Biol Chem* 274:12933-12938
- El-Merhie N, Baumgart-Vogt E, Pilatz A, Pfreimer S, Pfeifer B, Pak O, Kosanovic D, Seimetz M, Schermuly RT, Weismann N, Karnati S (2017) Differential alterations of the mitochondrial morphology and respiratory chain complexes during postnatal development of the mouse lung. *Oxid Med Cell Longi* in press

References

- Endo H, Oka T (1991) An immunohistochemical study of bronchial cells producing surfactant protein A in the developing human fetal lung. *Early Hum Dev* 25:149-156
- Fahimi HD (1968) Cytochemical localization of peroxidase activity in rat hepatic microbodies (peroxisomes). *J Histochem Cytochem* 16:547-550
- Fahimi HD (1969) Cytochemical localization of peroxidatic activity of catalase in rat hepatic microbodies (peroxisomes). *J Cell Biol* 43:275-288
- Fahimi HD, Beier K, Lindauer M, Schad A, Zhan J, Pill J, Rebel W, Völkl A, Baumgart E (1996) Zonal heterogeneity of peroxisome proliferation in rat liver. *Ann N Y Acad Sci* 804:341-361
- Fanucchi MV, Buckpitt AR, Murphy ME, Plopper CG (1997a) Naphthalene cytotoxicity of differentiating Clara cells in neonatal mice. *Toxicol Appl Pharmacol* 144:96-104
- Fanucchi MV, Murphy ME, Buckpitt AR, Philpot RM, Plopper CG (1997b) Pulmonary cytochrome P450 monooxygenase and Clara cell differentiation in mice. *Am J Respir Cell Mol Biol* 17:302-314
- Fattman CL, Chang LY, Termin TA, Petersen L, Enghild JJ, Oury TD (2003) Enhanced bleomycin-induced pulmonary damage in mice lacking extracellular superoxide dismutase. *Free Radic Biol Med* 35:763-771
- Fernandez IE, Eickelberg O (2012) The impact of TGF-beta on lung fibrosis: from targeting to biomarkers. *Proc Am Thorac Soc* 9:111-116
- Fringes B, Gorgas K, Reith A (1988a) Clofibrate increases the number of peroxisomes and of lamellar bodies in alveolar cells type II of the rat lung. *Eur J Cell Biol* 46:136-143
- Fringes B, Gorgas K, Reith A (1988b) Modification of surfactant metabolizing cells in rat lung by clofibrate, a hypolipidemic peroxisome proliferating agent. Evidence to suggest that clofibrate influences pulmonary surfactant metabolism. *Virchows Arch B Cell Pathol Incl Mol Pathol* 54:232-240
- Fringes B, Reith A (1988) Two hypolipidemic peroxisome proliferators increase the number of lamellar bodies in alveolar cells type II of the rat lung. *Exp Mol Pathol* 48:262-271
- Fruchart JC, Duriez P (2006) Mode of action of fibrates in the regulation of triglyceride and HDL-cholesterol metabolism. *Drugs Today (Barc)* 42:39-64
- Gabele E, Froh M, Arteel GE, Uesugi T, Hellerbrand C, Scholmerich J, Brenner DA, Thurman RG, Rippe RA (2009) TNFalpha is required for cholestasis-induced liver fibrosis in the mouse. *Biochem Biophys Res Commun* 378:348-353
- Gail DB, Lenfant CJ (1983) Cells of the lung: biology and clinical implications. *Am Rev Respir Dis* 127:366-387
- Gärtner J (2003) Is there a phenotype/genotype correlation in peroxisome biogenesis disorders (PBDs)? *Adv Exp Med Biol* 544:59-65
- Genovese T, Mazzon E, Di Paola R, Muia C, Crisafulli C, Caputi AP, Cuzzocrea S (2005) ROLE OF ENDOGENOUS AND EXOGENOUS LIGANDS FOR THE PEROXISOME PROLIFERATOR-ACTIVATED RECEPTOR alpha IN THE DEVELOPMENT OF BLEOMYCIN-INDUCED LUNG INJURY. *Shock* 24:547-555
- Gharaee-Kermani M, Hu B, Phan SH, Gyetko MR (2009) Recent advances in molecular targets and treatment of idiopathic pulmonary fibrosis: focus on TGFbeta signaling and the myofibroblast. *Curr Med Chem* 16:1400-1417
- Ghosh S, Janocha AJ, Aronica MA, Swaidani S, Comhair SA, Xu W, Zheng L, Kaveti S, Kinter M, Hazen SL, Erzurum SC (2006) Nitrotyrosine proteome survey in asthma identifies oxidative mechanism of catalase inactivation. *J Immunol* 176:5587-5597
- Giangreco A, Reynolds SD, Stripp BR (2002) Terminal bronchioles harbor a unique airway stem cell population that localizes to the bronchoalveolar duct junction. *Am J Pathol* 161:173-182

References

- Gilks CB, Price K, Wright JL, Churg A (1998) Antioxidant gene expression in rat lung after exposure to cigarette smoke. *Am J Pathol* 152:269-278
- Gosset P, Charbonnier AS, Delerive P, Fontaine J, Staels B, Pestel J, Tonnel AB, Trottein F (2001) Peroxisome proliferator-activated receptor gamma activators affect the maturation of human monocyte-derived dendritic cells. *Eur J Immunol* 31:2857-2865
- Gould SJ, Valle D (2000) Peroxisome biogenesis disorders: genetics and cell biology. *Trends Genet* 16:340-345
- Gowdy KM, Fessler MB Emerging roles for cholesterol and lipoproteins in lung disease. *Pulm Pharmacol Ther* 26:430-437
- Grabenbauer M, Fahimi HD, Baumgart E (2001) Detection of peroxisomal proteins and their mRNAs in serial sections of fetal and newborn mouse organs. *J Histochem Cytochem* 49:155-164
- Grant P, Ahlemeyer B, Karnati S, Berg T, Stelzig I, Nenicu A, Kuchelmeister K, Crane DI, Baumgart-Vogt E (2013) The biogenesis protein PEX14 is an optimal marker for the identification and localization of peroxisomes in different cell types, tissues, and species in morphological studies. *Histochem Cell Biol* 140:423-442
- Haefeli-Bleuer B, Weibel ER (1988) Morphometry of the human pulmonary acinus. *Anat Rec* 220:401-414
- Hajra AK, Burke CL, Jones CL (1979) Subcellular localization of acyl coenzyme A: dihydroxyacetone phosphate acyltransferase in rat liver peroxisomes (microbodies). *J Biol Chem* 254:10896-10900
- Hansen MK, Connolly TM (2008) Nuclear receptors as drug targets in obesity, dyslipidemia and atherosclerosis. *Curr Opin Investig Drugs* 9:247-255
- Harris JB, Chang LY, Crapo JD (1991) Rat lung alveolar type I epithelial cell injury and response to hyperoxia. *Am J Respir Cell Mol Biol* 4:115-125
- Hayashi H, Takahata S (1991) Role of peroxisomal fatty acyl-CoA beta-oxidation in phospholipid biosynthesis. *Arch Biochem Biophys* 284:326-331
- Hecker L, Vittal R, Jones T, Jagirdar R, Luckhardt TR, Horowitz JC, Pennathur S, Martinez FJ, Thannickal VJ (2009) NADPH oxidase-4 mediates myofibroblast activation and fibrogenic responses to lung injury. *Nat Med* 15:1077-1081
- Heijnen HF, van Donselaar E, Slot JW, Fries DM, Blachard-Fillion B, Hodara R, Lightfoot R, Polydoro M, Spielberg D, Thomson L, Regan EA, Crapo J, Ischiropoulos H (2006) Subcellular localization of tyrosine-nitrated proteins is dictated by reactive oxygen species generating enzymes and by proximity to nitric oxide synthase. *Free Radic Biol Med* 40:1903-1913
- Hermans C, Knoop B, Wiedig M, Aarsalane K, Toubreau G, Falmagne P, Bernard A (1999) Clara cell protein as a marker of Clara cell damage and bronchoalveolar blood barrier permeability. *Eur Respir J* 13:1014-1021
- Herriges M, Morrisey EE (2014) Lung development: orchestrating the generation and regeneration of a complex organ. *Development* 141:502-513
- Hill LHaP, C.G. (1979) Use of large block embedding for correlated LM, TEM and SEM characterization of pulmonary airways of known anatomic location. *Proc Southeast Electron Microsc Soc*, :2:24
- Hilliard M, Frohnert C, Spillner C, Marcone S, Nath A, Lampe T, Fitzgerald DJ, Kehlenbach RH (2010) The anti-inflammatory prostaglandin 15-deoxy-delta(12,14)-PGJ2 inhibits CRM1-dependent nuclear protein export. *J Biol Chem* 285:22202-22210
- Hiltunen JK, Filppula SA, Koivuranta KT, Siivari K, Qin YM, Hayrinen HM (1996) Peroxisomal beta-oxidation and polyunsaturated fatty acids. *Ann N Y Acad Sci* 804:116-128

- Hirai K, Yamauchi M, Witschi H, Cote MG (1983) Disintegration of lung peroxisomes during differentiation of type II cells to type I cells in butylated hydroxytoluene-administered mice. *Exp Mol Pathol* 39:129-138
- Hirai KI, Witschi H, Cote MG (1977) Electron microscopy of butylated hydroxytoluene-induced lung damage in mice. *Exp Mol Pathol* 27:295-308
- Huang TH, Razmovski-Naumovski V, Kota BP, Lin DS, Roufogalis BD (2005) The pathophysiological function of peroxisome proliferator-activated receptor-gamma in lung-related diseases. *Respir Res* 6:102
- Huang W, Glass CK (2010) Nuclear receptors and inflammation control: molecular mechanisms and pathophysiological relevance. *Arterioscler Thromb Vasc Biol* 30:1542-1549
- Iber D, Menshykau D (2013) The control of branching morphogenesis. *Open Biol* 3:130088
- Immenschuh S, Baumgart-Vogt E (2005) Peroxiredoxins, oxidative stress, and cell proliferation. *Antioxid Redox Signal* 7:768-777
- Islinger M, Li KW, Seitz J, Volkl A, Luers GH (2009) Hitchhiking of Cu/Zn superoxide dismutase to peroxisomes--evidence for a natural piggyback import mechanism in mammals. *Traffic* 10:1711-1721
- Islinger M, Lüers GH, Zischka H, Ueffing M, Völkl A (2006) Insights into the membrane proteome of rat liver peroxisomes: microsomal glutathione-S-transferase is shared by both subcellular compartments. *Proteomics* 6:804-816
- Issemann I, Green S (1990) Activation of a member of the steroid hormone receptor superfamily by peroxisome proliferators. *Nature* 347:645-650
- Jarvinen K, Pietarinen-Runtti P, Linnainmaa K, Raivio KO, Krejsa CM, Kavanagh T, Kinnula VL (2000) Antioxidant defense mechanisms of human mesothelioma and lung adenocarcinoma cells. *Am J Physiol Lung Cell Mol Physiol* 278:L696-702
- Jat PS, Noble MD, Ataliotis P, Tanaka Y, Yannoutsos N, Larsen L, Kioussis D (1991) Direct derivation of conditionally immortal cell lines from an H-2Kb-tsA58 transgenic mouse. *Proc Natl Acad Sci U S A* 88:5096-5100
- Jedlitschky G, Mayatepek E, Keppler D (1993) Peroxisomal leukotriene degradation: biochemical and clinical implications. *Adv Enzyme Regul* 33:181-194
- Jeffery PKaR, L. (1977) Ultrastructure of airway epithelium and submucosal glands during the development. In: *Development of the lung* WA Hodson, ed Marcel Dekker, New York:87-134
- Jorens PG, Sibille Y, Goulding NJ, van Overveld FJ, Herman AG, Bossaert L, De Backer WA, Lauwerys R, Flower RJ, Bernard A (1995) Potential role of Clara cell protein, an endogenous phospholipase A2 inhibitor, in acute lung injury. *Eur Respir J* 8:1647-1653
- Junn E, Lee KN, Ju HR, Han SH, Im JY, Kang HS, Lee TH, Bae YS, Ha KS, Lee ZW, Rhee SG, Choi I (2000) Requirement of hydrogen peroxide generation in TGF-beta 1 signal transduction in human lung fibroblast cells: involvement of hydrogen peroxide and Ca²⁺ in TGF-beta 1-induced IL-6 expression. *J Immunol* 165:2190-2197
- Karnati S (2009) Functional characterization of peroxisomes and pathological consequences of peroxisomal dysfunction in the lung. VVB Laufersweiler Verlag 1st
- Karnati S, Baumgart-Vogt E (2008) Peroxisomes in mouse and human lung: their involvement in pulmonary lipid metabolism. *Histochem Cell Biol* 130:719-740
- Karnati S, Baumgart-Vogt E (2009) Peroxisomes in airway epithelia and future prospects of these organelles for pulmonary cell biology. *Histochem Cell Biol* 131:447-454
- Karnati S, Graulich T, Oruqaj G, Pfreimer S, Seimetz M, Stamme C, Mariani TJ, Weissmann N, Muhlfeld C, Baumgart-Vogt E (2016a) Postnatal development of the bronchiolar club cells of distal airways in the mouse lung: stereological and molecular biological studies. *Cell Tissue Res* 364:543-557

References

- Karnati S, Kosanovic, D., Schermuly, R.T., Weissmann, N., Baumgart-Vogt, E., Seimetz, M. (2014) PPAR γ regulation is cell type dependent: Can it reverse COPD? *PVRI Chronicle* 1:33-37
- Karnati S, Luers G, Pfreimer S, Baumgart-Vogt E (2013) Mammalian SOD2 is exclusively located in mitochondria and not present in peroxisomes. *Histochem Cell Biol* 140:105-117
- Karnati S, Palaniswamy S, Alam MR, Oruçaj G, Stamme C, Baumgart-Vogt E (2016b) C22-bronchial and T7-alveolar epithelial cell lines of the immortomouse are excellent murine cell culture model systems to study pulmonary peroxisome biology and metabolism. *Histochem Cell Biol* 145:287-304
- Katzenstein AL, Myers JL (1998) Idiopathic pulmonary fibrosis: clinical relevance of pathologic classification. *Am J Respir Crit Care Med* 157:1301-1315
- Keller GA, Barton MC, Shapiro DJ, Singer SJ (1985) 3-Hydroxy-3-methylglutaryl-coenzyme A reductase is present in peroxisomes in normal rat liver cells. *Proc Natl Acad Sci U S A* 82:770-774
- Keller GA, Warner TG, Steimer KS, Hallewell RA (1991) Cu,Zn superoxide dismutase is a peroxisomal enzyme in human fibroblasts and hepatoma cells. *Proc Natl Acad Sci U S A* 88:7381-7385
- Kendall RT, Feghali-Bostwick CA Fibroblasts in fibrosis: novel roles and mediators. *Front Pharmacol* 5:123
- Kersten S, Desvergne B, Wahli W (2000) Roles of PPARs in health and disease. *Nature* 405:421-424
- Kilgore KS, Billin AN (2008) PPARbeta/delta ligands as modulators of the inflammatory response. *Curr Opin Investig Drugs* 9:463-469
- Kim B, Kim JE, Kim HS Caffeic acid induces keratinocyte differentiation by activation of PPAR-alpha. *J Pharm Pharmacol* 66:84-92
- Kim CF, Jackson EL, Woolfenden AE, Lawrence S, Babar I, Vogel S, Crowley D, Bronson RT, Jacks T (2005) Identification of bronchioalveolar stem cells in normal lung and lung cancer. *Cell* 121:823-835
- Kim EH, Surh YJ (2006) 15-deoxy-Delta12,14-prostaglandin J2 as a potential endogenous regulator of redox-sensitive transcription factors. *Biochem Pharmacol* 72:1516-1528
- Kim HJ, Jeong JS, Kim SR, Park SY, Chae HJ, Lee YC (2013) Inhibition of endoplasmic reticulum stress alleviates lipopolysaccharide-induced lung inflammation through modulation of NF- κ B/HIF-1 α signaling pathway. *Sci Rep* 3:1142
- Kinnula VL, Fattman CL, Tan RJ, Oury TD (2005) Oxidative stress in pulmonary fibrosis: a possible role for redox modulatory therapy. *Am J Respir Crit Care Med* 172:417-422
- Kinnula VL, Myllarniemi M (2008) Oxidant-antioxidant imbalance as a potential contributor to the progression of human pulmonary fibrosis. *Antioxid Redox Signal* 10:727-738
- Kinnula VL, Yankaskas JR, Chang L, Virtanen I, Linnala A, Kang BH, Crapo JD (1994) Primary and immortalized (BEAS 2B) human bronchial epithelial cells have significant antioxidative capacity in vitro. *Am J Respir Cell Mol Biol* 11:568-576
- Kintscher U, Lyon C, Wakino S, Bruemmer D, Feng X, Goetze S, Graf K, Moustakas A, Staels B, Fleck E, Hsueh WA, Law RE (2002) PPARalpha inhibits TGF-beta-induced beta5 integrin transcription in vascular smooth muscle cells by interacting with Smad4. *Circ Res* 91:e35-44
- Kira Y, Sato EF, Inoue M (2002) Association of Cu,Zn-type superoxide dismutase with mitochondria and peroxisomes. *Arch Biochem Biophys* 399:96-102
- Kliment CR, Oury TD (2010) Oxidative stress, extracellular matrix targets, and idiopathic pulmonary fibrosis. *Free Radic Biol Med* 49:707-717
- Koch A, Thiemann M, Grabenbauer M, Yoon Y, McNiven MA, Schrader M (2003) Dynammin-like protein 1 is involved in peroxisomal fission. *J Biol Chem* 278:8597-8605

References

- Kondrikov D, Caldwell RB, Dong Z, Su Y (2011) Reactive oxygen species-dependent RhoA activation mediates collagen synthesis in hyperoxic lung fibrosis. *Free Radic Biol Med* 50:1689-1698
- Konstandi M, Shah YM, Matsubara T, Gonzalez FJ Role of PPAR α and HNF4 α in stress-mediated alterations in lipid homeostasis. *PLoS One* 8:e70675
- Kostadinova R, Wahli W, Michalik L (2005) PPARs in diseases: control mechanisms of inflammation. *Curr Med Chem* 12:2995-3009
- Kovacs WJ, Tape KN, Shackelford JE, Duan X, Kasumov T, Kelleher JK, Brunengraber H, Krisans SK (2007) Localization of the pre-squalene segment of the isoprenoid biosynthetic pathway in mammalian peroxisomes. *Histochem Cell Biol* 127:273-290
- Kuhn C, McDonald JA (1991) The roles of the myofibroblast in idiopathic pulmonary fibrosis. Ultrastructural and immunohistochemical features of sites of active extracellular matrix synthesis. *Am J Pathol* 138:1257-1265
- Kulkarni AA, Woeller CF, Thatcher TH, Ramon S, Phipps RP, Sime PJ (2012) Emerging PPAR γ -Independent Role of PPAR γ Ligands in Lung Diseases. *PPAR Res* 2012;2012:705352
- Kulkarni AAW, C.F.; Thatcher, TH.; Ramon, S.; Phipps, R.P.; Sime, P.J. (2012) Emerging PPAR γ -Independent Role of PPAR γ Ligands in Lung Diseases. *PPAR Res* 2012;2012:705352
- Lakatos HF, Thatcher TH, Kottmann RM, Garcia TM, Phipps RP, Sime PJ (2007) The Role of PPARs in Lung Fibrosis. *PPAR Res* 2007:71323
- Lawrence DA (1996) Transforming growth factor-beta: a general review. *Eur Cytokine Netw* 7:363-374
- Lawson GW, Van Winkle LS, Toskala E, Senior RM, Parks WC, Plopper CG (2002) Mouse strain modulates the role of the ciliated cell in acute tracheobronchial airway injury-distal airways. *Am J Pathol* 160:315-327
- Lazarow PB (1977) Three hypolipidemic drugs increase hepatic palmitoyl-coenzyme A oxidation in the rat. *Science* 197:580-581
- Lazarow PB, De Duve C (1976) A fatty acyl-CoA oxidizing system in rat liver peroxisomes; enhancement by clofibrate, a hypolipidemic drug. *Proc Natl Acad Sci U S A* 73:2043-2046
- Lazarow PB, Fujiki Y (1985) Biogenesis of peroxisomes. *Annu Rev Cell Biol* 1:489-530
- Leask A, Abraham DJ (2004) TGF-beta signaling and the fibrotic response. *FASEB J* 18:816-827
- Li X, Baumgart E, Morrell JC, Jimenez-Sanchez G, Valle D, Gould SJ (2002) PEX11 beta deficiency is lethal and impairs neuronal migration but does not abrogate peroxisome function. *Mol Cell Biol* 22:4358-4365
- Li X, Gould SJ (2002) PEX11 promotes peroxisome division independently of peroxisome metabolism. *J Cell Biol* 156:643-651
- Lin Q, Fang LP, Zhou WW, Liu XM Rosiglitazone inhibits migration, proliferation, and phenotypic differentiation in cultured human lung fibroblasts. *Exp Lung Res* 36:120-128
- Lowrie PMA, W.S. (1973) Selection and preparation of specific regions for TEM using large epoxy-embedded blocks. *Proc 31st Ann Mtg EMSA* 148:324-325
- Mallampalli RK, Floerchinger CS, Hunninghake GW (1992) Isolation and immortalization of rat pre-type II cell lines. *In Vitro Cell Dev Biol* 28A:181-187
- Manoury B, Nenan S, Leclerc O, Guenon I, Boichot E, Planquois JM, Bertrand CP, Lagente V (2005) The absence of reactive oxygen species production protects mice against bleomycin-induced pulmonary fibrosis. *Respir Res* 6:11
- Marklund SL (1984) Extracellular superoxide dismutase and other superoxide dismutase isoenzymes in tissues from nine mammalian species. *Biochem J* 222:649-655

References

- Martinez M (1996) Docosahexaenoic acid therapy in docosahexaenoic acid-deficient patients with disorders of peroxisomal biogenesis. *Lipids* 31 Suppl:S145-152
- McCord JM, Fridovich I (1969) Superoxide dismutase. An enzymic function for erythrocyte hemoglobin. *J Biol Chem* 244:6049-6055
- McKeown S, Richter AG, O'Kane C, McAuley DF, Thickett DR (2009) MMP expression and abnormal lung permeability are important determinants of outcome in IPF. *Eur Respir J* 33:77-84
- Miao L, St Clair DK (2009) Regulation of superoxide dismutase genes: implications in disease. *Free Radic Biol Med* 47:344-356
- Michael LF, Lazar MA, Mendelson CR (1997) Peroxisome proliferator-activated receptor gamma1 expression is induced during cyclic adenosine monophosphate-stimulated differentiation of alveolar type II pneumocytes. *Endocrinology* 138:3695-3703
- Michalik L, Auwerx J, Berger JP, Chatterjee VK, Glass CK, Gonzalez FJ, Grimaldi PA, Kadowaki T, Lazar MA, O'Rahilly S, Palmer CN, Plutzky J, Reddy JK, Spiegelman BM, Staels B, Wahli W (2006) International Union of Pharmacology. LXI. Peroxisome proliferator-activated receptors. *Pharmacol Rev* 58:726-741
- Milam JE, Keshamouni VG, Phan SH, Hu B, Gangireddy SR, Hogaboam CM, Standiford TJ, Thannickal VJ, Reddy RC (2008) PPAR-gamma agonists inhibit profibrotic phenotypes in human lung fibroblasts and bleomycin-induced pulmonary fibrosis. *Am J Physiol Lung Cell Mol Physiol* 294:L891-901
- Moldovan L, Moldovan NI (2004) Oxygen free radicals and redox biology of organelles. *Histochem Cell Biol* 122:395-412
- Molnar F, Matilainen M, Carlberg C (2005) Structural determinants of the agonist-independent association of human peroxisome proliferator-activated receptors with coactivators. *J Biol Chem* 280:26543-26556
- Moodley YP, Misso NL, Scaffidi AK, Fogel-Petrovic M, McAnulty RJ, Laurent GJ, Thompson PJ, Knight DA (2003) Inverse effects of interleukin-6 on apoptosis of fibroblasts from pulmonary fibrosis and normal lungs. *Am J Respir Cell Mol Biol* 29:490-498
- Moore MW, Herzog EL (2013) Regulation and Relevance of Myofibroblast Responses in Idiopathic Pulmonary Fibrosis. *Curr Pathobiol Rep* 1:199-208
- Moraes LA, Piqueras L, Bishop-Bailey D (2006) Peroxisome proliferator-activated receptors and inflammation. *Pharmacol Ther* 110:371-385
- Moras D, Gronemeyer H (1998) The nuclear receptor ligand-binding domain: structure and function. *Curr Opin Cell Biol* 10:384-391
- Moreno S, Nardacci R, Ceru MP (1997) Regional and ultrastructural immunolocalization of copper-zinc superoxide dismutase in rat central nervous system. *J Histochem Cytochem* 45:1611-1622
- Moriguchi K, Higashi N, Kitagawa S, Takase K, Ohya N, Uyeda T, Hirai K (1984) Differentiation of human pulmonary alveolar epithelial cells revealed by peroxisome changes in pulmonary proteinosis. *Exp Mol Pathol* 40:262-270
- Moser HW (1999) [Disorders associated with alterations in single peroxisomal proteins, including X-linked adrenoleukodystrophy]. *Rev Neurol* 28 Suppl 1:S55-58
- Muller R, Rieck M, Muller-Brusselbach S (2008) Regulation of Cell Proliferation and Differentiation by PPARbeta/delta. *PPAR Res* 2008:614852
- Mundel P, Reiser J, Zuniga Mejia Borja A, Pavenstadt H, Davidson GR, Kriz W, Zeller R (1997) Rearrangements of the cytoskeleton and cell contacts induce process formation during differentiation of conditionally immortalized mouse podocyte cell lines. *Exp Cell Res* 236:248-258

References

- Nenicu A, Lüers GH, Kovacs W, Otte D, Zimmer A, Bergmann M, Baumgart-Vogt E (2007) Peroxisomes in human and mouse testis: differential expression of peroxisomal proteins in germ cells and distinct somatic cell types of the testis. *Biol Reprod* 77:1060-1072
- Noble PW, Homer RJ (2005) Back to the future: historical perspective on the pathogenesis of idiopathic pulmonary fibrosis. *Am J Respir Cell Mol Biol* 33:113-120
- Nolte RT, Conlin RM, Harrison SC, Brown RS (1998) Differing roles for zinc fingers in DNA recognition: structure of a six-finger transcription factor IIIA complex. *Proc Natl Acad Sci U S A* 95:2938-2943
- Noppen M, De Waele M, Li R, Gucht KV, D'Haese J, Gerlo E, Vincken W (2000) Volume and cellular content of normal pleural fluid in humans examined by pleural lavage. *Am J Respir Crit Care Med* 162:1023-1026
- Novikoff AB, Goldfischer S (1969) Visualization of peroxisomes (microbodies) and mitochondria with diaminobenzidine. *J Histochem Cytochem* 17:675-680
- Nozik-Grayck E, Suliman HB, Piantadosi CA (2005) Extracellular superoxide dismutase. *Int J Biochem Cell Biol* 37:2466-2471
- Ogata T, Miyauchi T, Sakai S, Irukayama-Tomobe Y, Goto K, Yamaguchi I (2002) Stimulation of peroxisome-proliferator-activated receptor alpha (PPAR alpha) attenuates cardiac fibrosis and endothelin-1 production in pressure-overloaded rat hearts. *Clin Sci (Lond)* 103 Suppl 48:284S-288S
- Okado-Matsumoto A, Fridovich I (2001) Subcellular distribution of superoxide dismutases (SOD) in rat liver: Cu,Zn-SOD in mitochondria. *J Biol Chem* 276:38388-38393
- Orgeig S, Daniels CB (2001) The roles of cholesterol in pulmonary surfactant: insights from comparative and evolutionary studies. *Comp Biochem Physiol A Mol Integr Physiol* 129:75-89
- Ortiz LA, Lasky J, Hamilton RF, Jr., Holian A, Hoyle GW, Banks W, Peschon JJ, Brody AR, Lungarella G, Friedman M (1998) Expression of TNF and the necessity of TNF receptors in bleomycin-induced lung injury in mice. *Exp Lung Res* 24:721-743
- Orugaj G (2015) Reactive Oxygen Species (ROS) and lipid metabolism in idiopathic pulmonary fibrosis - role of peroxisomes in the pathogenesis of this devastating disease. PhD dissertation
- Oruqaj G, Karnati S, Vijayan V, Kotarkonda LK, Boateng E, Zhang W, Ruppert C, Gunther A, Shi W, Baumgart-Vogt E (2015) Compromised peroxisomes in idiopathic pulmonary fibrosis, a vicious cycle inducing a higher fibrotic response via TGF-beta signaling. *Proc Natl Acad Sci U S A* 112:E2048-2057
- Ossendorp BC, Voorhout WF, van Golde LM, Wirtz KW, Batenburg JJ (1994) Identification of the non-specific lipid-transfer protein (sterol carrier protein 2) in peroxisomes of lung type II cells. *Biochem Biophys Res Commun* 205:1581-1588
- Palumbo K, Zerr P, Tomcik M, Vollath S, Dees C, Akhmetshina A, Avouac J, Yaniv M, Distler O, Schett G, Distler JH (2011) The transcription factor JunD mediates transforming growth factor {beta}-induced fibroblast activation and fibrosis in systemic sclerosis. *Ann Rheum Dis* 70:1320-1326
- Pantelidis P, Fanning GC, Wells AU, Welsh KI, Du Bois RM (2001) Analysis of tumor necrosis factor-alpha, lymphotoxin-alpha, tumor necrosis factor receptor II, and interleukin-6 polymorphisms in patients with idiopathic pulmonary fibrosis. *Am J Respir Crit Care Med* 163:1432-1436
- Pardo A, Selman M (2002) Molecular mechanisms of pulmonary fibrosis. *Front Biosci* 7:d1743-1761

References

- Pascual G, Fong AL, Ogawa S, Gamliel A, Li AC, Perissi V, Rose DW, Willson TM, Rosenfeld MG, Glass CK (2005) A SUMOylation-dependent pathway mediates transrepression of inflammatory response genes by PPAR-gamma. *Nature* 437:759-763
- Patel HJ, Belvisi MG, Bishop-Bailey D, Yacoub MH, Mitchell JA (2003) Activation of peroxisome proliferator-activated receptors in human airway smooth muscle cells has a superior anti-inflammatory profile to corticosteroids: relevance for chronic obstructive pulmonary disease therapy. *J Immunol* 170:2663-2669
- Peake JL, Reynolds SD, Stripp BR, Stephens KE, Pinkerton KE (2000) Alteration of pulmonary neuroendocrine cells during epithelial repair of naphthalene-induced airway injury. *Am J Pathol* 156:279-286
- Petrik P (1971) Fine structural identification of peroxisomes in mouse and rat bronchiolar and alveolar epithelium. *J Histochem Cytochem* 19:339-348
- Phan SH (2002) The myofibroblast in pulmonary fibrosis. *Chest* 122:286S-289S
- Piguet PF, Vesin C (1994) Treatment by human recombinant soluble TNF receptor of pulmonary fibrosis induced by bleomycin or silica in mice. *Eur Respir J* 7:515-518
- Plopper CG, Halsebo JE, Berger WJ, Sonstegard KS, Nettesheim P (1983) Distribution of nonciliated bronchiolar epithelial (Clara) cells in intra- and extrapulmonary airways of the rabbit. *Exp Lung Res* 5:79-98
- Plopper CG, Macklin J, Nishio SJ, Hyde DM, Buckpitt AR (1992a) Relationship of cytochrome P-450 activity to Clara cell cytotoxicity. III. Morphometric comparison of changes in the epithelial populations of terminal bronchioles and lobar bronchi in mice, hamsters, and rats after parenteral administration of naphthalene. *Lab Invest* 67:553-565
- Plopper CG, Pinkerton KE (1991) Overview of diversity in the respiratory system of mammals. In *Comparative Biology of the Normal Lung* 1:3-5 CRC Press. Boca Raton, FL
- Plopper CG, Suverkropp C, Morin D, Nishio S, Buckpitt A (1992b) Relationship of cytochrome P-450 activity to Clara cell cytotoxicity. I. Histopathologic comparison of the respiratory tract of mice, rats and hamsters after parenteral administration of naphthalene. *J Pharmacol Exp Ther* 261:353-363
- Plopper CG, Weir AJ, Morin D, Chang A, Philpot RM, Buckpitt AR (1993) Postnatal changes in the expression and distribution of pulmonary cytochrome P450 monooxygenases during Clara cell differentiation in rabbits. *Mol Pharmacol* 44:51-61
- Polvani S, Tarocchi M, Galli A (2012) PPARgamma and Oxidative Stress: Con(beta) Catenating NRF2 and FOXO. *PPAR Res* 2012:641087
- Purdue PE, Lazarow PB (2001) Peroxisome biogenesis. *Annu Rev Cell Dev Biol* 17:701-752
- Qian G, Fan W, Ahlemeyer B, Karnati S, Baumgart-Vogt E (2015) Peroxisomes in Different Skeletal Cell Types during Intramembranous and Endochondral Ossification and Their Regulation during Osteoblast Differentiation by Distinct Peroxisome Proliferator-Activated Receptors. *PLoS One* 10:e0143439
- Qiu Z, Fujimura M, Kurashima K, Nakao S, Mukaida N (2004) Enhanced airway inflammation and decreased subepithelial fibrosis in interleukin 6-deficient mice following chronic exposure to aerosolized antigen. *Clin Exp Allergy* 34:1321-1328
- Raghu G, Masta S, Meyers D, Narayanan AS (1989) Collagen synthesis by normal and fibrotic human lung fibroblasts and the effect of transforming growth factor-beta. *Am Rev Respir Dis* 140:95-100
- Rahman I (2006) Antioxidant therapies in COPD. *Int J Chron Obstruct Pulmon Dis* 1:15-29
- Rahman I, Adcock IM (2006) Oxidative stress and redox regulation of lung inflammation in COPD. *Eur Respir J* 28:219-242

References

- Rahman I, Biswas SK, Kode A (2006) Oxidant and antioxidant balance in the airways and airway diseases. *Eur J Pharmacol* 533:222-239
- Rahman I, MacNee W (1996) Role of oxidants/antioxidants in smoking-induced lung diseases. *Free Radic Biol Med* 21:669-681
- Rahman I, MacNee W (2000) Regulation of redox glutathione levels and gene transcription in lung inflammation: therapeutic approaches. *Free Radic Biol Med* 28:1405-1420
- Rahman I, Morrison D, Donaldson K, MacNee W (1996) Systemic oxidative stress in asthma, COPD, and smokers. *Am J Respir Crit Care Med* 154:1055-1060
- Rajasekaran S, Vaz M, Reddy SP (2012) Fra-1/AP-1 transcription factor negatively regulates pulmonary fibrosis in vivo. *PLoS One* 7:e41611
- Reynders V, Loitsch S, Steinhauer C, Wagner T, Steinhilber D, Bargon J (2006) Peroxisome proliferator-activated receptor alpha (PPAR alpha) down-regulation in cystic fibrosis lymphocytes. *Respir Res* 7:104
- Reynolds SD, Malkinson AM (2010) Clara cell: progenitor for the bronchiolar epithelium. *Int J Biochem Cell Biol* 42:1-4
- Rice WR, Conkright JJ, Na CL, Ikegami M, Shannon JM, Weaver TE (2002) Maintenance of the mouse type II cell phenotype in vitro. *Am J Physiol Lung Cell Mol Physiol* 283:L256-264
- Rigamonti E, Chinetti-Gbaguidi G, Staels B (2008) Regulation of macrophage functions by PPAR-alpha, PPAR-gamma, and LXRs in mice and men. *Arterioscler Thromb Vasc Biol* 28:1050-1059
- Robillard R, Fontaine C, Chinetti G, Fruchart JC, Staels B (2005) Fibrates. *Handb Exp Pharmacol*:389-406
- Rodney A, David, RB. (2013) *Medical Physiology: Principles for Clinical Medicine*. Wolters Kluwer and Lippincott Williams & Wilkins Fourth edition
- Rosan RC, Lauweryns JM (1972) Mucosal cells of the small bronchioles of prematurely born human infants (600-1700 g). *Beitr Pathol* 147:145-174
- Roy S, Khanna S, Azad A, Schnitt R, He G, Weigert C, Ichijo H, Sen CK (2010) Fra-2 mediates oxygen-sensitive induction of transforming growth factor beta in cardiac fibroblasts. *Cardiovasc Res* 87:647-655
- Rüdiger M, Kolleck I, Putz G, Wauer RR, Stevens P, Rüstow B (1998) Plasmalogens effectively reduce the surface tension of surfactant-like phospholipid mixtures. *Am J Physiol* 274:L143-148
- Ryerse JS, Hoffmann JW, Mahmoud S, Nagel BA, deMello DE (2001) Immunolocalization of CC10 in Clara cells in mouse and human lung. *Histochem Cell Biol* 115:325-332
- Saito F, Tasaka S, Inoue K, Miyamoto K, Nakano Y, Ogawa Y, Yamada W, Shiraishi Y, Hasegawa N, Fujishima S, Takano H, Ishizaka A (2008) Role of interleukin-6 in bleomycin-induced lung inflammatory changes in mice. *Am J Respir Cell Mol Biol* 38:566-571
- Savov J, Wright JR, Young SL (2000) Incorporation of biotinylated SP-A into rat lung surfactant layer, type II cells, and clara cells. *Am J Physiol Lung Cell Mol Physiol* 279:L118-126
- Schatz G (1987) 17th Sir Hans Krebs lecture. Signals guiding proteins to their correct locations in mitochondria. *Eur J Biochem* 165:1-6
- Schneeberger EE (1972a) A comparative cytochemical study of microbodies (peroxisomes) in great alveolar cells of rodents, rabbit and monkey. *J Histochem Cytochem* 20:180-191
- Schneeberger EE (1972b) Development of peroxisomes in granular pneumocytes during pre- and postnatal growth. *Lab Invest* 27:581-589
- Schoonjans K, Staels B, Auwerx J (1996) Role of the peroxisome proliferator-activated receptor (PPAR) in mediating the effects of fibrates and fatty acids on gene expression. *J Lipid Res* 37:907-925

References

- Schrader M, Costello J, Godinho LF, Islinger M (2015) Peroxisome-mitochondria interplay and disease. *J Inherit Metab Dis* 38:681-702
- Schrader M, Fahimi HD (2004) Mammalian peroxisomes and reactive oxygen species. *Histochem Cell Biol* 122:383-393
- Schrader M, Fahimi HD (2006) Peroxisomes and oxidative stress. *Biochim Biophys Acta* 1763:1755-1766
- Schrader M, Reuber BE, Morrell JC, Jimenez-Sanchez G, Obie C, Stroh TA, Valle D, Schroer TA, Gould SJ (1998) Expression of PEX11beta mediates peroxisome proliferation in the absence of extracellular stimuli. *J Biol Chem* 273:29607-29614
- Scotton CJ, Chambers RC (2007) Molecular targets in pulmonary fibrosis: the myofibroblast in focus. *Chest* 132:1311-1321
- Seibert K, Zhang Y, Leahy K, Hauser S, Masferrer J, Isakson P (1997) Distribution of COX-1 and COX-2 in normal and inflamed tissues. *Adv Exp Med Biol* 400A:167-170
- Shannon JM, Jennings SD, Nielsen LD (1992) Modulation of alveolar type II cell differentiated function in vitro. *Am J Physiol* 262:L427-436
- Sheppard D (2006) Transforming growth factor beta: a central modulator of pulmonary and airway inflammation and fibrosis. *Proc Am Thorac Soc* 3:413-417
- Shimizu M, Takeshita A, Tsukamoto T, Gonzalez FJ, Osumi T (2004) Tissue-selective, bidirectional regulation of PEX11 alpha and perilipin genes through a common peroxisome proliferator response element. *Mol Cell Biol* 24:1313-1323
- Shimoda-Matsubayashi S, Matsumine H, Kobayashi T, Nakagawa-Hattori Y, Shimizu Y, Mizuno Y (1996) Structural dimorphism in the mitochondrial targeting sequence in the human manganese superoxide dismutase gene. A predictive evidence for conformational change to influence mitochondrial transport and a study of allelic association in Parkinson's disease. *Biochem Biophys Res Commun* 226:561-565
- Shull S, Heintz NH, Periasamy M, Manohar M, Janssen YM, Marsh JP, Mossman BT (1991) Differential regulation of antioxidant enzymes in response to oxidants. *J Biol Chem* 266:24398-24403
- Simon DM, Arian MC, Srisuma S, Bhattacharya S, Andalcio T, Shapiro SD, Mariani TJ (2006) Epithelial cell PPARgamma is an endogenous regulator of normal lung maturation and maintenance. *Proc Am Thorac Soc* 3:510-511
- Singh AK, Dobashi K, Gupta MP, Asayama K, Singh I, Orak JK (1999) Manganese superoxide dismutase in rat liver peroxisomes: biochemical and immunochemical evidence. *Mol Cell Biochem* 197:7-12
- Singh G, Katyal SL (1984) An immunologic study of the secretory products of rat Clara cells. *J Histochem Cytochem* 32:49-54
- Sisson TH, Mendez M, Choi K, Subbotina N, Courey A, Cunningham A, Dave A, Engelhardt JF, Liu X, White ES, Thannickal VJ, Moore BB, Christensen PJ, Simon RH (2010) Targeted injury of type II alveolar epithelial cells induces pulmonary fibrosis. *Am J Respir Crit Care Med* 181:254-263
- Sivarajah K, Jones KG, Fouts JR, Devereux T, Shirley JE, Eling TE (1983) Prostaglandin synthetase and cytochrome P-450-dependent metabolism of (+/-)benzo(a)pyrene 7,8-dihydrodiol by enriched populations of rat Clara cells and alveolar type II cells. *Cancer Res* 43:2632-2636
- Slot JW, Geuze HJ, Freeman BA, Crapo JD (1986) Intracellular localization of the copper-zinc and manganese superoxide dismutases in rat liver parenchymal cells. *Lab Invest* 55:363-371
- Smith BT (1977) Cell line A549: a model system for the study of alveolar type II cell function. *Am Rev Respir Dis* 115:285-293

References

- Sorokin SA (1961) A study of development in organ cultures of mammalian lungs *Dev Biol* 3:60-83
- Sorokin SP (1988) The Respiratory System: Cell and Tissue Biology. In: Weiss L (ed): Chapter 25, Sixth edn, Urban and Schwarzenberg, Munich:751-814, ISBN: 753-541-72176-72176
- Spite M, Serhan CN (2010) Novel lipid mediators promote resolution of acute inflammation: impact of aspirin and statins. *Circ Res* 107:1170-1184
- Staels B (2005) Fluid retention mediated by renal PPARgamma. *Cell Metab* 2:77-78
- Steinberg SJ, Dodt G, Raymond GV, Braverman NE, Moser AB, Moser HW (2006) Peroxisome biogenesis disorders. *Biochim Biophys Acta* 1763:1733-1748
- Strieter RM, Mehrad B (2009) New mechanisms of pulmonary fibrosis. *Chest* 136:1364-1370
- Subramani S (1998) Components involved in peroxisome import, biogenesis, proliferation, turnover, and movement. *Physiol Rev* 78:171-188
- Sugahara K, Rubin JS, Mason RJ, Aronsen EL, Shannon JM (1995) Keratinocyte growth factor increases mRNAs for SP-A and SP-B in adult rat alveolar type II cells in culture. *Am J Physiol* 269:L344-350
- Sugiyama H, Nonaka T, Kishimoto T, Komoriya K, Tsuji K, Nakahata T (2000) Peroxisome proliferator-activated receptors are expressed in human cultured mast cells: a possible role of these receptors in negative regulation of mast cell activation. *Eur J Immunol* 30:3363-3370
- Suki B, Stamenovic D, Hubmayr R (2011) Lung parenchymal mechanics. *Compr Physiol* 1:1317-1351
- Sullivan DE, Ferris M, Nguyen H, Abboud E, Brody AR (2009) TNF-alpha induces TGF-beta1 expression in lung fibroblasts at the transcriptional level via AP-1 activation. *J Cell Mol Med* 13:1866-1876
- Sureshbabu A, Tonner E, Allan GJ, Flint DJ (2011) Relative Roles of TGF-beta and IGFBP-5 in Idiopathic Pulmonary Fibrosis. *Pulm Med* 2011:517687
- Tarrier N, Cooke EC, Lader MH (1978) Electrodermal and heart-rate measurements in chronic and partially remitted schizophrenic patients. *Acta Psychiatr Scand* 57:369-376
- Terlecky SR, Fransen M (2000) How peroxisomes arise. *Traffic* 1:465-473
- Terlecky SR, Koepke JI, Walton PA (2006) Peroxisomes and aging. *Biochim Biophys Acta* 1763:1749-1754
- Terlecky SR, Terlecky LJ, Giordano CR (2012) Peroxisomes, oxidative stress, and inflammation. *World J Biol Chem* 3:93-97
- Thannickal VJ, Day RM, Klinz SG, Bastien MC, Larios JM, Fanburg BL (2000) Ras-dependent and -independent regulation of reactive oxygen species by mitogenic growth factors and TGF-beta1. *FASEB J* 14:1741-1748
- Thompson SL, Krisans SK (1990) Rat liver peroxisomes catalyze the initial step in cholesterol synthesis. The condensation of acetyl-CoA units into acetoacetyl-CoA. *J Biol Chem* 265:5731-5735
- Tölle A, Meier W, Rüdiger M, Hofmann KP, Rüstow B (2002) Effect of cholesterol and surfactant protein B on the viscosity of phospholipid mixtures. *Chem Phys Lipids* 114:159-168
- Toskala E, Smiley-Jewell SM, Wong VJ, King D, Plopper CG (2005) Temporal and spatial distribution of ciliogenesis in the tracheobronchial airways of mice. *Am J Physiol Lung Cell Mol Physiol* 289:L454-459
- Trifilieff A, Bench A, Hanley M, Bayley D, Campbell E, Whittaker P (2003) PPAR-alpha and -gamma but not -delta agonists inhibit airway inflammation in a murine model of asthma: in vitro evidence for an NF-kappaB-independent effect. *Br J Pharmacol* 139:163-171

References

- Uhal BD (1997) Cell cycle kinetics in the alveolar epithelium. *Am J Physiol* 272:L1031-1045
- Van Scott MR, McIntire MR, Henke DC (1990) Arachidonic acid metabolism and regulation of ion transport in rabbit Clara cells. *Am J Physiol* 259:L213-221
- Van Veldhoven P, Mannaerts GP (1985) Comparison of the activities of some peroxisomal and extraperoxisomal lipid-metabolizing enzymes in liver and extrahepatic tissues of the rat. *Biochem J* 227:737-741
- Van Vyve T, Chanez P, Bernard A, Bousquet J, Godard P, Lauwerijs R, Sibille Y (1995) Protein content in bronchoalveolar lavage fluid of patients with asthma and control subjects. *J Allergy Clin Immunol* 95:60-68
- Vaughan MB, Howard EW, Tomasek JJ (2000) Transforming growth factor-beta1 promotes the morphological and functional differentiation of the myofibroblast. *Exp Cell Res* 257:180-189
- Verjee LS, Verhoekx JS, Chan JK, Krausgruber T, Nicolaidou V, Izadi D, Davidson D, Feldmann M, Midwood KS, Nanchahal J (2013) Unraveling the signaling pathways promoting fibrosis in Dupuytren's disease reveals TNF as a therapeutic target. *Proc Natl Acad Sci U S A* 110:E928-937
- Verrecchia F, Vindevoghel L, Lechleider RJ, Uitto J, Roberts AB, Mauviel A (2001) Smad3/AP-1 interactions control transcriptional responses to TGF-beta in a promoter-specific manner. *Oncogene* 20:3332-3340
- Vijayan V, Srinu T, Karnati S, Garikapati V, Linke M, Kamalyan L, Mali SR, Sudan K, Kollas A, Schmid T, Schulz S, Spengler B, Weichhart T, Immenschuh S, E. B-V (2017) A New Immunomodulatory Role for Peroxisomes in Macrophages Activated by the TLR4 Ligand Lipopolysaccharide. *J Immunol* Mar 15;198(6):2414-2425.
- Visser WF, van Roermund CW, Ijlst L, Waterham HR, Wanders RJ (2007) Metabolite transport across the peroxisomal membrane. *Biochem J* 401:365-375
- Waghray M, Cui Z, Horowitz JC, Subramanian IM, Martinez FJ, Toews GB, Thannickal VJ (2005) Hydrogen peroxide is a diffusible paracrine signal for the induction of epithelial cell death by activated myofibroblasts. *FASEB J* 19:854-856
- Wahli W, Michalik L (2012) PPARs at the crossroads of lipid signaling and inflammation. *Trends Endocrinol Metab* 23:351-363
- Wallaert B, Lassalle P, Fortin F, Aerts C, Bart F, Fournier E, Voisin C (1990) Superoxide anion generation by alveolar inflammatory cells in simple pneumoconiosis and in progressive massive fibrosis of nonsmoking coal workers. *Am Rev Respir Dis* 141:129-133
- Wan XS, Devalaraja MN, St Clair DK (1994) Molecular structure and organization of the human manganese superoxide dismutase gene. *DNA Cell Biol* 13:1127-1136
- Wanders RJ, Denis S (1992) Identification of superoxide dismutase in rat liver peroxisomes. *Biochim Biophys Acta* 1115:259-262
- Wang AC, Dai X, Luu B, Conrad DJ (2001) Peroxisome proliferator-activated receptor-gamma regulates airway epithelial cell activation. *Am J Respir Cell Mol Biol* 24:688-693
- Wang XY, Keefe KM, Jensen-Taubman SM, Yang D, Yan K, Linnoila RI (2012) Novel method for isolation of murine clara cell secretory protein-expressing cells with traces of stemness. *PLoS One* 7:e43008
- Warburton D, Shi W, Xu B (2013) TGF-beta-Smad3 signaling in emphysema and pulmonary fibrosis: an epigenetic aberration of normal development? *Am J Physiol Lung Cell Mol Physiol* 304:L83-85
- Ward JE, Tan X (2007) Peroxisome proliferator activated receptor ligands as regulators of airway inflammation and remodelling in chronic lung disease. *PPAR Res* 2007:14983

References

- Warner BB, Burhans MS, Clark JC, Wispe JR (1991) Tumor necrosis factor-alpha increases Mn-SOD expression: protection against oxidant injury. *Am J Physiol* 260:L296-301
- Weibel ER (2009) What makes a good lung? *Swiss Med Wkly* 139:375-386
- Weisiger RA, Fridovich I (1973a) Mitochondrial superoxide simutase. Site of synthesis and intramitochondrial localization. *J Biol Chem* 248:4793-4796
- Weisiger RA, Fridovich I (1973b) Superoxide dismutase. Organelle specificity. *J Biol Chem* 248:3582-3592
- Weller BL, Crapo JD, Slot J, Posthuma G, Plopper CG, Pinkerton KE (1997) Site- and cell-specific alteration of lung copper/zinc and manganese superoxide dismutases by chronic ozone exposure. *Am J Respir Cell Mol Biol* 17:552-560
- Whitehead RH, VanEeden PE, Noble MD, Ataliotis P, Jat PS (1993) Establishment of conditionally immortalized epithelial cell lines from both colon and small intestine of adult H-2Kb-tsA58 transgenic mice. *Proc Natl Acad Sci U S A* 90:587-591
- Wiese S, Gronemeyer T, Ofman R, Kunze M, Grou CP, Almeida JA, Eisenacher M, Stephan C, Hayen H, Schollenberger L, Korosec T, Waterham HR, Schliebs W, Erdmann R, Berger J, Meyer HE, Just W, Azevedo JE, Wanders RJ, Warscheid B (2007) Proteomics characterization of mouse kidney peroxisomes by tandem mass spectrometry and protein correlation profiling. *Mol Cell Proteomics* 6:2045-2057
- Williams K, Malarkey D, Cohn L, Patrick D, Dye J, Toews G (2004) Identification of spontaneous feline idiopathic pulmonary fibrosis: morphology and ultrastructural evidence for a type II pneumocyte defect. *Chest* 125:2278-2288
- Willson TM, Brown PJ, Sternbach DD, Henke BR (2000) The PPARs: from orphan receptors to drug discovery. *J Med Chem* 43:527-550
- Woerly G, Honda K, Loyens M, Papin JP, Auwerx J, Staels B, Capron M, Dombrowicz D (2003) Peroxisome proliferator-activated receptors alpha and gamma down-regulate allergic inflammation and eosinophil activation. *J Exp Med* 198:411-421
- Wong GH, Goeddel DV (1988) Induction of manganoous superoxide dismutase by tumor necrosis factor: possible protective mechanism. *Science* 242:941-944
- Wouters FS, Bastiaens PI, Wirtz KW, Jovin TM (1998) FRET microscopy demonstrates molecular association of non-specific lipid transfer protein (nsL-TP) with fatty acid oxidation enzymes in peroxisomes. *EMBO J* 17:7179-7189
- Wright JR (2005) Immunoregulatory functions of surfactant proteins. *Nat Rev Immunol* 5:58-68
- Zhang N (1996) Characterization of the 5' flanking region of the human MnSOD gene. *Biochem Biophys Res Commun* 220:171-180
- Zhao J, Shi W, Wang YL, Chen H, Bringas P, Jr., Datto MB, Frederick JP, Wang XF, Warburton D (2002) Smad3 deficiency attenuates bleomycin-induced pulmonary fibrosis in mice. *Am J Physiol Lung Cell Mol Physiol* 282:L585-593
- Zheng D, Limmon GV, Yin L, Leung NH, Yu H, Chow VT, Chen J (2013) A cellular pathway involved in Clara cell to alveolar type II cell differentiation after severe lung injury. *PLoS One* 8:e71028

9 Acknowledgments

I wish to express my profound heart felt thanks to my supervisor Prof. Baumgart-Vogt. She has been a great support for me throughout my career from PhD to PD. Her observations and critical suggestions have intensified my thinking into finding new ways to deal with the research. Discussions with her always used to give good clues and I appreciate her keen interest, time and her attitude of helping in crucial times.

I am also thankful to Dr. Klaus Peter Valerius for his support in all times. Special warm-hearted thanks to Dr. Wieland Stöckmann for this timely help in all times without any hesitation. I express my sincere gratitude to PD. Dr. Barbara Ahlemeyer for her helpful discussions. No work would be completed with out the help of technical staff and I owe my deep sense of gratitude to Bianca Pfeiffer and Susanne Pfreimer. Furthermore, I am grateful to, Andreas Textor, Petra Hahn-Kohlberger, Elke Rodenberg-Frank for the technical support.

I am grateful to work with intelligent colleagues Dr Lakshmikanth Kotarkonda, Dr Gani Oruqaj, Harshavardhan Janga, Srinu Tumpara, Dr. El Merhi, Eistine Boateng and Dr. Vijith Vijayan and Dr. Claudia Colasante.

I am indebted to all the staff at Institute for Anatomy and Cell Biology II for their whole hearted help and making my research work comfortable. I am thankful to Silvia Heller for her friendly helping nature and nice working atmopshere.

Friends have always been my strength and it is a delight to acknowledge all those who have been with me for various periods. Specially, I would like to address thanks to my dear wife **Dr Manvi Porwal** for her immense love, support, suggestion and patience. I also would like to acknowledge my parents **late Mr. Karnati Sathyanarayana** and **Mrs. Swarajya Laxmi**, my parent in-laws **Dr. R.K. Porwal, Mrs. Renu Porwal**, my sisters, and all family members and friends for their continuous support and encouragement through out my thesis work.

Original und übersichtarbeiten

Original- und Übersichtsarbeiten

I

Karnati S*, Graulich T, Oruqaj G, Pfreimer S, Seimetz M, Stamme C, Mariani TJ, Weissmann N, Mühlfeld C, Baumgart-Vogt E (2016). Postnatal development of the secretory cells of the distal airways, the bronchiolar club cells in the mouse lung: stereological and molecular biological studies. *Cell and Tissue Research*. Jun;364(3):543-57.

II

Karnati S, Baumgart-Vogt E (2009) Peroxisomes in airway epithelia and future prospects of these organelles for pulmonary cell biology. *Histochem Cell Biol.* Apr: 131(4):447-54.

III

Karnati S, Lüers G, Pfreimer S and Baumgart-Vogt E (2013) Manganese Superoxide dismutase 2 (MnSOD) is localized to mitochondria but not in peroxisomes. *Histochemistry and Cell Biology*, Aug:140(2):105-17

IV

Karnati S, Palaniswamy S, Alam MR, Orujaj G, Stamme C, Baumgart-Vogt E (2015) C22-bronchial and T7-alveolar epithelial cell lines of the immortomouse are excellent murine cell culture model systems to study pulmonary peroxisome biology and metabolism. *Histochemistry and Cell Biology* Mar;145(3):287-304.

Oruqaj G[§], **Karnati S[§]**, Vijayan V, Kotarkonda LK, Boateng E, Zhang W, Ruppert C, Günther A, Shi W, Baumgart-Vogt E (2015) Compromised peroxisomes in idiopathic pulmonary fibrosis, a vicious cycle inducing a higher fibrotic response via TGF- β signaling. *Proc Natl Acad Sci.* 112(16):E2048-57.

[§] both authors contributed equally to the study.

VI

Boateng E, El-Merhie N, Trompak O, Tumpara S, Seimetz M, Pilatz A, Baumgart-Vogt E, **Karnati S*** (2016) Targeting PPAR γ in Lung fibroblasts: Prospects of therapeutic treatment for IPF. *PVRI Chronicle* vol 3, issue 2, p33-37

VII

Vijayan V, Tumpara S, **Karnati S**, Garikapati V, Linke M, Kamalyan L, Mali SR, Sudan K, Kollas A, Schmid T, Schulz S, Spengler B, Weichhart T, Immenschuh S, Baumgart-Vogt E (2017) A new immunomodulatory role for peroxisomes in macrophages activated by the TLR-4 ligand LPS. *Journal of Immunology* Mar 15;198(6):2414-2425

Postnatal development of the bronchiolar club cells of distal airways in the mouse lung: stereological and molecular biological studies

Srikanth Karnati¹ · Tilman Graulich² · Gani Orujaj¹ · Susanne Pfreimer¹ · Michael Seimetz³ · Cordula Stamme⁴ · Thomas J. Mariani⁵ · Norbert Weissmann³ · Christian Mühlfeld^{6,7} · Eveline Baumgart-Vogt¹

Received: 22 March 2015 / Accepted: 17 December 2015 / Published online: 21 January 2016
© Springer-Verlag Berlin Heidelberg 2016

Abstract Club (Clara) cells are nonciliated secretory epithelial cells present in bronchioles of distal pulmonary airways. So far, no information is available on the postnatal differentiation of club cells by a combination of molecular biological, biochemical, and stereological approaches in the murine lung. Therefore, the present study was designed to investigate the changes in the club cell secretory proteins (CC10, surfactant proteins A, B and D) and club cell abundance within the epithelium of bronchioles of distal airways during the postnatal development of the mouse lung. Perfusion-fixed murine lungs of three developmental stages (newborn, 15-day-old and adult) were used. Frozen, unfixed lungs were used for cryosectioning and subsequent laser-assisted microdissection of bronchiolar epithelial cells and RT-PCR analyses. High resolution analyses of the three-dimensional structures and composition of lung airways were obtained by scanning electron microscopy. Finally, using

design-based stereology, the total and average club cell volume and the volume of secretory granules were quantified by light and transmission electron microscopy. Our results reveal that murine club cells are immature at birth and differentiate postnatally. Further, increase of the club cell volume and number of intracellular granules are closely correlated to the total lung volume enlargement. However, secretory granule density was only increased within the first 15 days of postnatal development. The differentiation is accompanied by a decrease in glycogen content, and a close positive relationship between CC10 expression and secretory granule abundance. Taken together, our data are consistent with the concept that the morphological and functional differentiation of club cells is a postnatal phenomenon.

Keywords Clara · CC10 · Stereology · Lung · Electron microscopy · Surfactant proteins · BASCs

Electronic supplementary material The online version of this article (doi:10.1007/s00441-015-2354-x) contains supplementary material, which is available to authorized users.

✉ Srikanth Karnati
Srikanth.Karnati@anatomie.med.uni-giessen.de;
<http://www.med.uni-giessen.de/anat/>

✉ Eveline Baumgart-Vogt
Eveline.Baumgart-Vogt@anatomie.med.uni-giessen.de;
<http://www.med.uni-giessen.de/anat/>

¹ Institute for Anatomy and Cell Biology II, Division of Medical Cell Biology, Justus Liebig University, Aulweg 123, D-35385 Giessen, Germany

² Department of Trauma, Hannover Medical School, Hannover, Germany

³ Excellence Cluster Cardio-Pulmonary System (ECCPS), Member of the German Center for Lung Research (DZL), Universities of Giessen

and Marburg Lung Center (UGMLC), Justus Liebig University Giessen, Giessen, Germany

⁴ Division of Cellular Pneumology, Research Center Borstel, Leibniz-Center for Medicine and Biosciences, Borstel, Germany and Department of Anesthesiology, University of Lübeck, Lübeck, Germany

⁵ Division of Neonatology and Pediatric Molecular and Personalized Medicine Program, University of Rochester Medical Center, Rochester, NY, USA

⁶ Biomedical Research in Endstage and Obstructive Lung Disease Hannover (BREATH), Member of the German Center for Lung Research (DZL), Hannover, Germany

⁷ Institute of Functional and Applied Anatomy, Hannover Medical School, Hannover, Germany

Introduction

The nonciliated columnar cell, formerly called Clara cell, is one of the two types of secretory epithelial cells present in distal airways in mammals. It was recently renamed club cell and the term “Clara cell *secretory* protein” was also replaced by club cell *secretory* protein by a Forum of International Respiratory Societies (Irwin et al. 2013; Winkelmann and Noack 2010). In the adult mouse lung, club cells are well characterized by specific secretory dense granules, large peroxisomes and mitochondria with only a few cristae and abundant smooth endoplasmic reticulum (Kamati and Baumgart-Vogt 2008; Plopper et al. 1980).

The terminal bronchiole is the last part of the distal conducting airways that undergoes continuous cellular maturation, where club cells constitute the majority of the bronchiolar epithelium in rodents (Plopper et al. 1983b). Although extensive morphological and transgenic studies on club cells were performed in previous years, their physiological functions in pulmonary biology have not yet been entirely clarified. To date, known parts of their major functions include (1) a progenitor/stem cell role for ciliated cells or self-renewal (Gras et al. 2013), (2) metabolism of xenobiotic materials via the P450 monooxygenase system (Plopper et al. 1993), and (3) immunomodulatory function exhibiting anti-inflammatory and cytokine-decreasing properties (Singh and Katyal 1984). Moreover, club cells synthesize the club cell 10-kDa marker protein CC10 and the surfactant proteins (SP) A, B, and D.

The postnatal differentiation of club cells has been analyzed by stereological methods in different species such as rats (Massaro et al. 1984), rabbits (Plopper et al. 1983a) and monkeys (Plopper et al. 1986). However, in mouse lungs, only a single study has addressed the postnatal differentiation of club cells exclusively at electron microscopic level (Ten Have-Opbroek and De Vries 1993). In addition, several studies have focused on the club cell differentiation either by staining for club cell secretory proteins or its enzyme activity (Fanucchi et al. 1997a, b). However, no knowledge is available on morphological and functional differentiation of the club cells by a combination of techniques through different analyses via light and electron microscopic techniques in conjunction with design-based stereology in the murine lung, as well as laser microdissection molecular analyses of specific mRNAs and proteins. However, more information on this cell type especially in mice is desirable to elucidate club cell biology and pathology from both functional and comparative points of view through various postnatal stages. Indeed, the small conducting airways of the lung are the most important targets of early dysfunction in the pathogenesis of chronic bronchitis and emphysema, for the study of which mouse models are frequently used (Cosio et al. 1978; Cudmore et al. 1962). Furthermore, club cell secretory proteins are strongly reduced in chronic lung disease such as asthma, chronic obstructive pulmonary

disease (COPD), and post-transplant obliterative bronchiolitis. It has been proposed that CC10 protein levels could act as a biomarker for club cell damage (Bernard et al. 1992; Bourdin et al. 2012; Jorens et al. 1995; Shijubo et al. 1999; Van Vyve et al. 1995). Mice deficient in CC10 are susceptible to hyperoxia-induced pulmonary injury and display an altered composition of epithelial airway lining fluid (Johnston et al. 1997; Stripp et al. 2002). Of note, CC10 controls the integrity of airways and mediates a swift repair response to injury, partly through their self-renewal and differentiation properties (Gras et al. 2013).

Therefore, the purpose of this study was to characterize the differentiation of club cells of distal airways by a combined light and fluorescence microscopic, scanning and transmission electron microscopic approach together with design-based stereology of the mouse lungs, as well as microdissection with subsequent RT-PCR analysis. We used different stages of postnatal lung development (newborn, 15-day-old and adult lungs) (1) to analyze the gene expression of distinct club cell secretory proteins, (2) to investigate structural modifications by characterizing the surface of club cells, (3) to characterize the morphology of the club cells and their secretory granules, and (4) to quantify the alterations of the secretory granules during postnatal differentiation of terminal bronchioles.

Materials and methods

Experimental animals

Fifteen adult (12 weeks of age) male mice, ten 15-day-old males and ten newborn male pups of C57BL/6 J genetic background were obtained from Charles River, Sulzfeld, Germany. The mice were kept on a normal laboratory diet and water ad libitum and housed in cages under standardized environmental conditions (12 h light/dark cycle, 23 °C ± 1 °C and 55 % ± 1 % relative humidity) at the central animal facility (ZTL) of the Justus Liebig University, Giessen. After delivery of the newborn pups in the morning, they were taken directly out of the animal facility. All experiments with laboratory mice were approved by the governmental ethics committee for animal welfare (Regierungspräsidium Giessen, Germany, permit number: V 54–19 C 20/15 c GI 20/23). CC10 wild-type and KO lung paraffin blocks were a kind gift from the Barry Strip group (Departments of Medicine and Cell Biology, Duke University Medical Center, Durham, NC, USA).

Perfusion fixation, sampling and tissue processing for light microscopy (LM) and transmission electron microscopy (TEM)

Five animals per group (P15 and adult) were killed by cervical dislocation and the newborn pups were killed by decapitation. The lungs were fixed by vascular perfusion fixation through

the right ventricle with 1.5 % paraformaldehyde, 1.5 % glutaraldehyde in 0.15 M Hepes buffer, pH 7.4 and additional tracheal instillation with the same fixative at a hydrostatic pressure of 20 cm H₂O for 2 min. The trachea was ligated around the cannula to prevent outflow of the fixative. The lungs were excised and the total lung volumes of the left and right lung were gained separately by Archimedes' principle (Scherle 1970). The left and right lungs were each cut longitudinally into approximately 1-mm-thick slices. Tissue samples were taken from different regions and were randomly assigned for either LM or TEM using systematic uniform random sampling (Gundersen and Jensen 1987; Mayhew 2008). Each slice for TEM preparation was once again sampled and cut into 1-mm³ blocks and further immersion-fixed in the same fixative for another 24 h. Due to this sampling method, all parts of lung regions had an equal chance of being selected for the analysis. Thereafter, tissue blocks were rinsed for 1 h in 0.1 M cacodylate buffer (4–6 changes), postfixed in 1 % osmiumtetroxide in aqua dest for 2 h at room temperature and washed several times in 0.1 M cacodylate buffer. After a short rinse in aqua dest, the samples were contrasted en bloc with half-saturated aqueous uranyl acetate for 18–24 h at 4 °C. Thereafter, the blocks of tissue were rinsed several times with distilled water and dehydrated in a series of ascending percentages of watery acetone solutions (70–100 % acetone) and embedded into the epoxid Agar 100 Resin[®] (Agar Scientific, Stansted, UK) followed by polymerization for 3 days at 60 °C. Embedded tissue blocks were trimmed with a diamond trimmer (Reichert TM 60; Austria) and ultrathin sections (80 nm) were cut with a Leica Ultracut E ultramicrotome (Leica, Nussloch, Germany). Ultrathin sections were collected on formvar-coated nickel grids and contrasted with uranyl acetate for 2 min and lead citrate for 45 s, followed by examination in a LEO 906 TEM (LEO Electron Microscopy, Oberkochen, Germany) equipped with a 2k-camera (TRS; Troendle Systems, Göttingen, Germany).

For LM, tissue slices were embedded in the glycol methacrylate resin Technovit 7100 (Heraeus Kulzer, Wehrheim, Germany). Briefly, for light microscopy, the samples were postfixed with 0.5 % osmiumtetroxide in water followed by half-saturated aqueous uranyl acetate, dehydrated in a series of ascending percentages of acetone–water solutions (70–100 % acetone), infiltrated with the methacrylate solution and finally polymerized in the glycol methacrylate overnight. Semi-thin sections of 1.5 μm thickness were cut and stained with the methylene blue-based Richardson's stain.

Stereology

Stereological analyses were performed with an Olympus BX51 LM (Olympus, Hamburg, Germany) using an Olympus DP72 digital camera and a computer with the

newCast software (Visiopharm, Horsholm, Denmark) or a LEO 906 TEM (LEO Electron Microscopy). For LM and TEM, systematic uniform random fields of view (FOV) were generated from the lung (Muhlfeld and Ochs 2013; Ochs and Muhlfeld 2013). Each FOV was included and point counting for volume density was performed (Table 1) (Weibel 1979). Points hitting a compartment of interest (P(comp)) and the reference volume (P(ref)) were counted and the volume fraction of the compartment was then calculated by $V_V(\text{comp}/\text{ref}) = P(\text{comp})/P(\text{ref})$. Using the single-section disector and the rotator, the number-weighted mean volume of club cells was calculated (Howard and Reed 2005; Sterio 1984; Vedel Jensen and Gundersen 1993), whenever a cell was sampled based on the appearance of a nucleolus, the rotator was used to provide a measure of the cell volume. From the whole estimates of one animal, the arithmetic mean was calculated (v_N). All other formulas are given in Table 4.

Post-embedding immunoelectron microscopy

To test the specificity of the CC10 antibody and to analyze its localization to the correct intracellular compartment (secretory granules in club cells) post-embedding immunoelectron microscopy was performed on adult mice samples (see Table 1 and immunofluorescence). The detailed protocol for perfusion fixation, processing of lungs, embedding into LR white and post-embedding immuno-EM with protein A-gold method was described previously (Karnati and Baumgart-Vogt 2008, 2009). Briefly, ultrathin sections of lung tissue were incubated overnight in a wet chamber with CC10 antibody [1:200 in 0.1 % BSA in TBS (TBSA); see Table 1]. The next morning, the sections were washed on a series of 12 TBSA drops. Subsequently, the grids were incubated for 60 min with the protein A-gold complex (PAG, gold particle size 15 nm) diluted 1:75 in TBSA (Slot and Geuze 1981). Thereafter, the grids with sections were washed briefly in a flow of distilled water and air-dried. Incubated sections were contrasted with uranyl acetate for 2 min and lead citrate for 45 s followed by examination in a LEO 906 TEM.

Scanning electron microscopy (SEM)

Three animals per group (P15 and adult) were killed by cervical dislocation and newborn pups were decapitated and the lungs were fixed by vascular perfusion fixation as mentioned above in 2. After fixation, the lung samples were rinsed 3 × 10 min each with 0.15 M Hepes buffer, pH 7.4 at RT. Thereafter, the lungs were again postfixed with 1 % osmiumtetroxide in distilled water for 1 h. After washing with water, the samples were dehydrated through a graded series of ethanol (30–100 %, 2 min each). The SEM samples were

Table 1 List of primary and secondary antibodies

Primary antibodies	Host	Dilution (IF)	Dilution (WB)	Supplier
Club cell protein 10 (CC10)	Rabbit, polyclonal	1:1,000	1:1,000	Santa Cruz, Cat no: sc-25555
Surfactant protein A (SP-A), rabbit	Rabbit, polyclonal	1:1,000	1:1,000	Chemicon, Cat. no: AB3420
Surfactant protein B (SP-B), rabbit	Rabbit, polyclonal	–	1:5,000	Santa Cruz, Cat no: sc-13798
Pro surfactant protein C (SP-C), rabbit	Rabbit, polyclonal	1:1,000	–	Chemicon, Cat. no: AB3786
β -actin, human	Rabbit, polyclonal	–	1:3,000	Abchem, Cat no: AB8227
Secondary antibodies	Host	Dilution		Supplier
Anti-Rabbit-IgG AlexaFluor488	Donkey	1:1,000		Molecular Probes/Invitrogen, Cat. no: A21206
Anti-Goat-IgG AlexaFluor594	Chicken	1:1,000		Molecular Probes/Invitrogen, Cat. no: A11058
Counterstaining of nuclei for immunofluorescence				
Hoechst 33342 (1 μ g/ml)	-	1:1,000		Molecular Probes/Invitrogen, Cat. no: 33342
TOTO [®] -3 iodide	-	1:1,000		Molecular Probes/Invitrogen, Cat. no: T-3604

critical point dried in a Balzers apparatus using CO₂ as the transitional fluid (Peao et al. 1992a, b). The dried blocks of remaining lung tissue were dissected longitudinally through the lumen of the mediastinal airways extending from the lobar bronchus to the distal airways. The preparations were mounted onto metal stubs fixed with Leit-C overnight and subjected to sputter coating by gold under vacuum (Polaron E5000 Sputter coater; Quorum, UK). They were examined in a Philips XL30 SEM.

Immunofluorescence

The detailed protocol for perfusion fixation, paraffin-embedding, sectioning of tissues and subsequent immunofluorescence for newborn, P15 and adult lungs has been described previously (Kamati and Baumgart-Vogt 2008, 2009). Briefly, perfusion-fixed lungs (4 % PFA in PBS, pH 7.4) were embedded into paraffin (Paraplast; Sigma, St. Louis, MO, USA) using a Leica TP 1020 automated vacuum infiltration tissue processor. Paraffin sections (2 μ m) were cut with a Leica RM2135 rotation microtome and processed for double immunofluorescence. Dilutions of the primary and secondary antibodies used are listed in Table 1. Negative controls for secondary antibody reaction were processed in parallel by addition of TBST buffer instead of the first antibodies. Nuclei were visualized with 1 μ M TOTO-3 iodide for 10 min at RT. Samples were analyzed by confocal laser scanning microscopy (CLSM) with a Leica TCS SP2 (Leica Mikrosysteme Vertrieb, Wetzlar, Germany). All images were processed with Adobe Photoshop CS2 (v.9).

Laser capture microdissection (LCM)

Newborn, P15, and adult lungs were isolated without fixation and embedded directly into a cryo-preserved solution (Optimal Cutting Temperature; Tissue-Tek) in freezing molds

and placed in liquid nitrogen. In preparation for LCM, frozen tissues were taken out of the liquid nitrogen and mounted quickly without thawing on tissue holders and sectioned at -20 °C. Next, 10 μ m thick cryosections were mounted on 1-mm polyethylene naphthalate (PEN) membrane-covered slides (Catalogue Nr: 1440–1000; PALM Microlaser Technologies, Bernried, Germany) fixed in 70 % ethanol and 1 min hematoxylin-stained for analysis of morphologic and nuclear details as previously described (Stelzig et al. 2013). The duration of RT exposure before LCM of dried sections was ≤ 10 min. The bronchial epithelial cells, which were identified by their anatomic location and morphology, were then marked on the computer screen (“painted”) and dissected by laser microdissection and pressure catapulting (LMPC) technology (PALM Microlaser Technologies) with the laser using the $\times 20$ objective, a beam width of 7.5 μ m and a beam intensity of 50 mW. Dissected bronchiolar epithelial cells catapulted into the cap of a microfuge tube were treated with lysis buffer (RLT-buffer; Qiagen, Hilden, Germany). All dissected samples were immediately frozen in liquid nitrogen.

RT-PCR for bronchiolar epithelial cells isolated by LCM

Total RNA was isolated from microdissected bronchiolar epithelial cells using the Qiagen microdissection kit (RNeasy Plus Qiagen kit). Reverse-transcription was performed by using the QuantiTect reverse transcription-PCR kit (Qiagen) as recommended by the manufacturer. Briefly, contaminating DNA was destroyed with gDNA Wipeout buffer by incubating the total sample at 42 °C for 2 min followed by addition of 20 μ l of a reverse transcription mixture consisting of 14 μ l sample, 4 μ l RT buffer (Qiagen), 1 μ l QuantiTect reverse transcriptase and 1 μ l of RT primer and incubated for 15 min at 42 °C. The reaction was stopped by increasing the final temperature to 95 °C for 3 min and the sample subsequently placed on ice. The concentration of the resultant

cDNA was measured by using a Bio-Rad spectrophotometer (Bio-Rad, Heidelberg, Germany). The subsequent PCR was performed with a primer concentration of 10 pmol/μl in a Bio-Rad iCycler and the following program: denaturation at 94 °C for 4 min, and 45 cycles of denaturation at 94 °C for 30 s, annealing at 58–64 °C depending on the primer pairs for 30 s, extension at 72 °C for 1 min, and a final round of product elongation at 72 °C for 5 min. The detailed list of primers used for RT-PCR analyses and their conditions are listed in Tables 2 and 3. An amount of 10 μl of each PCR reaction was analyzed on 2 % agarose gels in 1× TAE buffer and bands were visualized under the UV-Transilluminator of the Gel Doc system from Bio-Rad. 28S rRNA served as the housekeeping gene and “Water” negative controls were run in parallel without specific cDNA product. All RT-PCR experiments were performed three times and data is represented from three individual experiments.

Preparation of whole lung homogenates for protein analysis (western blotting)

Dissected lungs from newborn, P15, and adult mice were stored at –80 °C prior to homogenization. The tissues were homogenized with a Potter-Elvehjem homogenizer (Potter-S, B. Braun, Melsungen, Germany) at 1000 rpm (1 stroke, 60 s) in 2 ml ice-cold homogenization buffer (HMB): 0.25 M sucrose and 5 mM MOPS, pH 7.4, 1 mM EDTA, 0.1 % ethanol, 0.2 mM DTT, 1 mM aminocaproic acid and 10 % cocktail of Serva protease inhibitors (Serva, Heidelberg, Germany). The quality of the homogenization process was controlled by trypan blue staining with an LM. Thereafter, homogenates were centrifuged (Multifuge 3 SR; Heraeus, Hanau, Germany) for 20 min at 500g at 4 °C and the supernatant was used for further analysis.

Western blotting

Amounts of 50 μg of protein samples derived from newborn, P15, and adult lungs were separated on 12 % SDS-polyacrylamide gels using a Bio-Rad gel electrophoresis apparatus (BioRad, Munich, Germany). Protein transfer

was done with a semi-dry Trans-Blot apparatus (Biorad) onto a polyvinylidene membrane (Millipore, Schwalbach, Germany) for 50 min at constant 200 V. Nonspecific protein binding-sites were blocked with 10 % non-fat milk powder (Carl Roth, Karlsruhe, Germany) in TBST [TBS plus 0.05 % Tween-20 (blocking buffer)]. Primary antibodies were diluted to the concentrations listed in Table 1 in 5 % blocking solution. The membranes were incubated with appropriate primary antibodies for 1 h at RT on a rotor shaker. After washing with TBST (3 × 10 min), blots were incubated for 1 h with alkaline phosphatase conjugated anti-rabbit IgG antibodies. After a final washing step, immunoreactive bands were visualized with the Immunostar™-AP detection kit (Bio-Rad) with chemiluminescent substrate followed by exposure of the membrane to BioMax MR-films (Kodak, Stuttgart, Germany). Blots of different gels were stripped several times with 10 % SDS and 0.7 % β-mercaptoethanol at 42 °C for 45 min and reprobed with other primary antibodies as described in Table 1.

Statistics

Data are expressed as mean ± standard deviation. Groups were compared with the nonparametric Mann–Whitney *U* test. Data were considered statistically significant if $p < 0.05$.

Results

The CC10 protein is exclusively localized to club cells

Before investigating the number of club cells and the abundance of the CC10 protein during the development of the lung, we opted to detect the subcellular localization of the CC10 protein. We started our investigations to localize the CC10 protein (Cat.no: sc-25555; Santa Cruz) in the lung of wild-type mice in comparison to CC10 knockout mice as controls for the specificity of the CC10 antibody. Our results suggested a specific abundance and localization of the CC10 protein exclusively in club cells of the bronchiolar epithelium whereas ciliated cells (asterisk in Fig. 1b) remained

Table 2 List of primers

Gene target	Gene accession no.	Sense primer (5'-3')	Antisense primer (5'-3')	Annealing temperature °C
<i>CC10</i>	NM_011681	ACTGTGGTCATGCTGTCCATCT	GCAAGTACAAGGCTTTAGCAG	58
<i>SP-A</i>	NM_023134	CCCTCTTCTGACTGTTGTTGCTG	GAGTCTGGCCTTCAATCACACCTA	58
<i>SP-B</i>	BC032785	AATGACCTGTGCCAAGAGTGTGAG	GCCATTCTTCTATCAGAGGCTCCA	58
<i>SP-C</i>	BC061137	CTGATGGAGAGTCCACCGATTAC	GAAGAATCGGACTCGGAACCAGTA	60
<i>SP-D</i>	BC003705	GGACCTCCAGGACTTCCAGGTATT	TGGCAGCATTCTCAGTAGCAGAAC	62
<i>28S rRNA</i>	NR_003279	CCTTCGATGTCGGCTCTTCCTAT	GGCGTTCAGTCATAATCCCACAG	65

Table 3 Methodological details of stereological parameters

Parameter	Section	Staining	Magnification	Probe
$V_V(\text{bronchiole/lung})$	Semithin section	Richardson's stain	$\times 10$	Points (25 per FOV)
$V_V(\text{club cell/bronchiole})$	Ultrathin section	Richardson's stain	$\times 6,000$	Points (25 per FOV)
$V_V(\text{granule/club cell})$	Ultrathin section	Uranyl acetate and Osmium	$\times 6,000$	Points (100 per FOV)
$v_N(\text{club cell})$	Semithin section	Richardson's stain	$\times 100$	IUR Rotator

$V_V(\text{bronchiole/lung})$ volume density of the bronchiole related to the lung, $V_V(\text{club cell/bronchiole})$ volume density of the club cells in the bronchiole, $V_V(\text{granule/club cell})$ volume density of the granule related to the club cell, $v_N(\text{club cell})$ number-weighted mean volume of the club cell

negative (Fig. 1a, b). Of note, the CC10 protein was completely absent in the bronchiolar epithelium of the CC10-deficient mice demonstrating the high mono-specificity of the antibody (Fig. 1c, d). In addition, parallel preparations of negative

controls without the primary antibody remained completely devoid of staining in both WT and CC10-deficient lung tissue strongly suggesting a high specificity of the secondary antibody reaction (Fig. 1e–h).

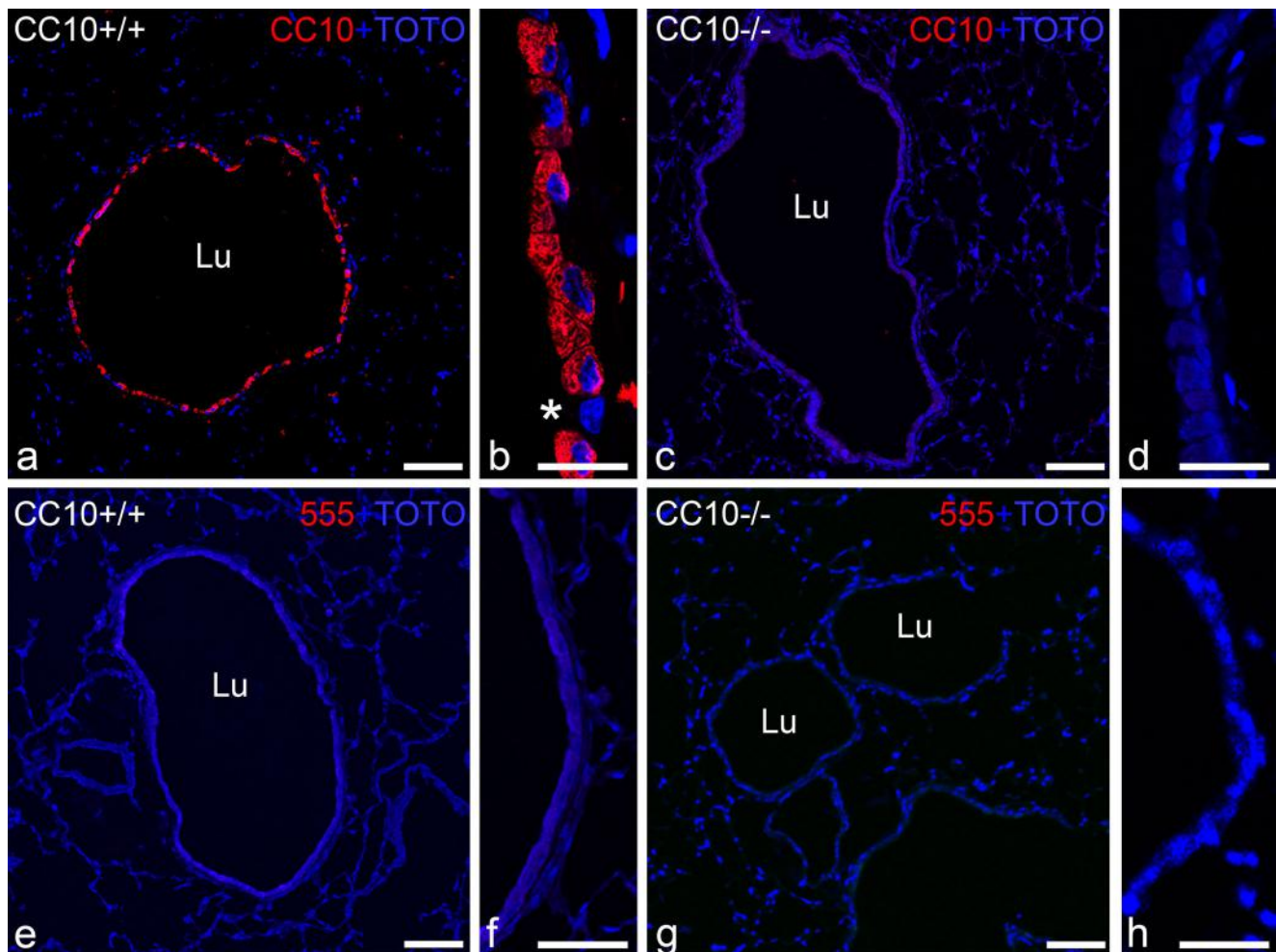


Fig. 1 Immunofluorescence detection of club cell marker protein CC10 in paraffin-embedded adult mouse lung tissue sections of wild-type (a, b) and CC10 knockout mice (c, d). Representative lower (a, c) and higher magnifications (b, d) of cross sections of terminal bronchioles in the mouse lung, stained for the localization of CC10. The CC10 protein is localized to club cells in WT lungs (a, b) whereas CC10 immunoreactivity is completely absent in the CC10 KO lungs (c, d)

demonstrating the high specificity of the antibody reaction. Furthermore, in parallel preparations, negative controls were incubated with anti-goat IgG-Alexa-555 which were completely devoid of staining, seen also in WT lung, suggesting an optimal specificity also of the secondary antibody and the high quality indirect immunofluorescence protocol used (e–h). Asterisk indicates a ciliated cell. Bars (a, c, e, g) 1000 μm , (b, d, f, h) 20 μm

Club cell secretory proteins are upregulated during the postnatal development of the lung and CC10 is exclusively localized to secretory granules

Next, we determined the abundance of the club cell secretory proteins CC10 and SP-A during the postnatal development of the lung by immunofluorescence. Our results revealed an increase in the protein abundance of CC10 and SP-A in club cells during the postnatal lung development. The CC10 protein was only weakly labeled in club cells of the newborn lungs but strongly increased in P15 and adult mice (Fig. 2a–f). Similarly, SP-A was only weakly labeled in club cells of the bronchiolar epithelium, whereas this protein was detected in higher abundance in alveolar epithelial cells type II (AECII) in the newborn lung (Fig. 2g, j). Further, the SP-A abundance was upregulated in 15-day-old lungs (Fig. 2h, k) and showed the strongest staining in adult lungs (Fig. 2i, l). We verified the subcellular localization of CC10 by post-embedding immunocytochemistry with the protein A-gold method on LR white sections of the adult lung. The gold particles were confined exclusively to the secretory granules of club cells depicting the high specificity of the antibody labeling (Fig. 2q). Other cell compartments, such as mitochondria and the nucleus were negative.

Moreover, microdissected bronchiolar epithelial cells were investigated for the expression of corresponding mRNAs of the club cell secretory proteins (Fig. 2m–p). We found an increase in the mRNA expression levels for CC10 and for the surfactant proteins A, B, and D during the postnatal development of the lung (Fig. 2r) which is in line with the data obtained by immunofluorescence. We used the SP-C mRNA as a marker for the quality of the microdissection, since only AECII cells synthesize SP-C and club cells do not produce SP-C (Fig. 2r). Further, western blot analysis revealed specific band patterns showing alterations of protein abundance for CC10, SP-A and SP-B in total homogenates during postnatal lung development. Indeed, the relative amount of these proteins was lower in newborn lungs and higher in 15-day-old and adult lungs (Fig. 2s). Overall, club cell secretory proteins and their mRNAs increased during the postnatal development of the lung, suggesting that club cell maturation occurs postnatally.

Surface view of club cells during postnatal development of the lung: observations by scanning electron microscopy (SEM)

In order to study the morphological surface alterations of the bronchiolar epithelium during the postnatal pulmonary development, lungs from newborn, 15-day-old, and adult mice were processed for SEM analysis (Fig. 3). Surface SEM views of the luminal side of bronchioles suggest the distinction of two types of cells defined by the presence or absence of cilia

(Fig. 3b, c, e–g, i–k). Club cells were scattered among the ciliated cells and displayed smooth and round surfaces facing the lumen of the bronchioles. Moreover, the club cells showed the typical anatomical features by the presence of dome-shaped projections (Fig. 3e–f, i–j). These apical dome formations were readily visible because they protruded from the epithelial surface into the bronchiolar lumen (arrowheads in Fig. 3f). While some of the club cells of newborn lungs possessed microvilli (Fig. 3c), in 15-day-old (Fig. 3e–g) and adult lungs (Fig. 3h–j), many of them were devoid of microvilli. Scanning electron microscopy of the luminal surface of the terminal bronchioles of different lung stages (NB, P15 and adult) demonstrated progressive ciliation (Fig. 3). After careful observations of bronchiolar areas, our results revealed that different phases in the surface of club cells were associated with secretion and release of the apical cytoplasm. Initially, formation of papillary projections extruding towards the bronchiolar lumen (P in Fig. 3j) was followed by a narrowing of the base of this projection and the formation of a cap-like body (C in Fig. 3k). Finally, the projections were either attached (white arrow in Fig. 3j) or detached (O in Fig. 3k) and appeared as separate bodies on the epithelial surface.

Stereologic analysis reveals a significant increase in total lung volume, bronchioles and club cells in 15-day-old mice in comparison to newborn lungs

The mean body weight increased from 1.41 ± 0.05 g in NB to 7.74 ± 0.038 g in 15-day-old mice and 22 ± 0.63 g in adult animals. The total lung volume increased $9.2\times$ from newborn to P15 animals ($P=0.004$) and increased $1.8\times$ from P15 to adult mice ($P=0.016$) (Fig. 4d). Further, bronchiole volume increased $7.2\times$ from newborn to P15 animals ($P=0.016$) (Fig. 4e), and the club cell volume increased $6.6\times$ from newborn to P15 animals ($P=0.032$) (Fig. 5d). We did not observe a statistically significant increase in the bronchiole volume and club cell volume between P15-day-old to adult lungs. The main results are presented in Table 4.

Postnatal changes in club cells and club cell secretory granules

Figure 5 shows the ultrastructure of club cells from newborn (A), 15-day-old (B) and adult mice (C). Two striking differences were clearly visible: (1) newborn murine club cells contain an enormous amount of glycogen (marked with asterisk), and (2) the club cells from the 15-day-old (B) and from the adult (C) contain a greater volume of secretory granules. Indeed, very few secretory granules were detected in the newborn mouse club cells even after an extensive search. The club cells underwent remarkable intracellular changes and increased in their total volume during the postnatal development of the lung (Fig. 5a–c). However, a significant increase in club

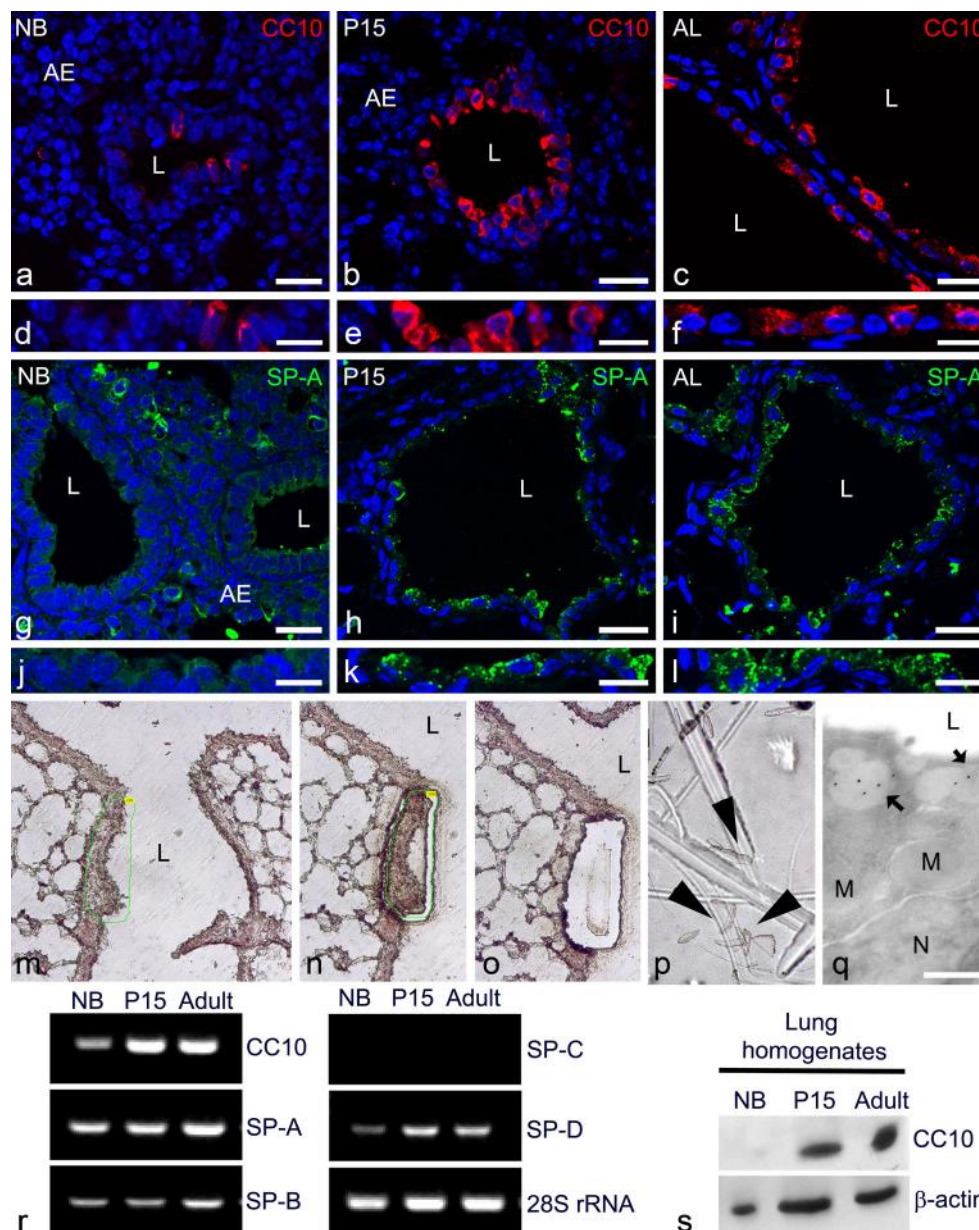


Fig. 2 Immunofluorescence detection of club cell marker proteins during the postnatal development of the mouse lung. Paraffin-embedded mouse lung tissue sections of newborn, 15-day-old and adult lungs were stained either with CC10 (a–c) or SP-A (g–i). Respective higher magnifications of these stainings are also depicted in (d–f) for CC10 and (j–l) for SP-A. Note that CC10 and SP-A protein abundance increased during postnatal lung development. Microdissection of bronchial epithelial cells isolated from newborn, P15, and adult lungs as well as RT-PCR analysis for specific mRNAs of club cell secretory proteins (m–p). All lung sections were stained with hematoxylin (m), the bronchiolar epithelium was marked (n)

and with the help of laser energy the marked sections were catapulted (o) into the lid of an Eppendorf tube (p). By post-embedding immunoelectron microscopy CC10 was exclusively localized to the secretory granules of the club cells (q). RT-PCR analysis for the amplification of specific mRNAs of club cell secretory proteins (r). For gene abbreviations and primer sequences, see Table 2. Western blot analysis of lung homogenates with affinity-purified antibodies to CC10 (s). Arrowheads microdissected regions, L lumen of the bronchioles, AE alveolar epithelium, N nucleus, M mitochondria. Arrows represent club cell secretory granules (q). Bars (a–c, g–i) 25 μ m, (d–f, j–l) 10 μ m, (q) 0.5 μ m

cell volume could only be measured in newborn versus 15-day-old and newborn versus adult but not in 15-day-old to adult mice (Fig. 5d). Furthermore, the total number of club cells in the lung increased 10 times during the first 15 days and nearly doubled from P15 to adult lungs. Our stereology analyses showed that the volume of intracellular secretory

granules in the lung significantly increased from newborn to P15 (214 \times) but not in 15-day-old to adult mice (Fig. 5e). Since the values were highly variable in P15 lungs, we did not observe a statistically significant increase ($p=0.095$) in the volume of club cell secretory granules between 15-day-old to adult lungs (Fig. 5e). Overall, there were changes between

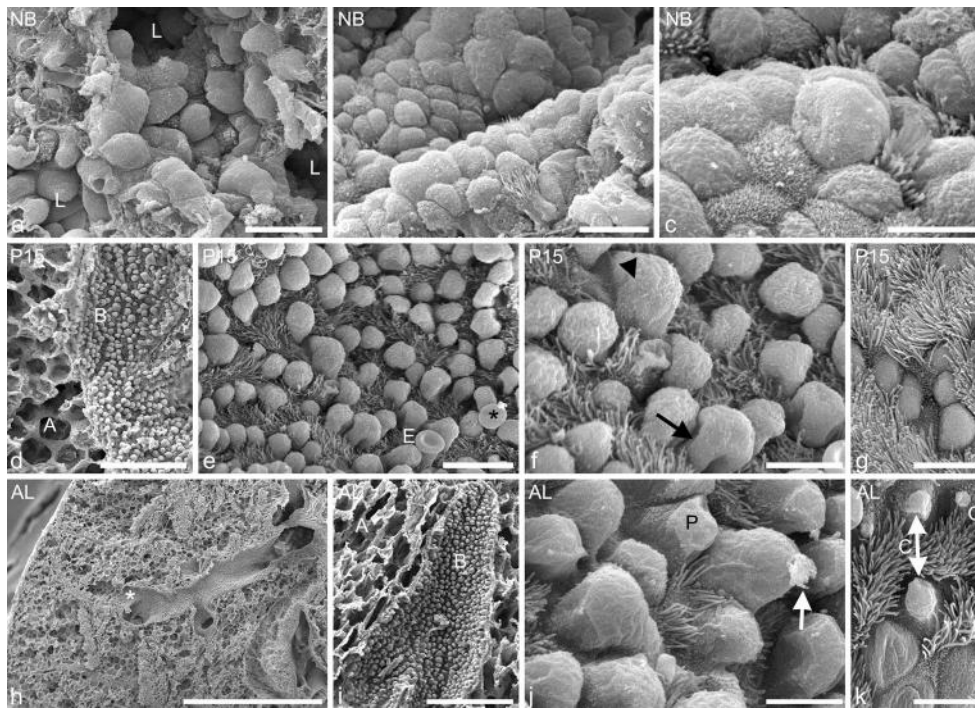


Fig. 3 Scanning electron microscopy (SEM) images of the surface of the terminal bronchiolar epithelium during postnatal development of the lung. **a** Lumen (*L*) of three terminal bronchioles of the newborn mouse lung. **b** View of luminal side of bronchiolar epithelial cells allowing the distinction of ciliated cells and club cells. **c** Higher magnification of ciliated cells and club cells. **d** SEM view showing the luminal side of bronchiolar epithelial cells (*B*) adjacent to the alveolar region (*A*) of a 15-day-old mouse lung. Ciliated cells and club cells can be clearly separated in these images. Club cells can be easily identified since they lack cilia. **e** Low magnification view of the bronchiolar surface with dome-shaped club cells projecting into the lumen and neighboring ciliated cells. Extrusion of the club cell secretory granules (*asterisk*) with neighboring erythrocyte (*E*). **f** High-magnification view of the apical dome-shaped cytoplasm of club cells with microvilli (*arrowhead*). Formation of thin

pedicles (*black arrow*), linking 2 cap-like bodies to the cytoplasm of two different club cells. **g** Higher-magnification views of the apical processes of the club cells, the surfaces of which are relatively smooth and protrude into the bronchiolar lumen. Note the increase in ciliation with age in comparison to the newborn lungs (**c**). **h** Low-magnification view of the terminal bronchiole and ductus alveolaris from adult mouse lung. **i** SEM view showing the luminal side of bronchiolar epithelial cells (*B*) adjacent to the alveolar region (*A*) of an adult mouse lung. **j** Increase in the length of apical dome-shaped club cells in adult in comparison to 15-day-old lungs (**e**). In particular, papillary projection (*P*) of the apical cytoplasm and extrusion of club cell granules before detachment (*white arrow*). Of interest, protrusions of apical cytoplasm of club cells towards the luminal side are above the cilia **k** Formation of cap-like body (*C*) and released cap-like bodies (*O*). Bars 5 μm

the P15 to adult animals but the precision of the estimates in combination with the low number of animals precluded to reach statistical significance in these two groups. Further, secretory granule density growth per bronchiole was only increased during the first 15 days (16.8 \times) compared to adult animals (0.9 \times). By the same token, the volume of secretory granule growth per club cell was also increased during the first 15 days (18.4 \times) compared to adult animals (0.9 \times). Furthermore, the number of secretory granules comprised 0.4 % of the total club cell volume in newborn lungs and 7.7 % in P15 and 6.9 % in adults (Table. 4; Fig. 5f). The mean club cell volume showed no statistical differences between all groups.

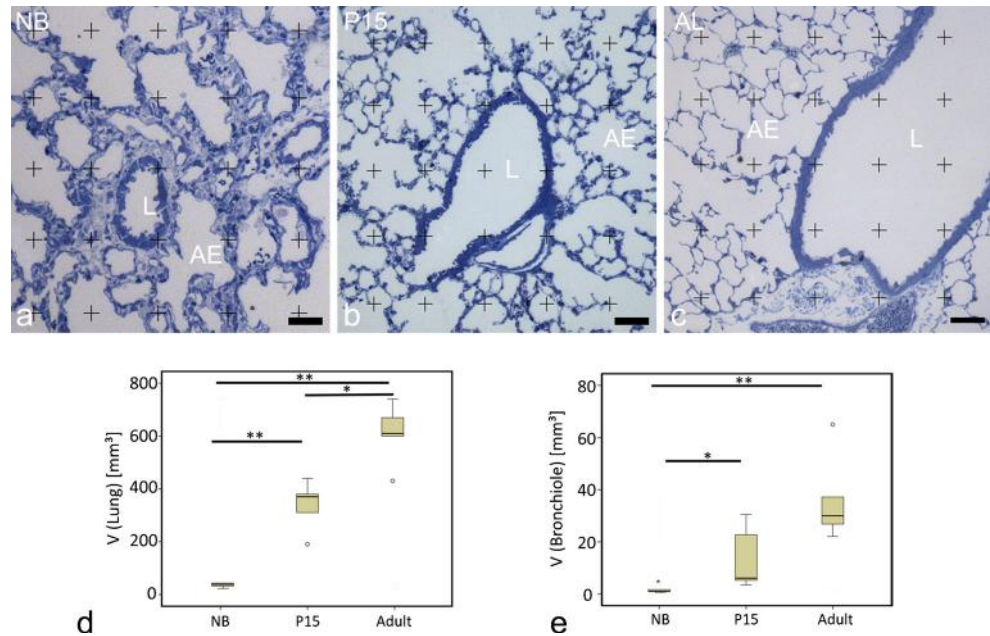
Discussion

Club cells, non-ciliated bronchiolar secretory epithelial cells, were first described as a morphologically distinct cell type by Kölliker in 1881, but were named Clara cells due to the seminal

study of human and rabbit bronchioles by Max Clara in 1937 (Clara 1937). Later, club cells were also identified in intra- and extrapulmonary airways of rabbits (Plopper et al. 1993). However, in our study, we mainly focused on the club cells of the distal airways during postnatal development of the mouse lung addressing their morphological and functional changes. Indeed, no detailed morphometric reports exist on club cell differentiation in the mouse lung based on design-based stereology.

An important aspect of our stereologic study was to select the club cells from the same anatomic location in the lungs of animals of newborn, 15-day-old and adult groups. Therefore, we have been able to demonstrate the changes in these cells over time. However, it must be pointed out that the distal airways may rearrange as the lung matures (Jeffery 1977). We therefore have employed the sampling procedure as rigorously as possible by conducting a large sample embedding procedure for light and electron microscopy (Hill and Plopper 1979; Lowrie and Tyler 1973). Based on these criteria, we quantitatively described the postnatal changes of

Fig. 4 Light microscopic images of lung parenchyma of newborn, P15 and adult mice subjected to stereological analysis. A point counting grid was placed onto the images for volume density analysis of bronchioles in the lung at magnification of $\times 10$ (a–c). Box plots of calculated values for total lung volume V (Lung) (d) and total bronchiole volume V (Bronchiole) (e). * = $p < 0.05$, ** = $p < 0.01$. L lumen of the bronchiole, AE alveolar epithelium. Bars (a–c) 50 μm



club cells and club cell secretory granules during the lung development. Our results from adult mice (C57/Bl 6 J) revealed that the majority (64 % of the volume) of bronchiolar epithelial cells lining the distal airways were club cells. In comparison, Fanucchi and colleagues described a higher percentage (77 %) club cells in the bronchiolar epithelium of

Swiss webster mice (Fanucchi et al. 1997a). This difference might be explained by either distinct mouse strain or different environmental conditions of the animals used. Interestingly, relative changes in the club cell volume fraction during post-natal lung development are comparable to the results obtained by Fanucchi and colleagues (Fanucchi et al. 1997a).

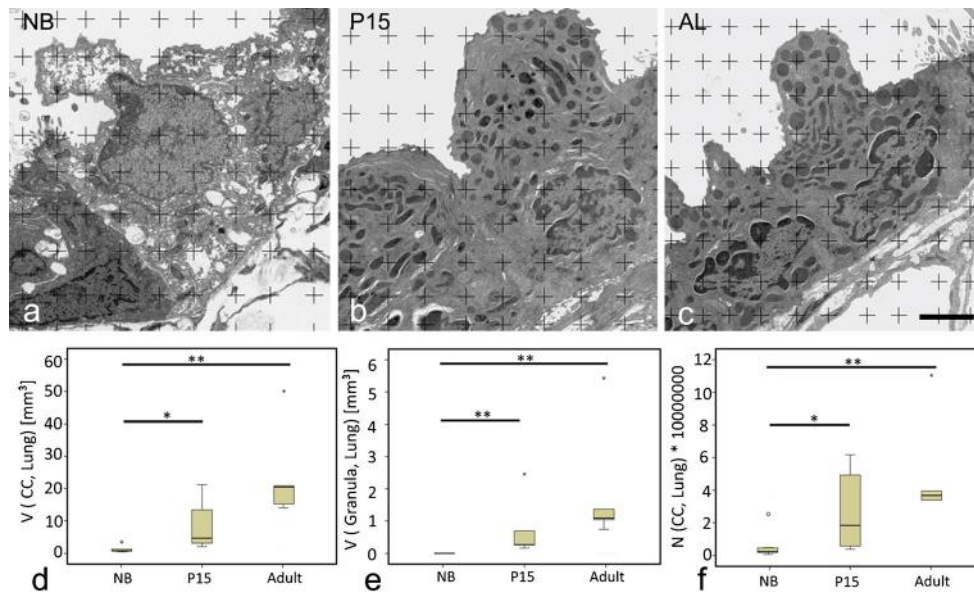


Fig. 5 Transmission electron micrographs of bronchioles containing club cells subjected to stereological analysis during the postnatal developmental stages of the lung. A point counting grid was placed onto the images for volume density of intracellular granules at a magnification $\times 6000$. Points hitting secretory granule structures and points hitting cell areas were counted and used to calculate the volume fraction of secretory granule in relation to club cell. Volume in combination with number and cell volume estimation, the total secretory granule volume can be calculated per cell and per lung (see

Table 4). White arrows showing club cell granules (b, c). Note the presence of abundant electron lucent glycogen fields in newborn club cells (asterisk in a). These areas were hardly visible in the 15-day-old (b) and adult mice (c). Box plots of calculated values for volume of club cells per lung volume, V (CC, Lung) (d), volume of club cell granules per lung volume V (Granule, Lung) (e) and number of club cells N (CC, Lung) (f). * $p < 0.05$, ** $p < 0.01$. CL club cell, CC ciliated cell, BL basal lamina. Bars (a–c) 5 μm

Table 4 Summary of stereological data

Parameter	Newborn	P15	Adult	<i>p</i> value
V(lung) [mm ³]	36.70 ± 7.03	338.00 ± 84.00	610.00 ± 102.00	0.016, 0.004, 0.004
V(Bronchiole, lung) [mm ³] = V _v (Bronchiole/lung)*V(lung)	1.87 ± 1.55	13.63 ± 10.88	36.21 ± 15.24	0.095, 0.008, 0.016
V(Club cell, lung) [mm ³] = V _v (CC/bronchiole)*V _v (bronchiole/lung)*V(lung)	1.35 ± 1.10	8.90 ± 7.32	24.13 ± 13.26	0.095, 0.008, 0.032
V(granule, lung) [mm ³] = VV(granule/CC)*V _v (CC/bronchiole)*V _v (bronchiole/lung)*V(lung)	0.0036 ± 0.0020	0.7714 ± 0.8633	1.9325 ± 1.7615	0.095, 0.008, 0.008
V(granule, lung)/V(bronchiole, lung) [mm ³ /mm ³]	0.0030 ± 0.0024	0.0505 ± 0.0165	0.0465 ± 0.0201	0.690, 0.008, 0.008
v _N (CC) [μm ³] = ΣV(CC)/N(CC)	474 ± 175	395 ± 134	513 ± 82	0.222, 0.690, 0.310
N(CC, lung)/1000000 = V(CC, lung)/ Volume rated mean volume(CC, lung)	2.87 ± 1.60	27.82 ± 23.52	49.13 ± 30.98	0.421, 0.008, 0.032

V(lung) total lung volume measured by water displacement, V(bronchiole, lung) total volume of lung bronchiole calculated by determining the bronchiole density in the lung [V_v(bronchiole/lung)] and multiplication with the total lung volume, V(club cell, bronchiole) means the total volume of club cells in the lung determined by multiplication of the CC density in the bronchiole [V_v(CC/bronchiole)] with the volume density of the bronchiole in the lung [V_v(bronchiole/lung)] and the total lung volume [V(lung)], V(granule, lung) total volume of the club cell granule in the lung determined by multiplication of the granule density in the CC [VV(granule/CC)] with the CC density in the bronchiole [V_v(CC/bronchiole)] with the volume density of the bronchiole in the lung, v_N(club cell) number-weighted mean volume of the club cells determined by division of the sum of the counted club cells in the lung [ΣV(club cells)] and the total number of all counted club cells [(N (club cells), N(club cells, lung)] total number of club cells in the lung determined by division of the total volume of club cells in the lung [V(club cells, lung)] and the number weighted mean volume of club cells in the lung

Interestingly, we observed a significant increase in the abundance of secretory granules between the newborn to P15 lungs (Table 4) which is in line with our western blot analysis for CC10 protein expression (Fig. 2s). The club cell granules tremendously increased during the first 15 days compared to adult animals and slightly elevated thereafter. Comparably, the overall CC10 protein abundance increased during the first 15 days and was higher in homogenates of the adult lungs revealing the postnatal differentiation of the club cell in the murine lung.

Antibodies that can recognize cell type-specific proteins, such as CC10 for club cells, are particularly useful for qualitative and quantitative identification of these cell types in organs, in particular in organs with more than 40 different cell types such as the lung (Sorokin 1988). To characterize the quality and specificity of the CC10 antibodies, we used our sensitive IF protocol to stain for the labeling for CC10 in wild-type (CC10^{+/+}) and CC10 knockout (CC10^{-/-}) animals as well as post-embedding immune TEM. Indeed, CC10 was exclusively detected in club cells and localized in a punctuate pattern in IF as well as the correct subcellular compartment, namely secretory granules at the ultrastructural level. Neighboring ciliated cells always remained negative and preparations of the CC10 knockout animals were devoid of labeling confirming the specificity of the reaction. In the CC10 knockout animals, no gross morphological differences of the lungs were observed in comparison to wild-type animals. CC10 knockout animals were devoid of secretory granules and the smooth endoplasmic reticulum (sER) differed strongly between WT and KO animals (Stripp et al. 2002). Electron-dense material was abundant in the lumen of the sER of club cells of WT animals, whereas it was not evident

in the KO animals. Furthermore, CC10 KO animals possessed large concentric whorls of endoplasmic reticulum within the apical portion of club cells. Moreover, the rER occupied <8 % of the cell volume in WT animals but only less than 0.5 % in KO animals (Stripp et al. 1996; Stripp et al. 2002).

Several studies have demonstrated that developmental changes of different cell types of the bronchiolar epithelium are highly variable (Cardoso et al. 1993; Plopper et al. 1993). Our study is the first comprehensive investigation of the club cell differentiation by combining light and fluorescence microscopic, scanning and transmission electron microscopic approaches together with design-based stereology of the mouse lungs, as well as microdissection with subsequent gene expression analysis. Here, we demonstrate that the club cell of the mouse lung is not a mature, fully differentiated cell at birth. Our experimental data are in line with the conclusions drawn by purely morphological studies performed on other species, such as rabbit (Plopper et al. 1983a), pig (Baskerville 1970) and human (Rosan and Lauweryns 1972).

We were only able to show a weak labeling for CC10 protein in the club cells of newborn mouse lungs, which is supported by studies performed in rat club cells on fetal day 19 (Singh and Katyal 1984), fetal day 19 in the mice (Fanucchi et al. 1997b) and fetal day 15 in the hamster (Strum et al. 1990).

Further, the distribution of club cells varies in distinct airway levels depending on the age of the animal. CC10 was not detected at all in the pseudoglandular stage of all airways in the mouse lung, whereas weakly stained club cells were detected only in the proximal airways of the canalicular stage (Fanucchi et al. 1997b). In the saccular stage, a weak labeling for CC10 was also detected in distal airways. At 1 day

postnatal age (1DPN), club cells were positively labeled both in proximal and distal airways. At 14 DPN, CC10 distribution and intensity in proximal and distal airways remained the same (Fanucchi et al. 1997b).

Our results showing that 15-day-old and adult club cells contain more apical dense secretory granules are in agreement with observations made about rat club cells (Bedetti et al. 1987). Furthermore, club cell secretory surfactant protein A was also similarly abundant in the 15-day-old and adult lungs (Fig. 2). However, there were several reports claiming that SP-A is not synthesized by club cells, instead exclusively by alveolar epithelial type II cells (Oomen et al. 1990; Ten Have-Opbroek and De Vries 1993). However, immunofluorescence results and gene expression analyses of microdissected bronchiolar epithelial cells in our study clearly demonstrate that club cells do express surfactant protein A, B and D mRNAs and contain the appropriate proteins in secretory granules. These results are in agreement with the studies performed by Endo and Oka (1991) and Horowitz et al. (1991) as well as by Sutherland et al. (2010). Further, Sutherland et al. showed the site-specific differences of the expression of genes coding for CC10, SP-A and SP-C in microdissected airway regions. Interestingly, this group demonstrated the importance of this technique by microdissecting terminal bronchiolar epithelial cells exhibiting 6-fold higher CC10 gene expression over the whole lung and 3-fold over the airway tree suggesting the use of microdissection technique in distal airways (Sutherland et al. 2010). In this context, it is of interest that the results of the comparison of gene expression patterns of CC10 between bronchiolar epithelial cells retrieved by LCM and whole lung homogenates were similar (Betsuyaku et al. 2001). This result is expected, because club cells are the only cells expressing CC10 mRNA in the whole lung, which is diluted in total RNA preparations of whole lung samples in comparison to LCM preparations of the bronchiolar epithelium, although LCM results do not necessarily reflect the analysis of whole-lung gene expression (Betsuyaku et al. 2001). The club cell secreting proteins CC10, SP-A, and SP-D are immunomodulators of lung physiology and pulmonary host defense (Reynolds and Malkinson 2010; Singh and Katyal 1984; Wright 2005). CC10-deficient mice have an increased IgA mRNA expression in peribronchial B lymphocytes suggesting an ability to induce inflammatory mechanisms consistent with the previous observations (Wang et al. 2001; Watson et al. 2001). Recently, anti-inflammatory properties of CC10 were shown to inhibit NF- κ B activation and suppress the phosphorylation of its inhibitor I κ B α , thereby suggesting that CC10 gene transfer may provide a new possibility in the therapy of airway inflammation (Long et al. 2012). Further, CC10-deficient animals showed an increased respiratory syncytial virus persistence, suggesting the importance of epithelial-derived pathogen clearance mechanisms as well as regulation of innate and adaptive immune response by epithelial-derived mediators (Harrod et al. 1998,

1999). The precise molecular mechanisms by which CC10 limits lung inflammation in vivo remain to be determined. Comparably, mice selectively deficient in SP-A or SP-D are highly susceptible to bacterial or viral challenge (Wright 2005). Interestingly, mice deficient in SP-A, secreted by club and AECII cells, also show increased inflammation to respiratory syncytial virus infections (Wang et al. 2003).

CC10 deficiency does not alter the regulation and synthesis of surfactant proteins (SP-A, SP-B and SP-D) and surfactant homeostasis but alters the composition of the airway surface fluid (Ikegami et al. 1999; Stripp et al. 2002). Surfactant protein synthesis, trafficking and their secretion into the bronchiolar lumen as well as the functional role in recycling of surfactant by club cells is still unknown (Auten et al. 1990; Endo and Oka 1991; Savov et al. 2000). Therefore, we attempted to investigate the structural modifications of club cells and their dynamics on the surface of the cells during the postnatal development of the lung. Strikingly, we detected extrusions of a significant portion of the apical cytoplasm of the club cells into the lumen of the bronchioles (Fig. 3j, k), which was suggested as an important key feature with functional physiological relevance on club cell secretory functions (Etherton et al. 1979; Mahvi et al. 1977). These extrusions were, however, in our study detected only in adult club cells, since this phenomenon is quite difficult to capture in normal healthy bronchioles without proper stimulation of club cell secretion. Peao and colleagues showed that only 6.3 % of total resting club cells in this time-frame showed the formation of these projections that will later be released into the bronchiolar lumen (Peao et al. 1993).

Our SEM results demonstrated progressive ciliation during postnatal development of the mouse lungs, which is in agreement with the observations by Toskala and colleagues (Toskala et al. 2005). In fact, ciliogenesis varies by airway generation and age; however, in this study, we mainly focused on the maturation of club cells. Club cells undergo a postnatal maturation process; AECII cells that are associated with surfactant system were already mature 1 day before birth (Desai et al. 2014; Williams 1977). The club cells in the newborn lung still contain large areas of glycogen and, apparently, glycogenolysis in the lung seems to be an important event for the development of the surfactant system of AECII cells, in particular prenatal increase of surfactant synthesis (Bourbon et al. 1982; Massaro and Massaro 1972). Furthermore, Maniscalco and colleagues demonstrated that a decrease in rat fetal lung glycogen coincided with an increase in the amount of pulmonary phosphatidylcholine and disaturated phosphatidylcholine (Maniscalco et al. 1978). Our results showing the absence of large glycogen fields in the 15-day-old and adult lungs and an increase in the club cell secretory granules is consistent with the previous observation (Cutz and Conen 1971; Plopper et al. 1980) and may suggest that glycogenolysis might be an indicator for the maturation of club cells as well as the synthesis of

secretory granules, containing high levels of CC10 and SP-A, SP-B, and SP-D thereby reflecting the club cell differentiation process. Moreover, since club cells are stem/progenitor cells of ciliated cells and repair and renew the airway epithelium upon injury, glycogenolysis may be an important process for energy delivery for the division of club cells (Reynolds and Malkinson 2010; Sorokin 1961; Wang et al. 2012). Interestingly, Kim and colleagues discovered bronchioalveolar stem cells (BASCs), a regional stem cell population at the junction between the conductive and respiratory part (the bronchioalveolar duct junction) in terminal bronchioles of adult mice (Kim et al. 2005). In our study, CC10 protein expression was also increased in BASCs during the postnatal development of the lung suggesting that BASCs are required for club cell differentiation (supplementary Fig. 1). Of note, tremendous remodeling and alveolarization of the gas exchange region of the lung indeed take place mainly in the second and third week of life (Amy et al. 1977). BASCs were also described to proliferate after injury of distinct lung epithelia such as 1 week after naphthalene treatment-induced club cell injury as well as after bleomycin-induced AECII cells (Kim et al. 2005). In 6–7 weeks after naphthalene treatment, the bronchiolar epithelium was restored and the number of BASCs was similar to untreated animals suggesting that BASCs are resistant to the damage and proliferate during repair processes of the bronchiolar epithelium. Moreover, recent evidence suggests that club cells differentiate into AECII cells during repair of the alveolar epithelium following severe pulmonary injury (Zheng et al. 2013). Furthermore, ciliated cells exhibit a remarkable plasticity to maintain an intact epithelial barrier when club cells were injured after naphthalene-induced injury (Lawson et al. 2002; Plopper et al. 1992a, b).

In summary, we studied the expression of secretory functional proteins during club cell differentiation. We found that club cell secretory function develops postnatally, involves a decrease in glycogen content, and exhibits a close association between CC10 expression and secretory granule abundance. Our morphometric analysis demonstrates a significant increase in the number of club cells and volume of secretory granules within 15 days after birth. Thus, our results indicate that mice may be an excellent animal model for studying the factors controlling club cell differentiation in the postnatal period.

Acknowledgments The excellent technical assistance of Bianca Pfeiffer, Gerd Magdowski, Gerhard Kripp, Ulrich Gärtner, Anika Seipp and Karina Greve is gratefully acknowledged. Further, we would like to thank Barry Stripp (Departments of Medicine and Cell Biology, Duke University Medical Center, Durham, North Carolina) for providing CC10 wild-type and knockout tissue samples. Our study was supported by LOM (Leistungsorientierte Mittel) performance-related resource allocation-funds of the Medical Faculty of the Justus Liebig University Giessen, and by the DFG via the Cluster of Excellence REBIRTH, Germany.

References

- Amy RW, Bowes D, Burri PH, Haines J, Thurlbeck WM (1977) Postnatal growth of the mouse lung. *J Anat* 124:131–151
- Auten RL, Watkins RH, Shapiro DL, Horowitz S (1990) Surfactant apoprotein A (SP-A) is synthesized in airway cells. *Am J Respir Cell Mol Biol* 3:491–496
- Baskerville A (1970) Ultrastructural studies of the normal pulmonary tissue of the pig. *Res Vet Sci* 11:150–155
- Bedetti CD, Singh J, Singh G, Katyal SL, Wong-Chong ML (1987) Ultrastructural localization of rat Clara cell 10 KD secretory protein by the immunogold technique using polyclonal and monoclonal antibodies. *J Histochem Cytochem* 35:789–794
- Bernard A, Marchandise FX, Depelchin S, Lauwerys R, Sibille Y (1992) Clara cell protein in serum and bronchoalveolar lavage. *Eur Respir J* 5:1231–1238
- Betsuyaku T, Griffin GL, Watson MA, Senior RM (2001) Laser capture microdissection and real-time reverse transcriptase/ polymerase chain reaction of bronchiolar epithelium after bleomycin. *Am J Respir Cell Mol Biol* 25:278–284
- Bourbon JR, Rieutort M, Engle MJ, Farrell PM (1982) Utilization of glycogen for phospholipid synthesis in fetal rat lung. *Biochim Biophys Acta* 712:382–389
- Bourdin A, Mifsud NA, Chanez B, McLean C, Chanez P, Snell G, Kotsimbos TC (2012) Donor clara cell secretory protein polymorphism is a risk factor for bronchiolitis obliterans syndrome after lung transplantation. *Transplantation* 94:652–658
- Cardoso WV, Stewart LG, Pinkerton KE, Ji C, Hook GE, Singh G, Katyal SL, Thurlbeck WM, Plopper CG (1993) Secretory product expression during Clara cell differentiation in the rabbit and rat. *Am J Physiol* 264:L543–L552
- Clara M (1937) Zur histobiologie des bronchialepithels. *Z Mikrosk Anat Forsch* 41:321–347
- Cosio M, Ghezzi H, Hogg JC, Corbin R, Loveland M, Dosman J, Macklem PT (1978) The relations between structural changes in small airways and pulmonary-function tests. *N Engl J Med* 298:1277–1281
- Cudmore RE, Emery JL, Mithal A (1962) Postnatal growth of the bronchi and bronchioles. *Arch Dis Child* 37:481–484
- Cutz E, Conen PE (1971) Ultrastructure and cytochemistry of Clara cells. *Am J Pathol* 62:127–141
- Desai TJ, Brownfield DG, Krasnow MA (2014) Alveolar progenitor and stem cells in lung development, renewal and cancer. *Nature* 507:190–194
- Endo H, Oka T (1991) An immunohistochemical study of bronchial cells producing surfactant protein A in the developing human fetal lung. *Early Hum Dev* 25:149–156
- Etherton JE, Purchase IF, Corrin B (1979) Apocrine secretion in the terminal bronchiole of mouse lung. *J Anat* 129:305–322
- Fanucchi MV, Buckpitt AR, Murphy ME, Plopper CG (1997a) Naphthalene cytotoxicity of differentiating Clara cells in neonatal mice. *Toxicol Appl Pharmacol* 144:96–104
- Fanucchi MV, Murphy ME, Buckpitt AR, Philpot RM, Plopper CG (1997b) Pulmonary cytochrome P450 monooxygenase and Clara cell differentiation in mice. *Am J Respir Cell Mol Biol* 17:302–314
- Gras D, Chanez P, Vachier I, Petit A, Bourdin A (2013) Bronchial epithelium as a target for innovative treatments in asthma. *Pharmacol Ther* 140:290–305
- Gundersen HJ, Jensen EB (1987) The efficiency of systematic sampling in stereology and its prediction. *J Microsc* 147:229–263
- Harrod KS, Mounday AD, Stripp BR, Whitsett JA (1998) Clara cell secretory protein decreases lung inflammation after acute virus infection. *Am J Physiol* 275:L924–L930

- Harrod KS, Trapnell BC, Otake K, Korfhagen TR, Whitsett JA (1999) SP-A enhances viral clearance and inhibits inflammation after pulmonary adenoviral infection. *Am J Physiol* 277:L580–L588
- Hill LH, Plopper CG (1979) Use of large block embedding for correlated LM, TEM and SEM characterization of pulmonary airways of known anatomic location. *Proc Southeast Electron Microsc Soc* 2:24
- Horowitz S, Watkins RH, Auten RL Jr, Mercier CE, Cheng ER (1991) Differential accumulation of surfactant protein A, B, and C mRNAs in two epithelial cell types of hyperoxic lung. *Am J Respir Cell Mol Biol* 5:511–515
- Howard CV, Reed MG (2005) *Unbiased stereology*, 2nd edn. Garland Science/BIOS Scientific, Abingdon, pp 143–163
- Ikegami M, Harrod KS, Whitsett JA, Jobe AH (1999) CCSP deficiency does not alter surfactant homeostasis during adenoviral infection. *Am J Physiol* 277:L983–L987
- Irwin RS, Augustyn N, French CT, Rice J, Tedeschi V, Welch SJ (2013) Spread the word about the journal in 2013: from citation manipulation to invalidation of patient-reported outcomes measures to renaming the Clara cell to new journal features. *Chest* 143:1–4
- Jeffery PK (1977) Ultrastructure of airway epithelium and submucosal glands during the development. In: *Development of the lung*. Marcel Dekker, New York, pp 87–134
- Johnston CJ, Mango GW, Finkelstein JN, Stripp BR (1997) Altered pulmonary response to hyperoxia in Clara cell secretory protein deficient mice. *Am J Respir Cell Mol Biol* 17:147–155
- Jorens PG, Sibille Y, Goulding NJ, van Overveld FJ, Herman AG, Bossaert L, De Backer WA, Lauwerys R, Flower RJ, Bernard A (1995) Potential role of Clara cell protein, an endogenous phospholipase A2 inhibitor, in acute lung injury. *Eur Respir J* 8:1647–1653
- Karnati S, Baumgart-Vogt E (2008) Peroxisomes in mouse and human lung: their involvement in pulmonary lipid metabolism. *Histochem Cell Biol* 130:719–740
- Karnati S, Baumgart-Vogt E (2009) Peroxisomes in airway epithelia and future prospects of these organelles for pulmonary cell biology. *Histochem Cell Biol* 131:447–454
- Kim CF, Jackson EL, Woolfenden AE, Lawrence S, Babar I, Vogel S, Crowley D, Bronson RT, Jacks T (2005) Identification of bronchioalveolar stem cells in normal lung and lung cancer. *Cell* 121:823–835
- Lawson GW, Van Winkle LS, Toskala E, Senior RM, Parks WC, Plopper CG (2002) Mouse strain modulates the role of the ciliated cell in acute tracheobronchial airway injury-distal airways. *Am J Pathol* 160:315–327
- Long XB, Hu S, Wang N, Zhen HT, Cui YH, Liu Z (2012) Clara cell 10-kDa protein gene transfection inhibits NF-kappaB activity in airway epithelial cells. *PLoS ONE* 7:e35960
- Lowrie PM, Tyler WS (1973) Selection and preparation of specific regions for TEM using large epoxy-embedded blocks. *Proc Annu Meet Electron Microsc Soc Am* 148:324–325
- Mahvi D, Bank H, Harley R (1977) Morphology of a naphthalene-induced bronchiolar lesion. *Am J Pathol* 86:558–572
- Maniscalco WM, Wilson CM, Gross I, Gobran L, Rooney SA, Warshaw JB (1978) Development of glycogen and phospholipid metabolism in fetal and newborn rat lung. *Biochim Biophys Acta* 530:333–346
- Massaro GD, Massaro D (1972) Granular pneumocytes. Electron microscopic radioautographic evidence of intracellular protein transport. *Am Rev Respir Dis* 105:927–931
- Massaro GD, Davis L, Massaro D (1984) Postnatal development of the bronchiolar Clara cell in rats. *Am J Physiol* 247:C197–C203
- Mayhew TM (2008) Taking tissue samples from the placenta: an illustration of principles and strategies. *Placenta* 29:1–14
- Muhlfeld C, Ochs M (2013) Quantitative microscopy of the lung: a problem-based approach. Part 2: stereological parameters and study designs in various diseases of the respiratory tract. *Am J Physiol Lung Cell Mol Physiol* 305:L205–L221
- Ochs M, Muhlfeld C (2013) Quantitative microscopy of the lung: a problem-based approach. Part 1: basic principles of lung stereology. *Am J Physiol Lung Cell Mol Physiol* 305:L15–L22
- Oomen LC, Ten Have-Opbroek AA, Hageman PC, Oudshoorn-Snoek M, Egberts J, van der Valk MA, Calafat J, Demant P (1990) Fetal mouse alveolar type II cells in culture express several type II cell characteristics found in vivo, together with major histocompatibility antigens. *Am J Respir Cell Mol Biol* 3:325–339
- Peao MN, Aguas AP, de Sa CM, Grande NR (1992a) Structural artifacts and advantages of cytocentrifugation of cells as viewed by scanning electron microscopy. *Scanning Microsc* 6:281–285
- Peao MN, Aguas AP, Grande NR (1992b) Cellular kinetics of inflammation in the pleural space of mice in response to the injection of exogenous particles. *Exp Lung Res* 18:863–876
- Peao MN, Aguas AP, de Sa CM, Grande NR (1993) Anatomy of Clara cell secretion: surface changes observed by scanning electron microscopy. *J Anat* 182(Pt 3):377–388
- Plopper CG, Mariassy AT, Hill LH (1980) Ultrastructure of the nonciliated bronchiolar epithelial (Clara) cell of mammalian lung: II. A comparison of horse, steer, sheep, dog, and cat. *Exp Lung Res* 1:155–169
- Plopper CG, Alley JL, Serabjitsingh CJ, Philpot RM (1983a) Cytodifferentiation of the nonciliated bronchiolar epithelial (Clara) cell during rabbit lung maturation: an ultrastructural and morphometric study. *Am J Anat* 167:329–357
- Plopper CG, Halsebo JE, Berger WJ, Sonstegard KS, Nettesheim P (1983b) Distribution of nonciliated bronchiolar epithelial (Clara) cells in intra- and extrapulmonary airways of the rabbit. *Exp Lung Res* 5:79–98
- Plopper CG, Alley JL, Weir AJ (1986) Differentiation of tracheal epithelium during fetal lung maturation in the rhesus monkey *Macaca mulatta*. *Am J Anat* 175:59–71
- Plopper CG, Macklin J, Nishio SJ, Hyde DM, Buckpitt AR (1992a) Relationship of cytochrome P-450 activity to Clara cell cytotoxicity. III. Morphometric comparison of changes in the epithelial populations of terminal bronchioles and lobar bronchi in mice, hamsters, and rats after parenteral administration of naphthalene. *Lab Invest* 67:553–565
- Plopper CG, Suverkropp C, Morin D, Nishio S, Buckpitt A (1992b) Relationship of cytochrome P-450 activity to Clara cell cytotoxicity. I. Histopathologic comparison of the respiratory tract of mice, rats and hamsters after parenteral administration of naphthalene. *J Pharmacol Exp Ther* 261:353–363
- Plopper CG, Weir AJ, Morin D, Chang A, Philpot RM, Buckpitt AR (1993) Postnatal changes in the expression and distribution of pulmonary cytochrome P450 monooxygenases during Clara cell differentiation in rabbits. *Mol Pharmacol* 44:51–61
- Reynolds SD, Malkinson AM (2010) Clara cell: progenitor for the bronchiolar epithelium. *Int J Biochem Cell Biol* 42:1–4
- Rosan RC, Lauweryns JM (1972) Mucosal cells of the small bronchioles of prematurely born human infants (600–1700 g). *Beitr Pathol* 147:145–174
- Savov J, Wright JR, Young SL (2000) Incorporation of biotinylated SP-A into rat lung surfactant layer, type II cells, and clara cells. *Am J Physiol Lung Cell Mol Physiol* 279:L118–L126
- Scherle W (1970) A simple method for volumetry of organs in quantitative stereology. *Mikroskopie* 26:57–60
- Shijubo N, Itoh Y, Yamaguchi T, Sugaya F, Hirasawa M, Yamada T, Kawai T, Abe S (1999) Serum levels of Clara cell 10-kDa protein are decreased in patients with asthma. *Lung* 177:45–52
- Singh G, Katyal SL (1984) An immunologic study of the secretory products of rat Clara cells. *J Histochem Cytochem* 32:49–54
- Slot JW, Geuze HJ (1981) Sizing of protein A-colloidal gold probes for immunoelectron microscopy. *J Cell Biol* 90:533–536
- Sorokin SA (1961) A study of development in organ cultures of mammalian lungs. *Dev Biol* 3:60–83

- Sorokin SP (1988) The respiratory system: cell and tissue biology. In: Weiss L (ed) Chapter 25, 6th edn. Urban and Schwarzenberg, Munich, p 751–814, ISBN: 753-541-72176-72176
- Stelzig I, Kamati S, Valerius KP, Baumgart-Vogt E (2013) Peroxisomes in dental tissues of the mouse. *Histochem Cell Biol* 140:443–462
- Sterio DC (1984) The unbiased estimation of number and sizes of arbitrary particles using the disector. *J Microsc* 134:127–136
- Stripp BR, Lund J, Mango GW, Doyen KC, Johnston C, Hultenby K, Nord M, Whitsett JA (1996) Clara cell secretory protein: a determinant of PCB bioaccumulation in mammals. *Am J Physiol* 271: L656–L664
- Stripp BR, Reynolds SD, Boe IM, Lund J, Power JH, Coppens JT, Wong V, Reynolds PR, Plopper CG (2002) Clara cell secretory protein deficiency alters clara cell secretory apparatus and the protein composition of airway lining fluid. *Am J Respir Cell Mol Biol* 27:170–178
- Strum JM, Singh G, Katyal SL, McDowell EM (1990) Immunochemical localization of Clara cell protein by light and electron microscopy in conducting airways of fetal and neonatal hamster lung. *Anat Rec* 227:77–86
- Sutherland KM, Combs TJ, Edwards PC, Van Winkle LS (2010) Site-specific differences in gene expression of secreted proteins in the mouse lung: comparison of methods to show differences by location. *J Histochem Cytochem* 58:1107–1119
- Ten Have-Oproek AA, De Vries EC (1993) Clara cell differentiation in the mouse: ultrastructural morphology and cytochemistry for surfactant protein A and Clara cell 10 kD protein. *Microsc Res Tech* 26: 400–411
- Toskala E, Smiley-Jewell SM, Wong VJ, King D, Plopper CG (2005) Temporal and spatial distribution of ciliogenesis in the tracheobronchial airways of mice. *Am J Physiol Lung Cell Mol Physiol* 289: L454–L459
- Van Vyve T, Chanez P, Bernard A, Bousquet J, Godard P, Lauwerijs R, Sibille Y (1995) Protein content in bronchoalveolar lavage fluid of patients with asthma and control subjects. *J Allergy Clin Immunol* 95:60–68
- Vedel Jensen EB, Gundersen HJG (1993) The rotator. *J Microsc* 170:35–44
- Wang SZ, Rosenberger CL, Espindola TM, Barrett EG, Tesfaigzi Y, Bice DE, Harrod KS (2001) CCSP modulates airway dysfunction and host responses in an Ova-challenged mouse model. *Am J Physiol Lung Cell Mol Physiol* 281:L1303–L1311
- Wang SZ, Rosenberger CL, Bao YX, Stark JM, Harrod KS (2003) Clara cell secretory protein modulates lung inflammatory and immune responses to respiratory syncytial virus infection. *J Immunol* 171: 1051–1060
- Wang XY, Keefe KM, Jensen-Taubman SM, Yang D, Yan K, Linnoila RI (2012) Novel method for isolation of murine clara cell secretory protein-expressing cells with traces of stemness. *PLoS ONE* 7: e43008
- Watson TM, Reynolds SD, Mango GW, Boe IM, Lund J, Stripp BR (2001) Altered lung gene expression in CCSP-null mice suggests immunoregulatory roles for Clara cells. *Am J Physiol Lung Cell Mol Physiol* 281:L1523–L1530
- Weibel ER (1979) Stereological methods. Practical methods for biological morphometry. Academic, London
- Williams MC (1977) Development of the alveolar structure of the fetal rat in late gestation. *Fed Proc* 36:2653–2659
- Winkelmann A, Noack T (2010) The Clara cell: a “Third Reich eponym”? *Eur Respir J* 36:722–727
- Wright JR (2005) Immunoregulatory functions of surfactant proteins. *Nat Rev Immunol* 5:58–68
- Zheng D, Limmon GV, Yin L, Leung NH, Yu H, Chow VT, Chen J (2013) A cellular pathway involved in Clara cell to alveolar type II cell differentiation after severe lung injury. *PLoS ONE* 8:e71028

Peroxisomes in airway epithelia and future prospects of these organelles for pulmonary cell biology

Srikanth Karnati · Eveline Baumgart-Vogt

Accepted: 29 January 2009 / Published online: 20 February 2009
© Springer-Verlag 2009

Abstract Peroxisomes are intimately involved in the metabolism of reactive oxygen species, in the synthesis of ether lipids and of polyunsaturated fatty acids as well as in the β -oxidation of bioactive and toxic lipid derivatives. Therefore, the metabolic pathways of this organelle might play an important role in pulmonary biology by protection of inner pulmonary surface epithelia against oxidative stress, induced by the high oxygen levels in the air and/or by regulation of the lipid homeostasis in pulmonary epithelia and the pulmonary surfactant film. In this article, original results on the distribution of peroxisomal marker proteins, involved in the biogenesis, ROS- and lipid-metabolism of this organelle in the bronchiolar epithelium and the alveolar region of the adult human lung in comparison to newborn and adult murine lungs are presented. In addition, we investigated the expression of the PEX11 β -mRNA, encoding a protein involved in peroxisomal division. Our study revealed significant differences in the abundance and distribution of peroxisomal proteins in distinct cell types of the lung and different developmental stages and led to the discovery of species-specific differences in the peroxisomal compartment in pulmonary epithelia between mouse and man. Finally, the structure and general biology of pulmonary airways—with special emphasis on Clara cells—are reviewed and discussed in relation to peroxisomal metabolism and proliferation. Future prospects of peroxisomes and Pex11 proteins for pulmonary cell biology are highlighted.

Keywords Catalase · Pex14p · ABCD3 · ACOXI · Thiolase · CC10 · Lung

Introduction

Peroxisomes are ubiquitous organelles, present in virtually all eukaryotic cells except for erythrocytes and spermatozoa. Their metabolic functions and enzyme composition varies between distinct cell types, tissues and organ systems. In addition, peroxisomes are very flexible organelles, adjusting their number and enzyme composition to metabolic needs and to cellular demands. Peroxisomal functions have been comprehensively investigated in liver and kidney, in which these organelles are intimately involved in the metabolism of reactive oxygen species (ROS) and lipids. In contrast, only very little is known about peroxisomal metabolism in the lung. Since the lung is the target of various forms of reactive oxygen and nitrogen species (ROS and RNS), due to exposition to high concentrations of oxygen on its large inner surface (Rahman and MacNee 2000), peroxisomes might perform important protective functions in this organ.

Pulmonary airways are exposed to high concentrations of environmental oxidants, eventually leading to oxidation of proteins, DNA and lipids and therefore causing direct lung injury. The first line of defence against the oxidants are non-enzymatic antioxidants, such as glutathione, vitamin C and β -carotene as well as ether lipids (plasmalogens) and polyunsaturated fatty acids (PUFA) in the plasma membranes of airway epithelial cells or in the surfactant film, covering the alveolar region. Interestingly, crucial steps in the synthesis of these lipids occur in peroxisomes. Enzymatic antioxidant enzymes are responsible for the second line of defence against ROS, such as superoxide dismutases, catalase, glutathione peroxidases and peroxiredoxins. They are degrading

Presented at the 50th anniversary symposium of the Society for Histochemistry, Interlaken, Switzerland, October 1–4, 2008.

S. Karnati · E. Baumgart-Vogt (✉)
Division of Medical Cell Biology,
Institute for Anatomy and Cell Biology II,
Justus Liebig University, Aulweg 123, 35385 Giessen, Germany
e-mail: Eveline.Baumgart-Vogt@anatomie.med.uni-giessen.de
URL: <http://www.med.uni-giessen.de/anat/>

various types of ROS and are localized in different pulmonary cell types as well as distinct intracellular subcompartments (Karnati and Baumgart-Vogt 2008; Immenschuh and Baumgart-Vogt 2005). If the fragile balance between the ROS production and the defensive capacity of the antioxidant system is severely disturbed, pathological alterations may occur in the affected tissue, leading to lung injury or diseases. In this respect, it is noteworthy that oxidative stress alters the transcriptional activity of various genes, including the ones encoding proteins of signalling pathways of the inflammatory response. Increased levels of ROS have been implicated in various airway diseases, such as asthma, chronic obstructive pulmonary disease and pulmonary fibrosis (Rahman and MacNee 2000).

Peroxisomes might protect the pulmonary airway epithelium by three different mechanisms: (1) their high and adaptable content in various antioxidative enzymes, (2) their involvement in the synthesis of plasmalogens and PUFA, as well as (3) their capacity to degrade a variety of the toxic and bioactive lipid derivatives via their β -oxidation systems (for a review see Karnati and Baumgart-Vogt 2008). In addition to the peroxisomal marker enzyme catalase, several other antioxidant enzymes have been described in this organelle, such as Cu, Zn-superoxide dismutase (SOD1), glutathione peroxidase and peroxiredoxins I, V and VI (Immenschuh and Baumgart-Vogt 2005). Our previous comprehensive paper on peroxisomes in the lung has mainly focussed on the alveolar region, in which we have revealed the overall distribution and the heterogeneity of this organelle in various cell types of the alveolus and discussed its possible role in pulmonary lipid metabolism (Karnati and Baumgart-Vogt 2008). However, in this article only little information was given on peroxisomes in pulmonary airway epithelia and to date, nothing is known on the overall distribution of peroxisomal proteins in bronchiolar epithelial cells—such as Clara cells—of the human lung.

Peroxisomal proteins in bronchiolar epithelial cells

In the 1970s, peroxisomes were revealed with certainty solely in alveolar epithelial cells II (AECII) and Clara cells in electron microscopic studies by using catalase cytochemistry with the alkaline DAB method (Petrik 1971; Schneeberger 1972). No information was available from the literature on the distribution of peroxisomal proteins in other cell types of the lung, until our group described with a variety of morphological techniques the localization and distribution of different peroxisomal proteins—catalase, Pex13p, Pex14p, ABCD3, ACOX1 and thiolase—in various cell types of the alveolar region and conducting airways, including Clara cells and ciliated cells of bronchioles in the adult mouse lung (Karnati and Baumgart-Vogt 2008).

Murine Clara cells possess larger peroxisomes, which are more abundant and contain stronger catalase activity in comparison to ciliated cells of the bronchiolar epithelium (Karnati and Baumgart-Vogt 2008). In addition, peroxisomes in murine Clara cells exhibit a strong heterogeneity in their enzyme content and are labelled with distinct intensities for the above mentioned peroxisomal markers (Karnati and Baumgart-Vogt 2008). Despite the limited information on peroxisomes in mouse lungs, no information is available on these organelles in the bronchiolar epithelium of the human lung. Therefore, the aim of this study is to give some more insights on peroxisomes in distinct pulmonary epithelial cells in newborn and adult murine as well as human lungs, to review the biology and to highlight the prospects of peroxisomes for the function of the epithelial cells of the bronchiolar epithelium.

Materials and methods

Most materials and methods were similar to the described details in one of our previous publications (Karnati and Baumgart-Vogt 2008). Shortly, human lung tissue was obtained from the University of Giessen Lung Center (UGLC). Non-transplanted areas of three human donor lungs, conserved for transplantation, fixed by immersion in 4% paraformaldehyde (PFA)-PBS and embedded into paraffin, were used. Adult mouse lungs were fixed by perfusion fixation as described (Karnati and Baumgart-Vogt 2008). In addition, the lungs of newborn or E18.5 mice were perfused via the heart with 4% PFA-PBS, pH 7.4. The paraffin-embedded left lung was cut and sections were further processed for application of immunohistochemical (IHC)-, immunofluorescence (IF)- and in situ hybridization (ISH)-procedures. The different labelling procedures were carried out according to Karnati and Baumgart-Vogt (2008) (for IHC and IF) and Grabenbauer et al. (2001) (for ISH). The digoxigenin-labelled cRNA-probe for the ISH-preparations was generated from a plasmid containing the PEX11 β -cDNA, described in detail by Schrader et al. (1998). An mRNA (sense) probe for PEX11 β was used in parallel for corresponding negative controls.

Results

Peroxisomes are abundant in the bronchiolar epithelium of the human lung

With the optimized immunofluorescence technique for the localization of peroxisomes in the lung, we were able to visualize these organelles in a punctuate staining pattern in ciliated cells and nonciliated Clara cells of the bronchiolar

epithelium of the human airways (Fig. 1a–e). In contrast to our results obtained in the adult mouse lung (see Fig. 2h, i), peroxisomes were of similar size and numerical abundance in both cell types in the human bronchiolar epithelium (Fig. 1a) and were mainly localized at the apical poles of ciliated cells and nonciliated Clara cells. Furthermore, with the anti-Pex14p antibody, we were able to stain peroxisomes in alveolar macrophages very prominently, which covered the surface of the bronchioles in some regions in the human donor lungs. In stainings for Pex14p, peroxisomes were labelled with similar intensity in Clara cells and ciliated cells (Fig. 1a). In contrast, Clara cells in human bronchioli seemed to be labelled slightly less intensively for catalase than neighbouring ciliated cells (Fig. 1b). Peroxisomes were also strongly labelled with an antibody against ABCD3, a lipid transporter of the peroxisomal membrane, in both cell types. With this antibody, Clara cells could be visualized that contained large clusters of tubular peroxisomes (Fig. 1c). In addition, peroxisomes of the bronchiolar epithelium also contained acyl-CoA oxidase I (data not shown), the rate-limiting enzyme of the β -oxidation pathway 1 in the peroxisomal matrix. With the rabbit antibody directed against mouse peroxisomal 3-keto-acyl-CoA thiolase, only peroxisomes in Clara cells could be visualized with certainty. The high levels of ABCD3 and β -oxidation enzymes in human Clara cells suggest an active peroxisomal lipid metabolism in this cell type. In the alveolar region of human lungs, peroxisomes were mainly present in high abundance in AECII and alveolar macrophages, which were intensively stained for Pex14p and catalase (Fig. 1f, g). ABCD3 and peroxisomal thiolase were also found in AECII of human lungs (Karnati and Baumgart-Vogt 2008). Parallel sections of corresponding negative controls revealed the specificity of our immunofluorescence protocol. These preparations were always devoid of reaction product and only exhibited autofluorescent staining of residual bodies (lysosomes), erythrocytes or components of the extracellular matrix (Fig. 1e, h).

Peroxisomal enzymes are already present at high numerical abundance at birth

Immunohistochemical analysis of catalase distribution and protein abundance on E18.5 mouse lung tissue revealed the highest protein levels for this enzyme in the distal conducting airways and AECII (Fig. 2b). In addition, also in immunofluorescence preparations, a high numerical abundance of peroxisomes and protein levels of the peroxisomal markers, Pex14p and catalase in these cell types were noted (Fig. 2c–e). In comparison to adult lungs (Fig. 2f–i), peroxisomes were still more generally abundant in different cell types of the distal airways and the undifferentiated alveolar regions of the E18.5 lungs (Fig. 2b–e). In addition, peroxisomes in most cells of the yet undifferentiated alveo-

lar region showed strong staining for catalase, most probably labelling AECII in the early phase in the process of their transdifferentiation into alveolar epithelial cells I (AECI). In contrast to E18.5 lungs, peroxisomes in the alveolar region of adult murine lungs were mainly present in high abundance in AECII and were more prominently stained for catalase than AECI (Fig. 2f, g). Stainings for Pex14p and catalase were also strong in large peroxisomes of Clara cells in bronchiolar epithelia of adult animals (Fig. 2h, i).

Furthermore, we wanted to visualize the distribution of Pex11 β p, a protein involved in the regulation of peroxisome division, proliferation and the control of numerical abundance of the organelle in different cell types. This protein is deeply embedded into the peroxisomal membrane and good antibodies are not available world-wide, hampering its morphological visualization on the organelles. Therefore, we decided to localize the PEX11 β mRNA in the newborn lung by using a large digoxigenin-labelled PEX11 β -cRNA as a probe with the ISH-technique established previously in our group for the localization of mRNAs encoding for other peroxisomal proteins (Grabenbauer et al. 2001). Our results showed that the PEX11 β mRNA is expressed in the lung at higher level than in the liver in newborn animals (Fig. 2a), even though peroxisomes are most abundant in hepatocytes, suggesting that the turnover of the organelles might be higher in the lung. The strongest expression of the PEX11 β mRNA was observed in the distal airway epithelium and AECII of the alveolar epithelium (Fig. 2a). Control incubations of parallel sections with corresponding mRNA (sense)-probes for the ISH procedure were consistently negative, confirming the specificity of the method (see inset in Fig. 2a).

Discussion

The results of the present article revealed that peroxisomes are highly abundant in the bronchiolar epithelium of pulmonary airways and that species-specific differences in the peroxisomal compartment in distinct pulmonary epithelial cells exist between man and mice.

Major cell types of pulmonary epithelia

Lung epithelia are differentiated into two distinct major portions—the epithelia of the conducting airways and the epithelium of the respiratory region—both having sets of specialized cells, serving different functions in the respiratory system (Gail and Lenfant 1983). The functional integrity of the airway and alveolar epithelia is essential for the regular process of respiration in the lung (Plopper and

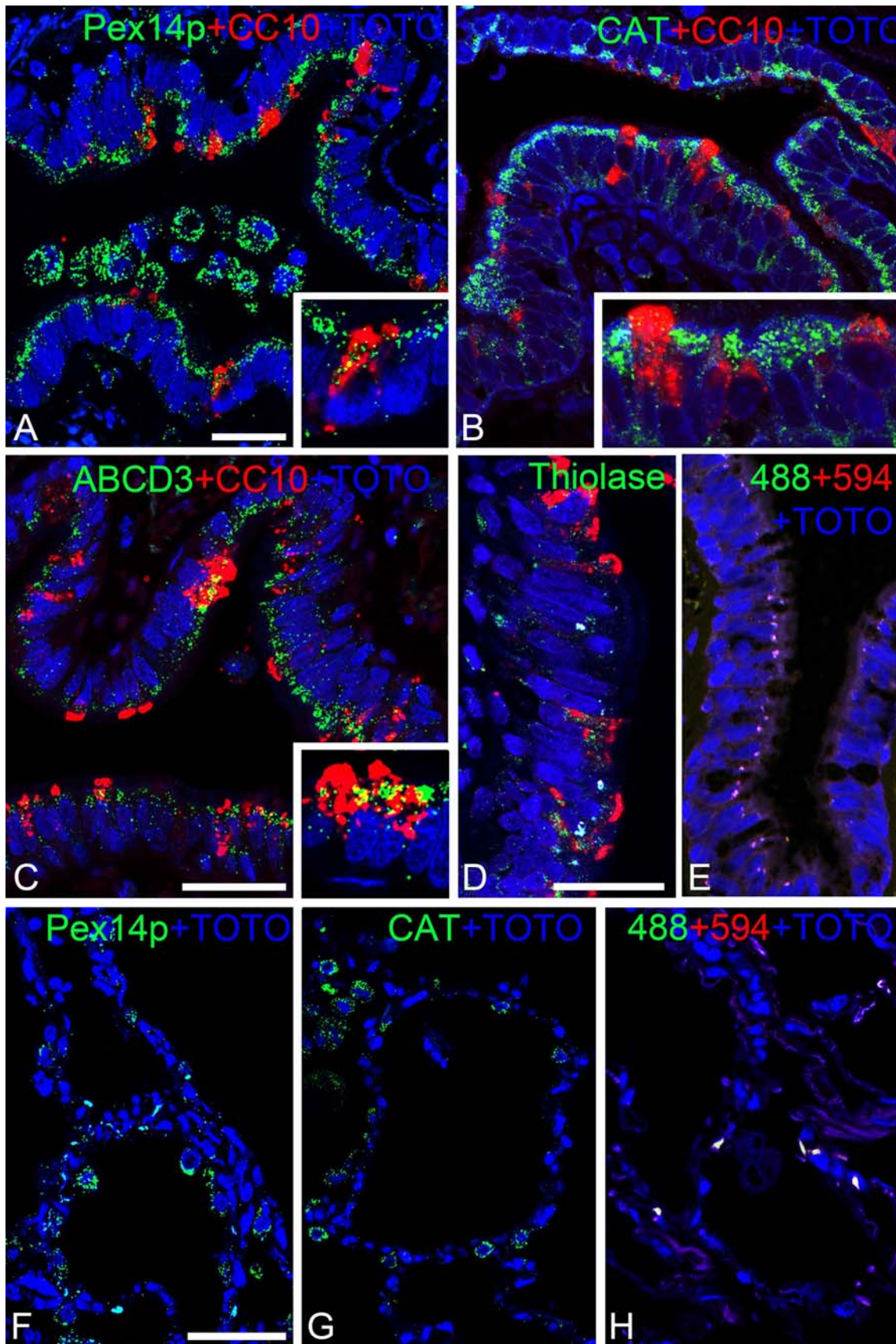


Fig. 1 Localization of peroxisomal proteins in the adult human lung. Double-IF preparations for Pex14p (a), catalase (CAT) (b), ABCD3 (c), and thiolase (d), combined with CC10-labelling, depicting the distribution of peroxisomal proteins in distinct cell types of the bronchiolar epithelium in the human lung. Stainings for the peroxisomal proteins Pex14p (f) and catalase (CAT) (g) in distinct cell types of the alveolar region. Note that AECII and alveolar macrophages are strongly labelled for peroxisomal proteins. Appropriate negative controls with anti-rabbit IgG-Alexa488 and anti-goat IgG-Alexa594 (e, h). Nuclei were counterstained with TOTO-3-iodide. Bars represent a–c: 50 μ m; f–h: 50 μ m; d, e: 25 μ m

Pinkerton 1992). Various cell types are present in the distinct lung epithelia, the major cell types of which—from proximal to distal regions—are: ciliated cells, intermediate and basal cells of the respiratory epithelium, mucous (goblet) cells, serous cells, nonciliated Clara cells and ciliated cells of the bronchiolar epithelium and AECI and AECII of the alveolar region (Sorokin 1988). Pulmonary epithelia are considered to be unique (1) for their exposure to high levels of environmental oxidants and (2) also for their unusual

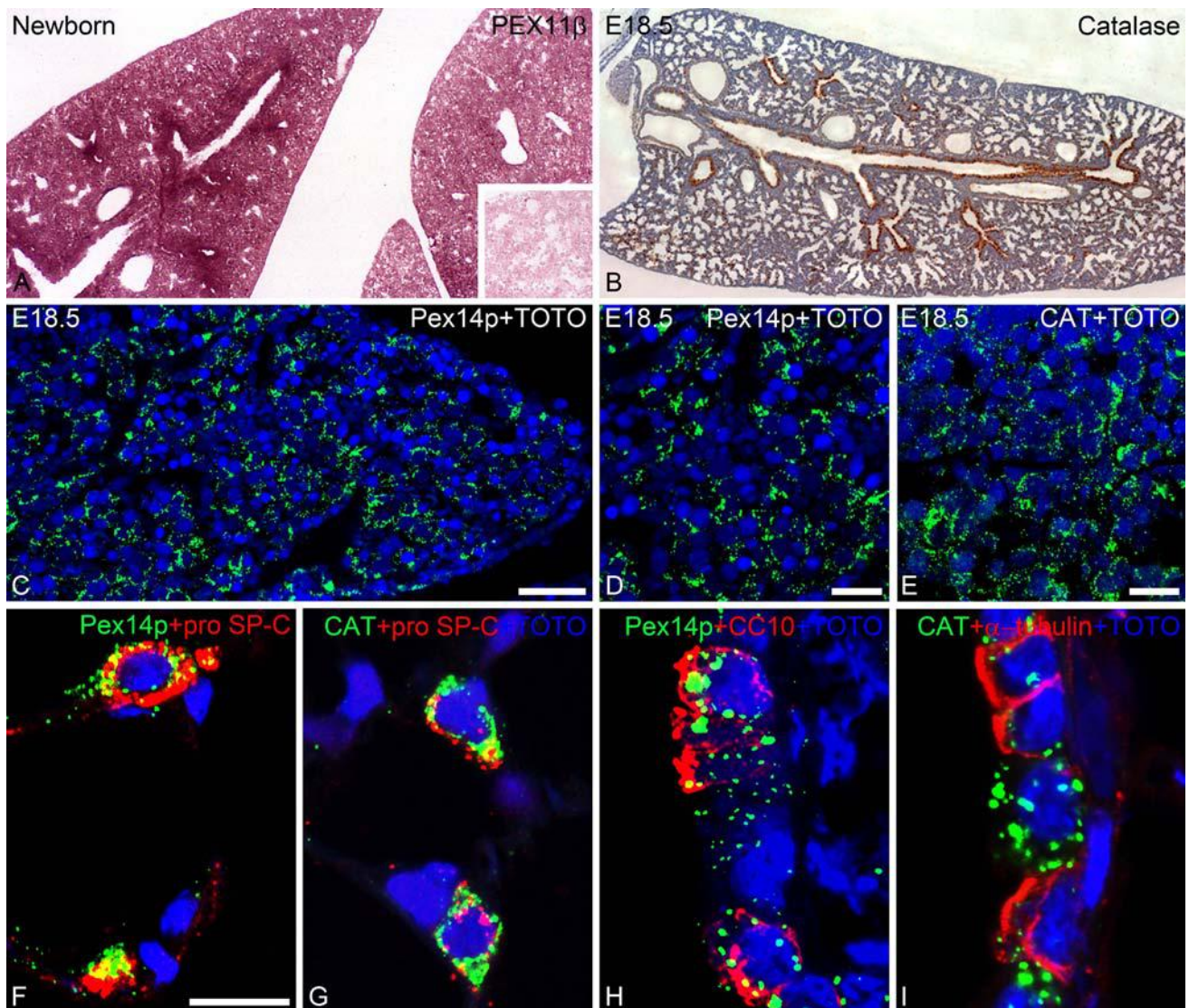


Fig. 2 Distribution of PEX11 β -mRNA and of peroxisomal proteins in the murine lung. In situ hybridization (ISH) for the PEX11 β -mRNA in newborn lung and liver tissues (a) and the corresponding mRNA (sense) control (*inset* in a), showing the high specificity of the ISH-reaction. Overviews of the immunohistochemical detection of catalase immunoreactivity (b) and an immunofluorescence (IF) preparation for Pex14p-labelling (c) in the left lung of E18.5 mice. Higher magnifica-

tion views of IF-preparations for Pex14p and catalase localization (d, e). Double-IF for Pex14p, combined with pro SP-C (f) or CC10 (h) as well as for catalase, combined with pro SP-C (g) or α -tubulin (i) in the adult mouse lung, depicting the distribution and abundance of different peroxisomal proteins in distinct pulmonary cell types. Bars represent c: 50 μ m; d, e: 25 μ m; f–i: 20 μ m

high concentrations of antioxidants and antioxidative enzymes (Halliwell and Gutteridge 1999).

Clara cell proteins and their involvement in ROS metabolism of the lung

Based upon morphology and histochemistry, Clara cells, the nonciliated cells of bronchioli, were first described by Kölliker (1881) and characterized in more detail by Clara (1937). Clara cells are nonmucous, nonserous, nonciliated, columnar to cuboidal secretory cells in the bronchiolar region of the pulmonary airways. The distribution and abundance of Clara cells in the airway epithelium is distinct among different species (e.g. mouse vs. human). In mouse bronchioli, Clara cells comprise 80% of the bronchiolar cells, whereas in the human lung, this cell type accounts only between 10 and 20% of the bronchiolar cells and ciliated cells predominate (Plopper et al. 1983). In contrast to this numerical difference, Clara cells of all species showed to be one of the most oxidant-resistant airway cell types. Their physiological role in pulmonary biology has not yet been entirely clarified, however, parts of their major functions include: (1) the secretion of the bronchioalveolar fluid as well as part of its constituent proteins and (2) the metabolism of xenobiotics, associated with cytochrome P450-dependent oxygenases. Moreover, precursor cells with Clara cell markers at the bronchioalveolar junction, expressing also low levels of the surfactant protein C (SP-C), are discussed as progenitor cells for the regeneration of the bronchiolar epithelium in the normal regeneration cycle and also during lung injury (Boyd 1977; Kim et al. 2005). Previous literature on this aspect showed that Clara cells actively regenerated the bronchiolar epithelium in an experimental animal model, using oxidant-induced damage to ciliated cells in rodent lungs (Evans et al. 1976). The major proteins secreted by Clara cells into the airway lumen and the extracellular lining fluid are the Clara cell 10-kDa protein (CC10) and the surfactant proteins A, B and D (SP-A, SP-B, SP-D). A series of investigations were carried out to elucidate the role of CC10 in airway biology, however, the exact functions of this protein remain elusive. Based on biochemical and biological properties of CC10 it was suggested that it (1) binds progestins or other lipophilic compounds, (2) binds calcium, (3) inhibits the secretory phospholipase A₂ and (4) decreases phagocyte chemotaxis (Singh and Katyal 2000). In addition, the involvement of CC10 in the protection against oxidative stress has been extensively investigated in recent years. Studies using chronic ozone exposure revealed that Clara cells compensate the ozone-induced oxidative stress by increasing their number and CC10 secretion, as well as increasing the activity of antioxidant enzymes. These results were further substantiated by investigations of Mango et al., exposing

CC10-deficient mice to an ozone challenge (Mango et al. 1998). Upon ozone exposure, these CC10-KO-mice showed elevated levels of oxidative stress, suggesting that the CC10 protein plays a vital role in regulating the ROS homeostasis of the airway epithelium. Furthermore, CC10-deficient mice are very sensitive to hyperoxia and exhibit alterations in inflammatory cytokine levels (Johnston et al. 1997). The high numerical abundance of peroxisomes in murine Clara cells and AECII and the prominent levels of peroxisomal enzymes in these cell types suggest that these organelles play a pivotal role in protecting the bronchiolar epithelium and the alveolar wall against high oxygen concentration and oxidative imbalance. In the human respiratory epithelium of bronchi (Karnati and Baumgart-Vogt 2008) and the bronchiolar epithelium (this article), the high numerical abundance of peroxisomes in ciliated cells may also contribute to the protection of the surface epithelia against ROS. Furthermore, peroxisomes might strongly influence the lipid metabolism in pulmonary epithelia, since they also contain high levels of lipid transporters and β -oxidation enzymes in these cell types (for a review on peroxisomal lipid metabolism in the lung see Karnati and Baumgart-Vogt 2008).

Alterations of “peroxisomal” antioxidant enzymes in airway epithelial cells

As mentioned in the “[Introduction](#)”, besides catalase, peroxisomes contain a variety of antioxidant enzymes, such as SOD1, glutathione peroxidase and peroxiredoxins I, V and VI. In addition, it is well known that oxidative stress also induces alterations in the peroxisomal compartment, such as tubulation of the organelles (Schrader and Fahimi 2006). Antibodies against SOD1, an enzyme with dual subcellular localization in the cytoplasm and the peroxisome, labelled the bronchiolar epithelium in healthy control subjects. Interestingly, the activity of this enzyme was decreased in asthmatic airway epithelia (Rahman et al. 2006). Furthermore, catalase and glutathione peroxidase activities also decreased in patients with asthma (Rahman et al. 2006). Therefore, it is most likely, that the peroxisomal compartment is affected in the airway epithelium of these patients. An altered peroxisomal lipid metabolism, such as a reduced ether lipid synthesis or a reduced peroxisomal β -oxidation of eicosanoids, important lipid mediators of inflammation, might perpetuate the inflammatory reaction. In this respect, it is noteworthy that activation of PPARs, the nuclear receptors regulating genes encoding peroxisomal proteins, ameliorates the inflammatory reaction in pulmonary airways (Paola and Cuzzocrea 2007). In addition, PPAR γ interferes also with the regulation of genes encoding for antioxidant proteins. Furthermore, some peroxisome proliferators, such as clofibrate or nafenopin, increase the number of

lamellar bodies in parallel to a significant increase in the number of peroxisomes in AECII of the rodent lung and it was suggested that surfactant synthesis is influenced in the lung by treatment with this compounds (Fringes et al. 1988; Fringes and Reith 1988). In addition, both compounds activate PPAR α , which induces the gene transcription of the PEX11 α gene, encoding a protein involved in peroxisome proliferation in the liver (Schrader et al. 1998). All of our results suggest a functional importance of the dynamic organelle “peroxisome” in airway protection and pulmonary cell biology.

Regulation of peroxisome proliferation by the proteins of the Pex11p family

The half life of the peroxisomes is only 3 days, wherefore peroxisomes are constantly formed or replaced by newly built peroxisomes, a process which is termed “peroxisomal biogenesis”. Peroxisomes are replicated by fission of pre-existing ones, regulated by proteins of the Pex11 family and DLP1/VpS1p (Delille et al. 2009). PEX11 proteins are components of the peroxisomal membrane in a wide variety of species including yeast, protozoan parasites and mammals. The mammalian family of Pex11 proteins contains three different isoforms: Pex11 α , Pex11 β , and Pex11 γ (Li et al. 2002a; b). PEX11 deletion studies in yeast or fibroblasts revealed a significant reduction in numerical peroxisome abundance, whereas overexpression of PEX11 β caused a pronounced increase in their abundance (Li and Gould 2002; Schrader et al. 1998). Overexpression of PEX11-cDNAs even led to a hyperproliferation of peroxisomes in distinct cell types. For more details on other proteins involved in peroxisome division and proliferation see Delille et al. (2009).

The vital importance of the Pex11 β p for the survival of the organism was revealed by the generation of PEX11 β deficient mice (Li et al. 2002b). Despite the presence of a reduced number of peroxisomes in all tissues, PEX11 β KO animals are severely growth retarded and die shortly after birth, a phenotype similar to patients with Zellweger syndrome (Baumgart et al. 2003; Gärtner 2003). Interestingly, however, plasmalogens and very-long-chain fatty acid levels were normal in PEX11 β KO-mice, suggesting that the defective peroxisome biogenesis rather than the disruption of peroxisomal metabolism led to the phenotype of these KO animals (Li and Gould 2002).

Future prospects for peroxisomes and Pex11 β on pulmonary biology

The presence of high levels of the PEX11 β -mRNA in distal airways in the newborn lung suggests that peroxisome proliferation and division is an important process in the

developing airways and during alveolarization. Indeed, PEX11 β -knockout mice exhibit less developed distal airways and reduced alveolarization in comparison to control animals (unpublished observation of E. Baumgart-Vogt). A detailed report on the pathological alterations of pulmonary airways and the alveolar region in these knockout animals will be published in a separate article in the near future. Delay and alterations in pulmonary development, however, certainly contribute to the early death of the PEX11 β animals shortly after birth. Therefore, studies with lung tissue of PEX11 β (-/-) animals for the elucidation of the molecular alterations due to peroxisome deficiency will provide more insights on the function of this organelle in pulmonary biology.

Acknowledgments The technical assistance of Andrea Klein, Elke Richter and Magdalena Gottwald is gratefully acknowledged. In addition, we thank Profs. D.I. Crane, S.J. Gould, P.P. Van Veldhoven and A. Völkl for providing of antibodies (for addresses see Karnati and Baumgart-Vogt 2008). We are indebted also to Dr. M. Schrader (University of Aveiro, Portugal) for the generous gift of the plasmid with the murine PEX11 β -cDNA. This study was supported by funds of the PhD-programme and LOM-funds of the Medical Faculty of the Justus Liebig University, Giessen.

References

- Baumgart E, Fahimi HD, Steininger H, Grabenbauer M (2003) A review of morphological techniques for detection of peroxisomal (and mitochondrial) proteins and their corresponding mRNAs during ontogenesis in mice: application to the PEX5-knockout mouse with Zellweger syndrome. *Microsc Res Tech* 61:121–138
- Boyd MR (1977) Evidence for the Clara cell as a site of cytochrome P450-dependent mixed-function oxidase activity in lung. *Nature* 269:713–715
- Clara M (1937) Zur Histobiologie des Bronchiaepithels. *Z Mikrosk Anat Forsch* 41:321–347
- Delille HK, Alves R, Schrader M (2009) Biogenesis of peroxisomes and mitochondria: linked by division. *Histochem Cell Biol*. doi:10.2007/s00418-009-0561-9
- Evans MJ, Johnson LV, Stephens RJ, Freeman G (1976) Cell renewal in the lungs of rats exposed to low levels of ozone. *Exp Mol Pathol* 24:70–83
- Fringes B, Reith A (1988) Two hypolipidemic peroxisome proliferators increase the number of lamellar bodies in alveolar cells type II of the rat lung. *Exp Mol Pathol* 48:262–271
- Fringes B, Gorgas K, Reith A (1988) Clofibrate increases the number of peroxisomes and of lamellar bodies in alveolar cells type II of the rat lung. *Eur J Cell Biol* 46:136–143
- Gail DB, Lenfant CJ (1983) Cells of the lung: biology and clinical implications. *Am Rev Respir Dis* 127:366–387
- Gärtner J (2003) Is there a phenotype/genotype correlation in peroxisome biogenesis disorders (PBDs)? *Adv Exp Med Biol* 544:59–65
- Grabenbauer M, Fahimi HD, Baumgart E (2001) Detection of peroxisomal proteins and their mRNAs in serial sections of fetal and newborn mouse organs. *J Histochem Cytochem* 49:155–164
- Halliwell B, Gutteridge JMC (1999) Free radicals in biology and medicine, 3rd edn. Oxford University Press, Oxford
- Immenschuh S, Baumgart-Vogt E (2005) Peroxiredoxins, oxidative stress, and cell proliferation. *Antioxid Redox Signal* 7:768–777

- Johnston CJ, Mango GW, Finkelstein JN, Stripp BR (1997) Altered pulmonary response to hyperoxia in Clara cell secretory protein deficient mice. *Am J Respir Cell Mol Biol* 17:147–155
- Karnati S, Baumgart-Vogt E (2008) Peroxisomes in mouse and human lung: their involvement in pulmonary lipid metabolism. *Histochem Cell Biol* 130:719–740
- Kim CF, Jackson EL, Woolfenden AE, Lawrence S, Babar I, Vogel S, Crowley D, Bronson RT, Jacks T (2005) Identification of bronchioalveolar stem cells in normal lung and lung cancer. *Cell* 121:823–835
- Kölliker A (1881) Zurkeniniss des Baues der Lunge des Menschen. *Verh Phys Med Ges* 16:1–24
- Li X, Gould SJ (2002) PEX11 promotes peroxisome division independently of peroxisome metabolism. *J Cell Biol* 156:643–651
- Li X, Baumgart E, Dong GX, Morrell JC, Jimenez-Sanchez G, Valle D, Smith KD, Gould SJ (2002a) PEX11alpha is required for peroxisome proliferation in response to 4-phenylbutyrate but is dispensable for peroxisome proliferator-activated receptor alpha-mediated peroxisome proliferation. *Mol Cell Biol* 22:8226–8240
- Li X, Baumgart E, Morrell JC, Jimenez-Sanchez G, Valle D, Gould SJ (2002b) PEX11 beta deficiency is lethal and impairs neuronal migration but does not abrogate peroxisome function. *Mol Cell Biol* 22:4358–4365
- Mango GW, Johnston CJ, Reynolds SD, Finkelstein JN, Plopper CG, Stripp BR (1998) Clara cell secretory protein deficiency increases oxidant stress response in conducting airways. *Am J Physiol* 275:L348–L356
- Paola RD, Cuzzocrea S (2007) Peroxisome proliferator-activated receptors and acute lung injury. *PPAR Res* 2007:63745
- Petrik P (1971) Fine structural identification of peroxisomes in mouse and rat bronchiolar and alveolar epithelium. *J Histochem Cytochem* 19:339–348
- Plopper CG, Pinkerton KE (1992) Overview of diversity in the respiratory system of mammals. In: Parent RA (ed) *Comparative biology of the normal lung I*. CRC Press, Boca Raton, FL, pp 3–5
- Plopper CG, Mariassy AT, Wilson DW, Alley JL, Nishio SJ, Nettesheim P (1983) Comparison of nonciliated tracheal epithelial cells in six mammalian species: ultrastructure and population densities. *Exp Lung Res* 5:281–294
- Rahman I, MacNee W (2000) Oxidative stress and regulation of glutathione in lung inflammation. *Eur Respir J* 16:534–554
- Rahman I, Biswas SK, Kode A (2006) Oxidant and antioxidant balance in the airways and airway diseases. *Eur J Pharmacol* 533:222–239
- Schneeberger EE (1972) A comparative cytochemical study of microbodies (peroxisomes) in great alveolar cells of rodents, rabbit and monkey. *J Histochem Cytochem* 20:180–191
- Schrader M, Fahimi HD (2006) Growth and division of peroxisomes. *Int Rev Cytol* 255:237–290
- Schrader M, Reuber BE, Morrell JC, Jimenez-Sanchez G, Obie C, Stroh TA, Valle D, Schroer TA, Gould SJ (1998) Expression of PEX11beta mediates peroxisome proliferation in the absence of extracellular stimuli. *J Biol Chem* 273:29607–29614
- Singh G, Katyal SL (2000) Clara cell proteins. *Ann N Y Acad Sci* 923:43–58
- Sorokin SP (1988) The respiratory system: cell and tissue biology. In: Weiss L (ed) *Chapter 25, Sixth edn*. Urban and Schwarzenberg, Munich, pp 751–814. ISBN: 753-541-72176-72176

Mammalian SOD2 is exclusively located in mitochondria and not present in peroxisomes

Srikanth Karnati · Georg Lüers · Susanna Pfreimer ·
Eveline Baumgart-Vogt

Accepted: 8 May 2013 / Published online: 7 June 2013
© Springer-Verlag Berlin Heidelberg 2013

Abstract Superoxide dismutases (SODs) are metalloenzymes that belong to the essential antioxidant enzyme systems of virtually all oxygen-respiring organisms. SODs catalyze the dismutation of highly reactive superoxide radicals into hydrogen peroxide and molecular oxygen. For the subcellular localization of the manganese superoxide dismutase (SOD2) in eukaryotic cells, a dual mitochondrial localization and peroxisomal localization were proposed in the literature. However, our own observation from immunofluorescence preparations of human and mouse tissues suggested that SOD2 serves as an excellent marker protein for mitochondria but never co-localized with peroxisomes. To clarify whether our observations were correct, we have carefully reinvestigated the subcellular localization of SOD2 using sensitive double-immunofluorescence methods on frozen and paraffin sections as well as in cell culture preparations. In addition, ultrastructural analyses were performed with post-embedding immunoelectron microscopy on LR White sections as well as labeling of ultrathin cryosections with various immunogold techniques. In all morphological experiments, the SOD2 localization was compared to one of the catalase, a typical marker protein for peroxisomes, solely localized in these organelles. Moreover, biochemical subcellular fractions of mouse liver was

used to isolate enriched organelles and highly purified peroxisomal fractions for Western blot analyses of the exact subcellular distributions of SOD2 and catalase. All results with the various methodologies, tissues, and cell types used revealed that catalase and SOD2 were always confined to distinct and separate subcellular compartments. SOD2 was unequivocally in mitochondria, but never present in peroxisomes. Furthermore, our results are supported by accumulating database information on organelle proteomes that also indicate that SOD2 is a pure mitochondrial protein.

Keywords Peroxisome · Lung · SOD2 · MnSOD · Catalase · Immunolabeling

Abbreviations

AECII	Alveolar epithelial cell type II
PFA	Paraformaldehyde
PBS	Phosphate-buffered saline
SOD2	Superoxide dismutase 2
CAT	Catalase
ROS	Reactive oxygen species

Introduction

Superoxide dismutases (SODs) are metalloenzymes that belong to the essential antioxidant enzyme systems of virtually all oxygen-respiring organisms. SODs catalyze the dismutation of highly reactive superoxide radicals into hydrogen peroxide and molecular oxygen (Miao and St. Clair 2009). The hydrogen peroxide can be further degraded by catalase, glutathione peroxidase, and peroxiredoxins (Immenschuh and Baumgart-Vogt 2005; Schrader and

S. Karnati · G. Lüers · S. Pfreimer · E. Baumgart-Vogt (✉)
Division of Medical Cell Biology, Institute for Anatomy
and Cell Biology II, Justus Liebig University, Aulweg 123,
35385 Giessen, Germany
e-mail: Eveline.Baumgart-Vogt@anatomie.med.uni-giessen.de
URL: <http://www.med.uni-giessen.de/anat/>

Present Address:

G. Lüers
Institute for Anatomy and Experimental Morphology, UKE,
Hamburg, Germany

Fahimi 2006). Three distinct forms of SODs have been identified and characterized in mammals depending on the metal content: a homodimeric Copper/Zinc superoxide dismutase (Cu/ZnSOD = SOD1) (McCord and Fridovich 1969); a homotetrameric Manganese (Mn) superoxide dismutase (MnSOD = SOD2) (Weisiger and Fridovich 1973b); and a homotetrameric glycosylated superoxide dismutase (SOD3) (Marklund 1982). SOD1 has been found in different cell compartments such as in the cytoplasm, nucleus, microsomes, and mitochondrial intermembrane space and also in peroxisomes (McCord and Fridovich 1969; Okado-Matsumoto and Fridovich 2001). SOD2 was first identified in *E. coli* (Keele et al. 1970) and was found across various phyla of archae, eubacteria, and eukaryotes (Culotta et al. 2006). In eukaryotes, SOD2 was described in the mitochondrial matrix and intermembrane space (Weisiger and Fridovich 1973a) and also in peroxisomes (Singh et al. 1999). In contrast to SOD1 and SOD2 which are present in different intracellular compartments, SOD3 was found in the extracellular matrix of mammalian tissues (Nozik-Grayck et al. 2005).

Peroxisomes are versatile organelles with distinct protein composition and abundance in different organs or cell types and are extensively involved in the metabolism of reactive oxygen species (ROS) and lipids (Karnati and Baumgart-Vogt 2008; Nenicu et al. 2007). Peroxisomes harbor a variety of antioxidative enzymes that are involved in the detoxification ROS including catalase, glutathione peroxidase, peroxiredoxin 1 and SOD1. As mentioned above, besides mitochondrial localization, SOD2 has been suggested to be present also in peroxisomes, based on immunostaining and on biochemical evidence (Singh et al. 1999). However, SOD2 has no peroxisomal targeting signal but a rather clear mitochondrial signal instead that is targeting SOD2 into mitochondria (Miao and St. Clair 2009; Shimoda-Matsubayashi et al. 1996).

Using specific antibodies to SOD2, we always observed an exclusively mitochondrial staining pattern in our immunofluorescence analyses of diverse mammalian tissues. We have therefore questioned the peroxisomal localization of SOD2, and here, we present refined subcellular localization data based on optimized and ultra-sensitive morphological and biochemical methods.

Materials and methods

Animals and human tissue material

Mice

Nine adult male mice, 12–15 weeks of age, and two pregnant mice of C57BL/6 J genetic background were

obtained from (Charles River, Sulzfeld, Germany) kept on a normal laboratory diet and water ad libitum and housed in cages under standardized environmental conditions (12 h light/dark cycle, 23 ± 1 °C and 55 ± 1 % relative humidity). New born pups were taken directly in the morning after the delivery ($P = 0.5$). All experiments with laboratory mice were approved by the German Government Commission of Animal Care. Human lung biopsies from three donors were obtained from the University of Giessen Lung Centre (UGLC) tissue collection bank. Characteristics of donors have been described in Karnati and Baumgart-Vogt (2008). The study protocol for human tissue use was approved by the local internal review board of the ethics committee of the Medical Faculty of the Justus Liebig University of Giessen (Germany), in accordance with national law and with “Good Clinical Practice/International Conference on Harmonisation” guidelines (see Karnati and Baumgart-Vogt 2008).

Cell culture and immunostaining of cells

The cell lines BGL166 (Lüers et al. Cytogenetic & genome research, 2003) and BGL190 (Islinger et al. 2006) were cultured in DMEM (PAA, Cölbe, Germany) supplemented with 10 % (v/v) FCS, 2 mM L-Glutamine, and 100 units/ml penicillin (PAA, Cölbe, Germany) at 37 °C in a humidified atmosphere of 5 % CO₂. BGL166 is a mouse fibroblast line derived from 3T3 cells and BGL190 is a human hepatoma cell line derived from HepG2 cells. Both cell lines are stably expressing a GFP-PTS1 fusion protein under the control of the murine phosphoglycerate kinase promoter. The GFP-PTS1 fusion protein is imported into the matrix of peroxisomes via its peroxisomal targeting signal (PTS1), which are labeled by the green fluorescent protein (GFP) in transgenic cells.

For colocalization studies of peroxisomal proteins, GFP-PTS1-transgenic cells cultured on coverslips were fixed at room temperature in 4 % freshly depolymerized paraformaldehyde in 0.15 M HEPES, pH 7.4 for 15 min. Cells were washed with PBS and permeabilized with 0.2 % Triton X-100 and 0.2 % Tween 20 in PBS (pH 7.4). To reduce non-specific binding of antibodies, cells were blocked for 30 min with Roti-Block (Roth, Karlsruhe, Germany) in PBS. Roti-Block was also used for dilution of specific antibodies. For routine immunostaining, cells were incubated for 2 h with polyclonal primary antibodies against SOD2 (Abcam, Cambridge, UK, Cat.no: ab13533). After washing of the coverslips 3 times for 5 min, they were incubated with a Cy3-conjugated goat anti-rabbit antibody (1:300; Dianova, Hamburg, Germany) for 1 h. After final washing (3 × 5 min) in PBS, the coverslips were mounted with 50 % glycerol in PBS containing 1.5 % (w/v) n-propyl gallate as an antifading agent.

Morphological methods

Processing of tissue for immunofluorescence

Three adult mice and new born mouse pups of 2 l were fixed via Cardiac perfusion with a fixative containing 4 % PFA in PBS (pH 7.4) either via the left ventricle for liver tissue or via the right ventricle for lung tissue. Briefly, mouse lungs were inflated with air via tracheal cannulation and the lungs thereafter perfused via the right ventricle. Lungs and trachea were dissected out and the trachea instilled for overnight immersion fixation in the same solution.

The detailed protocol procedure for paraffin embedding, sectioning of tissues, and subsequent immunofluorescence were followed as described previously in our publications (Karnati and Baumgart-Vogt 2008, 2009). The lungs were dissected out and further immersion-fixed in the same fixative. Fixed lung and liver samples were embedded into paraffin (Paraplast, Sigma, St. Louis, MO, USA) using a Leica TP 1020 automated vacuum infiltration tissue processor. Paraffin sections (2–3 μm) were cut with a Leica RM2135 rotation microtome and processed for double immunofluorescence as described in Karnati and Baumgart-Vogt (2008). Dilutions of the primary and secondary antibodies used are listed in Table 2. Negative controls were processed in parallel by addition of TBST buffer instead of the first antibodies. Nuclei were visualized with 1 μM TOTO-3 iodide for 10 min at room temperature (Table 1). Samples were analyzed by confocal laser scanning microscopy (CLSM) with a Leica TCS SP2 (Leica Mikrosysteme Vertrieb GmbH, Wetzlar, Germany).

Fixation of tissues for electron microscopy

For electron microscopy, newborn (postnatal day 0.5) and adult mice were fixed by Cardiac perfusion (right ventricle for lung; left ventricle for liver) with 4 % (w/v) PFA, 0.05 % (v/v) glutaraldehyde in 0.1 M sodium cacodylate buffer with 2 % (w/v) sucrose, pH 7.4. Thereafter, liver or lungs were dissected out and immersed in a fixative containing only 4 % (w/v) PFA in 0.1 M sodium cacodylate buffer with 2 % sucrose at 4 °C. Thin vibratome sections of liver or lung were cut from these tissues, and the lung slices placed in a vacuum desiccator for 1 h in immersion fixative solution at room temperature to remove the air. Liver vibratome slices were immediately processed for embedding into LR White or processed for cryo-electron microscopy (see below).

Post-embedding immunoelectron microscopy

Wet liver or lung sections, after dissection from adult animals or newborn pups, were dehydrated and embedded

in LR White (medium grade) (LR White Resin, Berkshire, England) according to the protocol of Newman and colleagues (Newman et al. 1983). Ultrathin sections (60 nm) of lung and liver tissue were collected on formvar-coated nickel grids and non-specific protein-binding sites were blocked by placing the grids with sections down on 1 % BSA in TBS, pH 7.4, for 30 min. Primary antibody incubations were done with anti-catalase or SOD2 antibodies (Table 1). The next morning, the sections on grids were washed 12 times on series of TBSA and subsequently incubated for 60 min with protein A-gold (PAG, gold particle size 15 nm), diluted 1:75 in TBSA (Slot and Geuze 1981). Thereafter, the grids with sections were washed shortly in a flow of distilled water and air dried. Incubated sections were contrasted with uranyl acetate for 2 min and lead citrate for 45 s followed by examination in a LEO 906 transmission electron microscope (LEO electron microscopy, Oberkochen, Germany). For negative controls, ultrathin sections were processed in parallel without primary antibody followed by the protein A-gold complex.

Immunolabeling of ultrathin cryosections

Liver tissue of adult and newborn mice was cut into 2 mm³ tissue blocks and immersed for cryoprotection. Fixed vibratome sections (100 μm thick) from newborn and adult mouse livers were immersed for cryoprotection in 2.3 M Sucrose in 0.1 M PBS (pH 7.4) on a rotating wheel overnight at 4 °C. The next morning, the solution was replaced by a fresh one and the tissue blocks further immersed for 2 days. Infiltrated tissue slices were mounted on an aluminum pin and frozen in liquid nitrogen. Ultrathin sections of newborn and adult livers (60 nm) for cryo-electron microscopy were cut at –120 °C with a cryo-diamond knife (Diatome, Switzerland). Sections were picked up from the knife with a loop dipped in 1.15 M sucrose and 1 % (w/v) Methylcellulose and transferred to formvar-coated nickel grids. Sections were incubated with the rabbit anti-SOD2 antibody (Abcam, Cambridge, UK, Cat.no: ab13533; 1:500) in 0.1 % BSA in TBS overnight. After washing with TBSA, the grids were incubated for 2 h with gold-labeled goat anti-rabbit Fab fragments (Table 1) (Aurion, Wageningen, Netherlands). The subsequent washing steps were performed as described above.

Biochemical techniques

Preparation of peroxisomal fractions from adult mouse liver tissue

Six adult male mice were fasted overnight and anesthetized, and the livers were perfused with physiological

Table 1 List of antibodies used in this study

Antigens	Species AB raised in (AB)	Molecular weight (kDa)	Dilution (IF)	Dilution (WB)	Dilution (EM)	Supplier
<i>Primary antibodies</i>						
Superoxide Dismutase 2, Human	Rabbit, polyclonal	25	1:2,000	1:20,000	1:50	Abcam, Cambridge, UK, Cat.no: ab13533
Superoxide Dismutase 2, Human	Rabbit, polyclonal	25	1:1,000	–	–	RDI Systems, Flanders, NJ, USA; Cat. No.: RDI-RTSODMabr
Catalase, Human	Goat, polyclonal	60	1:1,000	–	–	Abcam, Cambridge, UK, Cat.no: ab50434
Catalase, Mouse	Rabbit, polyclonal	60	1:2,000	1:50,000	1:50	Gift from Denis Crane, Biomolecular and Biophysical Sciences, Griffith University, Nathan, Brisbane, Australia; see reference Karnati and Baumgart-Vogt (2008)
<i>Secondary antibodies, protein A and ultrasmall immunogold</i>						
Secondary detection system used		Host	Method	Dilution	Supplier	
<i>Secondary antibodies, protein A and ultrasmall immunogold</i>						
Protein A-gold		–	EM	1:75	See Ref. Slot and Geuze (1981)	
Ultrasmall immunogold		Goat	EM	1:70	Aurion, Wageningen, Netherlands	
Anti-Rabbit-IgG AlexaFluor488		Donkey	IF	1:1,000	Molecular Probes/Invitrogen, Cat. no: B-6648	
Anti-Mouse-IgG AlexaFluor555		Donkey	IF	1:1,000	Molecular Probes/Invitrogen, Cat. no: A31570	
Anti-Goat-IgG AlexaFluor594		Chicken	IF	1:1,000	Molecular Probes/Invitrogen, Cat. no: A11058	
<i>Counterstaining of nuclei for IF</i>						
TOTO-3 nucleic acid staining		–	IF	1:1,000	Molecular Probes/Invitrogen, Cat. no: T-3604	

saline via the portal vein. Livers were excised and minced with a scissor in chilled homogenization buffer (HB) containing 0.25 M sucrose and 5 mM MOPS (pH 7.4), 1 mM EDTA, 0.1 % ethanol, 0.2 mM DTT, 1 mM aminocaproic acid and 100 μ l cocktail of protease inhibitors (# 39102, Serva, Germany).

Two gram of liver tissue was homogenized in 4 ml ice-cold HB with a single stroke for 60 s at 1,000 rpm of Potter–Elvehjem homogenizer held in an ice-water bath (B. Braun Biotech International, Melsungen, Germany). A differential centrifugation of liver homogenates and isolation of peroxisomes by an Optiprep™ cushion method were performed. Briefly, clumps of connective tissue and nuclei were sedimented by centrifugation of the homogenates at 100 \times g for 12 min at 4 °C. The supernatant was further processed by centrifugation (Sorvall Evolution RC centrifuge, Kendro Laboratory Products, Asheville, NC) at 3,000 \times g for 20 min at 4 °C to obtain a heavy mitochondrial fraction (P1) in the pellet. The supernatant (S2) was subjected to centrifugation at 20,000 \times g for 12 min to obtain a pellet with the light mitochondrial fraction (P2) that consists of a mixture of peroxisomes, light mitochondria, lysosomes, and few microsomes. Each of the pellets obtained was washed once by resuspension in an appropriate volume of homogenizing buffer using a glass rod and re-centrifuged under the same conditions. 1 ml of

the light mitochondrial fraction (P2) was layered on top of the Optiprep™ step gradient (4 ml of 30 % and 4 ml of 50 % (w/v) Iodixanol) in Sorvall tubes (Sorvall Centrifuge, Newton, USA). Gradient tubes were centrifuged at 60,000 \times g for 2.5 h in a SE 12 rotor (Sorvall ultra-centrifuge, Sorvall Evolution RC). After centrifugation, the peroxisomal fraction was removed by aspiration with a Pasteur pipette. This peroxisomal fraction consists primarily of peroxisomes with only minimal contamination by other cell organelles, for example, mitochondria and microsomes. Protein concentrations in all fractions were determined by using the Bradford method (Bradford 1976).

Western blot analysis

Polypeptides of all fractions obtained by differential centrifugation and the highly purified peroxisomal fractions were separated by SDS–PAGE using a Bio-Rad electrophoresis apparatus (Bio-Rad, Heidelberg, Germany). Proteins (10 μ g) from each sample and 5 μ l of color stained as well as 6 μ l of a (1:30 diluted) biotinylated marker (Precision markers from Bio-Rad) were separated by SDS–PAGE (12 % resolving gel). Protein transfer was done by semi-dry blotting onto polyvinylidene difluoride membranes (Millipore, Schwalbach, Germany) with a Trans-Blot semi-dryer (Bio-Rad). Non-specific protein-binding

Table 2 SOD2 is exclusively localized to mitochondria in various organ systems and cell types of five different species

Species	Organ	Cell type	SOD2 localization in mitochondria	CAT localization in peroxisomes	SOD2 localization in peroxisomes	
Monkey	Liver	Hepatocytes, Kupffer cells, Endothelial cells	✓	✓	×	
Rabbit	Liver	Hepatocytes, Kupffer cells, Endothelial cells	✓	✓	×	
Rat	Liver	Hepatocytes, Kupffer cells, Endothelial cells	✓	✓	×	
Mouse embryo	Liver	Hepatocytes, Kupffer cells, Endothelial cells	✓	✓	×	
	Intestine	Enterocytes	✓	✓	×	
	Lung	AECII, AECI, Clara, ciliated cells and macrophages	✓	✓	×	
	Kidney	Epithelial cells, Endothelial cells	✓	✓	×	
	Adrenal gland		✓	✓	×	
	Eye-retina		✓	✓	×	
	Epidermis	Epithelial cells	✓	✓	×	
	Connective tissue	Fibroblasts	✓	✓	×	
	Cartilage	Chondrocytes	✓	✓	×	
	Brown fat	Adipocytes	✓	✓	×	
	Bone	Osteoblasts, Osteoclasts	✓	✓	×	
	Muscle	Skeletal muscle cells	✓	✓	×	
	Brain	Leptomeningeal mesothelial cells	✓	✓	×	
	Plexus Choroideus	Neurons	✓	✓	×	
	Spinal Ganglion	Pseudounipolar neurons	✓	✓	×	
	Dog	Lung	AECII, Clara, ciliated cells and macrophages	✓	✓	×

Paraffin-embedded sections of various organs of five different species were subjected to double-IF with anti-SOD2 (Abcam, Cambridge, UK, Cat.no: ab13533) and anti-catalase (a kind gift from Denis Crane) antibodies. This table provides the subcellular localization of SOD2 and catalase in various cell types of different organ systems of five species. None of the results obtained from immunofluorescence experiments showed the localization of SOD2 in peroxisomes, whereas catalase solely localized to peroxisomes

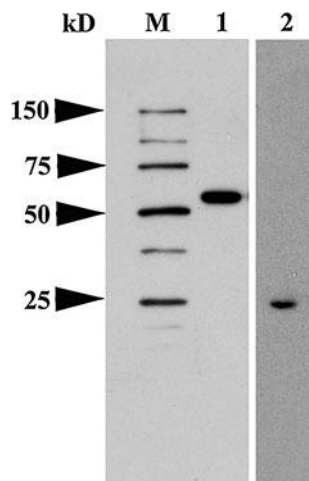


Fig. 1 Western blot analysis of catalase and SOD2 in adult mouse liver homogenate. 20 μ g of total protein was loaded from mouse liver homogenate and immunostained with anti-catalase (a kind gift from Denis Crane laboratory) (lane 1) and anti-SOD2 (Abcam, Cambridge, UK, Cat.no: ab13533) (lane 2). The size of markers is indicated on the left side

sites on membranes were blocked overnight at 4 °C in blocking solution consisting of 10 % fat-free milk powder (Carl Roth, Karlsruhe, Germany) in TBST (TBS plus

0.5 % Tween 20). Primary antibodies were diluted in 5 % blocking solution and the membranes incubated for 2 h at room temperature. Dilutions of antibodies are summarized in Table 1. After washing with TBST (3 \times 10 min), blots were incubated with alkaline phosphatase-conjugated anti-rabbit IgG (Sigma, Steinheim, Germany) for 2 h. After final washing with TBST (3 \times 10 min), immunoreactive bands were visualized with the ImmunostarTM detection kit (Bio-Rad, Hercules, CA) with a chemiluminescent substrate followed by exposure to BioMax MR-Film (Kodak, Stuttgart, Germany). Biotinylated marker proteins on membranes were visualized by incubation with streptavidin-AP conjugate.

Results

Highly sensitive monospecific antibodies against proteins of interest are a prerequisite for the correct localization of these proteins in distinct subcellular compartments. Therefore, the anti-SOD2 (Abcam, Cambridge, UK, Cat.no: ab13533) and catalase antibodies (a kind gift from Denis Crane, Griffith University, Brisbane, Australia) were tested in preliminary experiments by Western blot analysis

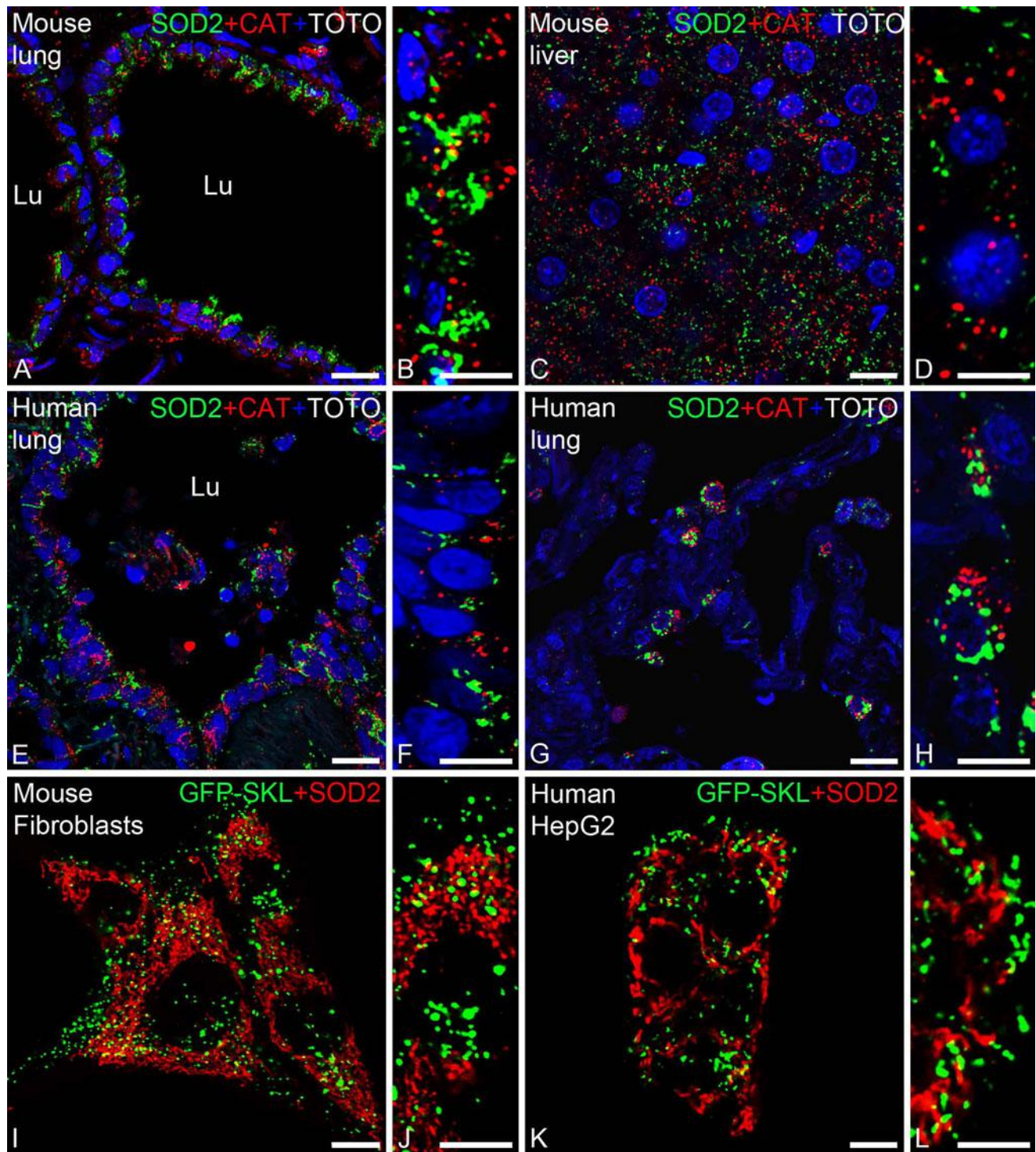


Fig. 2 Double-immunofluorescence localization of SOD2 and catalase in different cell compartments. Double-IF preparations for peroxisomal marker protein catalase (Abcam, Cambridge, UK, Cat.no:ab50434) combined with SOD2-labeling (Abcam, Cambridge, UK, Cat.no: ab13533) (a–h) depicted the clear subcellular distribution in individual subcellular compartments. Staining for the catalase with the SOD2 in the bronchiolar epithelium of the mouse (a, b) and human lung (e, f) as well as the alveolar epithelium mainly in AECII cells of the human lung (g, h) shows no signs of co-localization. The same observation was also detected in hepatocytes (c, d) in adult mouse liver preparations, in which

the organelles are more round and more easily distinguishable from each other. Nuclear counter staining in (a–h) was performed with TOTO-3-iodide. Double-immunofluorescence staining for SOD2 (red) and GFP-labeled peroxisomes (green) in the cultured mouse fibroblasts (i, j) and in human HepG2 (k, l) cells. Also in both cell monolayers, SOD2 is not co-localizing with GFP-labeled peroxisomes, suggesting that SOD2 is not a peroxisomal protein. Few yellow overlaps indicate a close neighborhood of both organelles with each other, under the limit of fluorescence microscopic resolution. Bars represent a, c, e, g 25 μm ; b, d, f, h 10 μm ; j, l 10 μm ; i, k 20 μm

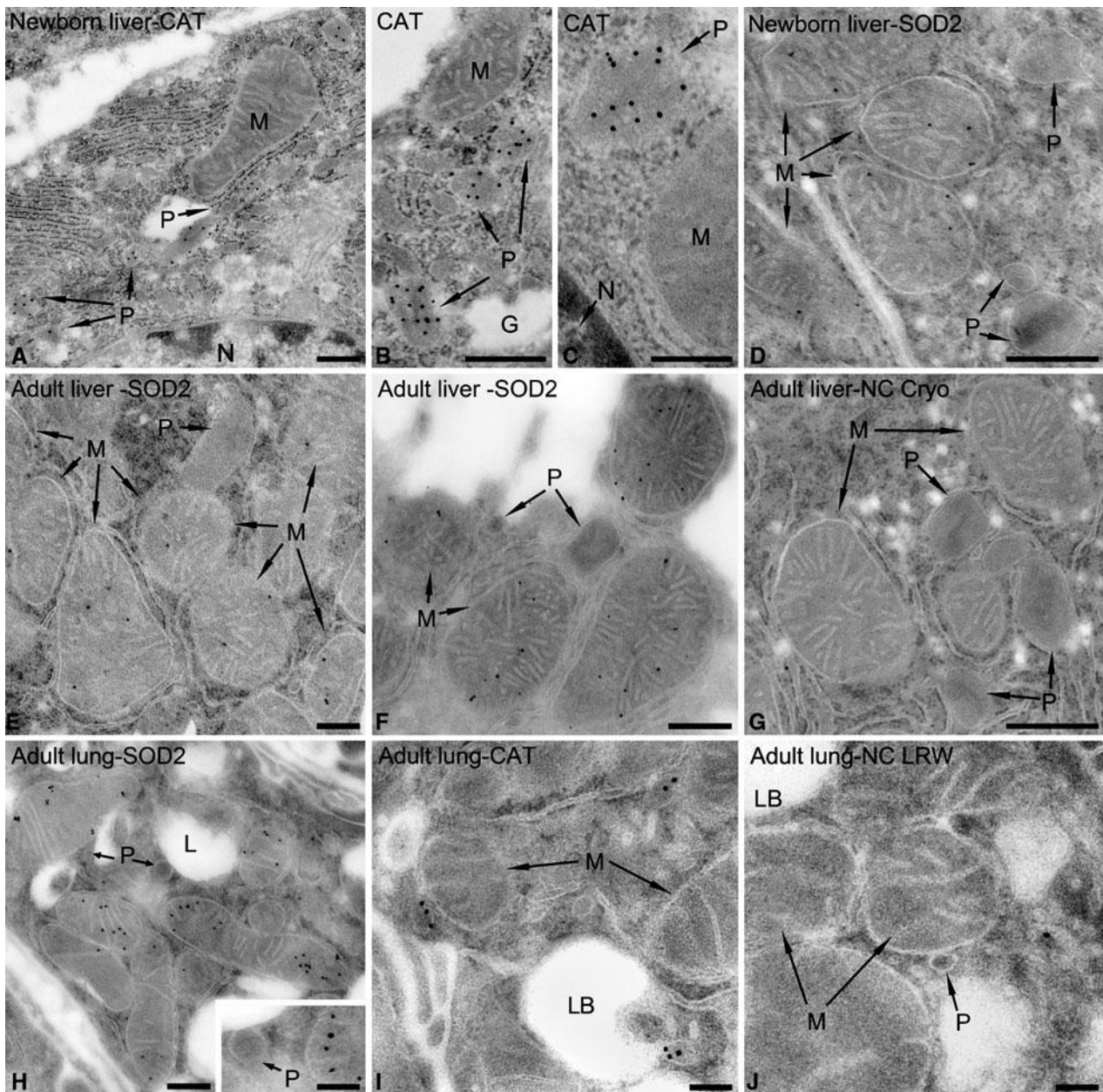


Fig. 3 Ultrastructural immunocytochemical localization of SOD2 and catalase in distinct organelles in AECII of mouse lung and hepatocytes of liver. Electron microscopic immunocytochemical localization of the catalase protein in the hepatocytes of newborn liver with the post-embedding protein A-gold technique on LR White sections (a–c). **a** Lower magnification views of several peroxisomes in the cytoplasm surrounded by mitochondria and glycogen particles adjacent to the nucleus of hepatocytes in the mouse liver. **b, c** Higher magnification view of a region containing peroxisomes and mitochondria. Electron micrograph exhibits a peroxisome with a negative urate oxidase core and the close neighborhood to a mitochondrion showing the high specificity for catalase labeling. **d** Immunocytochemical localization of the SOD2 protein in newborn and adult liver hepatocytes (e, f) in the ultrathin cryosections with ultrasmall gold-labeled Fab fragments and silver intensification. Also with this highly sensitive method, peroxisomes are devoid of SOD2, whereas this protein could clearly be localized in mitochondria of newborn (d) or adult hepatocytes (e, f). Negative

controls for the ultrasmall gold silver intensification methods were very clean and only seldom could gold particles with random distribution on ultrathin cryosections of the liver (g) be observed. Labeling for SOD2 in LR White sections with the ultrasmall gold silver intensification method exhibited the same results, but a clearly lower labeling intensity (h) for SOD2 was detected. A neighborhood of peroxisomes with mitochondria was observed in many instances, corroborating the fluorescence microscopic findings. Due to the high SOD2 content in the mitochondria of AECII cells of the adult mouse lung, the inset picture in the (h) clearly shows the SOD2 labeling only in mitochondria but not in the neighboring peroxisomes. Even though cross-section of peroxisomes is very small in AECII cells, these organelles can be clearly labeled for catalase already with the PAG method (i). Negative controls very seldom contained gold particles that were randomly distributed in AECII cells (j). *M* mitochondria, *G* glycogen, *N* nucleus, *P* peroxisomes, *Lu* lung, *LB* lamellar bodies. Bars represent a, d, e–g, i, j 1 μ m; b, c 0.5 μ m; h 0.25 μ m

of adult mouse liver homogenates (Fig. 1). In these Western blots, only bands with correct molecular weight at 24.6 kDa for SOD2 and 59 kDa for catalase were detected, suggesting a high specificity of both antibodies.

Catalase and SOD2 are localized in double-immunofluorescence preparations in distinct subcellular compartments

To analyze the localization of SOD2 in comparison with the localization of catalase, we performed double-immunofluorescence stainings for both proteins. In preliminary experiments, different antibodies against SOD2 (Abcam, Cambridge, UK, Cat.no: ab13533) and RDI Systems (Flanders, NJ, USA; Cat. No.: RDI-RTSODMabr) were tested for their specificity and for optimal concentrations to detect SOD2 by indirect immunofluorescence (data not shown). With optimized conditions, we could show in double-immunofluorescence preparations that catalase and SOD2 exhibited a different staining and distribution patterns in cells from liver and lung in mouse as well as in human samples (Fig. 2). A distinct compartmentalization could be shown in bronchiolar and alveolar type 2 epithelial cells (Fig. 2a, b, e–h) and in hepatocytes (Fig. 2c, d). Also at higher magnification (Fig. 2b, d, f, h), the SOD2 was not colocalized with catalase. In some instances, however, a minimal overlap of the fluorescence signal at the organelle periphery indicated that although both proteins were localized within different subcellular compartments, peroxisomes and mitochondria are in close proximity to each other within the cells, which is also observed in electron micrographs (Fig. 3). Furthermore, we have analyzed the distribution pattern of both proteins in transiently transfected human hepatoma cells (HepG2, Fig. 2k, l) and mouse fibroblasts (3T3, Fig. 2i, j), expressing a GFP-PTS1 fusion protein, which is imported into peroxisomes via its peroxisomal targeting signal (PTS1). Therefore, all peroxisomes were labeled by the green fluorescent protein (GFP), whereas immunostaining for SOD2 revealed that specific fluorescence signals were not colocalized as it was the case in liver and lung tissue sections.

SOD2 is a mitochondrial protein that could not be detected in peroxisomes even by highly sensitive immunoelectron microscopy on ultrathin cryosections

Since peroxisomes are best characterized in hepatocytes, we have used mouse liver for the standardization of the techniques and the first analysis of the subcellular localization of catalase and SOD2 at the ultrastructural level. At first, as a positive control, LR White sections as well as ultrathin cryosections of newborn liver and adult liver were

stained for catalase with the protein A-gold technique (15 nm gold size), whereby we could show that catalase was specifically localized in peroxisomes (Fig. 3a–c) and that other subcellular compartments such as the nucleus, cytoplasm, and mitochondria were devoid of gold particles. Subsequently, the localization of SOD2 was analyzed on LR White sections in parallel to catalase. With this technique, a specific labeling of mitochondria was obtained, however, with a relatively low labeling density. No other organelles were stained. Negative controls on LR White sections with the PAG method always showed very few randomly distributed gold particles. To obtain the highest sensitivity labeling for SOD2, both were done on LR White sections and more importantly ultrathin cryosections using ultrasmall gold-labeled Fab fragments and silver intensification as secondary detection method. As expected, we found that mitochondria were clearly labeled by silver-intensified ultragold particles used for visualization of SOD2 (Fig. 3d–f). We could not detect any gold particles in peroxisomes or any other cell compartments in immunostainings with antibodies against SOD2. Also with this labeling method, negative control preparations with LR White or ultrathin cryosections incubated in parallel with non-specific IgG or without primary antibody only very seldom exhibited non-specific labeling (Fig. 3g). Furthermore, we have analyzed the ultrastructural localization of SOD2 in the lung, since it is known from the literature that antioxidant enzymes are highly expressed in this organ and SOD2 activity in the adult lung is higher than in liver (Rickett and Kelly 1990). In the lung, LR White sections already showed a clear, specific staining pattern of SOD2 in mitochondria (Fig. 3h), whereas peroxisomes were

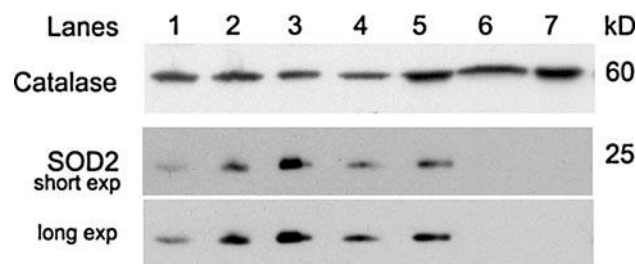


Fig. 4 Isolation of pure peroxisomal fractions using Optiprep gradient centrifugation from the liver of mice. Enriched organelles or highly purified peroxisomal fractions were isolated by differential centrifugation or density gradient centrifugation with Optiprep from mouse liver homogenates and subjected to SDS-PAGE Western blot analyses. Ten μ g of protein was loaded in each lane. Lanes 1 total homogenate, 2 supernatant 1 with all organelles, 3 heavy mitochondrial fraction, 4 supernatant 2, 5 light mitochondrial fraction (=enriched peroxisomes), 6 and 7 highly purified peroxisomal fractions from density gradients. Short- and long-term exposures of the SOD2 blot are depicted to show the absence of this protein in highly purified peroxisomal fractions with higher (6) and lower density (7)

devoid of SOD2 (see inset H) and similar results were found also for ultra-cryosections. AECII cells in the lung-secreted surfactant are stored in lipid lamellar bodies (LB) surrounded by many large mitochondria and small peroxisomes (Fig. 3h, i). The peroxisomal limiting membranes are clearly visible in all SOD2-stained preparations, and definitively, no labeling of gold particles for these organelles at the ultrastructural level was observed suggesting that SOD2 is not a peroxisomal protein as mentioned in the literature (Slot et al. 1986).

Highly purified isolated peroxisomes are devoid of SOD2

In order to compare the subcellular localization of SOD2 and catalase by biochemical means, the selective enrichment of both proteins in distinct fractions obtained by differential and density gradient centrifugation was analyzed. The protein abundance was analyzed by Western blotting with specific antibodies that were also used for immunostainings. SOD2 and catalase could specifically be localized in the corresponding fractions where mitochondria or peroxisomes were enriched and clearly showed distinct distribution patterns.

In accordance with the results obtained by immunofluorescence, a high level of SOD2 immunoreactivity was observed in the heavy mitochondrial fraction (Fig. 4 lanes 2, 3) in comparison with a lower level in the light mitochondrial fraction (Fig. 4 lanes 3, 5), whereas peroxisomal catalase was enriched in the fraction. Most importantly, in both highly purified peroxisome preparations obtained by density gradient centrifugation (Fig. 4, lanes 6–7), we could not detect any immunoreactivity for SOD2, whereas the peroxisomal marker protein catalase was highly abundant judged on the signal intensity. Even after long-term exposure, no signal was obtained for SOD2 in the highly purified peroxisomal fractions.

Database screening for SOD2 localization in different species: no signs of SOD2 localization in peroxisomes

Transcriptomics, proteomics, and tissue-specific analyses have recently started to be applied to organelles. An increasing amount of proteome studies on cell organelles has led to the identification of new proteins, and the accumulation of these data supports a realistic estimation of the typical localization of proteins. We have screened the original articles from the literature for the comparative localization of SOD2 and catalase in various tissues and cell types (Table 2) as well as supplementary materials on journal homepages of appropriate publications analyzing peroxisome-related proteomes for data regarding the presence of SOD2 (Table 3) (Emanuelsson et al. 2003; Kamada

et al. 2003; Kurochkin et al. 2005; Schafer et al. 2001). We have also used bioinformatics tools for predicting the subcellular localization of SOD2. Consistently, with our morphological and biochemical data, none of the groups that have analyzed the peroxisomal proteome has identified SOD2 neither in the peroxisomal membrane nor in the peroxisomal matrix suggesting that SOD2 is not a peroxisomal protein. Instead, an analysis of the proteome of mitochondria in mouse liver has identified a localization of SOD2 in mitochondria also associated with mitochondrial membranes (Da Cruz et al. 2003). Furthermore, none of the different bioinformatic prediction tools were able to locate SOD2 in the peroxisomal compartment (Table 3), and also the recently developed “LOCATE” subcellular database suggests that SOD2 is localized solely in the mitochondria.

Discussion

The subcellular localization of proteins and the intracellular trafficking of proteins are generally dependent on specific targeting signals that direct the proteins to their assigned location (Schatz 1987). Some proteins, however, have indeed a multicompartamental localization such as SOD1 (McCord and Fridovich 1969; Okado-Matsumoto and Fridovich 2001). Similarly, SOD2 has also been proposed to have multi-subcellular locations and has been suggested to be present not only in mitochondria (Da Cruz et al. 2003; Shimoda-Matsubayashi et al. 1996; Weisiger and Fridovich 1973a, b) but also in the peroxisomal matrix and the peroxisomal membrane (Singh et al. 1999). Because we always detected SOD2 solely in mitochondria in our microscopical analyses and never found this enzyme in purified peroxisomes, we have reanalyzed the correct subcellular localization of SOD2 by optimization of each step of morphological and biochemical methods for obtaining the highest sensitivity for immunolabeling and lowest possible antibody cross-reactivity or mitochondrial contamination of peroxisomal fractions used for Western blotting.

Establishment of highly sensitive and reliable methods to localize SOD2 at the subcellular level

Since mono-specificity and the use of correct concentrations of antibodies are prerequisites for correct intracellular localization of proteins of interest, we have carefully analyzed different antibodies against catalase and SOD2 for their quality and sensitivity. To obtain the best reliable results for the correct subcellular localization of SOD2 in comparison with catalase, we have established highly sensitive protocols of divergent methods for: (1) Western blot analyses of mono-specificities of several antibodies against

Table 3 Analysis of database screening for SOD2 localization using different approaches

Analysis	Species	Organ	References	Results
Proteomic analysis				
Mass spectrometry analysis of peroxisomal membrane proteins	Yeast		Schafer et al. (2001)	SOD2 is not detected
Quantitative proteomic analysis of Arabidopsis cell culture peroxisomes	Plants	Arabidopsis cells	Eubel et al. (2008)	SOD2 is not detected
Proteomic map of Spinach leaf peroxisomes	Plants	Spinach leaf	Babujee et al. (2010)	SOD2 is not detected
Proteomic analysis of leaf peroxisomal proteins in greening cotyledons	Plants	<i>Arabidopsis thaliana</i>	Fukao et al. (2002)	SOD2 is not detected
Proteomic analysis of rat liver peroxisomal membranes	Rat	Liver	Islinger et al. (2006)	SOD2 is not detected
Proteomic analysis of rat liver peroxisomes	Rat	Liver	Kikuchi et al. (2004)	SOD2 is not detected
Quantitative proteomic comparison of peroxisomes	Mouse	Liver and kidney	Mi et al. (2007)	SOD2 is not detected
Proteomic analysis of mitochondrial membranes	Mouse	Liver	Da Cruz et al. (2003)	SOD2 detected
Bioinformatic predictions				
In silico prediction of the peroxisomal proteome	Fungi, plants and human		Emanuelsson et al. (2003)	SOD2 is not detected
Sequence-based discovery of the peroxisomal proteome	Rodent and human		Kurochkin et al. (2005)	SOD2 is not detected
Expression profiles of peroxisomal genes in <i>Arabidopsis thaliana</i>	Plants	<i>Arabidopsis thaliana</i>	Kamada et al. (2003)	SOD2 is not detected
Software programmes				
LOCATE-subcellular localization database	SOD2 is detected only in mitochondria but not in peroxisomes		http://locate.imb.uq.edu.au/	
Peroxisomedb.org	No SOD2 references		http://peroxisomedb.org/	
Araperox database	No SOD2 is detected in the confirmed list		http://www3.uis.no/AraPeroxVI/	

This table provides the complete list of results from database searches performed for original literature information on peroxisomal and mitochondrial proteomic profiling for SOD2 in different species and organs. The following key words were used to search the PubMed database of the NCBI (www.ncbi.nlm.nih.gov/pubmed) were used: “peroxisomes,” “peroxisome proteome,” “peroxisome membranes proteome,” “peroxisome mass spectrometry,” “mitochondrial proteome.” Whereas mitochondrial SOD2 was clearly detected in the proteomic study of mitochondrial membranes (Da Cruz et al. 2003), none of the proteomic studies on peroxisomes revealed the presence of SOD2 in this organelle. In addition to the careful analysis of all figures and tables in the text of the original articles, all additional online information of the listed publications has been searched for SOD2 (or superoxide dismutase in general)

Furthermore, analyses using bioinformatic prediction tools (in silico prediction of the peroxisomal proteome) and searches of additional databases (LOCATE—mammalian protein localization database, Arapex—A database of putative proteins of Arabidopsis peroxisomes, PeroxisomeDB—Peroxisome database) were performed to find any information for SOD2 (or superoxide dismutase in general) in peroxisomal “virtual” proteomes in different species. With all of the online bioinformatic tools used, an exclusive mitochondrial localization of SOD2 was detected, whereas no additional indications for an eventual peroxisomal localization of this protein was found

these proteins in tissue homogenates with sensitive and stable enhanced chemiluminescence detection, (2) an optimized immunofluorescence method on very thin paraffin sections (1 μ m) (Baumgart et al. 2003; Karnati and Baumgart-Vogt 2008, 2009), (3) sophisticated highly sensitive immunoelectron microscopy on ultrathin cryosections, (4) a combination of elaborate subcellular fractionation and isolation methods for obtaining highly purified peroxisomal fractions with minimal contamination of mitochondria (or mitochondrial membranes), and (5) analyses of the protein distributions in all subcellular fractions.

It is quite challenging to visualize proteins with low abundance in small organelles at the ultrastructural level because unspecific binding of the antibody or high background staining of the secondary detection method might mask the specific subcellular localization of a protein of interest (Fahimi et al. 1996). We have therefore chosen to use a high dilution of a well-characterized rabbit anti-mouse catalase antibody for optimization of the best conditions for the secondary detection methods to obtain specific labeling of peroxisomes with high sensitivity at the ultrastructural level (Karnati and Baumgart-Vogt 2008;

Nenicu et al. 2007). Moreover, for standardization of the secondary detection methods, the incubations were performed on fetal or newborn mouse liver sections, since peroxisomes therein are smaller and catalase is less abundant in individual organelles in comparison with adult animals (Baumgart et al. 2003). Moreover, SOD2 is highly abundant in mitochondria of hepatocytes, exhibiting 10 times higher values than in other tissues (Marklund 1984), and “peroxisome-associated SOD2” was described by Singh and colleagues in this organ (Singh et al. 1999). Only after optimization of all steps in the protocol (including dilution series of the best anti-SOD2 antibody), the best possible conditions were applied for SOD2 labelings with various secondary detection methods (ultrasmall gold, protein A-gold) on ultrathin cryosections of frozen tissue or LR White-embedded material. By the combination of these highly sensitive and diverging analyses, all our results confirm that SOD2 is not present in peroxisomes.

Reasons for false-positive peroxisomal localization of superoxide dismutase 2 in hepatocytes

Superoxide dismutase 2 was isolated from purified chicken liver mitochondria by Weisiger and Fridovich already in 1973 and described as a manganoprotein, resembling the superoxide dismutases from bacteria (Keele et al. 1970; Vance et al. 1972; Weisiger and Fridovich 1973a), providing additional support of the endosymbiotic theory of the mitochondrial origin (Grace 1990; Mereschkowsky 1905; Wallin 1922). The suborganellar localization of SOD2 has been described in the mitochondrial matrix in close association with the inner membrane or the inner membrane itself (Da Cruz et al. 2003; Shimoda-Matsubayashi et al. 1996; Slot et al. 1986; Weisiger and Fridovich 1973a, b). Moreover, in addition to its mitochondrial localization, Avtar Singh and colleagues suggested a peroxisomal localization of this protein by the use of biochemical and morphological techniques (Singh et al. 1999). Since this article on the dual localization of SOD2 appeared, the citation on its peroxisomal localization continued in our research field (Abdelraheim et al. 2003; Antonenkov et al. 2009; Antonenkov and Hiltunen 2006; Dansen and Wirtz 2001; Moldovan and Moldovan 2004; Schrader and Fahimi 2006) with most authors stating its peroxisomal localization without any additional proof from the literature. Singh and colleagues described the localization of SOD2 in the peroxisomal membrane as well as peroxisomal core, whereas in the matrix of the organelle, no SOD2 was present (Singh et al. 1999). Their interpretation of data was based mainly on results of Western blots of purified peroxisomal fractions and subfractionation of the organelles as well as labeling of rat liver tissue samples embedded in an Epon 812 substitute (EMbed 812) on the

ultrastructural level with the protein A-gold technique (Roth 1982). However, as can be seen by the high activity of mitochondrial cytochrome c oxidase in their purified peroxisomal fractions (see Table 1 in Singh et al. 1999), an enzyme of complex 4 of the respiratory chain in the inner mitochondrial membrane, the SOD2 signal on the Western blots in this publication can be interpreted as mitochondrial contamination of their isolated peroxisomal fractions. Also the SOD2 enrichment in the membrane fraction (Table 2 in Singh et al. 1999) can be explained, since in mitochondria this enzyme tends to associate peripherally with the inner mitochondrial membrane and is not removed from the inner membrane preparation even with one incubation of sodium carbonate buffer (see supplementary Table 1 in Da Cruz et al. 2003). In contrast, our Western blot results with sensitive chemiluminescence detection revealed no obvious SOD2 signal in the isolated highly purified peroxisomal fraction even after overexposure of the film. Our results are supported by several proteomic studies (Table 3) using isolated peroxisomes or peroxisomal membrane fractions, in which no SOD2 peptide fragments were detected (Babujee et al. 2010; Da Cruz et al. 2003; Eubel et al. 2008; Fukao et al. 2002; Islinger et al. 2006; Kikuchi et al. 2004; Mi et al. 2007). Similarly, the localization of SOD2 in the peroxisome depicted in the electron micrograph presented in Fig. 2 of the article from Singh and colleagues could be explained by non-specific labeling with protein A-gold particles, since also several gold particles (even one cluster of 4 particles) can be noted in the cytoplasm surrounding the organelles. Moreover, the “real” specific labeling of SOD2 in the mitochondria present on this figure should be higher. The low labeling for SOD2 in the mitochondria in their publication, however, can be explained by the use of a fixative containing a mixture of 2 % paraformaldehyde combined with 1 % glutaraldehyde and embedding of the tissue into an Epon 812 substitute which is polymerized at 60 °C, both leading to the reduction of the antigenicity of many proteins (Baumgart 1997; Fahimi et al. 1996). In contrast, the tissue used in our study was fixed with 4 % paraformaldehyde combined with only 0.05 % glutaraldehyde and either embedded in LR White or cryoprotected for the use of ultrathin cryosections that preserve a high antigenicity and provide the best results for labeling of peroxisomal and mitochondrial proteins (Baumgart et al. 2003; Fahimi et al. 1996). Even by using the most sensitive methods in our study, SOD2 was shown to be solely localized in mitochondria and to be absent from peroxisomes.

Do peroxisomes contain superoxide dismutases?

In contrast to the false-positive localization of SOD2 in peroxisomes, SOD1 has been described in rat, mouse, and

human peroxisomes by several groups and morphological and biochemical methods as well as comprehensive proteomic studies (Dhaunsi et al. 1992; Islinger et al. 2009; Keller et al. 1991; Kira et al. 2002; Wanders and Denis 1992). Moreover, this protein seems to be induced by fibrate treatment in rat liver peroxisomes (ciprofibrate treatment: Dhaunsi et al. 1992). Accordingly, SOD1 was more easily found in proteomic studies with highly purified peroxisomal fractions from bezafibrate-treated rats (Islinger et al. 2007). Moreover, a 2D-gel map from mouse liver peroxisomes showed a clear spot (No. 8) for SOD1 around 20 kDa and PI 6.8. In contrast, no spot or peptides for SOD2 were described in both studies. Moreover, SOD1 has been localized by double-immunofluorescence (combined with catalase) in peroxisomes of human fibroblasts and hepatoma cells (HepG2) and on the ultrastructural level after overexpression of human SOD1 in yeast peroxisomes (Keller et al. 1991). Interestingly, the SOD1 labeling density seemed to be even higher in peroxisomes than in the cytoplasm, in which SOD1 was first isolated (Keller et al. 1991). Moreover, the abundance of peroxisomal and cytoplasmic SOD1 seems to be rather independent from each other as shown on the ultrastructural level in distinct neurons (Moreno et al. 1997).

Despite its peroxisomal localization, no typical peroxisomal targeting signal (PTS1 or PTS2) has been described in the SOD1 cDNA sequence, wherefore its targeted transport into the organelle remained enigmatic. Recently, Islinger and colleagues reported a “piggyback import mechanism” of SOD1 via binding to its chaperone CCS into peroxisomes (Islinger et al. 2009). The CCS protein possesses indeed a typical C-terminal PTS1 in domain III (Casareno et al. 1998). Islinger and colleagues showed that the CCS-domain II is required for hetero-dimer formation with SOD1, mediating the natural piggyback import into peroxisomes (Islinger et al. 2009). In contrast to SOD1, SOD2 possesses a clear mitochondrial signal, enabling SOD2 targeting into mitochondria (Miao and St. Clair 2009; Shimoda-Matsubayashi et al. 1996). Phylogenetic studies of all known vertebrate SOD genes showed a close similarity between SOD1 and SOD3 and a very low homology to SOD2 (Zelko et al. 2002). In contrast to SOD1, however, no SOD3 has been described in peroxisomes.

We are facing the problem that it is methodologically and conceptually easier to show the presence of a protein in a distinct localization rather than to provide evidence for its absence since there exists no positive experimental controls to support such a conclusion. Based on our data and the overwhelming evidence from databases and the literature, we strongly suggest that the view of the subcellular distribution of SOD2 suggesting a peroxisomal localization is

incorrect. Taken together, our results suggest a solely mitochondrial localization of SOD2 in mammals.

Acknowledgments The authors thank Dr. Klaus-Peter Valerius for help in animal perfusions. The excellent technical assistance of Elke Richter and Bianca Pfeiffer is gratefully acknowledged. We would like to thank Profs. Denis I. Crane for providing us the catalase antibody (see Table 1). Finally, we are indebted to Jessica Woods for carefully reading and correcting the manuscript.

References

- Abdelraheim SR, Spiller DG, McLennan AG (2003) Mammalian NADH diphosphatases of the Nudix family: cloning and characterization of the human peroxisomal NUDT12 protein. *Biochem J* 374:329–335
- Antononkov VD, Hiltunen JK (2006) Peroxisomal membrane permeability and solute transfer. *Biochim Biophys Acta* 1763:1697–1706
- Antononkov VD, Grunau S, Ohlmeier S, Hiltunen JK (2009) Peroxisomes are oxidative organelles. *Antioxid Redox Signal* 13:525–537
- Babujee L, Wurtz V, Ma C, Lueder F, Soni P, van Dorsselaer A, Reumann S (2010) The proteome map of spinach leaf peroxisomes indicates partial compartmentalization of phyloquinone (vitamin K1) biosynthesis in plant peroxisomes. *J Exp Bot* 61:1441–1453
- Baumgart E (1997) Application of in situ hybridization, cytochemical and immunocytochemical techniques for the investigation of peroxisomes. A review including novel data. Robert Feulgen Prize Lecture 1997. *Histochem Cell Biol* 108:185–210
- Baumgart E, Fahimi HD, Steininger H, Grabenbauer M (2003) A review of morphological techniques for detection of peroxisomal (and mitochondrial) proteins and their corresponding mRNAs during ontogenesis in mice: application to the PEX5-knockout mouse with Zellweger syndrome. *Microsc Res Tech* 61:121–138
- Bradford MM (1976) A rapid and sensitive method for the quantitation of microgram quantities of protein utilizing the principle of protein-dye binding. *Anal Biochem* 72:248–254
- Casareno RL, Waggoner D, Gitlin JD (1998) The copper chaperone CCS directly interacts with copper/zinc superoxide dismutase. *J Biol Chem* 273:23625–23628
- Culotta VC, Yang M, O’Halloran TV (2006) Activation of superoxide dismutases: putting the metal to the pedal. *Biochim Biophys Acta* 1763:747–758
- Da Cruz S, Xenarios I, Langridge J, Vilbois F, Parone PA, Martinou JC (2003) Proteomic analysis of the mouse liver mitochondrial inner membrane. *J Biol Chem* 278:41566–41571
- Dansen TB, Wirtz KW (2001) The peroxisome in oxidative stress. *IUBMB Life* 51:223–230
- Dhaunsi GS, Gulati S, Singh AK, Orak JK, Asayama K, Singh I (1992) Demonstration of Cu-Zn superoxide dismutase in rat liver peroxisomes. Biochemical and immunochemical evidence. *J Biol Chem* 267:6870–6873
- Emanuelsson O, Elofsson A, von Heijne G, Cristobal S (2003) In silico prediction of the peroxisomal proteome in fungi, plants and animals. *J Mol Biol* 330:443–456
- Eubel H, Meyer EH, Taylor NL, Bussell JD, O’Toole N, Heazlewood JL, Castleden I, Small ID, Smith SM, Millar AH (2008) Novel proteins, putative membrane transporters, and an integrated metabolic network are revealed by quantitative proteomic analysis of Arabidopsis cell culture peroxisomes. *Plant Physiol* 148:1809–1829

- Fahimi HD, Reich D, Volkl A, Baumgart E (1996) Contributions of the immunogold technique to investigation of the biology of peroxisomes. *Histochem Cell Biol* 106:105–114
- Fukao Y, Hayashi M, Nishimura M (2002) Proteomic analysis of leaf peroxisomal proteins in greening cotyledons of *Arabidopsis thaliana*. *Plant Cell Physiol* 43:689–696
- Grace SC (1990) Phylogenetic distribution of superoxide dismutase supports an endosymbiotic origin for chloroplasts and mitochondria. *Life Sci* 47:1875–1886
- Immenschuh S, Baumgart-Vogt E (2005) Peroxiredoxins, oxidative stress, and cell proliferation. *Antioxid Redox Signal* 7:768–777
- Islinger M, Lüers GH, Zischka H, Ueffing M, Völkl A (2006) Insights into the membrane proteome of rat liver peroxisomes: microsomal glutathione-S-transferase is shared by both subcellular compartments. *Proteomics* 6:804–816
- Islinger M, Luers GH, Li KW, Loos M, Volkl A (2007) Rat liver peroxisomes after fibrate treatment. A survey using quantitative mass spectrometry. *J Biol Chem* 282:23055–23069
- Islinger M, Li KW, Seitz J, Volkl A, Luers GH (2009) Hitchhiking of Cu/Zn superoxide dismutase to peroxisomes—evidence for a natural piggyback import mechanism in mammals. *Traffic* 10:1711–1721
- Kamada T, Nito K, Hayashi H, Mano S, Hayashi M, Nishimura M (2003) Functional differentiation of peroxisomes revealed by expression profiles of peroxisomal genes in *Arabidopsis thaliana*. *Plant Cell Physiol* 44:1275–1289
- Karnati S, Baumgart-Vogt E (2008) Peroxisomes in mouse and human lung: their involvement in pulmonary lipid metabolism. *Histochem Cell Biol* 130:719–740
- Karnati S, Baumgart-Vogt E (2009) Peroxisomes in airway epithelia and future prospects of these organelles for pulmonary cell biology. *Histochem Cell Biol* 131:447–454
- Keele BB Jr, McCord JM, Fridovich I (1970) Superoxide dismutase from *Escherichia coli* B. A new manganese-containing enzyme. *J Biol Chem* 245:6176–6181
- Keller GA, Warner TG, Steimer KS, Hallewell RA (1991) Cu, Zn superoxide dismutase is a peroxisomal enzyme in human fibroblasts and hepatoma cells. *Proc Natl Acad Sci USA* 88:7381–7385
- Kikuchi M, Hatano N, Yokota S, Shimozawa N, Imanaka T, Taniguchi H (2004) Proteomic analysis of rat liver peroxisome: presence of peroxisome-specific isozyme of Lon protease. *J Biol Chem* 279:421–428
- Kira Y, Sato EF, Inoue M (2002) Association of Cu, Zn-type superoxide dismutase with mitochondria and peroxisomes. *Arch Biochem Biophys* 399:96–102
- Kurochkin IV, Nagashima T, Konagaya A, Schonbach C (2005) Sequence-based discovery of the human and rodent peroxisomal proteome. *Appl Bioinform* 4:93–104
- Lüers GH, Schad A, Fahimi HD, Völkl A, Seitz J (2003) Expression of peroxisomal proteins provides clear evidence for the presence of peroxisomes in the male germ cell line GC1spg. *Cytogenet Genome Res* 103(3–4):360–365
- Marklund SL (1982) Human copper-containing superoxide dismutase of high molecular weight. *Proc Natl Acad Sci USA* 79:7634–7638
- Marklund SL (1984) Extracellular superoxide dismutase and other superoxide dismutase isoenzymes in tissues from nine mammalian species. *Biochem J* 222:649–655
- McCord JM, Fridovich I (1969) Superoxide dismutase. An enzymic function for erythrocyte (hemocuprein). *J Biol Chem* 244:6049–6055
- Mereschkowsky C (1905) über ber Natur und Ursprung der Chromatophoren in Pflanzenreiche. *Biol Centralbl* 25:593–604
- Mi J, Kirchner E, Cristobal S (2007) Quantitative proteomic comparison of mouse peroxisomes from liver and kidney. *Proteomics* 7:1916–1928
- Miao L, St. Clair DK (2009) Regulation of superoxide dismutase genes: implications in disease. *Free Radic Biol Med* 47:344–356
- Moldovan L, Moldovan NI (2004) Oxygen free radicals and redox biology of organelles. *Histochem Cell Biol* 122:395–412
- Moreno S, Nardacci R, Ceru MP (1997) Regional and ultrastructural immunolocalization of copper-zinc superoxide dismutase in rat central nervous system. *J Histochem Cytochem* 45:1611–1622
- Nenicu A, Luers GH, Kovacs W, David M, Zimmer A, Bergmann M, Baumgart-Vogt E (2007) Peroxisomes in human and mouse testis: differential expression of peroxisomal proteins in germ cells and distinct somatic cell types of the testis. *Biol Reprod* 77:1060–1072
- Newman GR, Jasani B, Williams ED (1983) A simple post-embedding system for the rapid demonstration of tissue antigens under the electron microscope. *Histochem J* 15:543–555
- Nozik-Grayck E, Suliman HB, Piantadosi CA (2005) Extracellular superoxide dismutase. *Int J Biochem Cell Biol* 37:2466–2471
- Okado-Matsumoto A, Fridovich I (2001) Subcellular distribution of superoxide dismutases (SOD) in rat liver: Cu, Zn-SOD in mitochondria. *J Biol Chem* 276:38388–38393
- Rickett GM, Kelly FJ (1990) Developmental expression of antioxidant enzymes in guinea pig lung and liver. *Development* 108:331–336
- Roth J (1982) Applications of immunocolloids in light microscopy. Preparation of protein A-silver and protein A-gold complexes and their application for localization of single and multiple antigens in paraffin sections. *J Histochem Cytochem* 30:691–696
- Schafer H, Nau K, Sickmann A, Erdmann R, Meyer HE (2001) Identification of peroxisomal membrane proteins of *Saccharomyces cerevisiae* by mass spectrometry. *Electrophoresis* 22:2955–2968
- Schatz G (1987) 17th Sir Hans Krebs lecture. Signals guiding proteins to their correct locations in mitochondria. *Eur J Biochem* 165:1–6
- Schrader M, Fahimi HD (2006) Peroxisomes and oxidative stress. *Biochim Biophys Acta* 1763:1755–1766
- Shimoda-Matsubayashi S, Matsumine H, Kobayashi T, Nakagawa-Hattori Y, Shimizu Y, Mizuno Y (1996) Structural dimorphism in the mitochondrial targeting sequence in the human manganese superoxide dismutase gene. A predictive evidence for conformational change to influence mitochondrial transport and a study of allelic association in Parkinson's disease. *Biochem Biophys Res Commun* 226:561–565
- Singh AK, Dobashi K, Gupta MP, Asayama K, Singh I, Orak JK (1999) Manganese superoxide dismutase in rat liver peroxisomes: biochemical and immunochemical evidence. *Mol Cell Biochem* 197:7–12
- Slot JW, Geuze HJ (1981) Sizing of protein A-colloidal gold probes for immunoelectron microscopy. *J Cell Biol* 90:533–536
- Slot JW, Geuze HJ, Freeman BA, Crapo JD (1986) Intracellular localization of the copper-zinc and manganese superoxide dismutases in rat liver parenchymal cells. *Lab Invest* 55:363–371
- Vance PG, Keele BB Jr, Rajagopalan KV (1972) Superoxide dismutase from *Streptococcus mutans*. Isolation and characterization of two forms of the enzyme. *J Biol Chem* 247:4782–4786
- Wallin IE (1922) A note on the morphology of bacteria symbiotic in the tissues of higher organisms. *J Bacteriol* 7:471–474
- Wanders RJ, Denis S (1992) Identification of superoxide dismutase in rat liver peroxisomes. *Biochim Biophys Acta* 1115:259–262
- Weisiger RA, Fridovich I (1973a) Mitochondrial superoxide dismutase. Site of synthesis and intramitochondrial localization. *J Biol Chem* 248:4793–4796
- Weisiger RA, Fridovich I (1973b) Superoxide dismutase. Organelle specificity. *J Biol Chem* 248:3582–3592
- Zelko IN, Mariani TJ, Folz RJ (2002) Superoxide dismutase multigene family: a comparison of the CuZn-SOD (SOD1), Mn-SOD (SOD2), and EC-SOD (SOD3) gene structures, evolution, and expression. *Free Radic Biol Med* 33:337–349

C22-bronchial and T7-alveolar epithelial cell lines of the immortomouse are excellent murine cell culture model systems to study pulmonary peroxisome biology and metabolism

Srikanth Karnati¹ · Saranya Palaniswamy¹ · Mohammad Rashedul Alam¹ · Gani Oruqaj¹ · Cordula Stamme^{2,3} · Eveline Baumgart-Vogt¹

Accepted: 29 October 2015 / Published online: 21 December 2015
© Springer-Verlag Berlin Heidelberg 2015

Abstract In pulmonary research, temperature-sensitive immortalized cell lines derived from the lung of the “immortomouse” (H-2k^b-tsA58 transgenic mouse), such as C22 club cells and T7 alveolar epithelial cells type II (AECII), are frequently used cell culture models to study CC10 metabolism and surfactant synthesis. Even though peroxisomes are highly abundant in club cells and AECII and might fulfill important metabolic functions therein, these organelles have never been investigated in C22 and T7 cells. Therefore, we have characterized the peroxisomal compartment and its associated gene transcription in these cell lines. Our results show that peroxisomes are highly abundant in C22 and T7 cells, harboring a common set of enzymes, however, exhibiting specific differences in protein composition and gene expression patterns, similar to the ones observed in club cells and AECII in situ in the lung. C22 cells contain a lower number of larger peroxisomes, whereas T7 cells possess more numerous tubular peroxisomes, reflected also by higher levels of PEX11

proteins. Moreover, C22 cells harbor relatively higher amounts of catalase and antioxidative enzymes in distinct subcellular compartments, whereas T7 cells exhibit higher levels of ABCD3 and plasmalogen synthesizing enzymes as well as nuclear receptors of the PPAR family. This study suggests that the C22 and T7 cell lines of the immortomouse lung are useful models to study the regulation and metabolic function of the peroxisomal compartment and its alterations by paracrine factors in club cells and AECII.

Keywords Peroxisomes · C22 · Club cells · T7 · AECII · Oxidative stress

Introduction

Peroxisomes are single-membrane-bound ubiquitous organelles that vary in number, size and shape (i.e., angular, tubular or elongated forms as well as networks of interconnected peroxisomes exist), depending on the organ and cell type investigated (Baumgart 1997). Peroxisomal metabolic functions and their enzyme composition are highly heterogeneous and vary between cell types, tissues and organ systems according to their metabolic needs (Baumgart 1997; Chang et al. 1999; Fahimi et al. 1996). In general, peroxisomal proteins are involved in various lipid metabolic pathways, such as synthesis of cholesterol and ether lipids and the degradation of various bioactive and pro-inflammatory lipid derivatives by β -oxidation as well as in the metabolism of reactive oxygen species (ROS) and reactive nitrogen species (RNS) (Islinger et al. 2006; Karnati and Baumgart-Vogt 2008; Wiese et al. 2007). These peroxisomal functions have been thoroughly investigated in hepatocytes of the liver; however, only scarce information is available on the function of peroxisomes in different lung

Electronic supplementary material The online version of this article (doi:10.1007/s00418-015-1385-4) contains supplementary material, which is available to authorized users.

✉ Eveline Baumgart-Vogt
Eveline.Baumgart-Vogt@anatomie.med.uni-giessen.de
<http://www.med.uni-giessen.de/anat/>

¹ Institute for Anatomy and Cell Biology, Medical Cell Biology, Justus Liebig University, Aulweg 123, 35385 Giessen, Germany

² Division of Cellular Pneumology, Research Center Borstel, Leibniz-Center for Medicine and Biosciences, Borstel, Germany

³ Department of Anesthesiology, University of Lübeck, Lübeck, Germany

cell types. Only few studies are available on peroxisomes in the lung, in which these organelles were described on the ultrastructural level first in AECII and club cells (formerly called Clara cells) (Winkelmann and Noack 2010), two cell types in which peroxisomes are most numerous and their marker protein catalase is very abundant [for a review on the literature, see (Karnati and Baumgart-Vogt 2008, 2009; Petrik 1971; Schneeberger 1972)]. Previously, we showed that peroxisomes are present in all cell types of the airway and alveolar epithelia of mice, however, harboring a distinct subset of enzymes in club cells and AECII with high levels of catalase, ABCD3 and thiolase in comparison with ciliated cells of the bronchiolar epithelium or AECI cells of the alveolus (Karnati and Baumgart-Vogt 2008). We also showed by in situ hybridization that the high expression levels of *Pex11 β* mRNA encoding a protein involved in the regulation of constitutive peroxisome number coincide with the highest numerical abundance of peroxisomes in these cell types (Karnati and Baumgart-Vogt 2008, 2009).

To study the regulation of peroxisomal functions in club cells and AECII by distinct intracellular signaling pathways or external factors, e.g., cytokines, growth factors, lipids and high levels of oxygen or hypoxia, experimental cell culture model systems in the best case primary cultures of both cell types are required. However, club cells are very difficult to isolate and to maintain in primary cell cultures (Wang et al. 2012). Similar to club cells, AECII lose their capacity to synthesize surfactant and dedifferentiate within 24–48 h in primary culture (Mason et al. 1977; Shannon et al. 1992). During the cell culture, AECII lose their apical microvilli (Diglio and Kikkawa 1977), lamellar body inclusion (Mason et al. 1977), production of phospholipids (Mason et al. 1977), and synthesis of surfactant proteins (Shannon et al. 1992). These difficulties could be overcome by using cell lines of the immortomouse containing the ts SV40 large T-antigen that allow studying the biology of club and AECII (Demello et al. 2002).

The C22 and T7 cell lines were isolated from the transgenic H-2k^b-tsA58 immortomouse (Jat et al. 1991) containing the major histocompatibility complex (MHC) H-2k^b class I promoter, coupled to the Simian virus 40 (SV40) T-antigen. The SV40 T-antigen is temperature sensitive, and its expression is controlled by γ -interferon (γ -INF). The non-tumor-derived immortalized cell lines, C22 and T7 cell lines proliferate at 33 °C in the presence of interferon- γ and show similar morphological features and secrete surfactant proteins as well as cell-type-specific marker proteins from the club cells and AECII of the lung (Demello et al. 2002; Ryerse et al. 2001). Moreover, T7 cells synthesize surfactant lipids and phosphatidyl choline, a major lipid component of the surfactant (deMello et al. 2000) that reduces the intra-alveolar surface tension at end expiration (Karnati and Baumgart-Vogt 2008). By using

immortomouse-derived cell lines, club cell and AECII physiology can be studied as well as the role of different organelles therein. Therefore, these cell lines could provide very good cell culture model systems to study the metabolic role of peroxisomes in club cells and AECII.

The present study is the first comprehensive investigation on the peroxisomal compartment and its associated gene expression in proliferating C22 and T7 cells cultured at 33 °C. Our results indeed reveal that the peroxisomes are very abundant in these cell lines and that the peroxisomal enzyme composition and gene expression are comparable to the one in club cells and AECII in situ in the mouse lung, exhibiting specific heterogeneous protein composition and characteristic gene expression patterns (Karnati and Baumgart-Vogt 2008). This study is a prerequisite for further investigations on the functional role of peroxisomes in C22 club cell and T7 AECII biology as well as their differentiation process and regulation by cytokines or growth factors.

Materials and methods

Animals

Ten adult male mice (12 weeks of age) of C57BL/6J genetic background were obtained from Charles River, Sulzfeld, Germany. The mice were kept on a normal laboratory diet and water ad libitum and housed in cages under standardized environmental conditions (12-h-light/dark cycle, 23 \pm 1 °C and 55 \pm 1 % relative humidity) at the central animal facility (ZTL) of the Justus Liebig University Giessen. The mice were transported to our institute on the day of experiments. All experiments with laboratory mice were approved by the governmental ethics committee for animal welfare (Regierungspräsidium Giessen, Germany, permit number: V 54-19 C 20/15 c GI 20/23).

Immunofluorescence of mouse lungs

The detailed protocol for perfusion fixation, paraffin embedding, sectioning of tissues and subsequent immunofluorescence for adult lungs was described previously (Karnati and Baumgart-Vogt 2008, 2009). Briefly, perfusion-fixed lungs (4 % PFA in PBS, pH 7.4) were embedded into paraffin (Paraplast, Sigma, St. Louis, MO, USA) using a Leica TP 1020 automated vacuum infiltration tissue processor. Paraffin sections (2 μ m) were cut with a Leica RM2135 rotation microtome and processed for indirect double immunofluorescence. All dilutions of the primary and secondary antibodies used are listed in Table 1. Negative controls for the secondary antibody reaction were processed in parallel by addition of TBST buffer (Tris-buffered saline/0.05 % Tween 20, pH 7.4) instead of the first

Table 1 List of primary antibodies used in this study

Primary antibody	Host	Dilution IF (T7)	Dilution IF (C22)	Dilution (WB)	Supplier
<i>Cell-type-specific antigens</i>					
Surfactant protein A (SP-A), rabbit	Rabbit, polyclonal	1:1000	1:1000	1:1000	Chemicon, Cat. no: AB3420 (Karnati and Baumgart-Vogt 2008)
Surfactant protein B (SP-B), rabbit	Rabbit, polyclonal	1:1000	1:1000	–	Santa cruz, Cat no: sc-13798 (Karnati and Baumgart-Vogt 2008)
Pro-surfactant protein C (pro-SP-C), human	Rabbit, polyclonal	1:1000	–	–	Chemicon, Cat. no: ab3786 (Karnati and Baumgart-Vogt 2008)
Club cell protein 10 (CC10), mouse	Rabbit, polyclonal	–	1:100	–	Santa cruz, Cat no: sc-25555 (Karnati and Baumgart-Vogt 2008)
<i>Peroxisomal biogenesis and metabolic protein</i>					
Peroxin 13 (PEX13p), mouse	Rabbit, polyclonal	–	–	1:5000	Gift from Denis I. Crane; School of Biomol. Biophys. Sci., Griffith Univ., Nathan, Brisbane, Australia (Karnati and Baumgart-Vogt 2008; Grant et al. 2013)
Peroxin 14 (PEX14p), mouse	Rabbit, polyclonal	1:1000	1:1000	1:3000	Gift from Denis I. Crane; (Karnati and Baumgart-Vogt 2008; Grant et al. 2013)
Catalase (CAT), mouse	Rabbit, polyclonal	1:2000	1:2000	1:30,000	Gift from Denis I. Crane (Karnati and Baumgart-Vogt 2008; Grant et al. 2013)
ABC-transporter D3 (ABCD3), mouse	Rabbit, polyclonal	1:1000	1:1000	–	Gift from Alfred Völkl, Dept. of Anatomy and Cell Biology, Heidelberg, Germany; (Karnati and Baumgart-Vogt 2008)
Thiolase, human	Rabbit, polyclonal	1:1000	1:1000	1:5000	Gift from Nancy E Braverman; Depts. of Human Genetics and Pediatrics, McGill University-Montreal Montreal, QC, Canada.
Alkylglycerone-phosphate synthase (AGPS), human	Mouse, monoclonal	–	–	1:500	Santa Cruz, Cat no: sc-374201
Glycerone-phosphate O-acyltransferase (GNPAT), human	Rabbit, polyclonal	1:500	1:500	–	Proteintech, Cat no: 14931-1-AP
<i>Nuclear receptors</i>					
Peroxisome proliferator-activated receptor alpha (PPARA), human	Rabbit, polyclonal	1:50	1:50	–	Santa Cruz, Cat no: sc-1985
Peroxisome proliferator-activated receptor beta (PPARB), rabbit	Goat, polyclonal	1:50	1:50	1:500	Santa Cruz, Cat no: sc-7197
Peroxisome proliferator-activated receptor gamma (PPARG), rabbit	Rabbit, polyclonal	1:50	1:50	–	Santa Cruz, Cat no: sc-7196
<i>Antioxidative enzymes from other cell compartments</i>					
Superoxide dismutase 1 (SOD-1), rat	Rabbit, polyclonal	–	–	1:1000	Research diagnostics, Cat no: RDI-RTSODMabR
Superoxide dismutase 2 (SOD-2), human	Rabbit, polyclonal	1:1000	1:1000	1:5000	Abcam, Cat.no: ab13533 (Karnati et al. 2013)
HO-1 rabbit	Rabbit, polyclonal	1:1000	1:1000	1:5000	Stressgen, Cat no: SPA-895
<i>Secondary antibodies</i>					
	Host	Dilution (T7)	Dilution (C22)	Supplier	
<i>Other marker proteins of different cell compartments</i>					
Anti-rabbit-IgG AlexaFluor488	Donkey	1:1000	–	–	Molecular Probes/Invitrogen, Cat. no: A21206
Anti-mouse-IgG AlexaFluor555	Donkey	1:1000	–	–	Molecular Probes/Invitrogen, Cat. no: A31570
Anti-goat-IgG AlexaFluor594	Chicken	1:1000	–	–	Molecular Probes/Invitrogen, Cat. no: A11058
Anti-rabbit-IgG Ultra-small gold	Goat	1:400	–	–	Aurion, Wageningen, Netherlands
<i>Counterstaining of nuclei for immunofluorescence</i>					
Hoechst 33342 (1 µg/ml)	–	1:1000	–	–	Molecular Probes/Invitrogen, Cat. no: 33342
TOTO [®] -3 iodide	–	1:1000	–	–	Molecular Probes/Invitrogen, Cat. no: T-3604

Tested, but not working properly for these methods used

antibodies. Nuclei were visualized with 1 μM TOTO-3 iodide for 10 min at room temperature (RT). Samples were analyzed by confocal laser scanning microscopy (CLSM) with a Leica TCS SP5 (Leica Mikrosysteme Vertrieb GmbH, Wetzlar, Germany). All images were processed with Adobe Photoshop CS2 (version 9).

Post-embedding immunoelectron microscopy of mouse lungs

The detailed protocol of lung perfusion fixation and embedding in LR white medium grade and subsequent post-embedding immunoelectron microscopy on ultrathin lung sections was described previously (Karnati and Baumgart-Vogt 2008, 2009). Briefly, ultrathin lung sections (80 nm) were collected on formvar-coated nickel grids and non-specific protein-binding sites were blocked by placing the grids on 1 % BSA in TBS, pH 7.4 for 30 min. Ultrathin sections of lung tissue were incubated overnight in a wet chamber with the rabbit anti-mouse catalase antibody (1:4000 in 0.1 % BSA in TBS (TBSA); gift from Prof. Denis Crane; see Table 1). The sections were washed on a series of 12 TBSA drops. Subsequently, the grids were incubated for 2 h with ultrasmall gold-labeled goat anti-rabbit Fab fragments (Table 1) (Aurion, Wageningen, Netherlands). Primary and secondary antibodies are listed in Table 1. Specificity of the primary antibodies used in this manuscript were tested previously (Karnati and Baumgart-Vogt 2008; Karnati et al. 2013; Nenicu et al. 2007; Xiao et al. 2012). Thereafter, the grids with sections were washed shortly in a flow of distilled water and air-dried. Incubated sections were subjected to silver intensification according to Danscher and thereafter contrasted with uranyl acetate for 3 min and lead citrate for 1 min, followed by examination in a LEO 906 transmission electron microscope (Danscher 1981).

Cell lines

The C22 cell line was grown in Dulbecco's modified Eagle's medium (DMEM) containing 2 % fetal bovine serum (FBS), 100 U/ml penicillin, 1 % streptomycin, 250 $\mu\text{g}/\text{ml}$ amphotericin B, 5 $\mu\text{g}/\text{ml}$ transferrin, 100 U/ml γ -INF, 10 $\mu\text{g}/\text{ml}$ insulin, 0.025 $\mu\text{g}/\text{ml}$ epidermal growth factor, 7.5 $\mu\text{g}/\text{ml}$ endothelial cell growth supplement, 40 nmol/ml endothelin-1, 0.36 $\mu\text{g}/\text{ml}$ hydrocortisone, 20 ng/ml T3 as previously described (DeMello et al. 2002). The T7 medium consisted of all the above-mentioned substances with 2 % Ultrosor G. Both the cell lines were cultured in 75 cm^2 T75 flasks (Cell star[®], Greiner Bio-one GmbH, Germany), containing 20 ml of the appropriate medium. The splitting ratios were 1:3 at each second day. For the following experiments, both cell lines were incubated for

24 h in 10 % CO_2 at 33 °C under permissive condition, in which cell proliferation occurs.

Immunofluorescence (IF) with C22 and T7 cells

Since C22 and T7 cells do not attach well onto the glass surfaces, coating with collagen IV (Becton–Dickinson, Bedford, MA) was performed to promote maximum attachment and spreading of the cells (deMello et al. 2000). The C22 and T7 cells (1.25×10^5 cells/ cm^2) were grown on the collagen IV-coated cover slips for 24 h. The confluent cells were first washed with PBS for 3 \times 5 min and fixed with 4 % paraformaldehyde (PFA) in phosphate-buffered saline (PBS), pH 7.4, for 20 min at room temperature (RT). The cells were then washed carefully with PBS, pH 7.4, for 3 \times 5 min at RT. For blocking of free aldehyde sites and permeabilization, the cells were incubated simultaneously with 1 % glycine/0.3 % Triton X-100 in PBS at RT for 10 min. Thereafter, they were washed again with PBS, pH 7.4, for 3 \times 5 min. Blocking of non-specific protein-binding sites was done with 1 % BSA in PBS (blocking solution) with 0.05 % Tween 20, pH 7.4, for 30 min at RT. The primary antibody incubation was done overnight at 4 °C (for the list of antibodies, see Table 1). Subsequently, the cover slips were washed 3 \times 5 min with PBS, pH 7.4, followed by incubation with the secondary antibody for 1 h, followed again by washing for 3 \times 5 min with PBS, pH 7.4. Nuclei were counterstained with Hoechst and TOTO-3-iodide (1:1000/1:1000 dilution) for 10 min. Thereafter, the cells were washed with PBS, pH 7.4, for 3 \times 5 min. The coverslips were mounted using Mowiol/n-propyl gallate (3:1 v/v). The slides were analyzed using a Leica TCS SP5 confocal laser scanning microscope (Leica Microsystems GmbH, Wetzlar, Germany). Images were captured with a 63 \times objective, setting at Airy 1 (=pinhole of 190), 1 \times zoom and 12 times sampling. All images were processed with Adobe Photoshop CS2 (version 9).

Post-embedding immunoelectron microscopy of C22 and T7 cell lines

C22 and T7 cells were trypsinized, and the cell suspensions were incubated with one volume of pre-warmed fixative containing 4 % paraformaldehyde in cacodylate buffer and 0.05 % glutaraldehyde in 0.1 M sodium cacodylate buffer with 2 % sucrose (pH 7.4), and one volume of cell culture suspension (1:1) for 30 min. Thereafter, the cell mixture was centrifuged for 10 min at 500 g. After centrifugation, the growth medium was aspirated, and the pellet was further fixed for 90 min with the same fixative at RT. After fixation, the supernatant was discarded and the pellet was rinsed for 1 h in 0.1 M cacodylate buffer (4–6 changes). Thereafter, the pellets were dehydrated in

70 % alcohol and embedded in LR white medium grade according to the protocol of Newman et al. (1983) (LR White Resin, Berkshire, England) followed by polymerization for 3 days at 50 °C. Ultrathin sections of C22 and T7 cells (80 nm) were incubated overnight in a wet chamber with a rabbit anti-mouse catalase antibody (1:4000 in 0.1 % BSA in TBSA) or rabbit anti-mouse CC10 (1:1000 in 0.1 % in TBSA or rabbit anti-mouse pro-SP-C (1:500 in 0.1 % TBSA). After washing, the grids were incubated for 2 h with ultrasmall gold-labeled goat anti-rabbit Fab fragments (Table 1) (Aurion, Wageningen, Netherlands). Incubated sections were subjected to silver intensification according to Danscher and contrasted thereafter with uranyl acetate for 3 min and lead citrate for 1 min, followed by examination in a LEO 906 transmission electron microscope.

Isolation and purification of RNA

The conditionally immortalized C22 and T7 cell lines were grown until confluence in six-well plates for 24 h (Becton–Dickinson, GmbH, Heidelberg, Germany). The medium was aspirated, and the cells were washed with PBS (Mg^{2+} and Ca^{2+} free). RLT buffer (350 μ l) from the RNeasy mini kit (Qiagen, Hilden, Germany) were added and the cells removed by using a cell scraper. Isolation of total RNA was performed with the RNeasy mini kit (Qiagen, Hilden, Germany) according to the manufacturer's protocol. The concentration of the purified total RNA was measured with a Smartspec™ 3000 spectrophotometer (Bio-Rad, München, Germany).

DNase I treatment and reverse transcription

To eliminate the genomic DNA, DNase I digestion was done to obtain pure total RNA preparations. One microgram of purified total RNA was treated with 1 U/ml of DNase I (Invitrogen) at 25 °C for 15 min in 10 μ l reaction volume prior to reverse transcription. The DNase I reaction was stopped by inactivation of the enzyme by adding 25 mM EDTA for 10 min at 65°. Reverse transcription was carried out as follows: One microgram RNA was incubated with a final concentration of 0.5 μ g oligo (dT) 12–18 primers and 10 mM dNTPs, and this RNA mixture was heated to 65 °C for 5 min and thereafter immediately placed on chilled ice. The reaction mixture was further incubated by adding 5x RT buffer, 0.1 M DTT, 40 U/ μ l RNaseOUT™ (all from Invitrogen, Karlsruhe, Germany) and heated for 2 min at 42 °C (Biometra TRIO-thermo block, Netherlands). Finally, 1 μ l of SuperScript™ II reverse transcriptase (200U/ml) was added and the reaction mixture incubated at 42 °C for 50 min for reverse transcription. The reaction was stopped by heating at 70 °C for 15 min.

Quantitative reverse transcriptase polymerase chain reaction (qRT-PCR)

Specific primers were designed with the Primer3 online software (<http://bioinfo.ut.ee/primer3-0.4.0/>) (Untergasser et al. 2012) and ordered online from Eurofins MWG Operon (<http://www.operon.com>). Primers used in this study are listed in Table 2. Quantitative RT-PCR analysis was carried out using the SYBR premix (Life Technologies, Darmstadt, Germany) on an iCycler PCR machine (Bio-Rad, Heidelberg, Germany), according to the manufacturer's instructions. Normalized values for different mRNAs of C22 and T7 cells were calculated by dividing the values for individual mRNAs with the values for *Gapdh* mRNA. All RT-PCR experiments were performed three times using the total RNA from three distinct isolation experiments. The qPCR was performed using triplicate and the reports were analyzed by an approximation method, taking $\Delta\Delta ct$ values into consideration, and the fold changes were calculated. Graphs were made by using the GraphPad prism software version 5, and the statistical significance was determined by using the unpaired *t* test.

Preparation of total homogenates from C22 and T7 cells

The C22 and T7 cells were grown until confluence in six-well plates for 24 h (Becton–Dickinson, GmbH, Heidelberg, Germany). The cells were removed by trypsinization for 3 min and collected by centrifugation at 300g for 5 min. The pellet was homogenized with a Potter–Elvehjem homogenizer (Potter-S, B. Braun, Melsungen, Germany) at 1000 rpm (1 stroke, 60 s) in 2 ml ice-cold homogenization buffer (HMB: 0.25 M sucrose and 5 mM MOPS, pH 7.4, 1 mM EDTA, 0.1 % ethanol, 0.2 mM DTT, 1 mM aminocaproic acid and 10 % cocktail of Serva protease inhibitors (Serva, Heidelberg, Germany). The quality of the homogenization process was controlled by trypan blue staining of 1 μ l of the homogenate by light microscopy. Thereafter, the homogenates were centrifuged for 20 min at 1000 rpm at 4 °C, and the supernatants were used for further analysis.

Western blotting

A total of 20 and 50 μ g of protein samples derived from C22 and T7 cells were separated on 12 % SDS-polyacrylamide gels and transferred onto a polyvinylidene difluoride membrane (PVDF from Millipore, Schwalbach, Germany) for 50 min at constant 200 V using a Bio-Rad electrophoresis apparatus (Bio-Rad, München, Germany). Non-specific protein-binding sites on the blotted membranes were blocked with Tris-buffered saline (TBS) containing 10 % non-fat milk powder (Carl Roth, Karlsruhe, Germany) in

Table 2 List of primers used for qRT-PCR analysis on total RNA of C22 and T7 cells

Gene target	Gene bank accession no.	Sense primer (5′–3′)	Antisense primer (5′–3′)	PCR product (bp)	Ann. Temp. °C
<i>Abcd1</i>	NM_007435.1	ACAGTGCCATCCGCTACCTA	ATGAGCTACTAGACGG CTTCG	65	59.5
<i>Abcd4</i>	NM_008991.2	TCAGAATGGGACGC TCATTGA	TGGCAGCGATGAAGTTG AATAA	86	57.0
<i>Acaa1</i>	AK143187.1	CAATGAACTGA AGCGTCGTG	CACCACTGTGG CACTCTCTG	141	59.0
<i>Acox1</i>	NM_015729.2	CCGCCACCTTCAATCC AGAG	CAAGTTCTCGATTTCTCG ACGG	86	61.0
<i>Acox2</i>	NM_001161667.1	ACGGTCCTGAACGCAT TTATG	TTGGCCCCATTTAGC AATCTG	125	57.9
<i>Acox3</i>	NM_030721.2	TTCTAGTGCTGATTAAC TGCCT	AGAAACGAAAACCTGTGG TTCCAA	98	58.0
<i>Agps</i>	AK_031049	TGTCCTCCGTGTCTGTTCCCT	CATGGTACAACCTGCCCTTC	141	59.4
<i>Cat</i>	BC013447	GGAGAGGAAACGCCTG TGTGA	GTCAGGGTGGACGTCAGTG AAA	103	64.0
<i>Cc10</i>	AK145844.1	GCCTCCAACCTCTA CCATGA	GGACTTGAAGAAATCC TGGGC	107	59.5
<i>Fdps</i>	AK140881.1	GAGAAGGAACACGCC AATGC	GACCTTTCCCGTC ACACTGG	111	60.0
<i>Gnpat</i>	AK_010896.1	TGAGGACGTGCAAG CCTTTG	TCCAGAAGCTGACGGGTG AA	121	58.0
<i>Gpx</i>	BC086649.1	TTGGTGATTACTGGC TGCAC	CATTAGGTGGAAAG GCATCG	145	57.3
<i>Gr</i>	AK040136.1	TGACAACATCCCTAC TGTGGTC	ACATCGGGGTAAAG GCAGTC	128	60.0
<i>Hmgcr</i>	AK079302.1	ACCTTCTACCTCAGCAAGCC	GTGCCACATAC AATTCGGGC	106	59.4
<i>Hmgcs</i>	AK135551.1	GCTCAGAGAGGACACAC ATCA	GTGGTCATTTGTGAAG GGGC	142	59.5
<i>Ho-1</i>	BC010757.1	CGCCTTCCTGCTCAACATT	TGTGTTCTCTGTCAGCATC AC	150	58.5
<i>Idi1</i>	AK160832.1	TGTTACAGCAGAGATCAG ATGC	CTGCTCGCTTCACACC AATG	126	59.0
<i>Mfp2</i>	NM_008292.4	TTAGGAGGGGACTTCAAG GGA	TCGCTGCTTCAACTG AATCG	119	59.8
<i>Mvd</i>	AK089354.1	TTGTGGCAGCTGTAAG ACAC	ATGATGTACTGGACCCCACC	148	59.0
<i>Mvk</i>	BC005606	GCTGACCAAGTTCCCTGAG ATT	TCCAGCCCCAGATACTTAG AGG	182	60.7
<i>Pex11γ</i>	NM_026951.2	CTAGTGGAACAATGCC CCAAC	AGGCCATACTGCTTAGTGT AGA	137	59.0
<i>Pex11α</i>	NM_011068.1	TCAACCGCGTGGTTTATT ACA	CGCCACCTTTGCCATTTC	98	65.7
<i>Pex11β</i>	NM_001162388.1	GACGAAAGTTGCTACG CCTG	GCTCGGTTGAGGTGACTG AC	118	60.0
<i>Pex13</i>	NM_023651.4	TGGATATGGAGCCTACGG	CGGTTAAAGCCCAAACC ATT	81	57.9
<i>Pex14</i>	NM_019781.2	GCCACCACATCAACC AACTG	GTCTCCGATTCAAAGAAG TCTT	97	59.0
<i>Pex5</i>	NM_008995.2	AATGCAACTCTTGTATCCC GA	GGCGAAAGTTTACTG TTCAATC	91	58.5
<i>Pmvk</i>	AK003607.1	AGATTGTGGAAGGCGTG TCC	GCCACTACTCGGACTG TCTG	118	60.0

Table 2 continued

Gene target	Gene bank accession no.	Sense primer (5′–3′)	Antisense primer (5′–3′)	PCR product (bp)	Ann. Temp. °C
<i>Ppara</i>	AK081709.1	TCCTTTCTGAATGGGCACTT	TAAACATTGGGCCG GTAAAG	125	55.0
<i>Pparβ</i>	AK089913.1	GCGGGCTCTAGAATTCCATC	CCGTCCTCTTAGCCACTGC	137	59.4
<i>Pparγ</i>	BC021798.1	TTTTCAAGGGTGCCAGTTTC	CATGGACACCATAC TTGAGCA	128	56.0
<i>Prx1</i>	BC083348.1	CATGATGTGGTGTGA TTCCAG	AACAGGTTGTTTTCT GTGACTGAT	134	57.9
<i>Sod1</i>	BC032986.1	AAAATGAGGTCCTGC ACTGG	AACCATCCACTTCGA GCAGA	145	57.3
<i>Sod2</i>	BC010548.1	GGGAGCACGCTTACT ACCTTC	GAGCCTGGCACTCAATGTG	150	60.0
<i>Sod3</i>	BC010975.1	CTAGACAGAGGCCCTC CCAGA	GTCCTGGACACAGAGG AACG	148	64.4
<i>Sp-a</i>	AK004788.1	ACAAGGGAGAGCCTG GAGAA	TGGATCCTTGCAAGCTG AGG	132	59.4
<i>Sp-b</i>	NM_0012820 1.1	ATCCCTGGAGTGTGC ACAAG	TGGCACAGGTCATTAG CTCC	126	59.4
<i>Sp-c</i>	BC061137	CTGATGGAGAGTCCAC CGGATTAC	GAAGAATCGGACTCGGA ACCAGTA	485	58.0
<i>Sqs</i>	AK162294.1	ACGTCCTCACCTACCTGTCA	TGCCCTTCCGAATCTTCAC	145	59.4
<i>Trx1</i>	AK149625.1	TGACAATGTCCCA ACGACTG	TTCCAATGGCCAAAAG AAAC	140	55.0
<i>Trx2</i>	BC013688.1	AGGCTTTGACCA GCAAATGT	AAGCATGATCCTCCCAAG TG	140	56.0

TBST (TBS plus 0.05 % Tween-20 blocking buffer). Primary antibodies were diluted in 5 % blocking solution and applied for 1 h at RT on a rotor shaker at concentrations listed in Table 1. After washing with TBST at RT (3 × 10 min), blots were incubated for 1 h with alkaline phosphatase-conjugated anti-rabbit or anti-mouse IgG antibodies. After a final washing step, immunoreactive bands were visualized with the Immunostar™—AP detection kit (Bio-Rad) with a chemiluminescent substrate for alkaline phosphatase, followed by exposure of the membrane to BioMax MR films (Kodak, Stuttgart, Germany). Blots of different gels were stripped several times with 10 % SDS and 0.7 % β-mercaptoethanol at 42 °C for 45 min and reprobed with other primary antibodies as described in Table 1. All Western blot analyses were performed three times with different membranes and therefore represent data from three individual experiments.

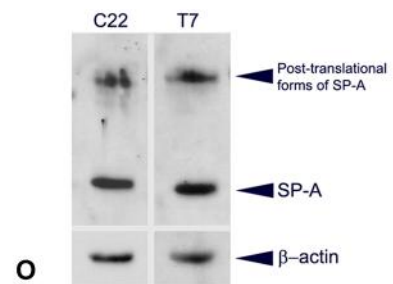
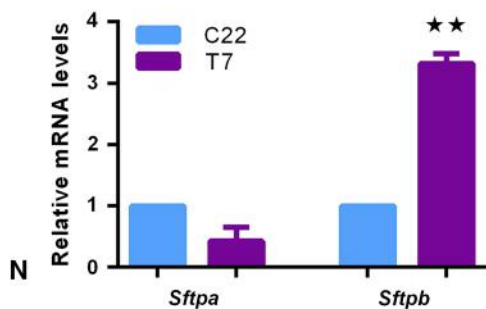
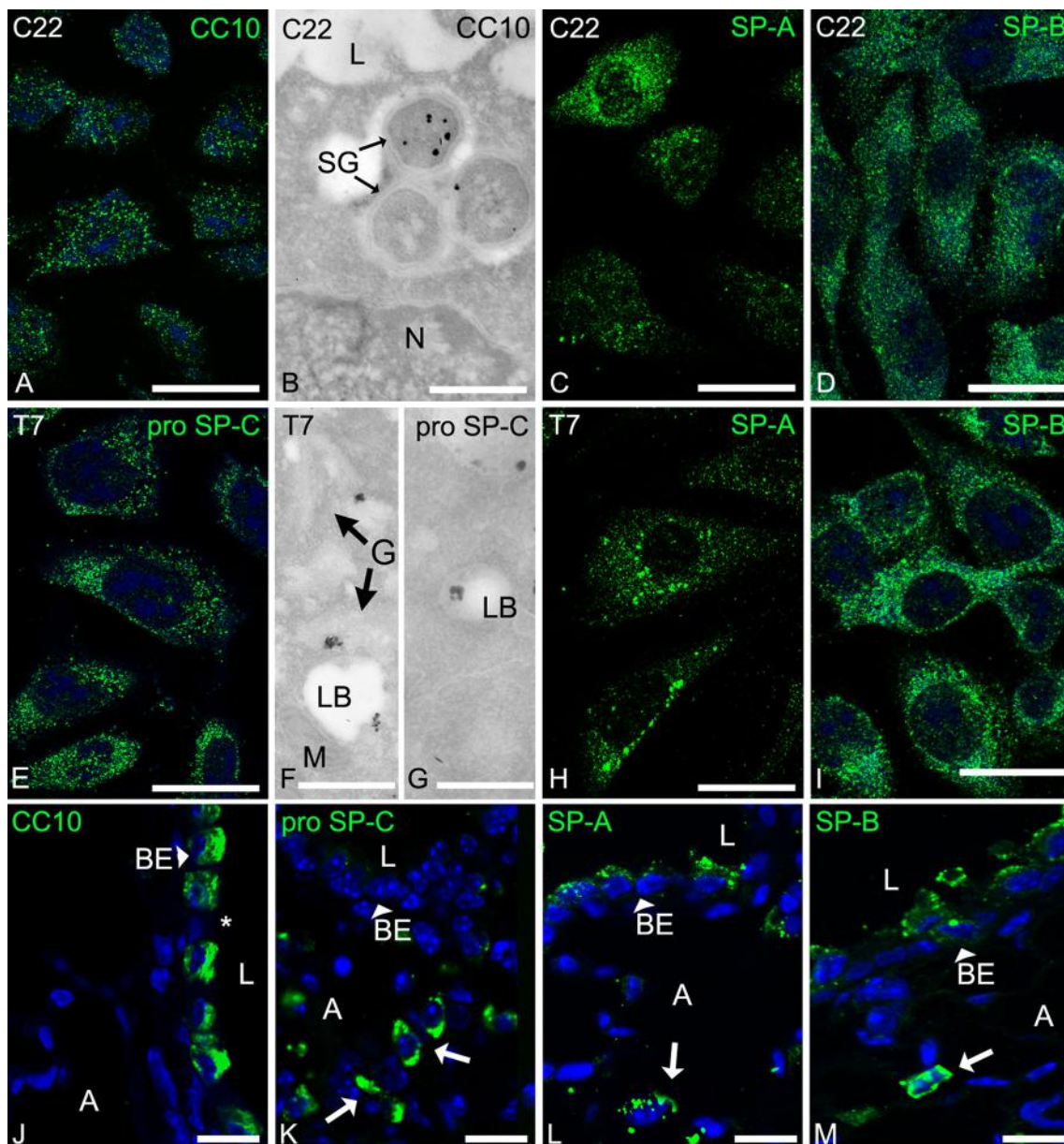
Results

In the human and mouse lung, club cells and AECII contain the highest numerical abundance of peroxisomes with characteristic heterogeneous enzyme content (Karnati and Baumgart-Vogt 2008, 2009). To establish model cell lines

to study the functional role of peroxisomes in these cell types, we have used conditionally immortalized C22 and T7 cell lines of the immortomouse to profile the peroxisomal compartment, its protein content and associated gene expression.

C22 and T7 cells express lung cell-type-specific marker proteins

Initially, we determined the cell-type-specific marker protein expression of these cell lines by using IF employing antibodies against the lung cell-type-specific marker proteins, such as the club cell protein 10 (CC10) (Fig. 1a) and pro-SP-C for AECII (Fig. 1e). The staining revealed strong labeling of these specific cell types with a pattern suggestive for the localization of both proteins in secretory granules, CC10 in granules of C22 cells (Fig. 1b) and pro-SP-C in lamellar bodies of T7 cells (Fig. 1g). We verified the correct subcellular localization of the CC10 protein or pro-SP-C by post-embedding immunocytochemistry on LR white sections of the adult lung. The gold particles were confined exclusively to the secretory granules of club cells or transport vesicles in the secretory pathway and lamellar bodies of the AECII depicting the high specificity of the antibody labeling (Fig. 1b, f). Other cell compartments such as



mitochondria and the nucleus were negative. Moreover, the specificity of these antibodies were verified by reciprocal staining of T7 cells with anti-CC10 and C22 cells with anti-pro-SP-C antibodies, which remained completely negative

(supplementary Fig. 1A and 1B). In contrast to the sole labeling of either C22 or T7 cells, both cell lines showed positive labeling for the surfactant proteins SP-A (Fig. 1c vs. h) and SP-B (Fig. 1d vs. i). Further, these results were

Fig. 1 Cell-type-specific marker proteins and mRNA expression in cultured C22 and T7 cells. IF used for the localization of the CC10 protein (a) and its subcellular localization in secretory granules (b). SP-A (b) and SP-B (c) were localized in C22 cells. The pro-SP-C protein was localized in T7 cells (e) and its subcellular localization in transport vesicles (f) and in lamellar bodies (g). The SP-A (h) and SP-B (i) were also expressed in these cells. Adult mouse lung sections were stained with CC10 (j), or pro-SP-C (k), SP-A (l) and SP-B (m). *SG* secretory granule, *N*: nucleus, *G* Golgi, *LB* lamellar bodies, *BE* bronchiolar epithelium, *arrow head* bronchiolar epithelium, ***ciliated cell *A*: alveoli, *arrows* AECII, *L*: lumen of the bronchiole. Bars represent a, c–e, h, i 25 μm , b, f, g 0.3 μm , j–m 15 μm . qRT-PCR analyses on C22 and T7 cells showing mRNA levels encoding for SP-A and SP-B proteins (** $P < 0.004$) (n). Western blots were probed with an affinity-purified antibody to SP-A (o). The membrane was stripped and reprobed for loading control (β -actin)

corroborated by IF analysis of paraffin sections of adult mouse lungs, revealing the same staining pattern (j–m). The CC10 protein was exclusively localized in club cells of the bronchiolar epithelium (BE), whereas neighboring ciliated cells (asterisk in Fig. 1j) remained negative. Similarly pro-SP-C was detected solely in AECII of the alveolar epithelium (AE), whereas AECI or the complete bronchiolar epithelium was not stained, verifying cell-type-specific localization of these marker proteins and the high monospecificity of the antibodies used (Fig. 1k). The SP-A and SP-B proteins were detected in both club cells and AECII in the adult mouse lung tissue. The SP-A protein exhibited hardly any differences in labeling intensities (Fig. 1l), whereas the SP-B protein demonstrated clear labeling intensity differences between the weaker labeled club cells and the stronger labeled AECII (Fig. 1m). This difference was also observed in C22 cells (Fig. 1c) in comparison with T7 cells (Fig. 1h). Negative controls without the primary antibodies remained completely unstained, confirming the specificity of the secondary antibody reactions (supplementary Fig. 1c–1f). Analysis of mRNA expression levels for *CC10*, *SP-C*, *Sftpa* and *Sftpb* corroborated the morphological results (Fig. 1n, supplementary Fig. 1g–h). The *CC10* mRNA was exclusively expressed in C22 club cells, whereas the one for *SP-C* was expressed in T7 cells. Western blot analysis for the SP-A protein yielded two specific bands at 36 and 72 kDa (Fig. 1n). In these Western blots, no clear differences in protein amounts for SP-A in C22 and T7 cells were observed.

Post-embedding immunocytochemistry for catalase localization revealed exclusive labeling of peroxisomes

We investigated the localization of the catalase protein by post-embedding immunocytochemistry in C22 and T7 cell lines in comparison with mouse lungs. Our results revealed that gold particles were confined exclusively to the matrix region of peroxisomes in club cells (2a), C22 cells (2b), AECII (2c) and T7 cells (2d). Mitochondria and other cell

organelles were negative. The largest peroxisomes were observed in the club cells of mouse lungs (2a) in comparison with C22 peroxisomes that were stained with catalase protein (2b). These results are in agreement with our previous observations on mouse club peroxisomes stained with the DAB method for catalase activity (Karnati and Baumgart-Vogt 2008). Peroxisomes in AECII were much smaller and more elongated and associated very closely with lamellar bodies (2c). A similar pattern was observed in T7 cells (2d) (Fig. 2).

Peroxisomes are more numerous, and the genes encoding for PEX5p and PEX11p proteins are highly expressed in T7 cells

We aimed at investigating the structure, distribution, numerical abundance and protein composition of the peroxisomal compartment in C22 and T7 cells. Peroxisomes in C22 cells were less numerous but larger and frequently round structures (Fig. 3a, b); the ones in the T7 were much higher in number and arranged in clusters of mostly tubular organelles (Fig. 3c, d). Comparable differences were also noted in situ in lung tissue sections (Karnati and Baumgart-Vogt 2008). Moreover, Western blot analysis for PEX13p and PEX14p corroborated the morphological results demonstrating clearly the higher abundance of both proteins in T7 cells in comparison with the C22 cells (Fig. 3e). Further, qRT-PCR analysis for all mRNAs of the *Pex11* family (*Pex11 α* , β , γ) were expressed at higher levels in T7 cells, corresponding to the higher number of organelles in this cell type (Fig. 3f). The most significant difference was observed for the mRNA levels for *Pex5* (** $P < 0.0002$; ** $P < 0.001$; * $P < 0.02$) between both cell types.

Peroxisomal β -oxidation enzymes of pathways 1 and 2 are differentially expressed in C22 and T7 cells

Peroxisomes contain at least 3 distinct lipid transporters of the ABCD family, from which the ABCD3 protein was selected as a marker protein for immunostaining. Staining for ABCD3 was much stronger in T7 cells (Fig. 4b) in comparison with C22 cells (Fig. 4a), which supports our previous in situ results in the mouse lung (Karnati and Baumgart-Vogt 2008). In contrast to ABCD3, IF analysis for ACOX1 (Fig. 4c, d) and peroxisomal thiolase (Fig. 4e, f) showed the highest protein levels in C22 in comparison with T7 cells. Also qRT-PCR analysis of mRNAs for lipid transporters for distinct ABCD family members revealed that the *Abcd3* mRNA exhibited a significantly higher expression levels in T7 cells in comparison with C22 cells (** $P < 0.0001$). These results correlated with the morphological analysis for ABCD3 in both

Fig. 2 Immunoelectron microscopic localization of catalase protein in peroxisomes. Catalase staining of peroxisomes in mouse lung club cells (**a**) and in C22 cells (**b**). Immunolocalization of catalase protein in peroxisomes of mouse lung AECII (**c**) and T7 cells (**d**). *SG* secretory granules, *LB* lamellar bodies. Bars represent 0.5 μ m

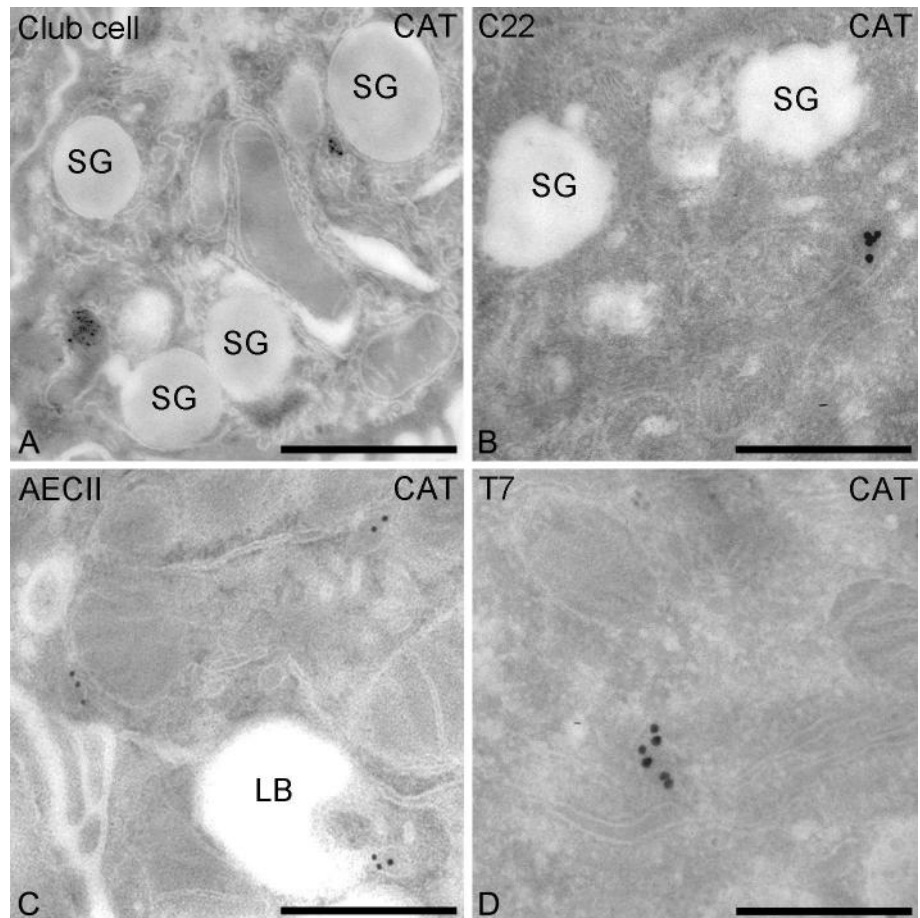
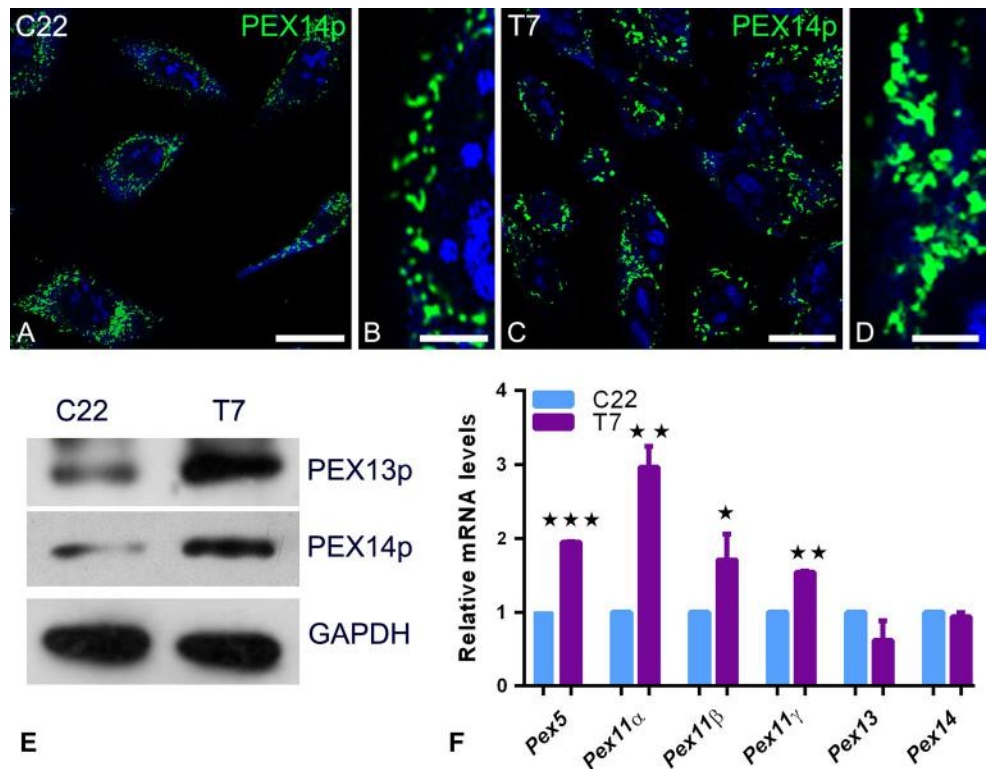


Fig. 3 Peroxisomal biogenesis proteins and mRNAs in cultured C22 and T7 cells. PEX14p (**c**, **d**) was more abundant in T7 cells in comparison with C22 cells (**a**, **b**) and their higher magnification in (**b**) and (**d**). Bars represent **a** and **c** 20 μ m, **b** and **d** 5 μ m. Western blot analysis of different blots was probed with antibodies to PEX13p, PEX14p (**e**). GAPDH was used as loading control (**e**). qRT-PCR analyses of Pex5, Pex11 α , β , γ , Pex13 and Pex14 mRNAs encoding for peroxisomal biogenesis protein, Pex5 ($***P < 0.0002$) and proteins involved in the proliferation of peroxisomes, such as Pex11 α ($*P < 0.027$) and Pex11 γ ($**P < 0.001$) which were highly expressed in T7 in comparison with C22 cells, whereas the ones for Pex13 and Pex14 mRNAs showed no statistical significance between the two cell types (**f**)



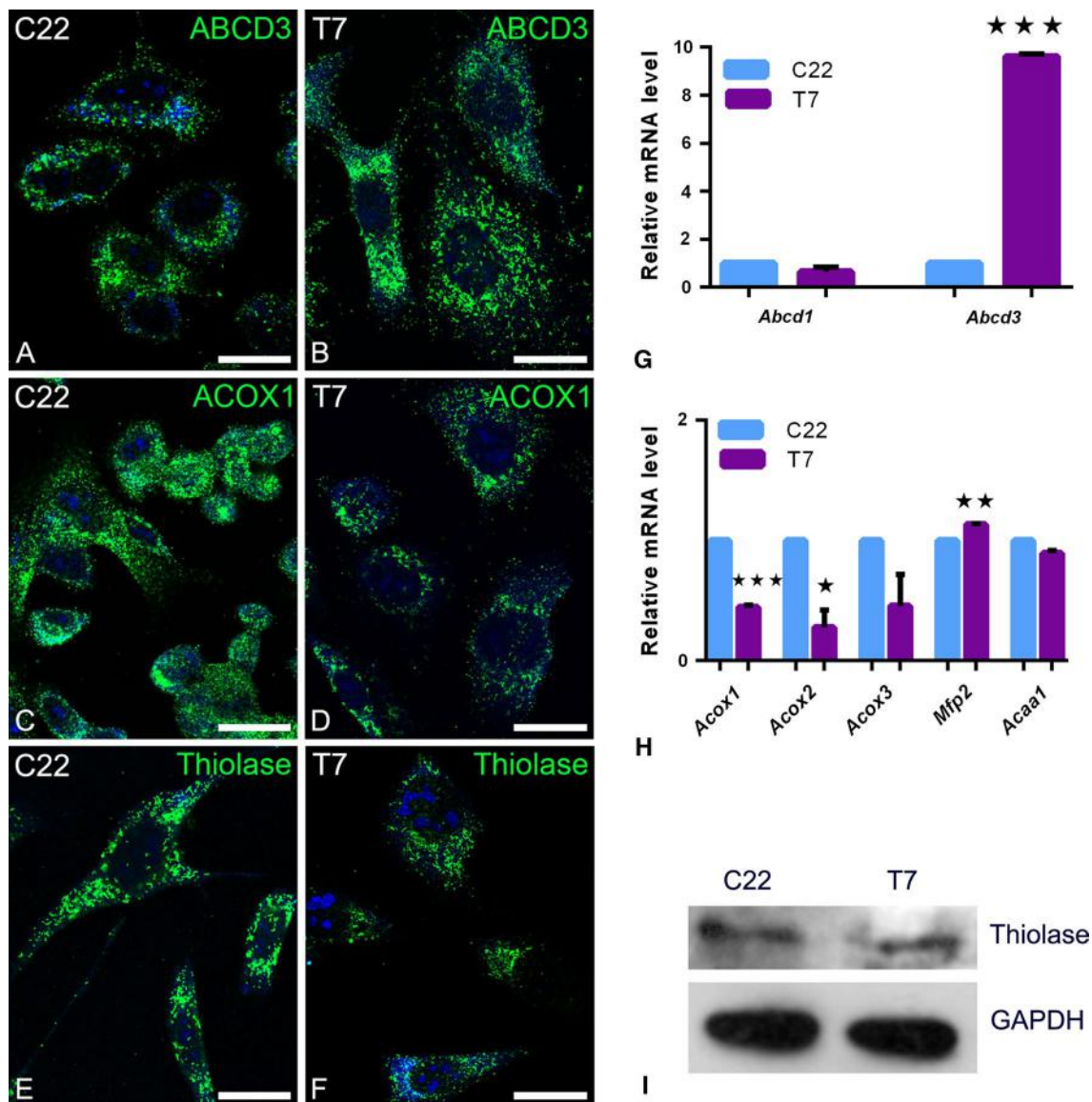


Fig. 4 Peroxisomal proteins and mRNAs involved in lipid transport and β -oxidation. IF detection of peroxisomal lipid transporter (ABCD3) (a, b), peroxisomal β -oxidation enzymes acyl-CoA oxidase 1 (ACOX1) (c, d) and 3-oxo-acyl-CoA thiolase (thiolase) (e, f)

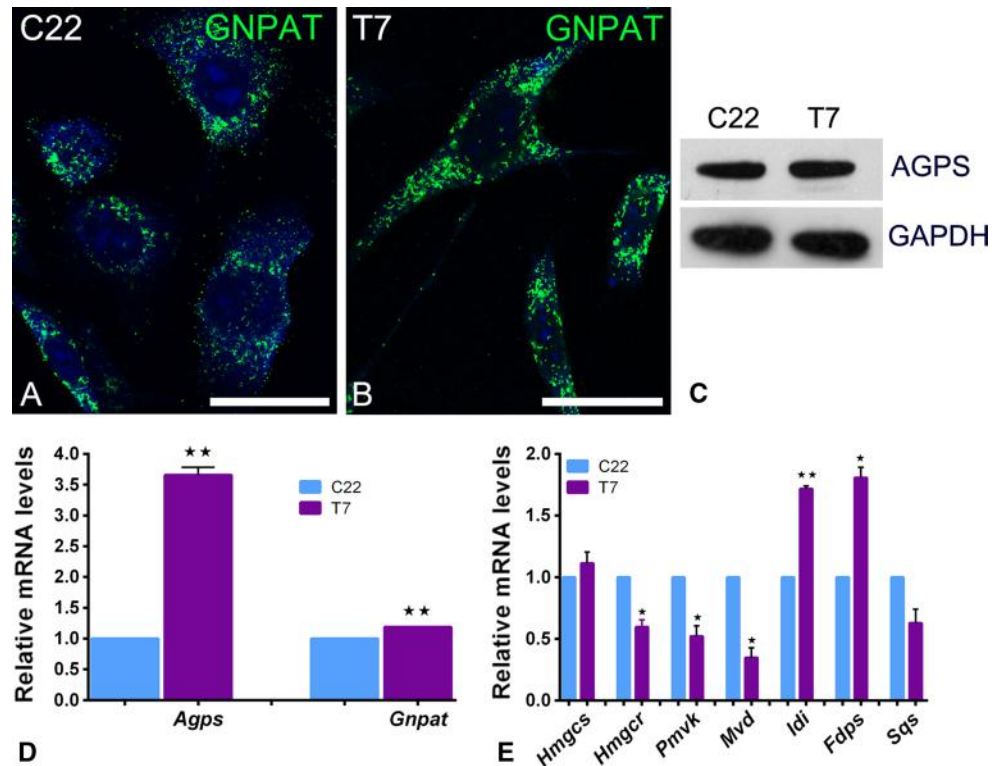
in cultured C22 and T7 cells. qRT-PCR analyses on C22 and T7 cells for mRNAs encoding lipid transporters (g) as well as β -oxidation enzymes (h). Western blot analysis for thiolase. GAPDH was used as loading control (i)

cell types (Fig. 4a, b). Also for genes encoding enzymes of the β -oxidation pathways 1 and 2, a clear heterogeneity was observed between expression levels in C22 cells in comparison with T7 cells (Fig. 4h), with the ones for the *Acox1* and *Acox2* being significantly highly expressed in C22 cells in comparison with T7 cells ($***P < 0.0001$; $*P < 0.0361$; Fig. 3h). Interestingly, the *Mfp2* mRNA showed a distinct pattern, exhibiting a slightly higher expression in T7 cells in comparison with C22 cells ($***P < 0.0035$). The relative amount of peroxisomal thiolase was higher in C22 cells corroborating the IF and qRT-PCR results (Fig. 4i).

Enzymes of plasmalogen synthesis are highly abundant in T7 cells

IF for ether lipid synthesizing enzyme glycerone-phosphate O-acyl transferase (GNPAT) revealed a clear localization of this enzyme in the peroxisomal compartment in both C22 and T7 cells with higher abundance in the organelles of T7 cells (Fig. 5a, b). Furthermore, mRNA levels for both enzymes *Agps* and *Gnpat*, encoding the peroxisomal steps of the plasmalogen synthesis, were significantly highly expressed in T7 cells in comparison with C22 cells ($**P < 0.0023$; $**P < 0.0019$; see Fig. 5d).

Fig. 5 Peroxisomal etherlipid and cholesterol synthesis in C22 and T7 cells. IF staining for GNPAT (**a, b**) was detected in both C22 and T7 cells. Western blot analysis for AGPS in both C22 and T7 cells (**c**) qRT-PCR analyses on C22 and T7 cells for the mRNAs for etherlipid synthesizing enzymes such as *Agps* (** $P < 0.002$) and *Gnpat* (** $P < 0.001$) as well as cholesterol synthesizing enzymes such as *Hmgcr* (* $P < 0.021$), *Pmvk* (** $P < 0.020$), *Mvd* (** $P < 0.015$), *Idi* (** $P < 0.001$) and *Fdps* (* $P < 0.010$). Bars represent 25 μm



Moreover, also the Western blot analysis for AGPS revealed a higher abundance of this plasmalogen synthesizing enzyme in peroxisomes of T7 cells (Fig. 5c).

C22 and T7 cells were also tested for their expression of cholesterol synthesizing enzymes

Differences were observed in the expression levels for mRNAs encoding cholesterol synthesizing enzymes located in peroxisomes with most of them being highly expressed in C22 cells in comparison with T7 cells (Fig. 5e). HMG-CoA reductase (*Hmgcr*) is one enzyme that is localized in both compartments, and the mRNA encoding for this protein was increased in C22 cells (* $P < 0.025$; see Fig. 5e). Further, phosphomevalonate kinase (*Pmvk*) (* $P < 0.3$; Fig. 5e) and mevalonate 5-diphosphate decarboxylase (*Mvd*) (* $P < 0.3$; Fig. 5e), localized exclusively in peroxisomes, were highly expressed in C22 cells. In contrast, isopentenyl diphosphate isomerase (*Idi*) (** $P < 0.001$; Fig. 5e) and farnesyl diphosphate synthase (*Fdps*) (* $P < 0.01$; Fig. 5e) mRNAs were expressed at higher levels in T7 cells in comparison with C22 cells.

Antioxidative enzymes of different cell compartments are differentially expressed in C22 and T7 cells

Clear differences in the subcellular localization and distribution between antioxidative enzymes were noted

by IF analysis of C22 and T7 cells, revealing the typical staining patterns for their corresponding organelles in which the enzymes are localized: (a) a typical more prominent perinuclear punctuate staining pattern for peroxisomal catalase, (b) extensive network formation and elongated tubular organellar structures for mitochondrial SOD2 and (c) a partial staining of the nuclear envelope as well as network of endoplasmic reticulum structures for HO-1 localization were observed (Fig. 6a–f). Interestingly, catalase, the most abundant antioxidative enzyme in the peroxisomal matrix, was highly abundant in the C22 cells and present in large peroxisomes. Labeling for catalase in T7 cells was weaker than in C22 cells (Fig. 6a, b). A similar pattern was observed for this enzyme also by Western blot analysis (Fig. 6i). Several other antioxidative enzymes of peroxisomes peroxiredoxin 1 (PRDX1), glutathione peroxidase 1 (GPX1) and super oxide dismutase 1 (SOD1) as well as of other subcellular compartments also followed this expression pattern SOD2, SOD3 and thioredoxin 2 (TRX2). In contrast, hemeoxygenase 1 (HO-1) and thioredoxin 1 (TRX1) both localized in the endoplasmic reticulum showed an opposite regulation with much stronger protein and mRNA levels in T7 cells. Also the glutathione reductase protein (GR) was clearly more abundant in T7 cells, whereas its corresponding mRNA exhibited only a slight difference (Fig. 6h, i).

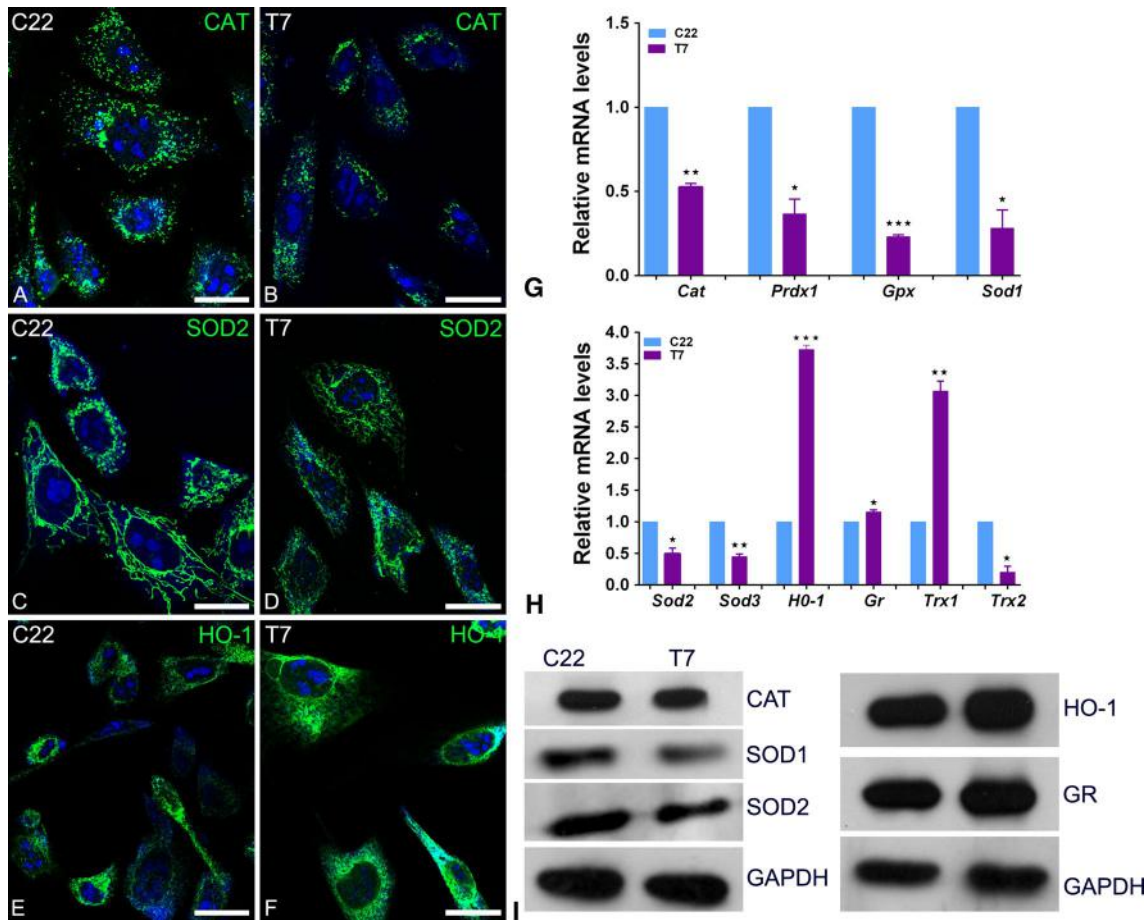


Fig. 6 Anti-oxidative enzymes of different cell compartments in C22 and T7 cell lines. Localization of catalase (a, b) in the peroxisomes, SOD2 (c, d) in the mitochondria was abundant in C22 cells in comparison with T7 cells. In contrast, HO-1 (e, f), an enzyme of the ER was highly abundant in T7 cells in comparison with C22 cells. qRT-PCR analysis for catalase (***P* < 0.02), Prdx1 (**P* < 0.01),

Gpx (***)*P* < 0.0001), Sod1 (**P* < 0.021), Sod2 (**P* < 0.029), Sod3 (***P* < 0.005) and Trx2 (**P* < 0.01) mRNAs in T7 cells in comparison with C22 cells (g, h). In contrast, Ho-1 (***)*P* < 0.0001), Gr (**P* < 0.03) and Trx1 (***)*P* < 0.005) mRNAs were highly expressed in T7 cells (h). Western blot analysis corroborated the IF and qRT-PCR results (i). GAPDH was used as loading control

Peroxisome proliferator-activated receptors (PPARs) are highly abundant in T7 cells

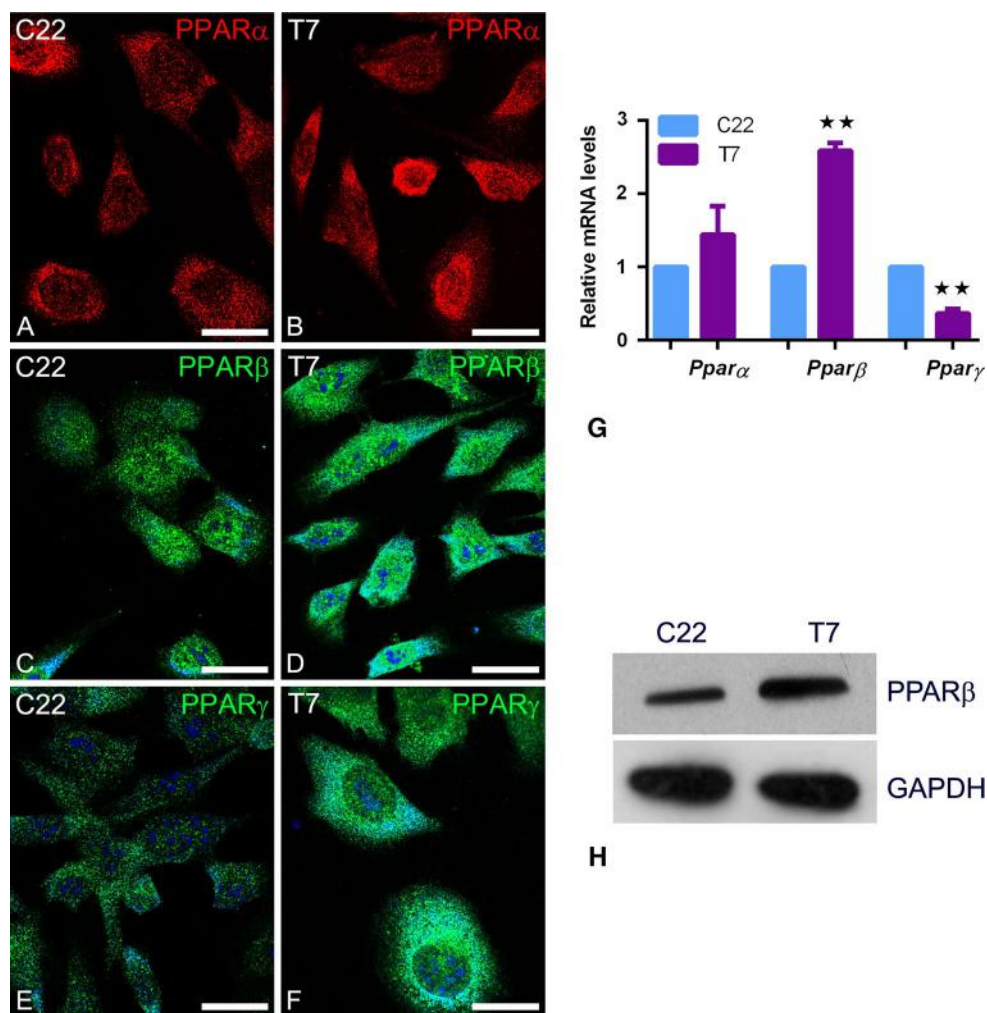
Since the genes for many peroxisomal proteins are regulated by nuclear receptors of the peroxisome proliferator-activated receptor family (PPAR), all three PPAR family members (PPARα, β/δ, γ) were localized in both cell types. PPARα, PPARβ and PPARγ are more abundant in T7 cells in comparison with C22 cells (Fig. 7a–f). Moreover, a clear nuclear staining pattern was observed in many T7 cells in the staining for PPARβ (Fig. 7d) and a weaker one for PPARα. In contrast, the relative protein content in the cytoplasm in comparison with the nucleus (cytoplasmic vs. nuclear pattern) was distinct in PPARγ preparations exhibiting much higher enrichment in the cytoplasm as well as stronger staining in T7 cells. Western blot analysis showed that PPARβ protein expression in T7 cells is higher than in C22 cells (Fig. 7h). These results were

corroborated by qRT-PCR analyses for *Pparα* and *Pparβ* mRNAs (Fig. 7g). In contrast, the *Pparγ* mRNA level was significantly lower in T7 cells (***P* < 0.008 for *Pparγ*) than in C22 cells, suggesting a distinct regulation of *Pparγ* mRNA and protein.

Discussion

C22 and T7 cells are frequently used model cell lines to study club cell and AECII biology and function. Previously, we described in lung tissue that club cells and AECII contain the highest number of peroxisomes in which these organelles might fulfill important metabolic functions (Karnati and Baumgart-Vogt 2008, 2009). To study the regulation of the peroxisomal compartment or their alterations by cytokines or growth factors, good cell culture model systems are necessary. Therefore, in the present study, we analyzed the

Fig. 7 Peroxisomal proliferator-activated receptors in C22 and T7 cells. PPAR α , PPAR β and PPAR γ are more abundant in T7 cells in comparison with C22 cells (a–f). qRT-PCR analysis did only confirm the results for PPAR α and β stainings (g). PPAR β (** $P < 0.004$) mRNA was significantly highly expressed in C22 cells compared to T7 cells. Further, at the protein level, PPAR β is more abundant in T7 cells compared to C22 cells (h) corroborating the morphological (c, d) and qRT-PCR (g) results



peroxisomal compartment in C22 and T7 cells with sensitive morphological, molecular biological and biochemical methods and a variety of peroxisomal markers to achieve insights on their possible metabolic roles in these cell lines. Our results reveal that peroxisomes are present in both cell lines at high abundance and show a comparable protein composition to AECII and club cells in lung tissue in situ.

Immortal cell lines are useful tools to study the function of cell types difficult to maintain in primary cell culture

Freshly isolated AECII or club cells can be placed in primary culture, but within a week the cells begin to dedifferentiate and are difficult to maintain in their phenotype. Also in good primary cell culture conditions, within 2–4 weeks these cells reach senescence and thereafter undergo apoptosis. Due to these difficulties, many physiological and functional studies of lung biology could not be performed in detail. This shortage can, however, be overcome by the use of conditionally immortal cell lines from the “immortomouse” (Demello et al. 2002). The transgenic H-2k^b-tsA58

“immortomouse” expressing a temperature-sensitive form of the SV40 T-antigen enables (Jat et al. 1991) to isolate and establish excellent model cell lines, resembling in their phenotype the original cell types in appropriate organs or tissues. Further, the “immortomouse” has helped to culture many difficult-to-maintain cell types, such as osteoclasts (Chambers et al. 1993), colonic and small bowel epithelial cells (Whitehead et al. 1993) or podocytes of the kidney (Mundel et al. 1997). T7 cells seem to resemble native AECII and C22 cells the native club cells, since they are able to produce corresponding cell-type-specific marker proteins (deMello et al. 2000, 2002).

Cell-type-specific marker proteins and surfactant proteins are synthesized in proliferating C22 and T7 cells

Indeed, the immortalized C22 and T7 cells used in our study expressed the mRNAs and synthesized cell-type-specific secretory proteins (for C22 cells: CC10 as well as SP-A and SP-B; for T7 cells: SP-C as well as SP-A, and SP-B),

suggesting that they resemble native club and AECII, supporting the data from Demello and colleagues (deMello et al. 2000, 2002; Wong et al. 1996). In comparison with their work, in our manuscript, these marker proteins were localized in addition also on the subcellular level in secretory granules or lamellar bodies by morphological means using our highly sensitive immunofluorescence protocol and post-embedding immunocytochemistry on LR white sections of C22 and T7 cells.

Peroxisomes in C22 and T7 cells lines

Peroxisomes are ubiquitous organelles and therefore also present in all cell types of the lung, in which they are most easily visualized in stainings for PEX14p, a biogenesis protein in the peroxisomal membrane, present ubiquitously in peroxisomes of distinct cell types (Grant et al. 2013; Karnati and Baumgart-Vogt 2008, 2009). However, the numerical density of peroxisomes and most metabolic matrix proteins as well as lipid transporters is more abundant in club cells and AECII, where they might also serve important metabolic functions, such as protection against oxidative stress and lipid toxicity and eventually synthesis of surfactant lipids (Karnati and Baumgart-Vogt 2008). Similar to the results obtained in situ in lung tissue, C22 cells and T7 cells contain a highly differentiated and abundant peroxisomal compartment, in which peroxisomes seem to divide frequently, since many tubular peroxisomes were observed and high-level expression of mRNAs encoding proteins of the Pex11 family was detected. The Pex11 β protein seems to regulate the constitutive numerical peroxisome abundance, whereas Pex11 α was suggested to be involved in induced peroxisome proliferation (Li et al. 2002; Li and Gould 2002; Schrader et al. 1998). By using a sensitive in situ hybridization technique in one of our earlier studies, we detected the strongest expression of the Pex11 β mRNA in the distal airway epithelium and AECII of the alveolar epithelium of newborn mice (Karnati and Baumgart-Vogt 2009). Finally, Pex11 γ seems to be involved in peroxisomal cluster formation (Li et al. 2002), which was also observed in C22 and T7 cells, corroborating the significant increase in Pex11 γ mRNA by qRT-PCR analysis (Fig. 3f). Similar to T7 cells, tubular peroxisomes have also been observed in AECII in the lung. In club cells of the bronchiolar epithelium in the mouse lung, peroxisomes are larger and mostly round or oval shaped, which is also reflected in a similar phenotype in C22 cells. In C22 cells less peroxisomes are elongated tubules in comparison with T7 cells, which is a typical distinguishing feature between club and AECII also in situ. Indeed, the number and morphological appearance of peroxisomes in distinct cell types depends on cell-specific functions and the metabolic environment (Baumgart 1997; Isseemann and Green 1990). Whereas PEX14p is present on

the surface of the whole tubular structures, metabolic matrix enzymes are sometimes localized only in special extended parts of these tubular network structures (Baumgart et al. 1989; Yamamoto and Fahimi 1987). Also peroxisomal catalase in C22 cells is mainly present in the larger and round parts of the peroxisomal compartment (Fig. 6).

Peroxisomal β -oxidation, cholesterol and plasmalogen synthesis are differentially expressed in C22 versus T7 cells

Peroxisomal β -oxidation is responsible not only for the degradation of a variety of toxic, insoluble, and bioactive lipids, e.g., eicosanoids, which are involved in the regulation of inflammatory processes, but also for the synthesis of polyunsaturated fatty acids (Hiltunen et al. 1996) that are vital components of surfactant and protect the surfactant film against ROS damage (Sosenko et al. 1991; Zoeller et al. 1999; Karnati and Baumgart-Vogt 2008; Mannaerts and Van Veldhoven 1993). ACOX 1–3 enzymes are the rate-limiting enzymes of the peroxisomal β -oxidation pathways and control the substrate flux through the β -oxidation chain (Baumgart et al. 1996; Karnati and Baumgart-Vogt 2008). Therefore, ACOX 1–3 also control the release of acetyl-CoA units from the peroxisomal β -oxidation chain. Indeed, the mRNAs for the regulatory enzymes of the distinct β -oxidation pathways, ACOX 1–3, are expressed in both cell types, however, with higher levels in C22 cells. The high levels of β -oxidation enzymes in C22 cells and club cells in situ in the mouse lung could protect the bronchiolar epithelium against proinflammatory eicosanoids released by activated macrophages on the bronchiolar surface. In this respect, it is of interest that also lipids involved in the resolution of inflammation (e.g., resolvins or maresins) are synthesized from docosahexanoic acid, which is synthesized via peroxisomal β -oxidation and is diminished in patients with peroxisomal disorders (Martinez 1996; Spite and Serhan 2010).

Peroxisomal β -oxidation could also be responsible for providing acetyl-CoA units for lipid synthetic pathways in peroxisomes of AECII, such as the synthesis of cholesterol precursors. All steps required for the synthesis of farnesyl-PP are present in peroxisomes, with the steps from mevalonate to FPP being exclusively localized in this organelle (Kovacs et al. 2002). Interestingly, the mRNAs for enzymes of the early “peroxisomal” steps are more abundant in C22 cells. In contrast, the mRNAs for IDI and FDPS, the last two enzymes involved in this pathway, located at a pathway branching-point and possibly necessary for isopentyl-tRNA synthesis, as well as the synthesis of heme a, ubiquinone (coenzyme Q10), dolichol-PP and prenylated proteins (FPP), are highly expressed in T7 cells. Therefore, peroxisomal intermediates in T7 cells might be

shuttled into the mentioned pathways and could therefore influence general translational fidelity, respiratory chain activity, N-glycosylation and isoprenylation of proteins, necessary for membrane interactions. Another lipid synthesizing pathway with higher expression in T7 cells mainly AGPS (synthesizing the ether bond) seems to be the one for the synthesis of ether lipids. Plasmalogens generated in peroxisomes are minor components of surfactant and might defend surfactant lipids against oxidative damage by trapping ROS. Moreover, ether lipids influence the movement of lipid molecules between tubular myelin and the mature surfactant film covering the surface of the alveolar region. Functional surfactant reduces the surface tension of the alveoli; therein plasmalogens and cholesterol seem to play an important role in viscosity regulation of the surfactant film (Tölle et al. 2002).

C22 and T7 cells contain high levels of antioxidative enzymes in distinct subcellular compartments

Lungs are well equipped with a set of antioxidative enzymes to protect against oxygen-induced pulmonary toxicity. In addition to catalase, the fastest enzyme degrading H_2O_2 , peroxisomes contain many other antioxidant enzymes which detoxify the H_2O_2 generated by a variety of peroxisomal oxidases during their substrate conversion (Karnati and Baumgart-Vogt 2008). Mitochondrial SOD2 is also highly abundant in C22 which is an important scavenging enzyme for superoxide radicals, generated by the mitochondrial respiratory chain that are converted by SOD2 into less toxic H_2O_2 in the mitochondrial matrix. H_2O_2 is further degraded by glutathione peroxidase and peroxiredoxin I which are present in peroxisomes, mitochondria and the cytoplasm (Immenschuh and Baumgart-Vogt 2005). In addition to H_2O_2 , an array of lipid hydroperoxides is degraded by the action of proteins of the peroxiredoxin family (Chae et al. 1994). Both C22 and T7 cells seem to harbor a specific set of antioxidant enzymes, which is also apparent from the distribution of distinct thioredoxin isoenzymes, TRX1 being high in T7 versus TRX2 being high in C22 cells. The cellular redox state is also influenced strongly by the availability of reduced glutathione levels, wherefore GSSG:GSH converting enzymes, especially the glutathione reductase, play an important role in the maintenance of the redox state. Interestingly, these cytoplasmic enzymes as well as hemoxygenase-1 from the endoplasmic reticulum are significantly enriched in T7 cells, suggesting that this cell type is protected by these enzymes. Redox-sensitive transcription factors, such as Nrf2 and NF- κ B, are mediating the up-regulation of the antioxidative enzyme genes, e.g., the one for HO-1, catalase as well as SOD2 (Polvani et al. 2012). In addition, other transcription factors, such as the ones for FOXO family and PPAR γ ,

contribute to the fine tuning of transcriptional activity of many antioxidative enzymes.

PPARs in C22 and T7 cells

PPAR γ seems to play an important role in club cell lipid metabolism and in the differentiation of the airway epithelium (Karnati and Baumgart-Vogt 2008). PPAR γ 1 is present in high abundance in murine AECII and club cells (Simon et al. 2006). Therefore, peroxisomal enzyme activation might in part be responsible also for the protective effects noted by PPAR γ induction in the molecular pathogenesis of several lung diseases associated with chronic oxidative stress (Lakatos et al. 2007). By IF and Western blot experiments, we revealed that PPAR β and γ proteins are more abundant in T7 cells in comparison with C22 cells, suggesting that these nuclear factors serve important regulatory functions in AECII. Together, these receptors might play an important role in the control of AECII lipid metabolism and epithelial differentiation (Michael et al. 1997). Particularly, PPAR γ 1 plays an important role in adipocyte differentiation which is in many aspects similar to the differentiation of AECII.

In addition to PPAR γ , PPAR α is a well-known inducer of peroxisome proliferation which is regulating also the transcription of the Pex11 α gene (Shimizu et al. 2004), ABCD transporters and β -oxidation enzymes by binding to a PPAR responsive element in their promoter region (Baumgart 1997; Baumgart et al. 1996). ABCD3 is involved in the transport of lipids in the peroxisomes (Visser et al. 2007) and is highly abundant in T7 AECII, suggestive for a high transport capacity and shuttling of lipid into peroxisomes of AECII for metabolization by the peroxisomal β -oxidation pathways. Recently, ABCD3 was shown to be involved in the transport of branched-chain fatty acids and bile acid precursor (C27 chain length) into peroxisomes, a crucial step in bile acid biosynthesis (Ferdinandusse et al. 2015). Oxysterols, also lipid derivatives, could also be metabolized in peroxisomes in a similar way. Whether ABCD3 is involved in the transport of these lipid derivatives that are important ligands for LXR, is not yet known.

Conclusion and future prospects

The results of our study revealed that C22 club cells and T7 AECII of the immortomouse are well suited as model systems to study the peroxisomal compartment and its associated metabolic and regulatory signaling pathways. Peroxisomes are highly abundant in both C22 club cells and T7 AECII, exhibiting heterogeneity in their structure, numerical abundance and enzyme content that are

reflecting the in situ situation in the lung. Peroxisomes in AECII or club cells possibly might play vital roles in the regulation of ROS levels and homeostasis of bioactive lipids and other lipid ligands for nuclear receptors. Future studies using non-permissive differentiating conditions for both cell types, high temperature (39 °C) cell culture to initiate the degradation of the temperature-sensitive SV40 T-antigen in T7 and C22 cells and addition of cell-type-specific growth or differentiation factors, will allow for the generation of excellent differentiated cell culture models with highest similarity to primary AECII and club cells to study peroxisome functions in these cell types and their alterations by external factors, such as cytokines or growth factors.

Acknowledgments The authors thank Elke Richter, Andrea Textor, Bianca Pfeiffer and Karina Greve for excellent technical assistance. Furthermore, we would like to thank Profs. Denis I. Crane, Stephen J. Gould, Paul P. Van Veldhoven, Alfred Völkl and Nancy Braverman for providing us with some antibodies (see Table 1). Our study was supported by performance-related resource allocation funds (LOM = Leistungsorientierte Mittel) of the Medical Faculty of the Justus Liebig University Giessen, Germany.

References

- Baumgart E (1997) Application of in situ hybridization, cytochemical and immunocytochemical techniques for the investigation of peroxisomes. A review including novel data. Robert Feulgen Prize Lecture 1997. *Histochem Cell Biol* 108:185–210
- Baumgart E, Völkl A, Hashimoto T, Fahimi HD (1989) Biogenesis of peroxisomes: immunocytochemical investigation of peroxisomal membrane proteins in proliferating rat liver peroxisomes and in catalase-negative membrane loops. *J Cell Biol* 108:2221–2231
- Baumgart E, Vanhooren JC, Franssen M, Marynen P, Puype M, Vandekerckhove J, Leunissen JA, Fahimi HD, Mannaerts GP, van Veldhoven PP (1996) Molecular characterization of the human peroxisomal branched-chain acyl-CoA oxidase: cDNA cloning, chromosomal assignment, tissue distribution, and evidence for the absence of the protein in Zellweger syndrome. *Proc Natl Acad Sci USA* 93:13748–13753
- Chae HZ, Robison K, Poole LB, Church G, Storz G, Rhee SG (1994) Cloning and sequencing of thiol-specific antioxidant from mammalian brain: alkyl hydroperoxide reductase and thiol-specific antioxidant define a large family of antioxidant enzymes. *Proc Natl Acad Sci USA* 91:7017–7021
- Chambers TJ, Owens JM, Hattersley G, Jat PS, Noble MD (1993) Generation of osteoclast-inductive and osteoclastogenic cell lines from the H-2Kb-tsA58 transgenic mouse. *Proc Natl Acad Sci USA* 90:5578–5582
- Chang CC, South S, Warren D, Jones J, Moser AB, Moser HW, Gould SJ (1999) Metabolic control of peroxisome abundance. *J Cell Sci* 112:1579–1590
- Danscher G (1981) Light and electron microscopic localization of silver in biological tissue. *Histochemistry* 71:177–186
- deMello DE, Mahmoud S, Padfield PJ, Hoffmann JW (2000) Generation of an immortal differentiated lung type-II epithelial cell line from the adult H-2K(b)tsA58 transgenic mouse. *In Vitro Cell Dev Biol Anim* 36:374–382
- Demello DE, Mahmoud S, Ryerse J, Hoffmann JW (2002) Generation and characterization of a conditionally immortalized lung clara cell line from the H-2k^b-tsA58 transgenic mouse. *In Vitro Cell Dev Biol Anim* 38:154–164
- Diglio CA, Kikkawa Y (1977) The type II epithelial cells of the lung. IV. Adaptation and behavior of isolated type II cells in culture. *Lab Invest* 37:622–631
- Fahimi HD, Beier K, Lindauer M, Schad A, Zhan J, Pill J, Rebel W, Völkl A, Baumgart E (1996) Zonal heterogeneity of peroxisome proliferation in rat liver. *Ann N Y Acad Sci* 804:341–361
- Ferdinandusse S, Jimenez-Sanchez G, Koster J, Denis S, Van Roermond CW, Silva-Zolezzi I, Moser AB, Visser WF, Gulluoglu M, Durmaz O, Demirkol M, Waterham HR, Gokcay G, Wanders RJ, Valle D (2015) A novel bile acid biosynthesis defect due to a deficiency of peroxisomal ABCD3. *Hum Mol Genet* 24:361–370
- Grant P, Ahlemeyer B, Karnati S, Berg T, Stelzig I, Nenicu A, Kuchelmeister K, Crane DI, Baumgart-Vogt E (2013) The biogenesis protein PEX14 is an optimal marker for the identification and localization of peroxisomes in different cell types, tissues, and species in morphological studies. *Histochem Cell Biol* 140:423–442
- Hiltunen JK, Filppula SA, Koivuranta KT, Siivari K, Qin YM, Hayrinen HM (1996) Peroxisomal beta-oxidation and polyunsaturated fatty acids. *Ann N Y Acad Sci* 804:116–128
- Immenschuh S, Baumgart-Vogt E (2005) Peroxiredoxins, oxidative stress, and cell proliferation. *Antioxid Redox Signal* 7:768–777
- Islinger M, Lüers GH, Zischka H, Ueffing M, Völkl A (2006) Insights into the membrane proteome of rat liver peroxisomes: microsomal glutathione-S-transferase is shared by both subcellular compartments. *Proteomics* 6:804–816
- Issemann I, Green S (1990) Activation of a member of the steroid hormone receptor superfamily by peroxisome proliferators. *Nature* 347:645–650
- Jat PS, Noble MD, Ataliotis P, Tanaka Y, Yannoutsos N, Larsen L, Kiousis D (1991) Direct derivation of conditionally immortal cell lines from an H-2k^b-tsA58 transgenic mouse. *Proc Natl Acad Sci USA* 88:5096–5100
- Karnati S, Baumgart-Vogt E (2008) Peroxisomes in mouse and human lung: their involvement in pulmonary lipid metabolism. *Histochem Cell Biol* 130:719–740
- Karnati S, Baumgart-Vogt E (2009) Peroxisomes in airway epithelia and future prospects of these organelles for pulmonary cell biology. *Histochem Cell Biol* 131:447–454
- Karnati S, Luers G, Pfreimer S, Baumgart-Vogt E (2013) Mammalian SOD2 is exclusively located in mitochondria and not present in peroxisomes. *Histochem Cell Biol* 140:105–117
- Kovacs WJ, Olivier LM, Krisans SK (2002) Central role of peroxisomes in isoprenoid biosynthesis. *Prog Lipid Res* 41:369–391
- Lakatos HF, Thatcher TH, Kottmann RM, Garcia TM, Phipps RP, Sime PJ (2007) The role of PPARs in lung fibrosis. *PPAR Res* 2007:71323
- Li X, Gould SJ (2002) PEX11 promotes peroxisome division independently of peroxisome metabolism. *J Cell Biol* 156:643–651
- Li X, Baumgart E, Morrell JC, Jimenez-Sanchez G, Valle D, Gould SJ (2002) PEX11 beta deficiency is lethal and impairs neuronal migration but does not abrogate peroxisome function. *Mol Cell Biol* 22:4358–4365
- Mannaerts GP, Van Veldhoven PP (1993) Peroxisomal beta-oxidation. *Verh K Acad Geneesk Belg* 55:45–78
- Martinez M (1996) Docosahexaenoic acid therapy in docosahexaenoic acid-deficient patients with disorders of peroxisomal biogenesis. *Lipids* 31(Suppl):S145–S152
- Mason RJ, Dobbs LG, Greenleaf RD, Williams MC (1977) Alveolar type II cells. *Fed Proc* 36:2697–2702
- Michael LF, Lazar MA, Mendelson CR (1997) Peroxisome proliferator-activated receptor gamma expression is induced during

- cyclic adenosine monophosphate-stimulated differentiation of alveolar type II pneumocytes. *Endocrinology* 138:3695–3703
- Mundel P, Reiser J, Zuniga Mejia Borja A, Pavenstadt H, Davidson GR, Kriz W, Zeller R (1997) Rearrangements of the cytoskeleton and cell contacts induce process formation during differentiation of conditionally immortalized mouse podocyte cell lines. *Exp Cell Res* 236:248–258
- Nenicu A, Lüers GH, Kovacs W, Otte D, Zimmer A, Bergmann M, Baumgart-Vogt E (2007) Peroxisomes in human and mouse testis: differential expression of peroxisomal proteins in germ cells and distinct somatic cell types of the testis. *Biol Reprod* 77:1060–1072
- Newman GR, Jasani B, Williams ED (1983) A simple post-embedding system for the rapid demonstration of tissue antigens under the electron microscope. *Histochem J* 15:543–555
- Petrik P (1971) Fine structural identification of peroxisomes in mouse and rat bronchiolar and alveolar epithelium. *J Histochem Cytochem* 19:339–348
- Polvani S, Tarocchi M, Galli A (2012) PPAR γ and oxidative stress: con(beta) catenating NRF2 and FOXO. *PPAR Res* 2012:641087
- Ryerse JS, Hoffmann JW, Mahmoud S, Nagel BA, deMello DE (2001) Immunolocalization of CC10 in Clara cells in mouse and human lung. *Histochem Cell Biol* 115:325–332
- Schneeberger EE (1972) A comparative cytochemical study of microbodies (peroxisomes) in great alveolar cells of rodents, rabbit and monkey. *J Histochem Cytochem* 20:180–191
- Schrader M, Reuber BE, Morrell JC, Jimenez-Sanchez G, Obie C, Stroh TA, Valle D, Schroer TA, Gould SJ (1998) Expression of PEX11beta mediates peroxisome proliferation in the absence of extracellular stimuli. *J Biol Chem* 273:29607–29614
- Shannon JM, Jennings SD, Nielsen LD (1992) Modulation of alveolar type II cell differentiated function in vitro. *Am J Physiol* 262:L427–L436
- Shimizu M, Takeshita A, Tsukamoto T, Gonzalez FJ, Osumi T (2004) Tissue-selective, bidirectional regulation of PEX11 alpha and perilipin genes through a common peroxisome proliferator response element. *Mol Cell Biol* 24:1313–1323
- Simon DM, Arikian MC, Srisuma S, Bhattacharya S, Tsai LW, Ingento EP, Gonzalez F, Shapiro SD, Mariani TJ (2006) Epithelial cell PPAR[γ] contributes to normal lung maturation. *FASEB J* 20:1507–1509
- Sosenko IR, Innis SM, Frank L (1991) Intralipid increases lung polyunsaturated fatty acids and protects newborn rats from oxygen toxicity. *Pediatr Res* 30:413–417
- Spite M, Serhan CN (2010) Novel lipid mediators promote resolution of acute inflammation: impact of aspirin and statins. *Circ Res* 107:1170–1184
- Tölle A, Meier W, Rüdiger M, Hofmann KP, Rüstow B (2002) Effect of cholesterol and surfactant protein B on the viscosity of phospholipid mixtures. *Chem Phys Lipids* 114:159–168
- Untergasser A, Cutcutache I, Koressaar T, Ye J, Faircloth BC, Remm M, Rozen SG (2012) Primer3—new capabilities and interfaces. *Nucleic Acids Res* 40:e115
- Visser WF, van Roermund CW, Ijlst L, Waterham HR, Wanders RJ (2007) Metabolite transport across the peroxisomal membrane. *Biochem J* 401:365–375
- Wang XY, Keefe KM, Jensen-Taubman SM, Yang D, Yan K, Linnoila RI (2012) Novel method for isolation of murine clara cell secretory protein-expressing cells with traces of stemness. *PLoS One* 7:e43008
- Whitehead RH, VanEeden PE, Noble MD, Ataliotis P, Jat PS (1993) Establishment of conditionally immortalized epithelial cell lines from both colon and small intestine of adult H-2k^b-tsA58 transgenic mice. *Proc Natl Acad Sci USA* 90:587–591
- Wiese S, Gronemeyer T, Ofman R, Kunze M, Grou CP, Almeida JA, Eisenacher M, Stephan C, Hayen H, Schollenberger L, Korosec T, Waterham HR, Schliebs W, Erdmann R, Berger J, Meyer HE, Just W, Azevedo JE, Wanders RJ, Warscheid B (2007) Proteomics characterization of mouse kidney peroxisomes by tandem mass spectrometry and protein correlation profiling. *Mol Cell Proteomics* 6:2045–2057
- Winkelmann A, Noack T (2010) The Clara cell: a “Third Reich eponym”? *Eur Respir J* 36:722–727
- Wong CJ, Akiyama J, Allen L, Hawgood S (1996) Localization and developmental expression of surfactant proteins D and A in the respiratory tract of the mouse. *Pediatr Res* 39:930–937
- Xiao Y, Karnati S, Qian G, Nenicu A, Fan W, Tchatalbachev S, Holand A, Hossain H, Guillou F, Luers GH, Baumgart-Vogt E (2012) Cre-mediated stress affects sirtuin expression levels, peroxisome biogenesis and metabolism, antioxidant and proinflammatory signaling pathways. *PLoS One* 7:e41097
- Yamamoto K, Fahimi HD (1987) Three-dimensional reconstruction of a peroxisomal reticulum in regenerating rat liver: evidence of interconnections between heterogeneous segments. *J Cell Biol* 105:713–722
- Zoeller RA, Lake AC, Nagan N, Gaposchkin DP, Legner MA, Lieberthal W (1999) Plasmalogens as endogenous antioxidants: somatic cell mutants reveal the importance of the vinyl ether. *Biochem J* 338(Pt 3):769–776

Compromised peroxisomes in idiopathic pulmonary fibrosis, a vicious cycle inducing a higher fibrotic response via TGF- β signaling

Gani Orujaj^{a,1}, Srikanth Karnati^{a,1}, Vijith Vijayan^a, Lakshmi Kanth Kotarkonda^a, Eistine Boateng^a, Wenming Zhang^b, Clemens Ruppert^{c,d}, Andreas Günther^{c,d}, Wei Shi^b, and Eveline Baumgart-Vogt^{a,2}

^aInstitute for Anatomy and Cell Biology, Medical Cell Biology, Justus Liebig University, Giessen 35392, Germany; ^bSaban Research Institute, Children's Hospital Los Angeles, Los Angeles, CA 90027; and ^cDepartment of Internal Medicine, Medical Clinic II, and ^dGerman Center for Lung Research (DZL), Universities of Giessen and Marburg Lung Center, Giessen 35392, Germany

Edited by David A. Schwartz, University of Colorado, Aurora, CO, and accepted by the Editorial Board March 10, 2015 (received for review August 25, 2014)

Idiopathic pulmonary fibrosis (IPF) is a devastating disease, and its pathogenic mechanisms remain incompletely understood. Peroxisomes are known to be important in ROS and proinflammatory lipid degradation, and their deficiency induces liver fibrosis. However, altered peroxisome functions in IPF pathogenesis have never been investigated. By comparing peroxisome-related protein and gene expression in lung tissue and isolated lung fibroblasts between human control and IPF patients, we found that IPF lungs exhibited a significant down-regulation of peroxisomal biogenesis and metabolism (e.g., PEX13p and acyl-CoA oxidase 1). Moreover, in vivo the bleomycin-induced down-regulation of peroxisomes was abrogated in transforming growth factor beta (TGF- β) receptor II knockout mice indicating a role for TGF- β signaling in the regulation of peroxisomes. Furthermore, in vitro treatment of IPF fibroblasts with the profibrotic factors TGF- β 1 or tumor necrosis factor alpha (TNF- α) was found to down-regulate peroxisomes via the AP-1 signaling pathway. Therefore, the molecular mechanisms by which reduced peroxisomal functions contribute to enhanced fibrosis were further studied. Direct down-regulation of *PEX13* by RNAi induced the activation of Smad-dependent TGF- β signaling accompanied by increased ROS production and resulted in the release of cytokines (e.g., IL-6, TGF- β) and excessive production of collagen I and III. In contrast, treatment of fibroblasts with ciprofibrate or WY14643, PPAR- α activators, led to peroxisome proliferation and reduced the TGF- β -induced myofibroblast differentiation and collagen protein in IPF cells. Taken together, our findings suggest that compromised peroxisome activity might play an important role in the molecular pathogenesis of IPF and fibrosis progression, possibly by exacerbating pulmonary inflammation and intensifying the fibrotic response in the patients.

peroxisome | lung | fibrosis | inflammation | TGF- β 1

Idiopathic pulmonary fibrosis (IPF) is a chronic, devastating, and lethal fibrotic disorder in human lung. IPF is characterized by a worsening of pulmonary function and persistent alterations of the lung parenchyma as a result of fibrotic foci formation by activated fibroblasts/myofibroblasts and excessive production and deposition of extracellular matrix components (ECM) (1–4). It is well accepted that transforming growth factor beta (TGF- β) signaling plays a critical role in IPF development. Inhibition of TGF- β signaling by blocking its downstream Smad3 gene expression protects against bleomycin-induced fibrosis in animal models (5, 6). In addition, there is increasing evidence that tumor necrosis factor alpha (TNF- α) also plays an important role in initiation and perpetuation of the fibrotic processes, possibly by activating TGF- β signaling pathway (7). However, the mechanisms by which TGF- β and TNF- α promote the fibrotic response in IPF are incompletely known.

Peroxisomes are single membrane bounded ubiquitous organelles, present in all types of cells. Particularly, type II alveolar epithelial cells and club cells (Clara) in the lung have highly

abundant peroxisomes (8). These organelles are involved in a variety of metabolic pathways, including degradation of reactive oxygen species (ROS) and bioactive lipid mediators (prostaglandins and leukotrienes) and synthesis of antioxidant lipids (polyunsaturated fatty acids, plasmalogens, etc.) (9). Absence or dysfunction of peroxisomes results in increased cellular oxidative stress, leading to severe pathological consequences in many organ systems (10, 11). Lung is one of the organs with highest exposure to various forms of reactive oxygen and nitrogen species (ROS and RNS) due to oxygen and different environmental oxidants in the inspired air, causing oxidation of cellular DNA, proteins and lipids, consequently a direct lung injury (12). Studies have shown that the most severe phenotype of a peroxisome biogenesis disorder (e.g., Zellweger syndrome) is associated with progressive liver fibrosis or cirrhosis, leading to early death of the patients during childhood (11). Moreover, mice with peroxisome dysfunction caused by *PEX11* knockout died during their first days of life and exhibit morphological alterations of the lungs (13). In contrast, treatment of rats with an agonist specific for peroxisome proliferator-activated receptor alpha (PPAR- α) significantly ameliorated tubulointerstitial renal fibrosis (14). Despite the fact that peroxisomal metabolism might play an important role in other tissue fibrosis, the role of peroxisomes in

Significance

This study enhances the knowledge on the molecular pathogenesis of idiopathic pulmonary fibrosis (IPF). To date, there is no information available on the role of peroxisomes in lung fibrosis. In our study we demonstrate that peroxisomal biogenesis and metabolism is compromised in tissue samples as well as in fibroblasts of IPF patients and in bleomycin-induced fibrosis mouse model. Moreover, RNAi-mediated knockdown of peroxisomal biogenesis leads to a profibrotic response in control and IPF fibroblasts suggesting that the reduction of peroxisomal function in IPF would contribute to the profibrotic phenotype of this devastating disease. Our work opens a new field of research in the area of lung fibrosis and might lead to novel treatment strategies against IPF by modulating the peroxisomal compartment.

Author contributions: G.O., S.K., V.V., W.S., and E.B.-V. designed research; G.O., S.K., V.V., L.K.K., E.B., W.Z., and C.R. performed research; A.G. contributed new reagents/analytic tools; G.O., S.K., V.V., C.R., W.S., and E.B.-V. analyzed data; G.O., S.K., V.V., W.S., and E.B.-V. wrote the paper; and E.B.-V. guided doctoral students as supervisor.

The authors declare no conflict of interest.

This article is a PNAS Direct Submission. D.A.S. is a guest editor invited by the Editorial Board.

¹G.O. and S.K. contributed equally this work.

²To whom correspondence should be addressed. Email: Eveline.Baumgart-Vogt@anatomie.med.uni-giessen.de.

This article contains supporting information online at www.pnas.org/lookup/suppl/doi:10.1073/pnas.1415111112/-DCSupplemental.

lung fibrosis onset and progression seen in IPF patients has never been reported (1, 15).

Herein, using human IPF and control fibroblast cultures as well as a bleomycin-induced mouse lung fibrosis model, we demonstrate that peroxisomal biogenesis and metabolism is compromised in the lung and in fibroblasts of IPF patients, in which a down-regulation of peroxisomal proteins leads to activation and release of profibrotic factors such as TGF- β 1 and collagen. In contrast, peroxisome proliferation by treatment with PPAR- α agonist (ciprofibrate, WY14643) significantly reduces the TGF- β 1-induced myofibroblast differentiation in IPF fibroblast cultures.

Results

Peroxisome Biogenesis, Lipid Metabolism, and Redox Balance Are Compromised in IPF Patients. First we analyzed control and patient tissue samples for peroxisomal alterations. Stainings of paraffin-embedded tissue sections of human lung biopsies of controls and IPF patients revealed that peroxisomal markers (PEX14p and cat) in fibroblasts were found to be significantly (Fig. S1E) reduced in IPF lungs (Fig. 1). Next we analyzed whereas lung fibroblasts isolated from these human IPF patients would exhibit similar peroxisomal alterations. IPF fibroblasts retained their profibrotic activity also in cell culture such as the expression of α -SMA (Fig. 2A) and expressed increased mRNA levels of the profibrotic markers TGF- β 1, COL1A2, and IL-6 (Fig. 2B) compared with the fibroblasts isolated from controls. The profibrotic phenotype was also confirmed by increased TGF- β signaling in IPF cells via luciferase reporter assay studies using a smad-binding element (SBE)-luciferase reporter plasmid (Fig. 2C).

Analysis of protein abundance by immunofluorescence revealed that the peroxisomal biogenesis protein PEX13p, the lipid transporter protein ABCD3, the β -oxidation enzyme acyl-CoA oxidase 1 (ACOX1), as well as the antioxidative enzyme catalase were reduced in IPF fibroblasts (Fig. 2D and E). The down-regulation of the peroxisomal biogenesis protein PEX13p was also observed at the mRNA level between control and IPF fibroblasts by qRT-PCR and confirmed by Western blot analysis (Fig. 2F). Because catalase (Fig. 2E) was down-regulated, we

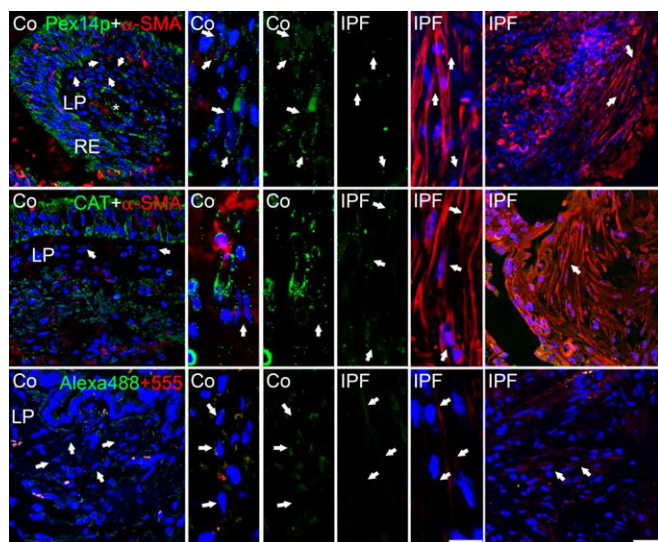


Fig. 1. Expression of peroxisomal proteins in human lung biopsies of control and IPF tissues. Immunofluorescence for PEX14p and catalase (CAT) in control and IPF lung tissue. Negative control for the secondary antibody reaction with donkey anti-rabbit Alexa488 and donkey anti-mouse Alexa555. Co, control; IPF, idiopathic pulmonary fibrosis; LP, Lamina propria; RE, respiratory epithelium. Arrow, fibroblasts in the lamina propria. (Scale bar: 10 μ m).

hypothesized that IPF fibroblasts might have an impaired antioxidant response. DHE stainings revealed that IPF fibroblasts exhibited a higher ROS production in comparison with control fibroblasts (Fig. 2G). Interestingly, a series of antioxidant enzymes such as SOD1, heme oxygenase (HO-1), glutathione reductase (GR), and the redox-sensitive transcription factor Nrf2 were decreased in IPF fibroblasts (SI Materials and Methods and Fig. S1A–D). Moreover, reporter gene analyses showed that Nrf2 binding element (ARE)-driven luciferase activity was significantly decreased in IPF fibroblasts (fivefold reduction) ($P < 0.05$) (Fig. S1F), whereas the luciferase expression of the AP1 reporter construct was not significantly changed in IPF fibroblasts in basal unstimulated conditions (Fig. S1F). To summarize, these results indicate that in IPF tissues as well as in IPF fibroblasts peroxisomal proteins were significantly down-regulated and IPF fibroblast exhibit an imbalance in the antioxidant response.

PEX13p Knockdown Activates Smad-Dependent TGF- β 1 Pathway and Increases COL1 Production. Alterations in peroxisomal proteins in IPF samples may be a collateral effect due to persistent fibrosis or could also be a significant factor that contributes to the pathogenesis of this devastating condition. To address this question, PEX13p, one of the peroxin proteins involved in peroxisomal biogenesis, was knocked down using a siRNA-mediated approach. The strong knockdown of PEX13 expression in both control and IPF fibroblasts was verified by quantitative RT-PCR and Western blot analysis (Fig. 3A and B), and disruption of peroxisomal biogenesis, leading in consequence to mistargeting of catalase into the cytoplasm (Fig. S4C). Interestingly, disruption of the peroxisomal biogenesis triggered the production of the profibrotic markers COL1A2 and TGF- β 1 at mRNA level and of the COL1 protein in Western blot analysis (Fig. 3A and B). This disruption was associated with increased collagen and TGF- β 1 also in the culture medium (Fig. 3C and D). Furthermore, increased COL1A2 promoter activity and activation of TGF- β signaling upon PEX13 knockdown was confirmed in COL1A2 and SBE luciferase reporter gene assays, respectively (Fig. 3E and F). It is noteworthy that also control fibroblasts exhibit an increased fibrotic phenotype after peroxisomal knockdown, even though to a lesser extent in comparison with the transfected IPF fibroblasts (Fig. 3A–F). Additionally, PEX13 knockdown also led to the intracellular elevation of profibrotic markers such as collagen I, collagen 3A1 (COL3A1), and prolyl 4-hydroxylase beta polypeptide (PDI) as revealed by immunofluorescence studies and also by increased mRNA levels of matrix metalloproteinase 2 (MMP2) which have been implicated in excessive TGF- β 1 activation (Figs. S2 and S3A and E). The increased fibrotic response of TGF- β 1 and COL1A2 was also observed with semiquantitative RT-PCR in cells with a PEX13 knockdown (Fig. S3A–D). To summarize, these results indicate that the down-regulation of peroxisomes in both control and IPF fibroblasts leads to an increased fibrotic phenotype in these cells associated with an increased production of collagen and TGF- β 1 as well as an activation of TGF- β signaling.

Knockdown of Peroxisomes Leads to Increased ROS and Proinflammatory Cytokine IL-6 in Fibroblasts. As shown above, IPF fibroblasts exhibit an increased production of ROS (Fig. 2G). Because peroxisomes are able to produce and scavenge ROS and are down-regulated in IPF fibroblasts, we questioned whether they are involved in the cellular ROS production observed. Indeed, the knockdown of PEX13 led to an increase in the production of ROS as measured by dihydroethidine staining both in control as well as IPF fibroblasts (Fig. 4A). However, unlike in the basal conditions of IPF fibroblasts (Fig. S1F), the increased ROS production was also paralleled with an increase in Nrf2 and AP-1 activity (Fig. 4B), and also induced a high antioxidative response

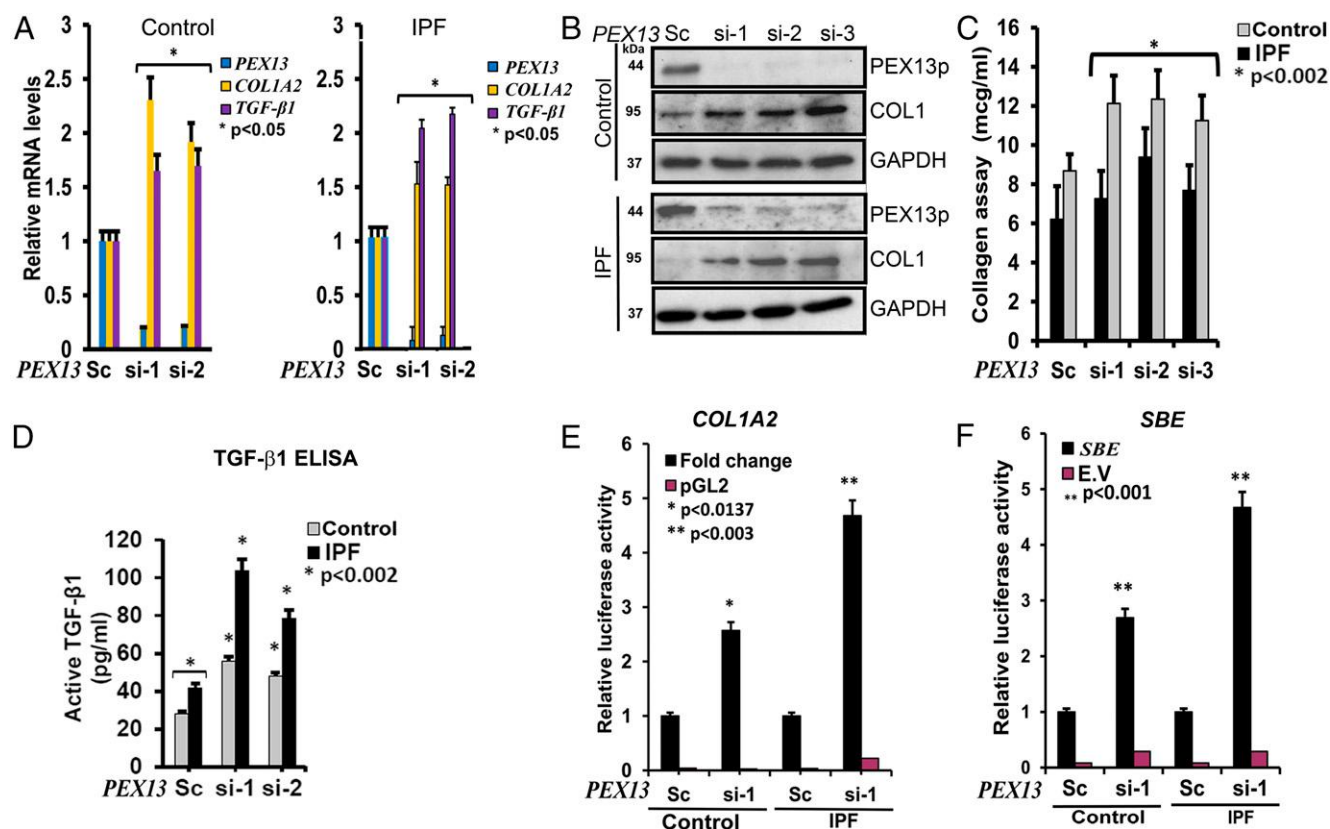


Fig. 3. Activation of TGF- β 1 Smad dependent pathway in *PEX13* siRNA treated control and IPF fibroblasts. (A) qPCR mRNA expression of peroxisome biogenesis *PEX13* and fibrotic markers *TGF- β 1* and *Col1A2* in *PEX13* siRNA fibroblasts. The expressions of *28S rRNA* and of the *HPRT1* gene were used as controls for normalization, * $P < 0.005$. (B) Western blots depicting the abundance of peroxisomal biogenesis genes and collagen I in *PEX13* knockdown. The expression of GAPDH was used as control. (C) Collagen Sircol assay, measuring the production of collagen released in medium by control and IPF fibroblasts. Sc (scrambled siRNA control), si-1 (siRNA *PEX13*-1), si-2 (siRNA *PEX13*-2), si-3 (siRNA *PEX13* 1, 2). (D) TGF- β 1 release in supernatant measured by TGF- β 1 ELISA Assay. (E and F) SBE, *COL1A2*, luciferase reporter assays in siRNA treated control and IPF fibroblasts. The activity of firefly luciferase was measured in cell lysates and normalized to the activity of renilla. (E.V., empty vector). Data represent \pm SD of three independent experiments. P value, unpaired Student t test.

membrane that was also reduced in IPF lungs (Fig. 1) was used. Indeed, bleomycin treatment in control mice down-regulated peroxisomes (PEX14p) on day 7 after treatment, followed by a recovery on day 14 and 28 compared with day 7, but still at lower protein abundance than in appropriate control animals (Fig. 5D). Strikingly, bleomycin treatment in TGF- β receptor II knockout mice did not induce the down-regulation of peroxisomes as detected by staining with PEX14p, indicating a direct relation for TGF- β -induced signaling in the down-regulation of peroxisomes (Fig. 5D). TGF- β 1 treatment also increased ROS production in these fibroblasts (Fig. 5E). In summary, these findings indicate that TGF- β 1 signaling down-regulates peroxisomes in fibroblasts and induce the production of ROS.

AP-1 Signaling Is Involved in TGF- β 1-Mediated Down-Regulation of *PEX13* in Human IPF Fibroblasts. Earlier reports indicate a cross-talk between TGF- β 1 signaling and the transcriptional factor AP-1, which as shown was also up-regulated in *PEX13* knock-down fibroblasts. Hence, we questioned whether the transcriptional factor AP-1, normally activated during profibrotic and proinflammatory responses, would play a role in the observed down-regulation of PEX13p. For a comparison we also used the luciferase reporter vector (*ARE*) for the ROS-activated transcriptional factor Nrf2. Indeed, stimulation with TGF- β 1 induced the activity of the *AP-1* luciferase reporter construct (Fig. 6A), but the activity of the *ARE*-luciferase construct remained unchanged (Fig. 6B). Furthermore, the AP-1-specific inhibitor

SR11302 partially blocked the TGF- β 1 stimulated activity of both the *AP-1*-luciferase construct and also the *ARE*-luciferase construct (Fig. 6A and B). This inhibition was expected as the AP-1 binding element shares the consensus sequence of the Nrf2 binding element but not vice versa. The luciferase reporter assays revealed that the inhibitor luteolin used generally as Nrf2 inhibitor is not specific, because it also inhibits the TGF- β 1-induced activation of *AP-1* (Fig. 6A) in addition to the inhibition of *ARE* luciferase (Fig. 6B). Interestingly, pretreatment of cells with an AP-1 specific inhibitor SR11302 or the Nrf2/AP-1 inhibitor luteolin blocked the TGF- β 1-mediated SBE activation, indicating a role for AP-1 in the TGF- β 1-mediated Smad-dependent pathway (Fig. 6C). Moreover, pretreatment with SR11302 and luteolin also reversed the TGF- β 1-mediated down-regulation of the PEX13p protein (Fig. 6D). To summarize, the profibrotic factor TGF- β 1 might down-regulate *PEX13* through the transcriptional factor *AP-1*.

Proinflammatory Cytokines TNF- α and IL-6 also Suppress the Peroxisome Biogenesis Protein PEX13p in Human IPF Fibroblasts. In a complex condition such as IPF, factors other than TGF- β 1 may also contribute to the down-regulation of peroxisomal genes in vivo. Macrophage-mediated TNF- α production might play an important paracrine role in this process. To determine whether TNF- α affects peroxisome biogenesis, IPF fibroblasts were treated with 10 ng/mL of TNF- α for the indicated time points (Fig. 7A and C). TNF- α induced a significant down-regulation of the *PEX13* mRNA as early as 1 h (Fig. 7A), as well as the protein

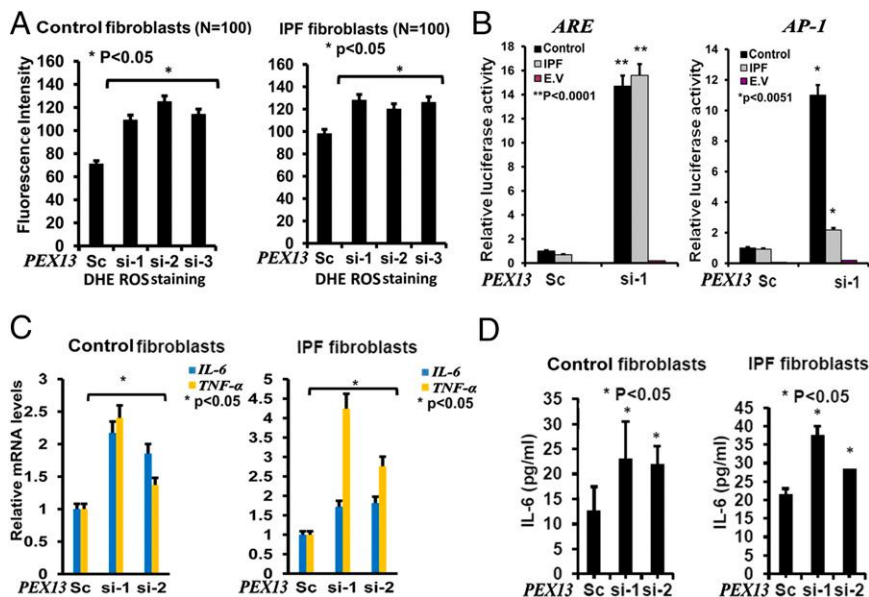


Fig. 4. Induction of ROS and cytokine production (IL-6) in *PEX13* knockdown control and IPF fibroblasts. (A) Generation of reactive oxygen species (ROS) detection with dihydroethidine (DHE) and quantification in control and IPF siRNA treated fibroblasts, (*N*-number of cells for quantification). (B) *ARE* and *AP-1* luciferase reporter assays in *PEX13* knockdown control and IPF fibroblasts, si vs. Sc (E.V., empty vector). The activity of firefly luciferase was measured in cell lysates and normalized to the activity of renilla. (C) qPCR mRNA expression of cytokines (*TNF- α* and *IL-6*) in *PEX13* knockdown of control and IPF fibroblasts. (D) Human *IL-6* secretory levels measured by Quantikine ELISA in siRNA *PEX13* treated control and IPF fibroblasts. Sc (scrambled siRNA control), si-1 (siRNA *PEX13*-1), si-2 (siRNA *PEX13*-2). Data represent \pm SD of three independent experiments. *P* value, unpaired Student *t* test.

abundance of *PEX13p* after 10 h (Fig. 7*B*). Similar to *TGF- β 1*, *TNF- α* also induced the activity of the *AP-1* luciferase construct and also increased the luciferase activity of the *ARE*-luciferase construct (Fig. 7*C*). Interestingly, the *AP-1* inhibitor SR11302 reversed the *TNF- α* -mediated down-regulation of *PEX13p* (Fig. 7*D*). Finally, treatment with the proinflammatory cytokine *IL-6* also induced the down-regulation of *PEX13p* (Fig. 7*E*). In summary, proinflammatory cytokines (*TNF- α* and *IL-6*) down-regulate *PEX13p* in IPF fibroblasts. Moreover, *TNF- α* -mediated down-regulation of *PEX13p* is at least partially mediated through *AP-1* signaling.

PPAR- α Agonists Proliferate Peroxisomes and Block the *TGF- β 1*-Induced Profibrotic Response in IPF Fibroblasts. As suggested by the studies above, reduced peroxisome biogenesis is associated with an increased profibrotic response as shown by the activation of *TGF- β 1* signaling and collagen production. This reduction raises the possibility that increasing peroxisomal biogenesis may be beneficial as a treatment strategy in IPF. To evaluate this we used two structurally distinct *PPAR- α* agonists (ciprofibrate and WY14643), classical peroxisome proliferators, and investigated the relationship between peroxisome proliferation and *TGF- β 1*-induced myofibroblast differentiation (as shown by α -SMA) and up-regulation of collagen I protein. Treatment with either ciprofibrate or WY14643 for 48 h resulted in proliferation of peroxisomes as detected by *PEX14p* stainings (Fig. 8*A*). The peroxisomal biogenesis protein *PEX13p* was also induced after treatment of IPF cells with ciprofibrate or WY14643 (Fig. 8*B*). *PPAR- α* has been shown to exert multiple effects on cellular targets that are independent of peroxisome proliferation, wherefore it is important to distinguish the peroxisome-dependent antifibrotic effects of *PPAR- α* agonists. To do this, the experimental setup (mentioned in detail in *SI Materials and Methods*) contained two different controls: (i) IPF cells, which were pretreated with *PPAR- α* agonists for 48 h, after which the medium was replaced with the *PPAR- α* antagonist to block endogenous *PPAR- α* activation. Ideally, these cells then contain proliferated peroxisomes

but further *PPAR- α* activation is blocked. (ii) IPF cells pretreated with *PPAR- α* agonists only for 2 h before *TGF- β 1* stimulation and hence will exhibit an activation of *PPAR- α* but no peroxisome proliferation due to the insufficiently short time period of drug treatment. The concentration of *PPAR- α* agonist and antagonist that was used for this approach activated and inhibited the *PPAR*-response-element (*PPRE*)-luciferase reporter constructs, respectively (Fig. 8*C*). Interestingly, IPF cells pretreated with ciprofibrate or WY14643 for 48 h showed a significant reduction in the *TGF- β 1*-induced myofibroblast differentiation represented by the abundance of the α -SMA protein. The strongest reduction was observed in the cells pretreated with *PPAR- α* agonist for 48 h followed by pretreatment with *PPAR- α* antagonist for 1 h before the addition of *TGF- β 1* (Fig. 8*C* and *D*), whereas pretreatment with *PPAR- α* agonist for 2 h before *TGF- β 1* stimulation did not block the *TGF- β 1*-induced α -SMA protein. Similarly, *TGF- β 1*-induced *COL1* protein was also blocked by the addition of *PPAR- α* agonists treated for 48 h followed by antagonist, but not in IPF cells pretreated with *PPAR- α* agonists alone for 2 h or 48 h (Fig. 8*C* and *D*). In summary, these findings suggest that IPF cells containing proliferated peroxisomes block the *TGF- β 1*-induced up-regulation of myofibroblast differentiation and *COL1* protein and endogenous *PPAR* activity might interfere with this mechanism.

Discussion

The findings presented here provide compelling evidence that peroxisomes are protective organelles against the development of pulmonary fibrosis. Importantly, we show that, in lung tissue samples of IPF patients as well as in IPF fibroblast cultures, peroxisomal proteins are down-regulated. Moreover, siRNA-mediated down-regulation of the peroxisomal biogenesis protein *PEX13p* elicits a profibrotic response, characterized by the activation of *TGF- β* signaling and increased collagen production. Furthermore, treatment with *PPAR- α* agonists increased the peroxisomal abundance in IPF fibroblasts and decreased the *TGF- β 1*-induced myofibroblast differentiation.

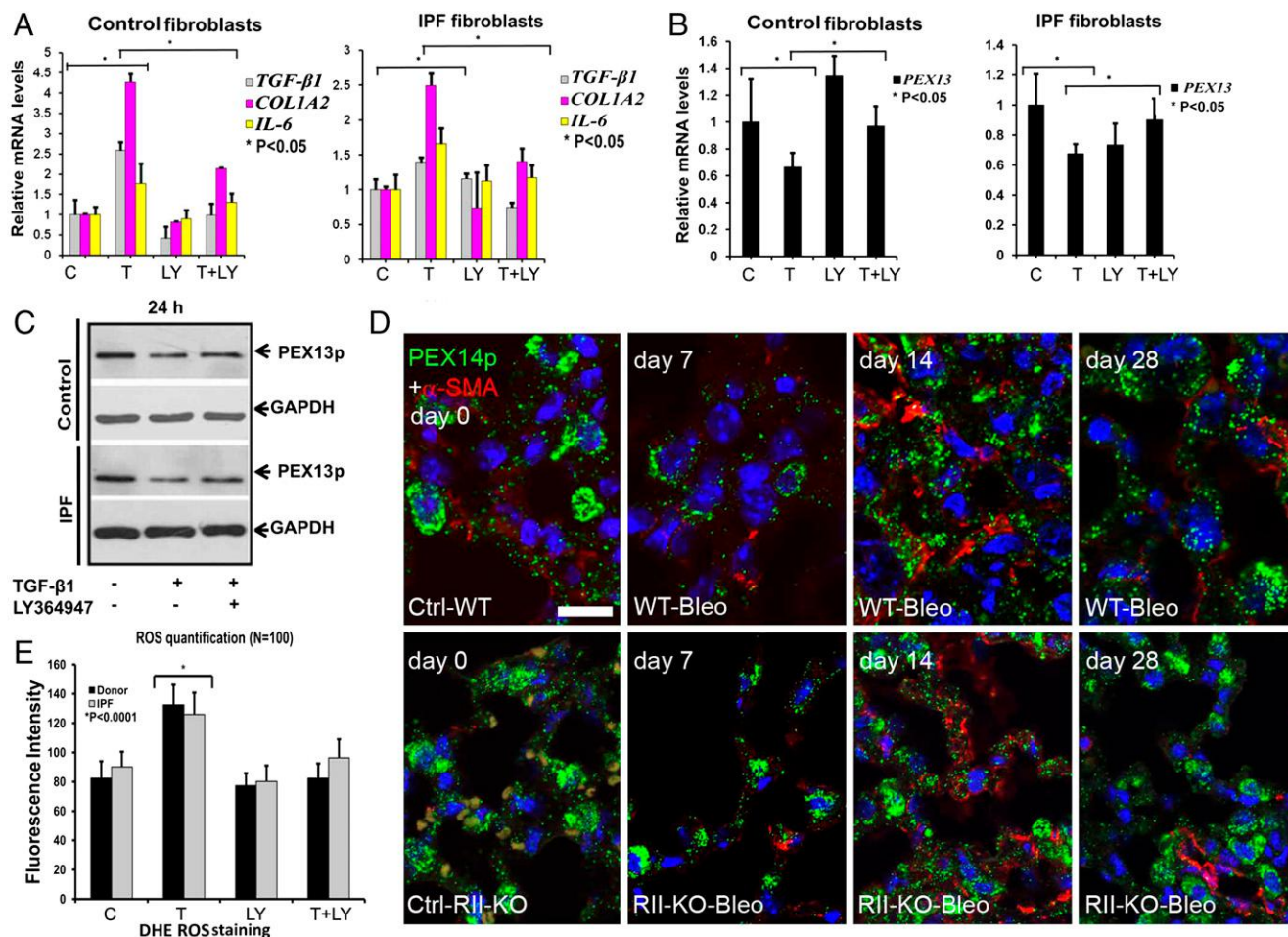


Fig. 5. TGF- β 1 signaling suppresses *PEX13* peroxisomal biogenesis protein in control/IPF and in a bleomycin-induced mouse model of lung fibrosis. Confluent control and IPF fibroblasts were pretreated with 5 μ M LY364947 (TGF- β 1 inhibitor) for 1 h, followed by a stimulation with 5 ng/mL TGF- β 1, or combined for 24 h. (A and B) RNA expression of *TGF- β 1*, *COL1A2*, *IL-6*, and *PEX13* was examined by real-time qRT-PCR. The results were normalized with *28S rRNA* and *HPRT* mRNA. (C) Total protein was isolated following 24 h incubation with TGF- β 1, LY364947, or combinations and subjected to Western blotting for indicated proteins. Relative density in donor and IPF fibroblasts treated with TGF- β 1 and the specific TGF- β 1 inhibitor LY364947. GAPDH was used as loading control. (D) Double immunofluorescence of PEX14 and α -SMA in bleomycin-induced mouse model of pulmonary fibrosis. Bleo, Bleomycin; Ctrl, Control; RII-KO, TGF- β receptor II knockout; WT, wild type. (E) TGF- β 1-induced reactive oxygen species (ROS) detection with dihydroethidine (DHE) in control and IPF fibroblasts. C, control; LY, LY364947; T, TGF- β 1; T+LY, TGF- β 1+LY364947. Data represent \pm SD of three independent experiments. *P* value, unpaired Student *t* test. (Scale bar: 10 μ m.)

Peroxisomes are present in different pulmonary cell types and exhibit strong heterogeneity in their abundance and enzyme composition (8). It is well known that the lung is one of the organs mostly exposed to the various forms of reactive oxygen species due to its high oxygen environment (12). In this respect, the protective role of peroxisomes in pulmonary fibrosis is closely associated with their functions in diminishing ROS species thus preventing excessive ROS production and inflammatory reactions (1, 8, 15). Accordingly, our findings also indicate that dysfunctional peroxisomes lead to increased cellular ROS production in IPF cells. This notion is in line with previous studies showing that the deficiency of peroxisomal proteins leads to increased ROS production and oxidative stress (10, 17).

The observation that IPF samples have reduced peroxisomal proteins is of particular interest because one of the clinical features of Zellweger syndrome, a peroxisomal disorder with complete absence or reduced number of peroxisomes, is the development of hepatic fibrosis (11). A continuous trigger would be necessary to induce this consistent down-regulation of peroxisomes in *in vitro* IPF fibroblast cultures because peroxisomal biogenesis will complement for this down-regulation over time.

Based on our findings that the SBE-luciferase activity was higher in IPF cells in their basal state and also contained increased concentrations of TGF- β 1 in the cell culture medium (Figs. 2C and 3D), we propose that the persistent activation of TGF- β signaling in these cells might be responsible for the observed down-regulation of peroxisomal proteins. This notion is also supported by the *in vivo* findings in the bleomycin-induced TGF- β receptor II knockout mouse model studies in which loss of TGF- β signaling prevented the bleomycin-induced down-regulation of peroxisomes (Fig. 5D). To our knowledge, this is the first study to show a direct role for TGF- β signaling in the regulation of peroxisomal genes.

In contrast, down-regulation of the peroxisomal genes by the proinflammatory cytokine TNF- α has been shown previously in the liver (18). In this study we extend our knowledge on the molecular mechanisms leading to the TNF- α -mediated down-regulation of peroxisomes by showing that TNF- α mediates this effect through activation of AP-1 (Fig. 7C and D). It is known that TNF- $\alpha^{-/-}$ mice develop less liver fibrosis in comparison with littermate controls, exhibit reduced levels of α -SMA, a marker for activated myofibroblasts, and reduced TGF- β 1 mRNA (19).

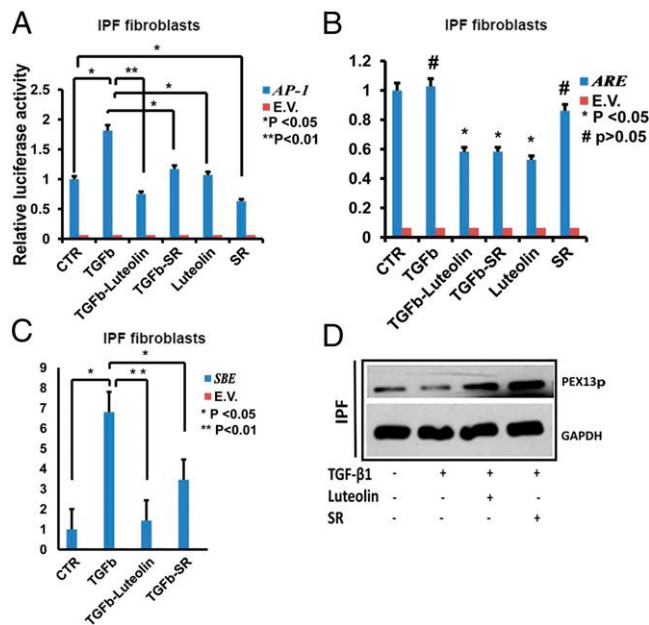


Fig. 6. AP-1 signaling is activated in TGF- β 1-mediated down-regulation of PEX13 in human IPF fibroblasts. Confluent IPF fibroblasts were pretreated 1 h before with luteolin 25 μ M or SR11302 (SR) 10 μ M. Then, cells were challenged with 5 ng/mL TGF- β 1 for 24 h as indicated. (A–C) AP1, ARE, and SBE luciferase reporter assays in IPF fibroblasts. The activity of firefly luciferase was measured in cell lysates and normalized to the activity of renilla. (E.V., empty vector). (D) Protein analysis of PEX13p in IPF fibroblasts treated with TGF- β 1, luteolin or SR11302. GAPDH was used as loading control. Data represent \pm SD of three independent experiments. *P* value, unpaired Student *t* test.

Consistent with our findings are the existing evidences from the literature that TNF- α is crucial in initiation and progression of the fibrotic processes via AP-1 in Swiss 3T3 fibroblasts (7, 20). Similarly, the interplay between Smad-dependent TGF- β signaling and AP-1 that we observed in our study has also been reported in numerous studies and are contradicting. In one study, the transcriptional factor AP-1 was reported to be essential for ROS-mediated TGF- β 1 activation and TGF- β 1-induced IL-6 production (21), which is in line with our finding that AP-1 signaling activates Smad-dependent SBE activation (Fig. 6C). In contrast to this observation, Verrecchia and colleagues reported that the Jun family of AP-1 factors act as inhibitors of Smad-dependent signaling (22). The AP-1 family of transcriptional factors is a broad class of transcriptional factors that can form hetero and homo dimers and are shown to be both profibrotic and antifibrotic based on the specific factors activated in different conditions (23, 24). Further studies to specifically identify the AP-1 factors activated in our experimental conditions are required to understand this observed profibrotic nature in our experimental conditions.

In the proposed mechanism TGF- β 1-mediated down-regulation of peroxisomes would lead to a synergistic effect on the proinflammatory and profibrotic responses and induce a vicious cycle. In agreement with this notion are the findings that PEX13 knockdown in fibroblast induce activation of TGF- β 1 signaling, increased ROS, collagen and IL-6 production. Several studies have reported that ROS and release of proinflammatory cytokines are the main triggers of TGF- β 1 signaling pathway, shown also during the peak of inflammation on day 7 using the bleomycin-induced lung fibrosis mouse model (1, 25). Interestingly, in our bleomycin model, the strongest down-regulation of peroxisomes is also observed during day 7 (Fig. 5D), which is consistent with our in vitro findings that proinflammatory cytokines

TNF- α and IL-6 down-regulate peroxisomes in IPF fibroblasts (Fig. 7D and E). IL-6 is known to mediate many inflammatory processes in the lung and has been implicated in the pathogenesis of a variety of respiratory disorders and a possible association between IL-6 and development of fibrosis (26, 27). In addition, IL-6 plays an important role in development of bleomycin-induced lung inflammation and subsequent fibrotic changes through the activation of TGF- β 1 (28).

ROS interferes with many cellular functions and results in activation of the master regulator of the cellular response to oxidative stress NRF2 and the antioxidant machinery (29). Although we were able to identify the activation of Nrf2 in our PEX13 knockdown fibroblasts based on the ARE-luciferase activity, luteolin which is commonly used in studies as a Nrf2 inhibitor was also found to inhibit the transcriptional factor AP-1. Hence at present we cannot conclude that the observed effect of luteolin on SBE activation is dependent on its ability as an Nrf2 inhibitor.

Finally, we also show that pretreatment of IPF cells with PPAR- α agonists for longer time points reduced the TGF- β 1-induced collagen and myofibroblast differentiation, provided that the endogenous PPAR- α activation during TGF- β 1 stimulation is blocked. This result is particularly interesting because several independent studies that reported antifibrotic effects of PPAR- α agonists have not considered peroxisome proliferation by these agonists into context. Their observation was largely based on the vast amount of accumulating evidence in the literature describing its broad antifibrotic and antiinflammatory properties of PPARs. In particular are the studies which report that PPAR- α agonists (*i*) inhibit cardiac fibrosis by inhibiting the

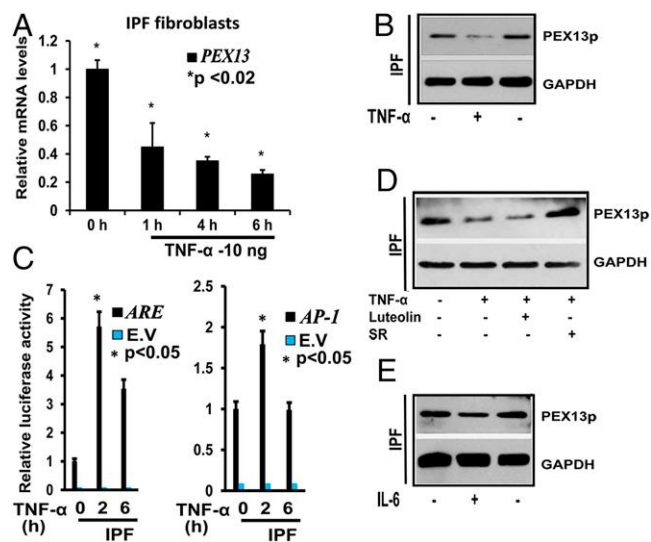


Fig. 7. TNF- α suppresses peroxisome biogenesis by induction of AP1 in human IPF fibroblasts. (A) IPF fibroblasts were treated with 10 ng/mL TNF- α for the indicated times, and the expression of PEX13 mRNA was determined by using qRT-PCR. (B) IPF fibroblasts were treated with 10 ng/mL TNF- α for 6 h, and cells were lysed for Western blot analysis. As loading control GAPDH was used. (C) ARE and AP-1 dual luciferase reporter assays of IPF fibroblasts treated with 10 ng/mL TNF- α for indicated times. The activity of firefly luciferase was measured in cell lysates and normalized to the activity of renilla luciferase. (D) IPF fibroblasts were treated with 10 ng/mL TNF- α for 6 h, cells were pretreated 1 h before with ARE inhibitor Luteolin and AP-1 inhibitor SR11302 (SR), PEX13 abundance was analyzed with Western blotting. GAPDH was used as loading control. (E) IPF fibroblasts were treated with 20 ng/mL IL-6 cytokine and PEX13 abundance was analyzed with Western blotting. GAPDH was used as loading control. Data represent the results of at least three experiments performed in triplicates (E.V., empty vector). (Mean \pm SEM, relative units, *n* = 3). *P* value, unpaired Student *t* test.

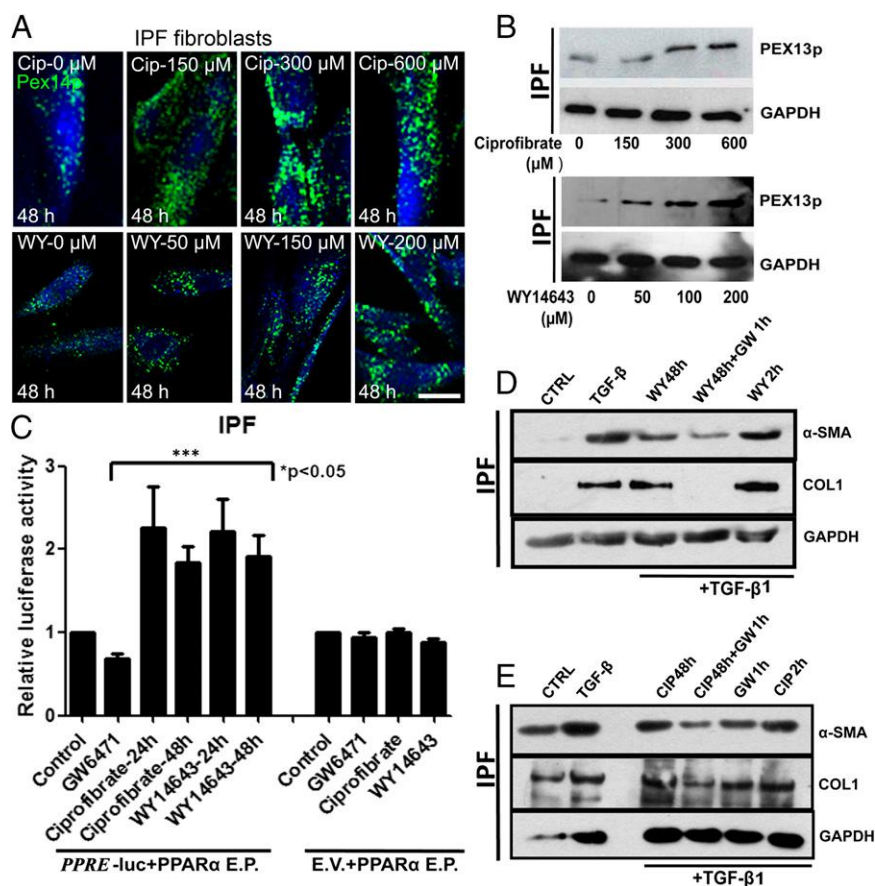


Fig. 8. Peroxisome proliferation by PPAR- α agonists ciprofibrate and WY14643 blocks the TGF- β 1-induced profibrotic response in IPF fibroblasts. (A) Staining of IPF fibroblasts treated with ciprofibrate or WY14643 for 48 h at the indicated concentrations with the peroxisomal marker PEX14p. (B) Western blot analysis of PEX13p in IPF cells treated with ciprofibrate or WY14643 for 48 h. (C) IPF cells cotransfected with PPAR- α expression vector (PPAR- α E.P.) and PPRE-luciferase-reporter vector (PPRE)/empty vector (E.V.) were treated with ciprofibrate (200 μ M) or WY14643 (100 μ M) or GW6471 (10 μ M) for the indicated times after which the firefly luciferase activity was measured in cell lysates and normalized to the activity of renilla luciferase. (D and E) Western blot analysis of IPF cells pretreated with WY14643 (100 μ M) or ciprofibrate (200 μ M) and/or GW6471 (10 μ M) for the indicated times followed by treatment with TGF- β 1 (5 ng/mL) for another 24 h. Note: After 48 h treatment of ciprofibrate/WY14643, the medium was replaced with fresh serum free medium before simulation with TGF- β 1, whereas the medium was not replaced before the addition of TGF- β 1 in cells pretreated with ciprofibrate/WY14643 for 2 h or GW6471 for 1 h. CIP, ciprofibrate; CTRL, control; GW, GW6471; WY, WY14643. Data are a representative of at least three reproducible experiments. Statistical analysis for luciferase assays was performed by ANOVA. (Scale bar: 10 μ m).

proliferation of cardiac fibroblasts (30), (ii) reduce the lung injury induced by bleomycin (31), and (iii) inhibit TGF- β -induced transcription of β 5 integrin in vascular smooth muscle cells (32). PPAR- α as a transcription factor mediates the peroxisome proliferation in rodent liver. A functional PPRE is found about 8.4 kb downstream of the *PEX11 α* promoter (33). Moreover, *PEX11 α* is one of the *PEX* genes responsible for peroxisome proliferation (33, 34). Lack of specific and potent peroxisome proliferators that are independent of PPARs is one of the main technical limitations in distinguishing the beneficial effects of peroxisome proliferation. Although the findings presented here suggest that peroxisome proliferation rather than the endogenous PPAR- α activation mediates the antifibrotic effects observed, we cannot rule out the possibility of other molecular targets being altered during this 48 h pretreatment with PPAR- α agonists. Similarly, it should also be taken into consideration that the PPAR- α antagonist, GW6471 used in this study might also interfere in the activation/regulation of other PPAR family members leading to secondary effects which could result in the inhibitory effect observed on TGF- β 1-induced α -SMA and collagen. Future studies have to be carried out to confirm the specificity of this PPAR- α antagonist and to get more insights into the complex interactions of distinct PPARs on the PPRES of

dependent genes, e.g., genes for peroxisomal proteins. Our study also highlights the necessity to design and synthesize new drugs with selective peroxisome proliferation activity that is independent of PPARs to resolve the technical difficulties in studying the beneficial effects of peroxisome proliferation in disease models.

Taken together, activation of TGF- β signaling during lung injury and subsequent induction of proinflammatory mediators such as TNF- α , ROS and IL-6 in IPF, leads to the down-regulation of peroxisomes specifically PEX13 via AP-1 transcription factor, thus enabling the persistence of a fibrotic phenotype, which in turn generates more ROS and elevates secretion of proinflammatory cytokines (e.g., IL-6) (Fig. 9). Moreover, the activation of TGF- β signaling (Smad-dependent pathway) by peroxisome down-regulation promotes an increased extracellular matrix production and generation of a fibrotic phenotype (Fig. 9). In summary, this study identifies a functionally relevant and potentially possible target for future development of new viable therapeutic approaches, and significantly extends the role of this organelle in the maintenance of normal cellular function by scavenging ROS, metabolizing lipid mediators, and by protecting against inflammatory processes leading eventually to exacerbations in patients with pulmonary fibrosis.

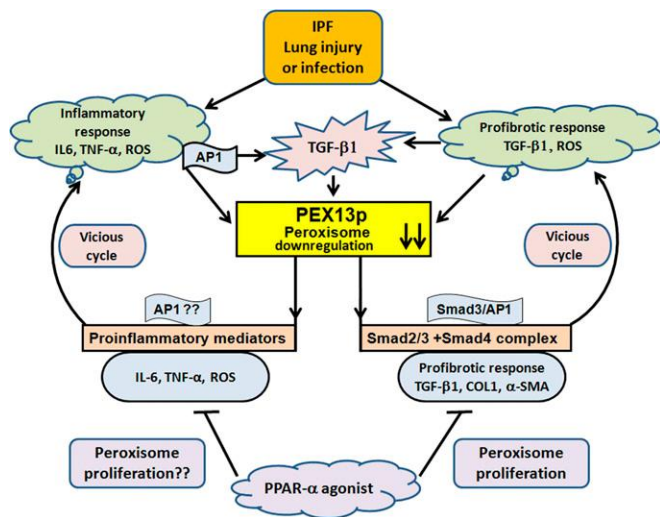


Fig. 9. Mechanism: Schematic illustration of TGF- β 1 effects on peroxisome function, described as proposed model in this study. In idiopathic pulmonary fibrosis, lung injury leads to the production of proinflammatory mediators such as TNF- α , IL-6, and ROS and the activation of profibrogenic TGF- β and AP-1 signaling. This damage leads to down-regulation of peroxisomes specifically PEX13p, which in turn generates more ROS, elevates secretion of cytokines such as IL-6 and promotes the activation of TGF- β and AP-1 signaling in a vicious cycle thus enabling the persistence of fibrotic phenotype and inflammatory exacerbation phases in IPF patients. In addition, this cycle also leads to increased production of collagen. In contrast, treatment with PPAR- α agonists induce the proliferation of peroxisomes and inhibit the profibrogenic factors such as α -SMA and collagen.

Materials and Methods

Detailed descriptions of cell culture, animal model, reagents, enzymatic treatments, confocal fluorescence microscopy, immunofluorescence, Western blotting, qRT-PCR and RT-PCR, and ELISAs are provided in *SI Materials and Methods*.

Cell Culture, Cell Isolation, and Tissue Sections. Lung tissue and fibroblasts were obtained from 10 IPF patients with typical IPF characteristics (mean age 49 ± 13 y; four females and six males) and 10 control subjects (organ donors, 56 ± 10 y, five females and five males) from the Giessen DZL-biobank at Universities of Giessen and Marburg Lung Center. The study protocol was approved by the Ethics Committee of the Justus-Liebig-University School of Medicine (AZ 31/93) in accordance with the national law and with the "Good Clinical Practice/International Conference on Harmonisation." Informed consent was obtained in written form from each subject for the study protocol. Control and IPF fibroblasts were cultured in Dulbecco's Modified Eagle's Medium (DMEM) low-glucose media supplemented with 2 mM L-glutamine, 10 U of penicillin/mL, 100 μ g of streptomycin/mL, and 10% FBS and maintained at 37 $^{\circ}$ C with 5% CO₂. Paraffin embedding sections and isolation of cells are described in detail in *SI Materials and Methods*.

Animal Model. C57BL/6J mice were housed under standard conditions in the central animal facility of the University of Southern California. Floxed TGF- β receptor II (T β RII) mice were provided Harold Moses (Vanderbilt University, Nashville, TN) (35, 36). C57BL/6J and TGF- β receptor II (T β RII) mice were used in experimental model in accordance with the National Institutes of Health (NIH) guidelines for animal care as approved by the USC Institutional Animal Care and Use Committee.

Bleomycin-Induced Pulmonary Fibrosis. C57BL/6J control and TGF- β receptor II (T β RII) female mice 8-wk-old, anesthetized with pentobarbital sodium (30–40 μ g/g ip) were administered with 4 U/kg bleomycin (BLM) (Sigma) diluted in 120 μ L of saline, or saline alone by intratracheal instillation using an intratracheal aerosolizer (MicroSprayer Aerosolizer, Model IA, Penn-Century) (37) on day 0 (6). The mouse lungs were then harvested 7, 14, and 28 d after BLM treatment. The harvesting and further processing of paraffin embedded sections was done as described in *SI Materials and Methods*.

PEX 13 siRNA Transfection. Control and IPF fibroblasts were transfected twice with 15 nM PEX 13 siRNA (Ambion, catalog no. AM16708), (Ambion, catalog no. AM16773), or silencer select negative control siRNA (Ambion, catalog no. 4390843), with Interferin reagent (Pqlab, catalog no. 13-409-10), processed after 72 h for harvesting and immunofluorescence as described in *SI Materials and Methods*.

IL-6 Treatment. IPF fibroblasts were seeded as described at a density of 8×10^4 cells per well in 12-well plates. After 24 h, they were challenged with 20 ng/mL human IL-6 (Biomol, catalog no. 50435), for 6 h duration. At the end of incubation period, the cells were processed for protein analysis with Western blotting.

Treatment of Fibroblast Cultures with Cytokines and Drugs. Treatment of cells with rhTGF- β 1 5 ng/mL, 24 h (R&D catalog no. 240-B); LY364947 5 μ M, 24 h (Tocris catalog no. 2718); rhTNF- α 10 ng/mL, 0 h, 1 h, 4 h, and 6 h duration (Biomol catalog no. 50435); interleukin 6, human recombinant (rhIL-6) (Biomol, catalog no. 50436) for 6 h; SR11302 (Tocris, catalog no. 2476), inhibitor of activator protein-1 (AP-1) transcription factor activity, for indicated times and concentrations; Lutecol (Sigma, L9283), an Nrf2 inhibitor for indicated concentration and duration; ciprofibrate, a PPAR- α agonist (Sigma-Aldrich Chemie), for 48 h, with the indicated concentrations: 0 μ M, 150 μ M, 300 μ M, 600 μ M; WY14643, a selective PPAR- α agonist (Tocris, catalog no. 1312) for 48 h for indicated concentrations: 0 μ M, 50 μ M, 100 μ M, 200 μ M; GW6471, a PPAR- α -specific antagonist (Tocris catalog no. 4618), for 24 h with the indicated concentration 10 μ M, were performed in cell culture for the indicated times and conditions as described in *SI Materials and Methods*.

Immunofluorescence. Control and IPF fibroblasts were plated on poly-L-lysine coated coverslips in 24-well plates for 24 h. Thereafter, cells were treated with the compounds mentioned above and described in detail in *SI Materials and Methods* for different time points. After treatment, they were subjected to an indirect immunofluorescence staining protocol as described (38).

Western Blot Analysis. Total cell lysates of control and IPF fibroblasts were separated by SDS/PAGE, transferred to PVDF membranes, and incubated with antibodies as described in *SI Materials and Methods* (8).

Quantitative RT-PCR. Control and IPF cells were grown in basal conditions as well as treated with the compounds described above and the cells were harvested after the respective time-points. Total RNA was isolated using the RNeasy kit (Qiagen), and cDNA was synthesized by reverse transcription with SuperScript II as described by the manufacturer (Applied Biosystems). The relative expression, fold change of a defined gene was calculated using the ddCT method. All primer pairs and incubation conditions are given in *SI Materials and Methods*.

Luciferase Reporter Gene Assay and Plasmid Constructs. Luciferase reporter gene assays were done for ARE, AP1, PPARE reporter, SBE elements, and the COL1A2 promoter. Plasmids were obtained from B. Vogelstein (SBE), E. Jung (COL1A2), W. E. Fahl (p-ARE), and C. A. Hauser (AP-1). PPARE reporter plasmid was from Qiagen Signal PPAR Reporter (luc) kit. PPAR- α expression plasmid pSG5 PPAR alpha was a gift from B. Spiegelman (Addgene plasmid no. 22751). Empty control vectors pGL2-basic and pGL3-basic were obtained from Promega. Transfection of plasmid DNA into cells was done with TransIT-LT1 (Mirus Bio) as described (39). See *SI Materials and Methods*.

Measurement of Reactive Oxygen Species. Reactive oxygen species (ROS) production was detected with dihydroethidine (DHE) final concentration of 5 μ M, incubated for 20 min. DHE is oxidized by superoxide to its fluorescent product, ethidine. Ethidine remains intracellularly after it is oxidized, thus allowing quantitative estimations of the intracellular ROS level (40). See *SI Materials and Methods*.

Cytokine ELISAs and Sircol Collagen Assay. Cytokine ELISAs and the collagen assay were used according to the manufacturer's instructions as described in detail in *SI Materials and Methods*. Collagen Sircol Assay (Biocolor; catalog no. S1000), human TGF- β 1 immunoassay (R&D, catalog no. DB100B) and human IL-6 Quantikine ELISA Kit (R&D, catalog no. D6050).

Statistics. All values are expressed as means \pm SEM where $n = 3$ or 4. An unpaired Student's t test or ANOVA were used to assess the difference between two groups. Image J was used for quantification of RT-PCR expression. Differences were considered statistically significant when $P < 0.05$.

ACKNOWLEDGMENTS. We thank Srinu Tumpara, Omelyan Trompak, Ranjithkumar Rajendran, Petra Hahn-Kohlberger, Andrea Textor, Elke Richter, Bianca Pfeiffer, and Gabriele Thiele for excellent technical assistance. We also thank Dr. Bert Vogelstein (The Ludwig Center and the Howard Hughes Medical Institute at Johns Hopkins Kimmel Cancer Center) for providing the luciferase reporter gene construct SBE (Smad binding element),

Dr. Eunsum Jung (BioSpectrum LifeScience Institute) for the COL1A2 luciferase construct, Dr. William E. Fahl (University of Wisconsin, Madison) for p-ARE luciferase plasmid, and Dr. C. A. Hauser (The Burnham Institute) for providing pAP-1 luciferase construct. Further, we also thank Denis I. Crane (Griffith University), Paul P. Van Veldhoven (Catholic University) and Alfred Völkl (Ruprecht-Karls-University), for providing us with some antibodies.

- Cui Y, et al. (2011) Oxidative stress contributes to the induction and persistence of TGF- β 1 induced pulmonary fibrosis. *Int J Biochem Cell Biol* 43(8):1122–1133.
- Katzenstein AL, Myers JL (1998) Idiopathic pulmonary fibrosis: Clinical relevance of pathologic classification. *Am J Respir Crit Care Med* 157(4 Pt 1):1301–1315.
- Kuhn C, McDonald JA (1991) The roles of the myofibroblast in idiopathic pulmonary fibrosis. Ultrastructural and immunohistochemical features of sites of active extracellular matrix synthesis. *Am J Pathol* 138(5):1257–1265.
- Pardo A, Selman M (2002) Molecular mechanisms of pulmonary fibrosis. *Front Biosci* 7: d1743–1761.
- Warburton D, Shi W, Xu B (2013) TGF- β -Smad3 signaling in emphysema and pulmonary fibrosis: An epigenetic aberration of normal development? *Am J Physiol Lung Cell Mol Physiol* 304(2):L83–L85.
- Zhao J, et al. (2002) Smad3 deficiency attenuates bleomycin-induced pulmonary fibrosis in mice. *Am J Physiol Lung Cell Mol Physiol* 282(3):L585–L593.
- Sullivan DE, Ferris M, Nguyen H, Abboud E, Brody AR (2009) TNF- α induces TGF- β 1 expression in lung fibroblasts at the transcriptional level via AP-1 activation. *J Cell Mol Med* 13(8B):1866–1876.
- Karnati S, Baumgart-Vogt E (2008) Peroxisomes in mouse and human lung: Their involvement in pulmonary lipid metabolism. *Histochem Cell Biol* 130(4):719–740.
- Karnati S, Baumgart-Vogt E (2009) Peroxisomes in airway epithelia and future prospects of these organelles for pulmonary cell biology. *Histochem Cell Biol* 131(4): 447–454.
- Ahlemeyer B, Gottwald M, Baumgart-Vogt E (2012) Deletion of a single allele of the Pex11 β gene is sufficient to cause oxidative stress, delayed differentiation and neuronal death in mouse brain. *Dis Model Mech* 5(1):125–140.
- Steinberg SJ, et al. (2006) Peroxisome biogenesis disorders. *Biochim Biophys Acta* 1763(12):1733–1748.
- Rahman I, Swarska E, Henry M, Stolk J, MacNee W (2000) Is there any relationship between plasma antioxidant capacity and lung function in smokers and in patients with chronic obstructive pulmonary disease? *Thorax* 55(3):189–193.
- Li X, et al. (2002) PEX11 beta deficiency is lethal and impairs neuronal migration but does not abrogate peroxisome function. *Mol Cell Biol* 22(12):4358–4365.
- Boor P, et al. (2011) The peroxisome proliferator-activated receptor- α agonist, BAY PP1, attenuates renal fibrosis in rats. *Kidney Int* 80(11):1182–1197.
- Rahman I, MacNee W (2000) Regulation of redox glutathione levels and gene transcription in lung inflammation: Therapeutic approaches. *Free Radic Biol Med* 28(9): 1405–1420.
- Grant P, et al. (2013) The biogenesis protein PEX14 is an optimal marker for the identification and localization of peroxisomes in different cell types, tissues, and species in morphological studies. *Histochem Cell Biol* 140(4):423–442.
- Baarine M, et al. (2012) Evidence of oxidative stress in very long chain fatty acid-treated oligodendrocytes and potentialization of ROS production using RNA interference-directed knockdown of ABCD1 and ACOX1 peroxisomal proteins. *Neuroscience* 213:1–18.
- Beier K, Völkl A, Fahimi HD (1997) TNF- α downregulates the peroxisome proliferator activated receptor- α and the mRNAs encoding peroxisomal proteins in rat liver. *FEBS Lett* 412(2):385–387.
- Gäbele E, et al. (2009) TNF α is required for cholestasis-induced liver fibrosis in the mouse. *Biochem Biophys Res Commun* 378(3):348–353.
- Verjee LS, et al. (2013) Unraveling the signaling pathways promoting fibrosis in Dupuytren's disease reveals TNF as a therapeutic target. *Proc Natl Acad Sci USA* 110(10): E928–E937.
- Junn E, et al. (2000) Requirement of hydrogen peroxide generation in TGF- β 1 signal transduction in human lung fibroblast cells: Involvement of hydrogen peroxide and Ca $^{2+}$ in TGF- β 1-induced IL-6 expression. *J Immunol* 165(4):2190–2197.
- Verrecchia F, et al. (2001) Smad3/AP-1 interactions control transcriptional responses to TGF- β 1 in a promoter-specific manner. *Oncogene* 20(26):3332–3340.
- Rajasekaran S, Vaz M, Reddy SP (2012) Fra-1/AP-1 transcription factor negatively regulates pulmonary fibrosis in vivo. *PLoS ONE* 7(7):e41611.
- Roy S, et al. (2010) Fra-2 mediates oxygen-sensitive induction of transforming growth factor beta in cardiac fibroblasts. *Cardiovasc Res* 87(4):647–655.
- Liu W, et al. (2013) Antiflammin-1 attenuates bleomycin-induced pulmonary fibrosis in mice. *Respir Res* 14:101.
- Pantelidis P, Fanning GC, Wells AU, Welsh KI, Du Bois RM (2001) Analysis of tumor necrosis factor- α , lymphotoxin- α , tumor necrosis factor receptor II, and interleukin-6 polymorphisms in patients with idiopathic pulmonary fibrosis. *Am J Respir Crit Care Med* 163(6):1432–1436.
- Qiu Z, Fujimura M, Kurashima K, Nakao S, Mukaida N (2004) Enhanced airway inflammation and decreased subepithelial fibrosis in interleukin 6-deficient mice following chronic exposure to aerosolized antigen. *Clin Exp Allergy* 34(8):1321–1328.
- Saito F, et al. (2008) Role of interleukin-6 in bleomycin-induced lung inflammatory changes in mice. *Am J Respir Cell Mol Biol* 38(5):566–571.
- Fourtounis J, et al. (2012) Gene expression profiling following NRF2 and KEAP1 siRNA knockdown in human lung fibroblasts identifies CCL11/Eotaxin-1 as a novel NRF2 regulated gene. *Respir Res* 13:92.
- Ogata T, et al. (2002) Stimulation of peroxisome-proliferator-activated receptor alpha (PPAR alpha) attenuates cardiac fibrosis and endothelin-1 production in pressure-overloaded rat hearts. *Clin Sci (Lond)* 103(Suppl 48):284S–288S.
- Genovese T, et al. (2005) Role of endogenous and exogenous ligands for the peroxisome proliferator-activated receptor alpha in the development of bleomycin-induced lung injury. *Shock* 24(6):547–555.
- Kintscher U, et al. (2002) PPARalpha inhibits TGF-beta-induced beta5 integrin transcription in vascular smooth muscle cells by interacting with Smad4. *Circ Res* 91(11): e35–e44.
- Shimizu M, Takeshita A, Tsukamoto T, Gonzalez FJ, Osumi T (2004) Tissue-selective, bidirectional regulation of PEX11 alpha and perilipin genes through a common peroxisome proliferator response element. *Mol Cell Biol* 24(3):1313–1323.
- Colasante C, Chen J, Ahlemeyer B, Baumgart-Vogt E (2015) Peroxisomes in cardiomyocytes and the peroxisome / peroxisome proliferator-activated receptor-loop. *Thromb Haemost* 113(3):452–463.
- Chytil A, Magnuson MA, Wright CV, Moses HL (2002) Conditional inactivation of the TGF- β type II receptor using Cre:Lox. *Genesis* 32(2):73–75.
- Sauer B (1993) Manipulation of transgenes by site-specific recombination: Use of Cre recombinase. *Methods Enzymol* 225:890–900.
- Bivas-Benita M, Zwier R, Junginger HE, Borchard G (2005) Non-invasive pulmonary aerosol delivery in mice by the endotracheal route. *Eur J Pharm Biopharm* 61(3): 214–218.
- Nenicu A, et al. (2007) Peroxisomes in human and mouse testis: Differential expression of peroxisomal proteins in germ cells and distinct somatic cell types of the testis. *Biol Reprod* 77(6):1060–1072.
- Vijayan V, Baumgart-Vogt E, Naidu S, Qian G, Immenschuh S (2011) Bruton's tyrosine kinase is required for TLR-dependent heme oxygenase-1 gene activation via Nrf2 in macrophages. *J Immunol* 187(2):817–827.
- Ahlemeyer B, Neubert I, Kovacs WJ, Baumgart-Vogt E (2007) Differential expression of peroxisomal matrix and membrane proteins during postnatal development of mouse brain. *J Comp Neurol* 505(1):1–17.



A New Immunomodulatory Role for Peroxisomes in Macrophages Activated by the TLR4 Ligand Lipopolysaccharide

This information is current as of January 24, 2019.

Vijith Vijayan, Tumpara Srinu, Srikanth Karnati, Vannuruswamy Garikapati, Monika Linke, Lilit Kamalyan, Srihari Reddy Mali, Kritika Sudan, Andreas Kollas, Tobias Schmid, Sabine Schulz, Bernhard Spengler, Thomas Weichhart, Stephan Immenschuh and Eveline Baumgart-Vogt

J Immunol 2017; 198:2414-2425; Prepublished online 8 February 2017;
doi: 10.4049/jimmunol.1601596
<http://www.jimmunol.org/content/198/6/2414>

Supplementary Material <http://www.jimmunol.org/content/suppl/2017/02/07/jimmunol.1601596.DCSupplemental>

References This article **cites 45 articles**, 14 of which you can access for free at: <http://www.jimmunol.org/content/198/6/2414.full#ref-list-1>

Why *The JI*? Submit online.

- **Rapid Reviews! 30 days*** from submission to initial decision
- **No Triage!** Every submission reviewed by practicing scientists
- **Fast Publication!** 4 weeks from acceptance to publication

**average*

Subscription Information about subscribing to *The Journal of Immunology* is online at: <http://jimmunol.org/subscription>

Permissions Submit copyright permission requests at: <http://www.aai.org/About/Publications/JI/copyright.html>

Email Alerts Receive free email-alerts when new articles cite this article. Sign up at: <http://jimmunol.org/alerts>

The Journal of Immunology is published twice each month by The American Association of Immunologists, Inc., 1451 Rockville Pike, Suite 650, Rockville, MD 20852
Copyright © 2017 by The American Association of Immunologists, Inc. All rights reserved.
Print ISSN: 0022-1767 Online ISSN: 1550-6606.



A New Immunomodulatory Role for Peroxisomes in Macrophages Activated by the TLR4 Ligand Lipopolysaccharide

Vijith Vijayan,^{*,†} Tumpara Srinu,^{*} Srikanth Karnati,^{*} Vannuruswamy Garikapati,^{*,‡} Monika Linke,[§] Lilit Kamalyan,^{*} Srihari Reddy Mali,^{*} Kritika Sudan,[†] Andreas Kollas,^{*} Tobias Schmid,[¶] Sabine Schulz,[‡] Bernhard Spengler,[‡] Thomas Weichhart,[§] Stephan Immenschuh,[†] and Eveline Baumgart-Vogt^{*}

Peroxisomes are proposed to play an important role in the regulation of systemic inflammation; however, the functional role of these organelles in inflammatory responses of myeloid immune cells is largely unknown. In this article, we demonstrate that the nonclassical peroxisome proliferator 4-phenyl butyric acid is an efficient inducer of peroxisomes in various models of murine macrophages, such as primary alveolar and peritoneal macrophages and the macrophage cell line RAW264.7, but not in primary bone marrow-derived macrophages. Further, proliferation of peroxisomes blocked the TLR4 ligand LPS-induced proinflammatory response, as detected by the reduced induction of the proinflammatory protein cyclooxygenase (COX)-2 and the proinflammatory cytokines TNF- α , IL-6, and IL-12. In contrast, disturbing peroxisome function by knockdown of peroxisomal gene *Pex14* or *Mfp2* markedly increased the LPS-dependent upregulation of the proinflammatory proteins COX-2 and TNF- α . Specifically, induction of peroxisomes did not affect the upregulation of COX-2 at the mRNA level, but it reduced the half-life of COX-2 protein, which was restored by COX-2 enzyme inhibitors but not by proteasomal and lysosomal inhibitors. Liquid chromatography–tandem mass spectrometry analysis revealed that various anti-inflammatory lipid mediators (e.g., docosahexaenoic acid) were increased in the conditioned medium from peroxisome-induced macrophages, which blocked LPS-induced COX-2 upregulation in naive RAW264.7 cells and human primary peripheral blood–derived macrophages. Importantly, LPS itself induced peroxisomes that correlated with the regulation of COX-2 during the late phase of LPS activation in macrophages. In conclusion, our findings identify a previously unidentified role for peroxisomes in macrophage inflammatory responses and suggest that peroxisomes are involved in the physiological cessation of macrophage activation. *The Journal of Immunology*, 2017, 198: 2414–2425.

Peroxisomes are eukaryotic membrane-bound subcellular organelles that compartmentalize several proteins or pathways for the metabolism of lipids and reactive oxygen species (ROS). A variety of bioactive lipid derivatives that cannot be degraded in the mitochondria is metabolized in peroxisomes (1). Peroxisomes are involved in cytoprotection by mediating intracellular lipid and ROS homeostasis (2) and, when compromised, are coupled with mitochondrial dysfunction (3, 4). The peroxisomal compartment and its metabolic capacity were suggested to be altered by bacterial compound endotoxin in the liver (5–7).

However, the role of peroxisomes in immune homeostasis has only recently been begun to be understood. Mitochondrial antiviral signaling protein, an adaptor protein primarily localized on the mitochondrial membrane, is also localized on peroxisomes, and this phenomenon is crucial for mounting an effective antiviral response (8). Follow-up studies identified peroxisomes as an important subcellular signaling platform for the production of IFN- λ during viral or intracellular bacterial infection (9). Similarly, peroxisome-derived ether lipids were shown to be vital for the maturation of invariant NK T cells in the thymus (10). Additionally,

^{*}Institute for Anatomy and Cell Biology II, Medical Cell Biology, Justus Liebig University Giessen, 35392 Giessen, Germany; [†]Institute for Transfusion Medicine, Hannover Medical School, 30625 Hannover, Germany; [‡]Institute of Inorganic and Analytical Chemistry, Justus Liebig University Giessen, 35392 Giessen, Germany; [§]Institute of Medical Genetics, Medical University of Vienna, 1090 Vienna, Austria; and [¶]Institute of Biochemistry I, Faculty of Medicine, Goethe University Frankfurt, 60596 Frankfurt, Germany

ORCID: 0000-0001-7410-736X (M.L.); 0000-0002-4349-0797 (T.W.); 0000-0002-8265-3763 (E.B.-V.).

Received for publication September 13, 2016. Accepted for publication January 16, 2017.

This work was supported by a post doctoral program Just'us (Junior Science and Teaching Units) stipend and consumable grant from Justus Liebig University Giessen (to V.V.), by grants from the Deutsche Forschungsgemeinschaft (DFG BA2465/1-2, DFG IM 20/4-1, and DFG SP 314/13-1 to E.B.-V., S.I., and B.S.), and a grant from the LandesOffensive zur Entwicklung Wissenschaftlich-ökonomischer Exzellenz excellence program of the State of Hesse (LandesOffensive zur Entwicklung Wissenschaftlich-ökonomischer Exzellenz-Focus Group MIBIE, Project A4 to E.B.-V.). V.G. was funded by a stipend from the Graduate School Scholarship Programme of the German Academic Exchange Service (2015-DAAD-GSSP, ID91566981), T.W. was funded by a grant from the Austrian Science Fund (FWF-P27701-B20), and M.L. was supported by the Doctoral Fellowship Programme of the Austrian Academy of Sciences.

V.V., T. Srinu, V.G., S.S., M.L., L.K., S.R.M., K.S., and A.K. conducted experiments; V.V., T. Schmid, S.K., V.G., B.S., T.W., S.I., and E.B.-V. designed experiments; and V.V., T. Srinu, T. Schmid, S.K., S.I., T.W., and E.B.-V. prepared the manuscript.

Address correspondence and reprint requests to Prof. Eveline Baumgart-Vogt, Institute for Anatomy and Cell Biology II, Medical Cell Biology, Justus Liebig University Giessen, Aulweg 123, 35392 Giessen, Germany. E-mail address: Eveline.Baumgart-Vogt@anatomie.med.uni-giessen.de

The online version of this article contains supplemental material.

Abbreviations used in this article: AA, arachidonic acid; AM, alveolar M Φ ; AP-1, activator protein-1; BMDM, bone marrow–derived M Φ ; CHX, cycloheximide; COX, cyclooxygenase; DHA, docosahexaenoic acid; ER, endoplasmic reticulum; HO-1, heme oxygenase-1; HU, hydroxy urea; LC-MS/MS, liquid chromatography–tandem MS; L-SF, L-sulforaphane; LTA, lipoteichoic acid; LT B_4 , leukotriene B $_4$; M Φ , macrophage; MEF, mouse embryonic fibroblast; Mfp2, multi-functional protein 2; MS, mass spectrometry; 4-PBA, 4-phenyl butyric acid; PM, peritoneal M Φ ; poly I:C, polyinosinic:polycytidylic acid; PPAR, peroxisome proliferator activated receptor; RAW, RAW264.7; ROS, reactive oxygen species; RT, room temperature; siRNA, small interfering RNA; ThT, thioflavin T.

Copyright © 2017 by The American Association of Immunologists, Inc. 0022-1767/17/\$30.00

our recent findings suggest that peroxisomal alterations in idiopathic pulmonary fibrosis lead to impaired TGF- β signaling and that the downregulation of peroxisomes in primary human lung fibroblasts causes a profibrotic phenotype in these cells (11).

The notion that peroxisomes are involved in the regulation of inflammation arises from three important functions attributed to the organelle. Peroxisomes are equipped with a series of antioxidant enzymes, such as catalase and peroxiredoxins, whose primary function is the neutralization of ROS generated during β -oxidation of lipids, but they may also play a role in maintaining cellular redox homeostasis (12). Indeed, various independent studies confirmed that deficiency of peroxisomes leads to increased oxidative stress (13). Peroxisomes were shown *in vitro* to metabolize leukotrienes (14) and PGs (15), which are crucial modulators of inflammation, and peroxisomes are the primary intracellular site for the production of docosahexaenoic acid (DHA) and eicosapentaenoic acid, which form the backbone for a series of resolution mediators of inflammation that includes resolvins, protectins, and maresins (12).

Despite their potential immunomodulatory properties, little is known about the specific role of peroxisomes in inflammatory responses in myeloid immune cells, such as monocytes, macrophages (M Φ s), and dendritic cells. We chose to address this issue in M Φ s, because they are unique in their capacity to initiate and resolve inflammation. M Φ s are broadly divided into two main subclasses: M1 (classically activated) and M2 (alternatively activated). M1 M Φ s exhibit a proinflammatory phenotype, whereas M2 M Φ s exhibit an anti-inflammatory phenotype (16). In this article, we report that induction of peroxisomes in M Φ s dampens the LPS-induced proinflammatory proteins cyclooxygenase (COX)-2, TNF- α , IL-6, and IL-12 without exhibiting the classical features of M2 M Φ s. In contrast, disruption of peroxisomal function leads to a hyperinduction of COX-2 and TNF- α . This peroxisome-driven anti-inflammatory effect was found to be mediated via extrinsic factors released by M Φ s upon LPS activation.

Materials and Methods

DMEM, RPMI 1640, and inactivated FBS were purchased from PAA Laboratories (Pasching, Austria), and polyvinylidene difluoride membranes were from Millipore (Darmstadt, Germany). LPS ultrapure (0111:B4), lipoteichoic acid (LTA), and polyinosinic:polycytidylic acid (poly I:C) were purchased from InvivoGen (San Diego, CA). PG (PG₂, PGD₂, PGE₂), leukotriene B₄ (LTB₄), arachidonic acid (AA), DHA, and deuterated internal standards LTB₄-d₄ and AA-d₁₁ were purchased from Cayman Chemical (distributor: Biomol, Hamburg, Germany). Strata-X polymeric SPE sorbents (33 μ m, 100 mg/3 ml tubes) were purchased from Phenomenex (Torrance, CA). All other chemicals were obtained from Sigma-Aldrich (St. Louis, MO) and Roche Applied Science (Penzberg, Germany), unless otherwise indicated.

Animals

Fifteen adult male mice (6–12 wk of age) on the C57BL/6J genetic background were obtained from Charles River (Sulzfeld, Germany). The mice were kept on a normal laboratory diet and water *ad libitum* and were housed in cages under standardized environmental conditions (12-h light/dark cycle, 23 \pm 1°C and 55 \pm 1% relative humidity) at the central animal facility of the Justus Liebig University Giessen. All experiments using laboratory mice were approved by the governmental ethics committee for animal welfare (Regierungspräsidium Giessen, Germany; permit number V 54-19 C 20/15 c GI 20/23).

Cell culture and treatment

RAW264.7 (RAW) cells were from the American Type Culture Collection, and primary mouse embryonic fibroblasts (MEFs) (17) were grown in DMEM supplemented with 10% FBS, 100 U/ml penicillin, and 100 μ g/ml streptomycin, as described previously (18). Murine alveolar M Φ (AMs), peritoneal M Φ s (PMs), and bone marrow-derived M Φ s (BMDMs) were isolated as described previously (19). AMs were cultured and maintained

in RPMI 1640 supplemented with 10% FBS, 100 U/ml penicillin, and 100 μ g/ml streptomycin. Peritoneal and bone marrow-derived macrophages were cultured and maintained in DMEM supplemented with 10% FBS, 100 U/ml penicillin, and 100 μ g/ml streptomycin. Conditioned medium obtained from culture of L-929 fibroblasts in DMEM supplemented with 10% FBS, 100 U/ml penicillin, and 100 μ g/ml streptomycin was used as a source of macrophage colony stimulating factors to differentiate bone marrow-derived cells to M Φ s. Peripheral blood-derived human M Φ s were obtained by Ficoll isolation of PBMCs from 50 ml of blood. Briefly, isolated PBMCs were plated onto bacterial petri dishes in RPMI 1640 + 5% AB serum (C.C.pro, Oberdola, Germany). The medium was replaced after 2 h to remove all nonadherent cells and was cultured for 5 d to differentiate into M Φ s. The following chemicals were used at the indicated concentrations: antimycin A (5–10 μ M), chloroquine (75 μ M), cycloheximide (CHX; 100 μ M), epoxomicin (1 μ M), hydroxy urea (HU; 100 μ M), L-sulforaphane (10 μ M), 3-methyladenine (5 mM), MG132 (10 μ M), NS-398 (20 μ M), and S-flurbiprofen (100 μ M).

All cell cultures were kept under air/CO₂ (19:1) at 100% humidity.

ELISA

Cell culture supernatants were briefly centrifuged and used fresh or stored at –80°C until use. ELISA kits for TNF- α , IL-6, IL-10, and IL-12 were purchased from eBioscience (San Diego, CA) and used according to the manufacturer's instructions.

Flow cytometry

Briefly, 1 \times 10⁶ cells were blocked with Fc blocker for 15 min on ice and stained with 0.25 μ g of anti-mouse CD86 or anti-mouse CD36 or the respective isotype controls (BioLegend, San Diego, CA) for 20 min before analysis by flow cytometry. For intracellular staining of PEX14p, the cells were fixed for 10 min in 2% paraformaldehyde, followed by permeabilization for 5 min using 0.2% Triton X-100. Cells were incubated for 30 min at 4°C with Ab against PEX14p (1:1200) in PBS containing 2% FCS+ 0.2% sodium azide. The cells were washed twice and incubated with donkey anti-rabbit IgG-Alexa Fluor 488 secondary Ab (Invitrogen, Carlsbad, CA) for 20 min, washed twice with 1 \times PBS, and analyzed using a BD FACSCanto II flow cytometer.

Immunofluorescence

Cells were plated on coverslips in 12- or 24-well plates and subjected to an indirect immunofluorescence staining protocol, as previously described (18). Briefly, cells grown on coverslips were washed three times with PBS, fixed using 4% paraformaldehyde and 2% saccharose, and permeabilized using 1% glycine containing 0.2% Triton X-100. Nonspecific binding sites were blocked with 1% BSA in TBS containing 0.05% Tween for 1 h at room temperature (RT), after which the coverslips were incubated overnight at 4°C with the primary Abs against PEX14p (1:2000; a generous gift from D. Crane), total p65 (1:400), phospho-c-jun (1:600), and COX-2 (1:1000) (Cell Signaling Technology, Danvers, MA). Coverslips were washed and incubated with Alexa Fluor 488-conjugated secondary Ab at 1:800 dilutions (Invitrogen). Nuclei were counterstained with 1 μ M Hoechst 33,342 for 5 min at RT and the coverslips were embedded in Mowiol 4-88 with *N*-propyl gallate as an antifading agent. All samples were examined with a Leica DMRS fluorescence microscope equipped with a DR4 camera or a confocal laser scanning microscope (Leica TCS SP5; Leica Mikrosystem Vertrieb, Wetzlar, Germany). All images were processed with Adobe Photoshop CS5 extended version.

Liquid chromatography–tandem mass spectrometry

Cell supernatants were collected from LPS-stimulated cultures of RAW cells, with or without pretreatment with 4-phenyl butyric acid (4-PBA), and stored at –80°C until further analysis. A total of 8.5 ml of each cell culture supernatant was spiked with deuterated internal standards (6 ng), and lipid species were extracted with a solid phase extraction method using solid phase extraction columns, according to the manufacturer's protocol. Briefly, the columns were equilibrated with 3.5 ml of 100% methanol, followed by 3.5 ml of water. After sample extraction, the columns were washed with 3.5 ml of 10% methanol, and the lipids were eluted with 1.5 ml of methanol. The methanol was dried down under a stream of nitrogen gas, and the dried extract was reconstituted with 55 μ l of 25% acetonitrile. Lipid species were quantified in cell supernatants by parallel reaction monitoring using a quadrupole orbital trapping mass spectrometer (Q Exactive; Thermo Scientific, Bremen, Germany) in high-resolution mode. Briefly, 10 μ l of final reconstituted extract was injected into a Dionex UltiMate 3000 UHPLC (Thermo Scientific), and separation was performed using a reverse-phase Kinetex C18 2.6- μ m column (100 \times 2.1 mm, 100 Å) with a flow rate of 500 μ l/min of binary solvent system consisting of mobile phase A (100%

water with 0.1% formic acid) and mobile phase B (100% acetonitrile with 0.1% formic acid). The gradient was 27–35% B in 15 min, 35–60% in 2 min, and 60–80% B in 10 min. The mass spectrometer was operated at a mass resolution of 70,000 at *m/z* 200 with electrospray ionization in negative ion mode. The method used consisted of full-scan mass spectrometry (MS) and targeted tandem MS of the lipid precursor with defined mass and retention time. The transitions of lipid species were selected based on previously published data (20, 21), and fatty acids were quantified from full-scan MS. Standard calibration curves were constructed by plotting the area under the curve of transition of lipids by extracted ion chromatogram against the concentrations of serial dilutions of lipid species ranging from 10 pg to 2.56 ng or in case of fatty acids, 1–256 ng on column.

MitoTracker staining

A total of 1×10^5 cells was plated on coverslips in a 12-well plate. After overnight culture, cells were treated with antimycin A (5–10 μ M) for 1 h, followed by staining with MitoTracker (150 nM; Molecular Probes), according to the manufacturer's instructions. The cells were fixed with 4% paraformaldehyde, and the images were captured using a Leica DMRS fluorescence microscope equipped with a DR4 camera. Digital photographs were processed with Adobe Photoshop version 9.

Quantitative real-time RT-PCR

Total RNA was isolated from cells using an RNeasy Kit (QIAGEN), and cDNA was synthesized by reverse transcription using a High-Capacity cDNA Reverse Transcription Kit (Applied Biosystems). One microgram of total RNA was used in each reverse transcription reaction. PCR analyses were performed with inventoried primer mixes for mouse *Arg-1*, *Cox-2*, *Il-6*, *Il-10*, *iNos*, and *Tnf- α* (Applied Biosystems). Amplification was performed using TaqMan Gene Expression Master Mix on a StepOnePlus Real-Time PCR System (Applied Biosystems), according to the manufacturer's instructions. Thermal cycling was performed at 95°C for 10 min, followed by 40 cycles at 95°C for 15 s and 60°C for 1 min. The constitutively expressed gene *Hprt* was used as a control for normalization of cDNA levels. The $\Delta\Delta$ threshold cycle method was used to semiquantify mRNA levels according to the manufacturer's protocol.

Small interfering RNA transfection

A total of 8×10^4 RAW cells was plated in a 12-well plate and cultured overnight. The next day, cells were transfected with 30 nM of control small interfering RNA (siRNA) (Ambion siRNA ID: AM4611), *Pex14* siRNA (Ambion siRNA ID: s80240), or *Mfp2* siRNA (Ambion siRNA ID: s67851) using ScreenFect A transfection reagent (Incella, Eggenstein-Leopoldshafen, Germany), according to the manufacturer's instructions. The cells were incubated for an additional 48 h, after which the medium was replaced with medium containing LPS wherever indicated.

Thioflavin T staining

Thioflavin T (ThT) staining was performed as previously mentioned (22). Briefly 5×10^4 cells were plated on coverslips in a 24-well plate and were left untreated or treated with 4-PBA (2.5–5 mM) for 72 h. Cells were washed with fresh medium and incubated with medium containing LPS (100 ng/ml) for 12 h. After incubation, the cells were fixed using 4% paraformaldehyde for 20 min, washed twice with PBS, and washed three times for 1 min each with double distilled H₂O. The cells were incubated with 5 μ M ThT in double distilled H₂O for 10 min and washed again with double distilled H₂O (three times for 1 min). Coverslips were mounted on slides with Mowiol 4-88 containing *N*-propyl gallate as an antifading agent. Images were taken using a Leica DMRS fluorescence microscope equipped with a DR4 camera. Digital photographs were processed with Adobe Photoshop version 9.

Western blot analyses

Western blot analyses were performed as described previously (18). Briefly, cells were washed with PBS, lysed, and the protein concentrations were estimated using Bradford's assay. Thirty micrograms of total protein was separated on 10% SDS-polyacrylamide gels and subsequently blotted onto polyvinylidene difluoride membranes. Membranes were blocked with TBS containing 5% skim milk, 50 mM Tris HCl (pH 7.6), 150 mM NaCl, and 0.1% Tween 20 for 1 h at RT. The blots were incubated overnight with primary Abs against COX-2 (1:1000; Cell Signaling Technology or Abcam, Cambridge, U.K.), Pex14p (1:14,000), multifunctional protein 2 (*Mfp2*; 1:1000; Abcam), heme oxygenase-1 (HO-1; 1:1000; Enzo Lifesciences, Loerach, Germany), β -actin (1:5000; Abcam), and GAPDH (1:10,000; Hytest, Turku, Finland). The secondary Ab mouse anti-rabbit IgG alkaline phosphatase or rabbit anti-mouse IgG (Sigma) was used at 1:30,000. Immun-Star alkaline

phosphatase substrate (Bio-Rad, Hercules, CA) was used for detection, according to the manufacturer's instructions. The bands were visualized by exposing the blots to Kodak BioMax MR Films or with a FluorChem (Alpha Innotec, San Leandro, CA) and quantified with ImageJ software.

Statistics

All values are expressed as mean \pm SEM. A Student *t* test or ANOVA was used to assess the difference between two groups. Differences were considered statistically significant when $p < 0.05$.

Results

4-PBA induces peroxisome proliferation in cell cultures of primary murine M Φ s and the RAW M Φ cell line

To elucidate the role of peroxisomes in the M Φ inflammatory response, we sought to compare M Φ activation by the prototypical proinflammatory stimulus LPS between control M Φ s with normal abundance of peroxisomes and M Φ s in which peroxisomes are induced. For this purpose, we used 4-PBA, a nonclassical peroxisome proliferator that was shown by us and other investigators to proliferate peroxisomes in cell cultures of mouse (23) and human (24) fibroblasts and is independent of the peroxisome proliferator activated receptor (PPAR)- α . Immunofluorescence studies revealed that treatment with 4-PBA for 72 h induced peroxisome proliferation, as detected by staining for the peroxisomal biogenesis protein PEX14p [which is an ideal marker for the abundance of peroxisomes (25)] in various M Φ cultures, such as the RAW murine M Φ cell line, murine primary AMs, and murine primary PMs (Fig. 1A–F). Unexpectedly, treatment with 4-PBA in primary BMDMs did not induce peroxisome proliferation (Fig. 1G, 1H). Similarly, Western blot analyses confirmed that PEX14p was induced after 4-PBA treatment in RAW M Φ s (Supplemental Fig. 1A) but not in primary BMDMs (Supplemental Fig. 1B).

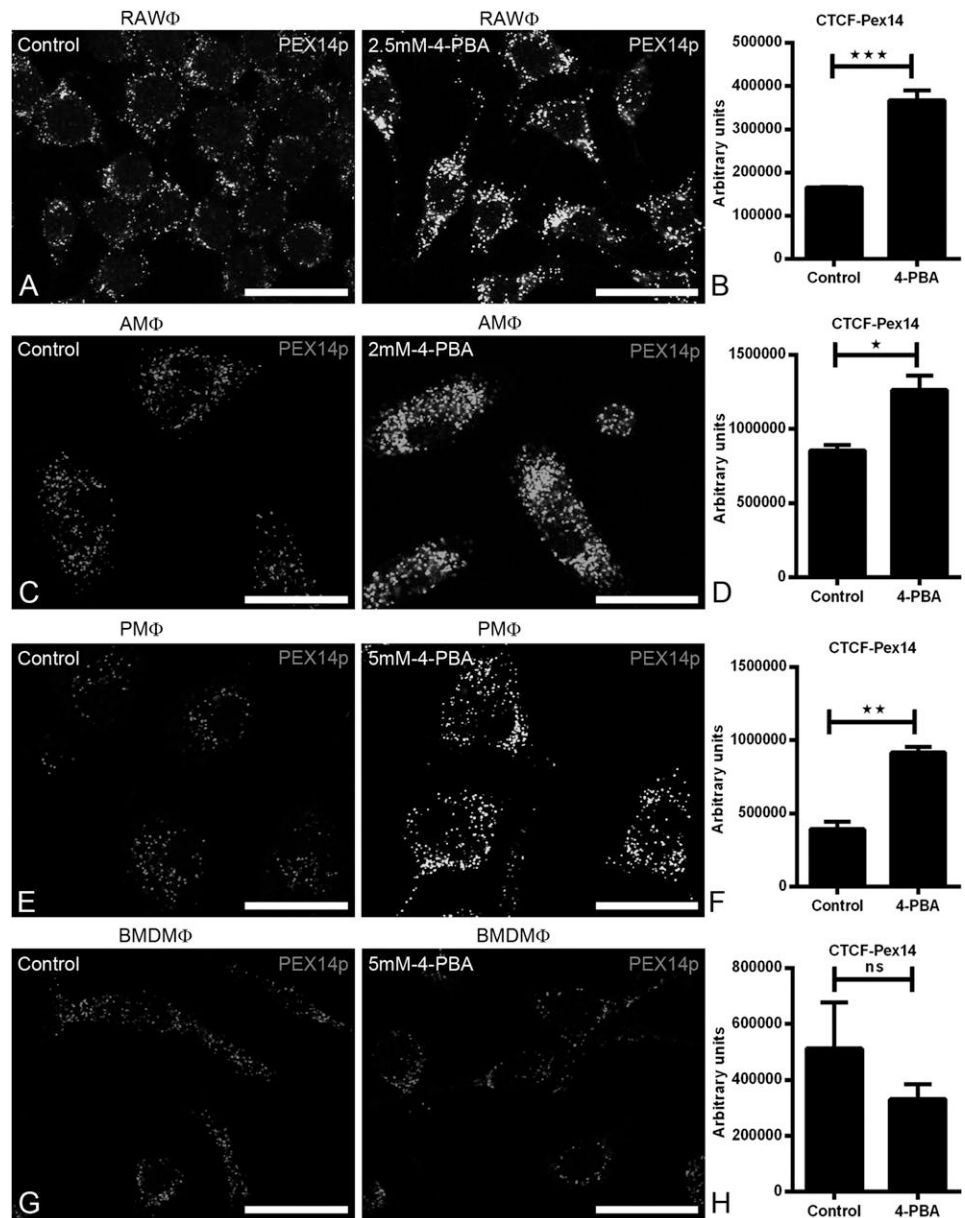
In summary, treatment with the peroxisome proliferator 4-PBA for 72 h induces peroxisome proliferation in murine primary AMs, primary PMs, and RAW M Φ s but not in primary BMDMs.

Induction of peroxisomes in M Φ s inhibits the LPS-induced proinflammatory response

Next, untreated control and 4-PBA-treated M Φ s were stimulated with LPS, and the induction of proinflammatory proteins was analyzed by immunofluorescence, Western blot analysis, and ELISA. LPS stimulation in primary AMs led to a strong increase in the staining for COX-2, a typical LPS-induced proinflammatory protein (18) involved in the production of proinflammatory PGs (Fig. 2A, middle panel). In contrast, AMs pretreated with 4-PBA for 72 h showed a very weak staining for COX-2 after LPS stimulation (Fig. 2A, right panel). Similarly, Western blot analyses confirmed that the LPS-induced upregulation of COX-2 was significantly reduced in 4-PBA-treated-RAW M Φ s and PMs (Fig. 2B, 2C, Supplemental Fig. 1C, 1D). Interestingly, treatment of RAW M Φ s with 4-PBA for only 2 h prior to LPS stimulation did not block LPS-induced COX-2 (Fig. 2B). Because 4-PBA did not induce peroxisomes in primary BMDMs, these cells were used as controls to test the peroxisome-independent effects of this compound. Accordingly, treatment with 4-PBA did not decrease LPS-induced COX-2 induction in BMDMs (Fig. 2D, Supplemental Fig. 1E). Unexpectedly, treatment with 4-PBA at a higher concentration (5 mM) enhanced LPS-dependent upregulation of COX-2 in BMDMs (Fig. 2D, Supplemental Fig. 1E).

To further substantiate the role of peroxisomes in M Φ s, two other peroxisome inducers, HU and L-sulforaphane (L-SF) (26), were applied. Pretreatment with HU or L-SF increased the protein abundance of PEX14p (Supplemental Fig. 2A, 2B) and subsequently blocked LPS-induced upregulation of COX-2 in RAW M Φ s (Supplemental Fig. 2C, 2D).

FIGURE 1. 4-PBA induces peroxisome proliferation in murine MΦs. RAW MΦs (**A** and **B**), primary murine AMs (**C** and **D**), primary murine PMs (**E** and **F**), and primary murine BMDMs (**G** and **H**) were cultured as described in *Materials and Methods*. Cells were left untreated (control) or treated with 4-PBA at the indicated concentration for 72 h and subjected to immunofluorescence analysis using an Ab against the peroxisomal marker protein PEX14p. Bar graphs shown the mean (\pm SEM) corrected total cell fluorescence (CTCF) quantified from images obtained from three independent experiments using ImageJ software. Scale bars, 50 μ m. * $p \leq 0.05$, ** $p \leq 0.01$, *** $p \leq 0.001$, Student *t* test. ns, not significant.



Recently, the global anti-inflammatory effect of 4-PBA in a LPS-induced lung inflammation model was suggested to be mediated via inhibition of endoplasmic reticulum (ER) stress (27). However, the concentration of 4-PBA (2.5 mM) used in our experimental setup did not inhibit LPS-induced ER stress, as indicated by ThT (Supplemental Fig. 2E). In contrast, a higher concentration of 4-PBA (5 mM) inhibited LPS-induced ER stress (Supplemental Fig. 2E). If the anti-inflammatory property of 4-PBA was mediated via inhibition of ER stress, then treatment of BMDM with 4-PBA should not inhibit ER stress. However, ThT staining in BMDMs revealed that LPS stimulation increased the intensity of ThT staining, and it was blocked when the cells were pretreated with 5 mM 4-PBA (Supplemental Fig. 2F).

To investigate a more global role for peroxisomes in the inflammatory response in MΦs, we measured important inflammatory cytokines by ELISA. 4-PBA-treated AMs, PMs, and RAW MΦs secreted significantly lower amounts of the proinflammatory cytokines TNF- α , IL-6, and IL-12 after stimulation by LPS in comparison with the respective controls (Fig. 2E). In contrast, pretreatment of BMDMs with 4-PBA did not reduce, but rather

stimulated, the expression of the proinflammatory cytokines secreted after LPS stimulation at higher concentrations of 4-PBA (Fig. 2F). Interestingly, ELISA measurements also revealed that the concentration of the anti-inflammatory cytokine IL-10 was significantly increased in 4-PBA-treated RAW MΦs stimulated with LPS (Fig. 2G). In contrast, 4-PBA treatment dose dependently reduced the LPS-induced secretion of the anti-inflammatory cytokine IL-10 in BMDMs (Fig. 2G). However, IL-10 was not detected by ELISA in PMs.

These results indicate that peroxisome induction in murine MΦs leads to suppression of the proinflammatory phenotype in these cells, which is independent of ER stress.

Knockdown of peroxisome biogenesis in MΦs causes a proinflammatory phenotype

The inhibitory effects of peroxisome induction on LPS-dependent upregulation of proinflammatory proteins may suggest that peroxisomes affect the proinflammatory phenotype of MΦs. To substantiate this hypothesis, we tested the proinflammatory response in MΦs, in which specific peroxisomal functions were modulated. Using an

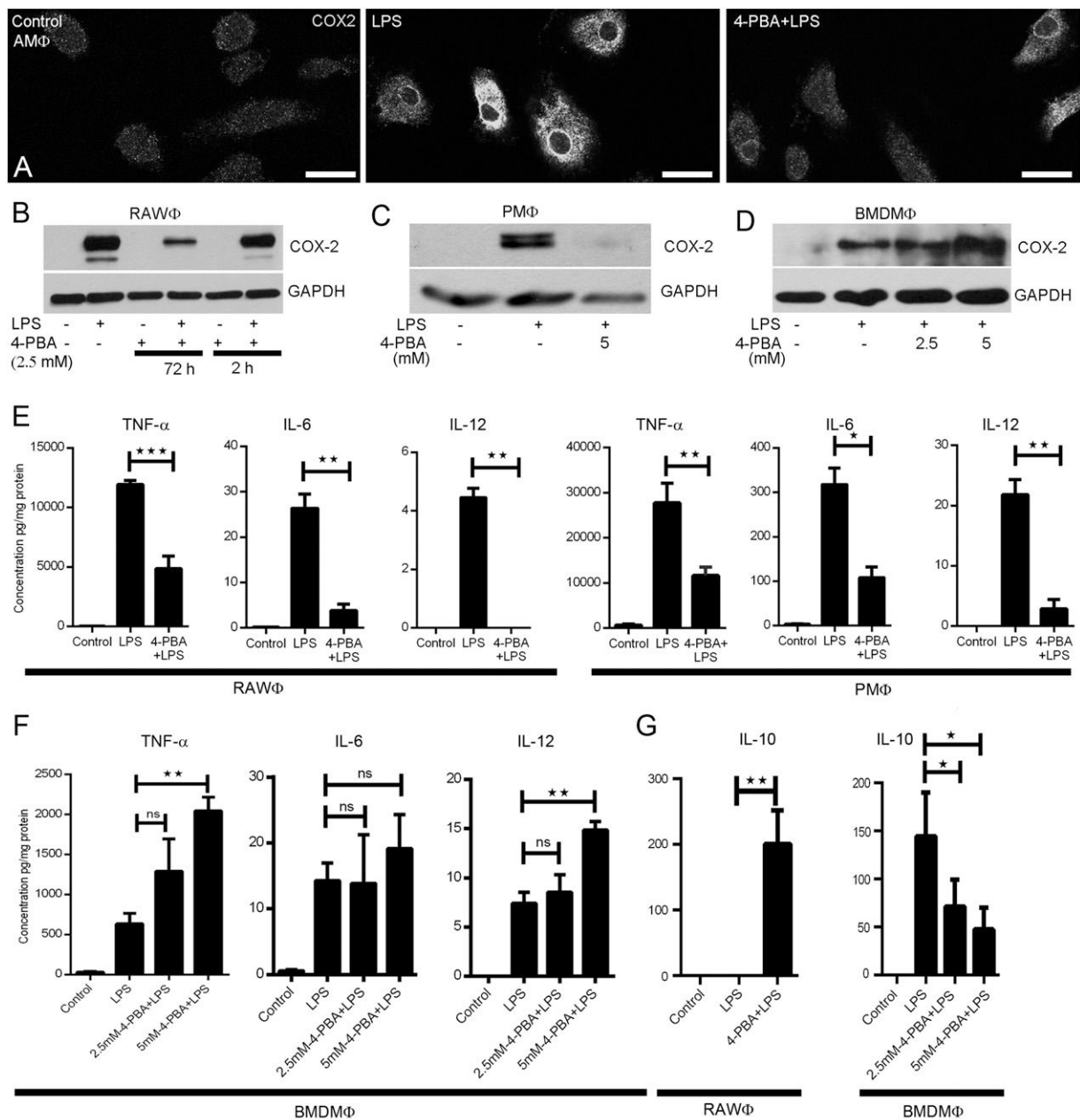
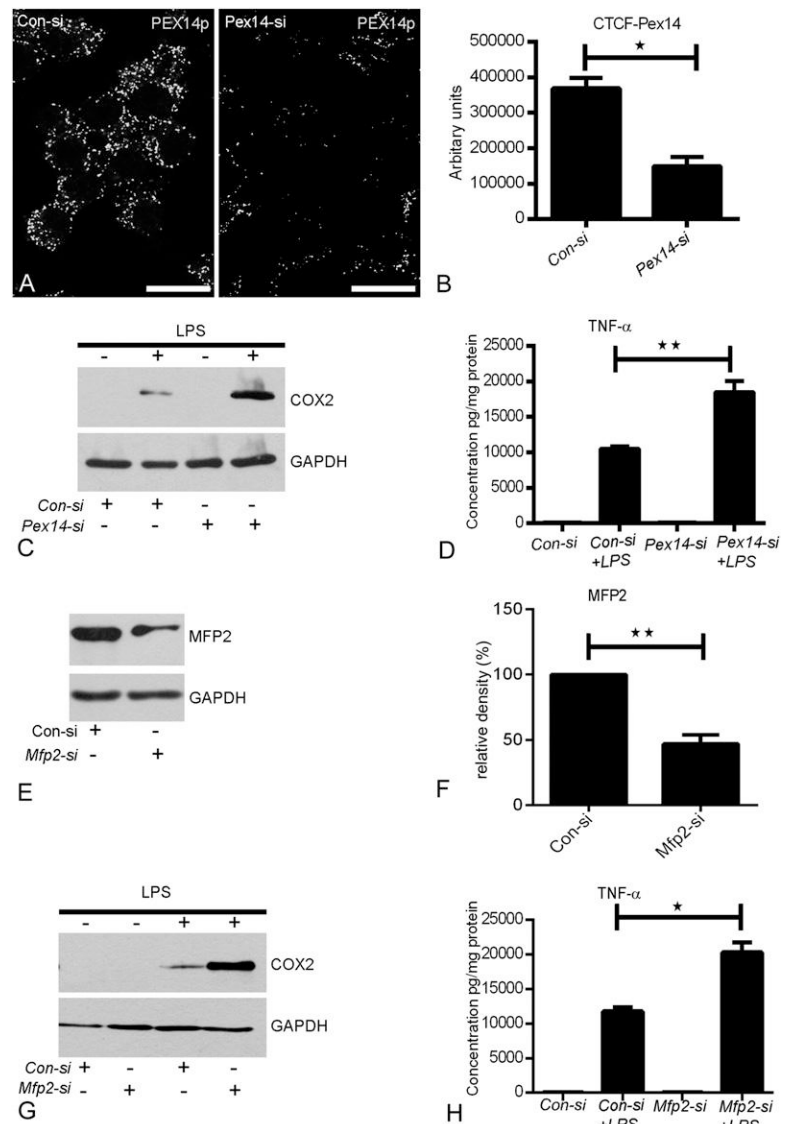


FIGURE 2. Treatment with 4-PBA abrogates the LPS-induced proinflammatory response. **(A)** Control untreated and 4-PBA-treated (72 h) primary AMs were stimulated with LPS (100 ng/ml) for 12 h and subjected to immunofluorescence analysis using an Ab against COX-2. A representative image from three independent experiments is shown. Scale bars, 30 μm. **(B–D)** The indicated MΦ cultures were treated with 4-PBA for 72 or 2 h as represented or left untreated, after which the medium was replaced with medium containing LPS (100 ng/ml) for an additional 12 h. Then cells were lysed, and the proteins were subjected to Western blot analyses and sequentially probed with Abs against COX-2 and GAPDH. A representative blot from three independent experiments is shown. **(E–G)** The indicated cells were left untreated or treated with 4-PBA for 72 h, after which the medium was replaced by medium containing LPS (100 ng/ml) for 12 h. The culture supernatants were subjected to ELISA for TNF-α, IL-6, IL-12, and IL-10. Data represent the mean (± SEM) concentration of the indicated cytokine normalized to the total protein content of the cells from three independent experiments. * $p \leq 0.05$, ** $p \leq 0.01$, *** $p \leq 0.001$, Student *t* test. ns, not significant.

siRNA-mediated approach, we targeted the peroxisomal biogenesis protein PEX14p, because earlier reports demonstrated that knockout of peroxisomal biogenesis proteins cause a lack of functional peroxisomes (3, 4, 28). Immunofluorescence studies revealed an efficient knockdown of PEX14p in RAW MΦs (Fig. 3A, 3B). Further, Western blot and ELISA analysis indicated that treatment with LPS in *Pex14* siRNA-transfected RAW MΦs significantly increased the protein levels of COX-2 and TNF-α in comparison with control siRNA-transfected RAW MΦs stimulated with LPS (Fig. 3C, 3D, Supplemental Fig. 3A).

Peroxisome deficiency may be coupled with mitochondrial alterations, including effects on the respiratory chain (3). Thus, it is conceivable that the regulatory effect on COX-2 expression might be indirectly caused by disturbance of the mitochondrial respiratory chain. To test this hypothesis, RAW MΦs were treated with the complex III inhibitor antimycin A, and mitochondrial dysfunction was evaluated by staining with MitoTracker (Supplemental Fig. 3B), which requires an intact mitochondrial potential to be incorporated into the mitochondria. Indeed, in cells treated with antimycin A, MitoTracker staining shifted from a mitochondrial pattern to a nuclear

FIGURE 3. Knockdown of peroxisomal genes leads to an increase in LPS-induced COX-2 and TNF- α . (**A** and **B**) RAW M Φ s were transfected with control-siRNA (Con-si) or *Pex14*-siRNA (Pex14-si) as indicated for 48 h. The knockdown was verified by immunofluorescence staining using an Ab against PEX14p. Scale bar, 30 μ m. (**B**) Data represent the mean (\pm SEM) corrected total cell fluorescence (CTCF) quantified from images obtained from three independent experiments using ImageJ software. (**C** and **D**) RAW M Φ s were transfected with control siRNA (Con-si) or *Pex14* siRNA (Pex14-si) as indicated for 48 h, after which the medium was replaced with medium containing LPS (100 ng/ml) for 12 h. (**C**) The isolated proteins were subjected to Western blot analyses and sequentially probed with Abs against COX-2 and GAPDH. (**D**) The culture supernatants were subjected to TNF- α ELISA. Data represent the mean (\pm SEM) concentration of TNF- α normalized to the total protein content of the cells ($n = 3$). (**E** and **F**) RAW M Φ s were transfected with control siRNA (Con-si) or *Mfp2* siRNA (Mfp2-si) for 48 h. (**E**) The knockdown was verified by Western blot analyses using an Ab against MFP2. A representative image of three independent experiments is shown. (**F**) Data are mean (\pm SEM) densitometric values of MFP2 normalized to the respective GAPDH obtained from three independent Western blot images ($n = 3$). (**G** and **H**) RAW M Φ s were transfected with control siRNA (Con-si) or *Mfp2*-siRNA (Mfp2-si) for 48 h, after which the medium was replaced with medium containing LPS (100 ng/ml) for 12 h. (**G**) The isolated proteins were subjected to Western blot analyses using COX-2 and GAPDH Abs. (**H**) The culture supernatants obtained were subjected to TNF- α ELISA. Data represent the mean (\pm SEM) concentration of TNF- α normalized to the total protein content of the cells ($n = 3$). n represents the number of experiments. * $p \leq 0.05$, ** $p \leq 0.01$, Student t test. ns, not significant.



pattern, indicating mitochondrial dysfunction (Supplemental Fig. 3B). Upon treatment with LPS, the COX-2 protein levels in antimycin A-treated cells were downregulated in comparison with control cells stimulated with LPS (Supplemental Fig. 3C). Thus, mitochondrial dysfunction per se may not induce upregulation of COX-2 protein in LPS-treated M Φ s.

To determine a potential role for the peroxisomal β -oxidation machinery in the regulation of COX-2, we knocked down *Mfp2*, a gene encoding a central peroxisomal β -oxidation enzyme, in RAW M Φ s (Fig. 3E, 3F). Similar to *Pex14* siRNA-transfected cells, stimulation with LPS in *Mfp2* siRNA-transfected RAW M Φ s led to a pronounced increase in COX-2 and TNF- α protein levels in comparison with LPS-treated control siRNA-transfected RAW M Φ s (Fig. 3G, 3H, Supplemental Fig. 3D). In summary, these results show that peroxisomes and their β -oxidation machinery negatively regulate COX-2 and TNF- α protein expression.

Regulation of COX-2 in 4-PBA-treated M Φ s via a posttranscriptional mechanism

TLR4-mediated signaling to proinflammatory genes is tightly regulated at the transcriptional level via the transcription factors NF- κ B and activator protein-1 (AP-1). Because LPS-dependent upregulation of proinflammatory proteins is suppressed in 4-PBA-

treated M Φ s, we hypothesized that induction of peroxisomes may affect the activation of these transcription factors. However, treatment with 4-PBA did not block LPS-induced activation of NF- κ B (as determined by the nuclear translocation of the NF- κ B subunit p65) (Fig. 4A–C) or AP-1 (as determined by phosphorylation of c-jun) (Fig. 4D–F). Accordingly, real-time PCR analysis revealed that LPS-induced mRNA expression of COX-2 and TNF- α were not reduced, but rather were increased in 4-PBA-treated RAW M Φ s in comparison with controls (Fig. 4G). Moreover, real-time PCR analysis showed that LPS-dependent induction of COX-2 and TNF- α mRNA levels was comparable in *Pex14* siRNA-, *Mfp2* siRNA-, and control siRNA-transfected M Φ s (Fig. 4H, 4I).

Because treatment with 4-PBA did not interfere with the transcriptional upregulation, we analyzed whether 4-PBA affects COX-2 protein stability. PMs were stimulated with LPS for 12 h and then treated with CHX for 2, 4, and 6 h, followed by Western blot analyses of COX-2 protein. In control PMs, COX-2 was not significantly reduced after up to 4 h of CHX treatment, and a reduction in COX-2 protein levels was only apparent after 6 h. In contrast, in 4-PBA-treated PMs, a reduction in COX-2 protein levels was evident as early as 2 h after CHX treatment and continued to decrease at 4 and 6 h (Fig. 5A, 5B). The calculated protein half-lives indicate that LPS-induced COX-2 protein has a much shorter half-life in 4-PBA-treated M Φ s (Fig. 5B).

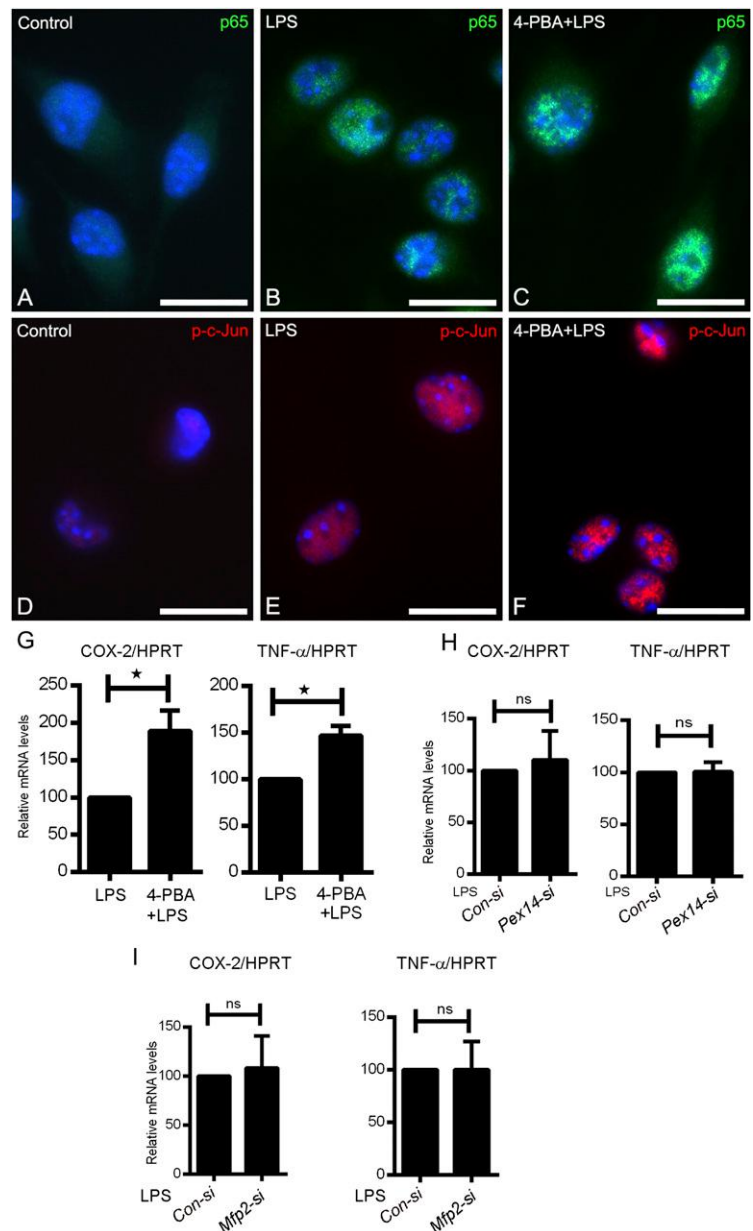


FIGURE 4. Treatment with 4-PBA does not block the LPS-induced activation of NF- κ B and AP-1 signaling pathways. (A–F) RAW MΦs were left untreated or were treated with 4-PBA for 72 h. Medium was replaced with medium containing LPS (100 ng/ml) and incubated for 1 h. The cells were fixed as described in *Materials and Methods* and subjected to immunofluorescence staining. Scale bars, 25 μ m. (A–C) A representative immunofluorescence staining against total p65 ($n = 3$). Hoechst 33,342 was used to stain the nucleus. (D–F) A representative immunofluorescence staining against phospho c-jun ($n = 3$). Hoechst 33,342 was used to stain the nucleus. (G–I) Real-time PCR analyses of COX-2 and TNF- α in RAW MΦs treated with 4-PBA (72 h) or transfected with the indicated siRNA (48 h) and stimulated with LPS (100 ng/ml) for 12 h. Expression of the housekeeping gene HPRT was used for normalization. The LPS-induced expression of COX-2 and TNF- α in control MΦs or control siRNA-transfected MΦs was taken as 100%, and the relative expression of these genes after LPS treatment in 4-PBA-treated/*Pex14*-siRNA/*Mfp2*-siRNA-transfected MΦs is shown. Data represent the mean (\pm SEM) relative fold induction from three independent experiments. n represents the number of experiments. * $p \leq 0.05$, Student t test. ns, not significant.

Because observations in RAW MΦs are similar to those in primary AMs and PMs (Figs. 1, 2), most of the following experiments were conducted in RAW MΦs (unless specified) to minimize the number of animals sacrificed.

To evaluate whether the observed protein degradation was mediated via a proteasomal or lysosomal pathway, we applied two chemical inhibitors to block these pathways. The concentration of the chemicals used was based on existing literature (29–32). However, pretreatment with proteasomal (MG132, epoxomicin) and lysosomal (3-methyladenine, chloroquine) inhibitors for 2 h did not block 4-PBA-mediated COX-2 protein degradation (Fig. 5C). Similar to our present findings, recent studies demonstrated a lysosome and proteasome-independent protein-degradation pathway for COX-2. This new COX-2-degradation pathway can be blocked by specific COX-2 enzyme inhibitors (33). To evaluate this possibility, 4-PBA-treated RAW MΦs were treated with the specific COX-2 inhibitor NS-398 and the general COX inhibitor S-flurbiprofen 2 h prior to the addition of LPS. As demonstrated in Fig. 5D and 5E, the blunted LPS induction of COX-2 protein was restored by these two inhibitors in 4-PBA-treated RAW MΦs.

In summary, LPS-induced COX-2 protein is destabilized in peroxisome-induced cells, which can be blocked by the inhibition of COX-2 enzyme activity but not by blocking classical protein-degradation pathways.

Regulation of COX-2 via peroxisome-derived extrinsic metabolite(s)

Because exposure of 4-PBA-treated MΦs to LPS led to release of the anti-inflammatory cytokine IL-10 into the medium, we specifically evaluated the effect of this cytokine on LPS-induced COX-2 expression. Pretreatment of RAW MΦs with recombinant mouse IL-10 for 24 h induced protein expression of the anti-inflammatory gene HO-1, as described in earlier reports (34), which was blocked when IL-10 was subjected to heat inactivation at 95°C for 30 min (Fig. 6A). However, pretreatment with IL-10 for 2 or 24 h did not block the upregulation of COX-2 by LPS (Fig. 6B). Alternatively, Cox-2 regulation in *Mfp2*-knockdown cells may implicate a role for peroxisomal β -oxidation machinery in this pathway. Hence, we asked whether a peroxisome-derived lipid mediator is involved in LPS-dependent regulation of COX-2. To test this, we collected

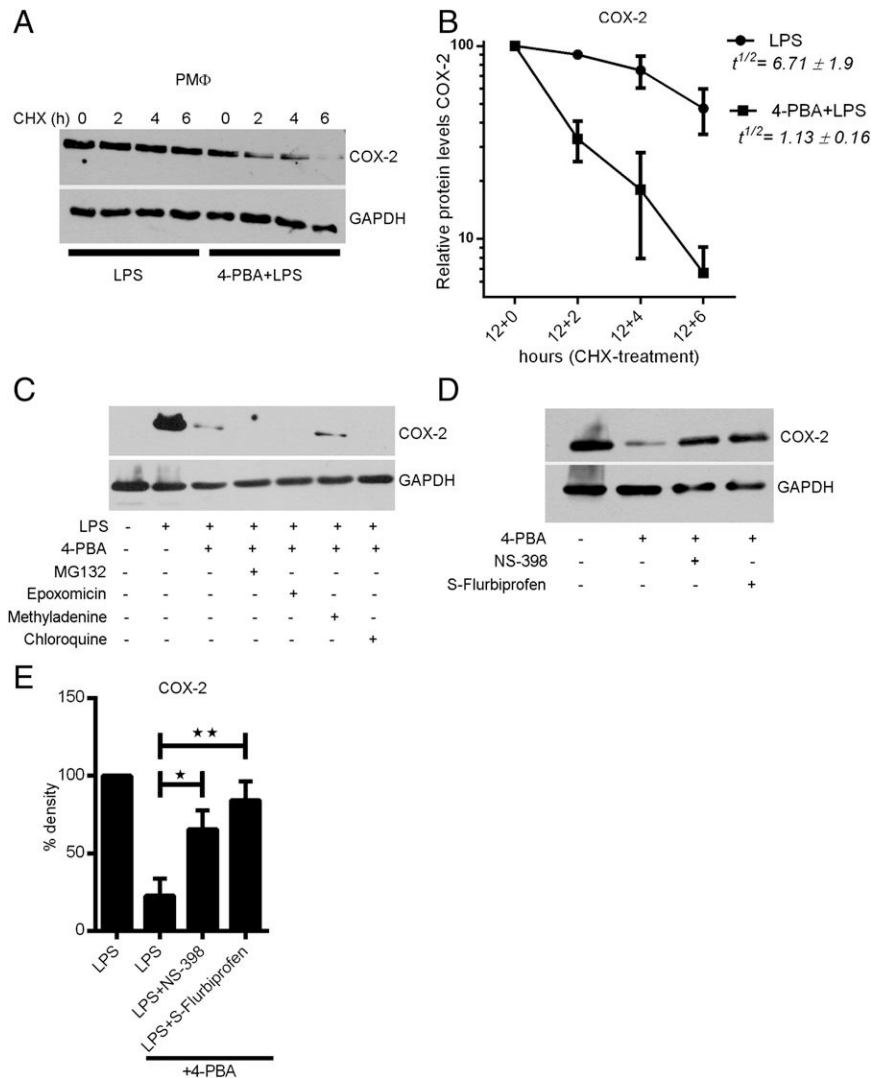


FIGURE 5. 4-PBA treatment induces protein degradation of COX-2, which is reversed by COX-2 inhibitors. **(A and B)** Primary murine PMs, treated or not with 4-PBA (4 mM) for 72 h, were stimulated with LPS (100 ng/ml) for an additional 12 h. The medium was replaced with medium containing CHX (100 μ M) for the indicated times. The cells were lysed, and proteins were isolated, subjected to Western blot analyses, and sequentially probed with Abs against COX-2 and GAPDH. **(A)** A representative Western blot image from three independent experiments. **(B)** Data represent the quantified densitometric values (\pm SEM) obtained for COX-2 normalized to the respective GAPDH from three independent experiments and are shown as relative protein levels for different time points in comparison with protein levels at time point 0 h of CHX. $t^{1/2}$ represent the half-life calculated by regression analysis of an Excel graph for the logarithmic scale of protein abundance versus time of CHX. **(C)** Control untreated or 4-PBA-treated RAW MΦs were treated with the indicated proteasomal and lysosomal inhibitors for 2 h, followed by the addition of LPS (100 ng/ml). The cells were lysed after 12 h of incubation, and the proteins were isolated, subjected to Western blot analyses, and probed sequentially with Abs against COX-2 and GAPDH. A representative Western blot image of three independent experiments is shown. **(D and E)** Control untreated or 4-PBA-treated RAW MΦs were treated with the indicated COX-2 inhibitors for 2 h, followed by the addition of LPS (100 ng/ml) and incubation for an additional 12 h. The isolated proteins were subjected to Western blot analyses and probed using Abs against COX-2 and GAPDH. **(D)** Representative Western blot image of three independent experiments. **(E)** Collective mean densitometric values for COX-2 normalized to the respective GAPDH values from three experiments are shown as relative fold induction. * $p \leq 0.05$, ** $p \leq 0.01$, ANOVA.

conditioned medium from 4-PBA-treated RAW MΦs stimulated with LPS and added them to naive RAW MΦs with an additional dose of LPS (100 ng/ml). We chose conditioned medium obtained from RAW MΦs treated with 5 mM 4-PBA because this concentration gave the maximum increase for peroxisomal protein PEX14p in our experimental set-up (Supplemental Fig. 4A). Interestingly, conditioned medium from 4-PBA-treated RAW MΦs, but not from control RAW MΦs, reduced LPS induction of COX-2 in naive RAW MΦs (Fig. 6C). To further evaluate the nature of this secreted cell-extrinsic anti-inflammatory mediator(s), conditioned medium was subjected to heat inactivation; however, this did not block its ability to reduce the LPS induction of COX-2 in naive RAW MΦs (Fig. 6D). Further, conditioned medium from murine RAW MΦs was

added to primary peripheral blood monocyte-derived human MΦs to test a potential species specificity of this effect. Conditioned medium from control RAW MΦs had minimal effects on the LPS induction of COX-2 in primary monocyte-derived human MΦs. In contrast, conditioned medium from 4-PBA-treated MΦs blunted the LPS-dependent induction of COX-2 protein in primary monocyte-derived human MΦs (Fig. 6E).

Next, the conditioned medium obtained from control RAW MΦs and 4-PBA-treated RAW MΦs stimulated with LPS were analyzed by liquid chromatography-tandem MS (LC-MS/MS) for the presence of lipid mediators. As expected, the levels of AA that are the substrate of COX-2 were higher in conditioned medium from 4-PBA-treated RAW MΦs (Fig. 6F). Interestingly,

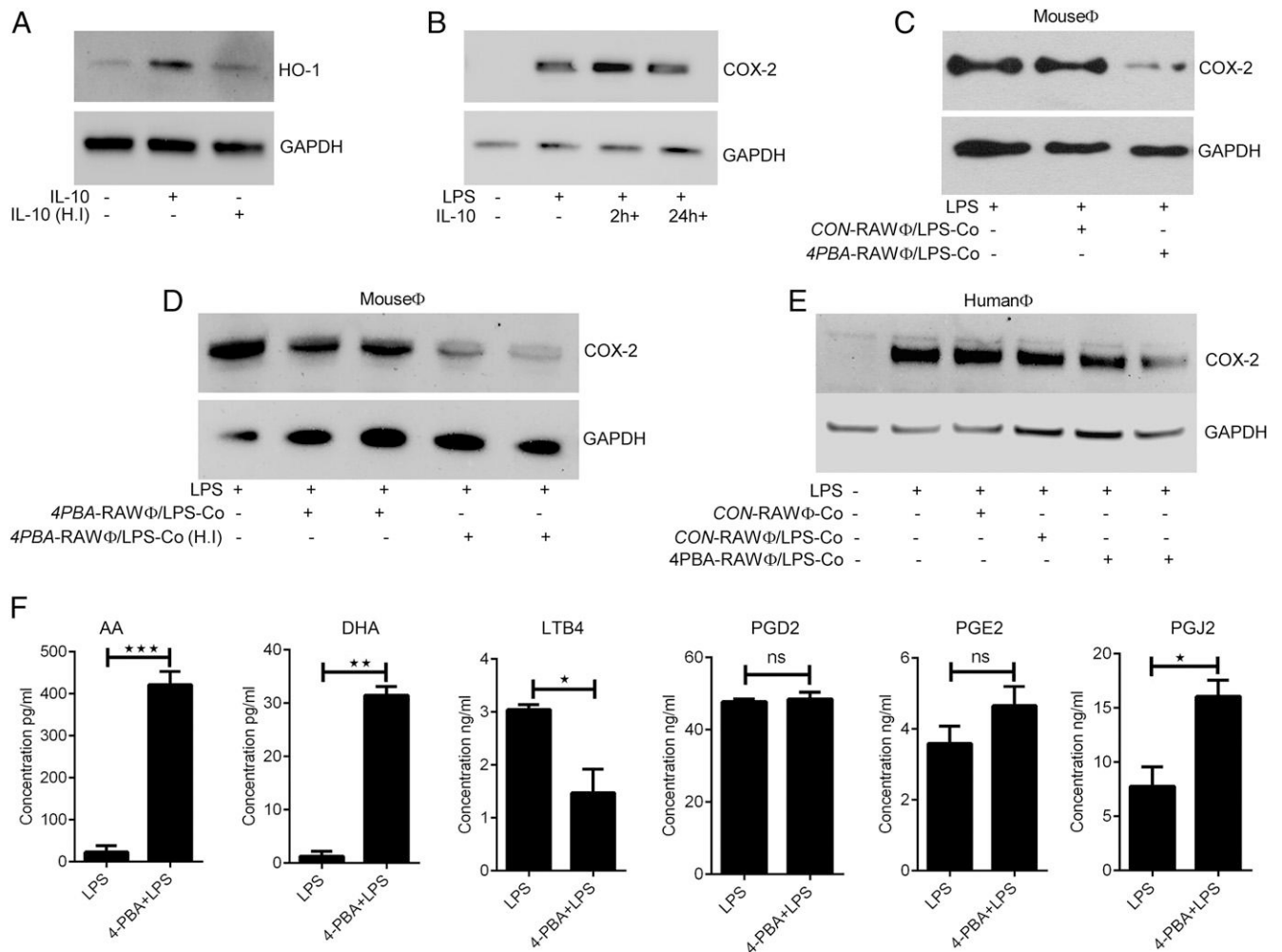


FIGURE 6. Conditioned medium from 4-PBA-treated MΦs partially blocks LPS-induced COX-2 in naive MΦs. **(A)** Western blot analyses of RAW MΦs that were left untreated or treated with mouse rIL-10 (20 ng/ml) or heat-inactivated (H.I.) mouse rIL-10 (20 ng/ml) for 24 h. The blot was sequentially probed with Abs for HO-1 and GAPDH. **(B)** RAW MΦs were treated with mouse rIL-10 for 2 or 24 h, as indicated, before the addition of LPS (100 ng/ml). The cells were incubated for an additional 12 h, subjected to Western blot analyses, and sequentially probed with Abs against COX-2 and GAPDH. **(C)** Conditioned medium, collected from LPS-stimulated RAW MΦs that were left untreated or were treated with 4-PBA, was added to fresh RAW MΦs with an additional dose of LPS (100 ng/ml) and incubated for 12 h. The proteins collected were analyzed by Western blot using Abs against COX-2 and GAPDH. **(D)** Conditioned medium collected from LPS stimulated 4-PBA-treated RAW MΦs was used as such or subjected to heat-inactivation (H.I.) at 95°C for 30 min. An additional dose of LPS (100 ng/ml) was added to the conditioned medium and applied to fresh RAW MΦs. After incubation for 12 h, the proteins collected were used for Western blot analyses and probed with Abs against COX-2 and GAPDH. **(E)** Conditioned medium, collected from LPS-stimulated RAW MΦs that were left untreated or were treated with 4-PBA, was added to primary human MΦs, as indicated, with an additional dose of LPS (1000 ng/ml). The cells were incubated for an additional 12 h, followed by Western blot analyses using Abs against COX-2 and GAPDH. **(F)** Conditioned medium, collected from LPS-stimulated RAW MΦs that were left untreated or pretreated with 4-PBA (5 mM), was analyzed by LC-MS/MS, as described in *Materials and Methods*. Data are the mean (\pm SEM) concentration of the indicated lipids per milliliter of cell medium. * $p \leq 0.05$, ** $p \leq 0.01$, *** $p \leq 0.001$, Student *t* test. ns, not significant.

DHA, which is the precursor of many lipid resolution mediators, and PGJ₂, metabolites of which are anti-inflammatory, were also significantly higher in conditioned medium from 4-PBA-treated RAW MΦs in comparison with conditioned medium obtained from LPS-treated control RAW MΦs (Fig. 6F). The concentration of the proinflammatory LTB₄, but not PGE₂/D₂, was significantly reduced in the conditioned medium from 4-PBA-treated MΦs (Fig. 6F).

In summary, peroxisome-derived regulation of COX-2 may be mediated by a heat-stable extrinsic factor(s) (most likely lipid in nature) released into the cell supernatant but not by IL-10.

Physiological induction of peroxisomes by LPS to restore homeostasis

Next, we asked whether treatment of MΦs with 4-PBA might affect the polarization to M2 MΦs that could explain the anti-inflammatory nature of these MΦs. To this end, we determined

levels of the M1 marker CD86 and the M2 marker CD36 by flow cytometry. To our surprise, the M1 marker CD86, but not the M2 marker CD36, was significantly higher in 4-PBA-treated MΦs in comparison with untreated control MΦs (Fig. 7A). Further, real-time PCR analysis revealed that the M1 marker inducible NO synthase was reduced, whereas IL-6 was induced, in 4-PBA-treated MΦs (Supplemental Fig. 4B). Similarly, expression of the M2 marker Arg-1 was significantly reduced and that of IL-10 was induced in 4-PBA-treated MΦs (Supplemental Fig. 4B). Stimulation with LPS induced expression of the M2 markers Arg-1 and IL-10 in 4-PBA-treated MΦs in comparison with control MΦs. In contrast, M1 markers inducible NO synthase and IL-6 did not change markedly (Supplemental Fig. 4B), indicating that 4-PBA treatment may not skew murine MΦs to the classical M2 phenotype that exhibits reduced gene expression of proinflammatory cytokines.

Next, we analyzed whether the peroxisome-dependent regulation of COX-2 may serve as a physiological negative-feedback mechanism in MΦs activated with LPS. To explore this possibility, BMDMs were treated with LPS for different periods of time. LPS stimulation induced PEX14p, as observed by Western blot, with a strong increase at 48 h (Fig. 7B, 7C). Strikingly, LPS induction of COX-2 protein was decreased after 48 and 72 h in comparison with 24 h (Fig. 7B). However, at the mRNA level, COX-2 was differentially regulated, with a maximum peak at 48 h (Fig. 7D). In conclusion, these findings show that upregulation of PEX14p correlates with the late-phase inhibition of COX-2 protein in LPS-activated MΦs. In conclusion, our findings indicate that induction of peroxisomes is a physiological anti-inflammatory response at late time points that potentially restores immune homeostasis.

Next, we also explored whether this peroxisome-dependent anti-inflammatory effect on MΦs was TLR4 specific. To address this we used two additional TLR ligands: LTA (a major component of Gram-positive bacteria) for TLR2 and poly I:C (mimicking double-stranded viral RNA) for TLR3. Treatment with LTA induced the protein expression of COX-2, which was blocked when cells were pretreated with 4-PBA for 72 h. In contrast, the minor induction of COX-2 upon poly I:C stimulation was not affected by pretreatment of MΦs with 4-PBA (Fig. 7E). To summarize, peroxisome induction blocks LPS- and LTA-induced COX-2 expression but not poly I:C-mediated COX-2 induction.

Finally, we also tried to address the cell specificity of the peroxisome-mediated anti-inflammatory response in a nonimmune

cell type. For this purpose, we used primary MEFs. Treatment with 4-PBA at a concentration of 3.5 mM for 5 d induced peroxisomes (Supplemental Fig. 4C). In contrast to MΦs, MEFs had a constitutive expression of COX-2, and stimulation with LPS only caused a minor induction of COX-2 (Fig. 7F). However, treatment with 4-PBA did not block COX-2 expression in MEFs (Fig. 7F). To summarize, peroxisome-dependent anti-inflammatory regulation of COX-2 may not exist in MEFs.

Discussion

Peroxisomes were initially described in 1954 as microbodies and were later identified in 1966 as organelles containing enzymes involved in H₂O₂ metabolism (35). In this study, we show that 4-PBA-mediated proliferation of peroxisomes leads to an attenuated LPS-mediated proinflammatory response in MΦs. In contrast, disturbing peroxisome function by knockdown of the peroxisome-specific genes *Pex14* and *Mfp2* causes an enhanced inflammatory response marked by an increase in the LPS-induced upregulation of proinflammatory proteins COX-2 and TNF-α, suggesting a direct immunomodulatory role for peroxisomes in MΦs.

4-PBA-mediated peroxisome induction exerts anti-inflammatory effects in MΦs

4-PBA is considered a nonclassical peroxisome proliferator, because it mediates peroxisome proliferation independent of PPAR-α and does not belong to the group of classical PPAR activators (23). To induce peroxisome proliferation, the primary choice is the classical PPAR agonists; however, in MΦ cultures, PPAR agonists

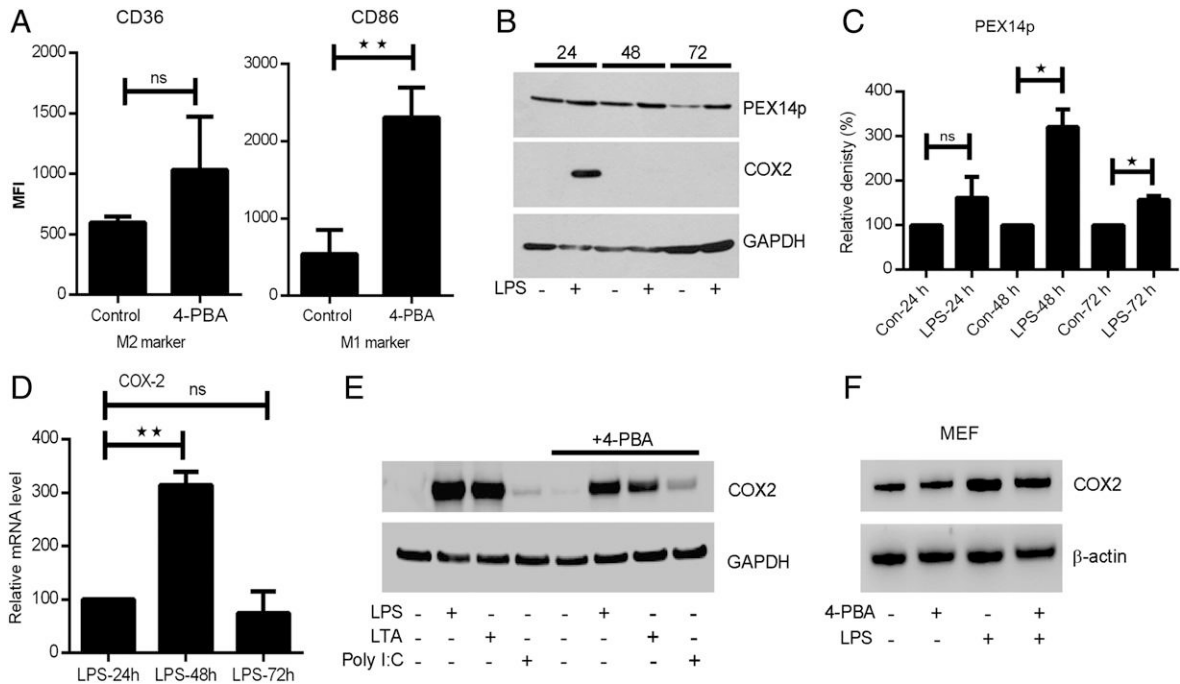


FIGURE 7. PEX14p upregulation correlates with the downregulation of LPS-induced COX-2 protein in MΦs. (A) RAW MΦs were left untreated or treated with 4-PBA (2.5 mM) for 72 h, stained with anti-mouse-CD86 (M1 marker) or anti-mouse-CD36 (M2 marker), and analyzed by flow cytometry as described in *Materials and Methods*. Data are the average mean fluorescence intensity (MFI) (± SEM) from three independent experiments. (B and C) Primary BMDM cultures were treated with LPS (100 ng/ml) for the indicated times. The proteins were isolated and analyzed by Western blot with Abs against PEX14p, COX-2, and GAPDH. (B) A representative Western blot image from three independent experiments. (C) Data are the quantified densitometric values (± SEM) obtained for COX-2 normalized to the respective GAPDH from three independent experiments and represented as relative fold inductions (D) Primary BMDM cultures were treated with LPS (100 ng/ml) for the indicated times. The RNA isolated was analyzed by real-time PCR for the expression of COX-2, which was normalized to the expression of HPRT and shown as relative fold inductions (n = 3). (E) RAW MΦs that were left untreated or treated with 4-PBA (2.5 mM) for 72 h were stimulated with LPS (100 ng/ml), LTA (5 μg/ml), and poly I:C (20 μg/ml) for an additional 16 h. The proteins were isolated and analyzed by Western blot with Abs against COX-2 and GAPDH. (F) MEFs that were left untreated or treated with 4-PBA (3.5 mM) for 5 d were stimulated with LPS (1 μg/ml) for 16 h. The proteins were isolated and analyzed by Western blot with Abs against COX-2 and β-actin. *p ≤ 0.05, **p ≤ 0.01, Student t test. ns, not significant.

exhibit pleiotropic anti-inflammatory effects, such as inhibition of NF- κ B and AP-1 signaling pathways that leads to the suppression of various proinflammatory genes (36). Thus, the use of a classical PPAR agonist would make it almost impossible to distinguish the specific effects of peroxisome proliferation from the described anti-inflammatory effects of PPAR activation. However, it is noteworthy that peroxisome proliferation by these agonists was never analyzed in connection with the anti-inflammatory effects observed. In this article, we report that 4-PBA is a potent inducer of peroxisomes in cell cultures of RAW M Φ s and various mouse primary M Φ s, such as AMs and PMs, but not primary BMDMs (Fig. 1). 4-PBA-mediated peroxisome proliferation subsequently downregulated the LPS-induced protein expression of the proinflammatory gene COX-2 and the proinflammatory cytokines TNF- α , IL-6, and IL-12. Similar results were observed with two other nonclassical peroxisome inducers: HU and L-SF. This conclusion is supported by the finding that 4-PBA treatment did not induce peroxisomes or provide an anti-inflammatory effect in BMDMs (Fig. 2). The importance of peroxisome proliferation to mediate the 4-PBA-dependent anti-inflammatory effect is also indicated by the observation that pretreatment with 4-PBA for 2 h, a period not sufficient for proliferation of peroxisomes, failed to abrogate LPS-induced COX-2 (Fig. 2). Additionally, a role for ER stress inhibition for these anti-inflammatory effects was ruled out, because the concentrations used in our experiments did not block ER stress (Supplemental Fig. 2). Furthermore, the anti-inflammatory effect of 4-PBA on COX-2 protein levels was not only TLR4 specific, it also was observed with the TLR2 ligand LTA but not with the TLR3 ligand poly I:C (Fig. 7E). TLR4 and TLR2 work as pathogen-associated molecular patterns for bacterial infection, whereas TLR3 is involved in a viral response. Because COX-2 was only weakly induced by the TLR3 ligand poly I:C, further studies need to be done to address whether there are specific differences in peroxisome-mediated anti-inflammatory responses upon stimulation with bacterial and viral agents.

Biological significance of peroxisomes in M Φ s

The homeostasis of M Φ s after proinflammatory activation is tightly controlled to prevent exacerbated pathological events. Activation of M Φ s is followed by a late-phase upregulation of anti-inflammatory proteins, such as Nod2, IL-10, and TGF- β , which act as inflammation suppressors/M Φ deactivators in an autocrine and paracrine fashion (37). The regulatory checkpoints for deactivation include transcriptional repression (repressors of signaling cascades) (37), posttranscriptional regulation (mRNA stability) (38), and translational silencing (39). These regulatory checkpoints exist independent of the M1-M2 paradigm of M Φ activation. Because proliferation of peroxisomes does not skew the M Φ s into a classical M2-like phenotype (Fig. 7A, Supplemental Fig. 4B), we propose that the upregulation of peroxisome proliferation may serve as an autoregulatory mechanism in M Φ s to protect against uncontrolled activation. This hypothesis is supported by our findings that knockdown of peroxisomal proteins led to an induction of proinflammatory proteins, indicating the existence of an intrinsic peroxisome-mediated regulation of proinflammatory proteins (Fig. 3). Moreover, the finding that LPS-dependent upregulation of PEX14p coincides with the downregulation of COX-2 (Fig. 7B) also supports this conclusion. Hence, we speculate that in vivo peroxisomes may act as late-phase inflammation suppressors at the posttranslational level to self-regulate inflammatory M Φ s. In line with this notion are the earlier findings that, in a mouse model of endotoxemia in vivo, peroxisomes are initially downregulated, followed by proliferation and increased abundance in the late phase of inflammation (40). Moreover, in the

earlier report, accumulation of nonfunctional peroxisomes was shown to aggravate the proinflammatory condition (40).

Mechanism of peroxisome-mediated anti-inflammatory regulation

COX-2, the inducible isoform of the PG synthase, is upregulated in inflammatory conditions and thought to have a major role in promoting inflammation via production of proinflammatory PGs (41). Peroxisome-dependent COX-2 regulation was mediated via a posttranslational mechanism independent of proteasomal and lysosomal protein degradation. These findings agree with previous reports showing that the COX-2 protein undergoes a distinct protein-degradation pathway in vitro as well as in vivo, which is dependent upon the substrate turnover (33, 42). Accordingly, LC-MS/MS analysis of conditioned medium from LPS-activated 4-PBA-treated M Φ s revealed a dramatic increase in the levels of free AA, which may induce the substrate-dependent suicidal pathway of COX-2, as shown by other investigators. Additionally, LC-MS/MS analysis revealed increased levels of PGJ₂ and DHA in the conditioned medium from 4-PBA-treated M Φ s. PG15d-PGJ₂ is anti-inflammatory in nature (43) and might be involved in the downregulation of proinflammatory proteins. Similarly, the increased levels of DHA that forms the backbone for lipid resolution mediators, such as resolvins, protectins, and maresins, may also have an impact on the anti-inflammatory nature of 4-PBA-treated M Φ s. Indeed, treatment of M Φ s with DHA was shown to downregulate the LPS induction of proinflammatory proteins (44, 45). Although the presence of peroxisome-derived cell extrinsic factors was confirmed, identification and individual application of these metabolites will be crucial to understand the exact nature of this phenomenon. Currently, we are characterizing the lipid metabolites produced in 4-PBA-treated M Φ s. Although our findings indicate that peroxisome-mediated effects on COX-2 expression may be M Φ specific (Fig. 7F), further characterization of the lipid mediators is necessary to evaluate the cell-type specificity of this phenomenon in other immune and nonimmune cell types. Peroxisome-mediated immunomodulation of M Φ inflammatory responses may open up new options for therapeutic interventions in chronic inflammatory conditions. 4-PBA is already in clinical use for treating a range of disorders, and phase II clinical trials for the treatment of cystic fibrosis were performed. Additionally, 4-PBA was shown to block LPS-induced expression of the proinflammatory cytokines TNF- α and IL-6 in an in vivo mouse model of lung inflammation (27). The beneficial effects of blocking proinflammatory proteins, such as COX-2 and TNF- α in various inflammatory disorders have been well documented. Moreover, the broad release of lipid-resolution mediators and the potent anti-inflammatory cytokine IL-10 further impact the resolution of inflammation. However, the lack of a PPAR-independent monospecific inducer of peroxisomes remains a limiting factor in exploring the complete potential of these organelles.

In summary, we showed that peroxisomes provide an anti-inflammatory phenotype to M Φ s and conclude that 4-PBA-mediated peroxisome proliferation may be beneficial for therapeutic interventions in chronic inflammatory disorders.

Acknowledgments

We thank Petra Hahn-Kohlberger, Andrea Textor (E.B.-V group), and Anette Sarti-Jacobi (S.I. group) for excellent technical assistance. We also thank Dr. Kashyap Krishnasamy (Department of Nephrology and Hypertension, Medical School Hannover) for valuable experimental discussions. Furthermore, we thank Prof. Dr. Denis I. Crane (School of Biomolecular and Physical Sciences, Griffith University, Brisbane, QLD, Australia) for providing the anti-PEX14 Ab and Privatdozent Dr. Christoph Rummel

(Faculty of Veterinary Medicine, Justus Liebig University Giessen) for providing some of the lipid standards.

Disclosures

The authors have no financial conflicts of interest.

References

- Colasante, C., J. Chen, B. Ahlemeyer, and E. Baumgart-Vogt. 2015. Peroxisomes in cardiomyocytes and the peroxisome/ Peroxisome proliferator-activated receptor-loop. *Thromb. Haemost.* 113: 452–463.
- Karnati, S., and E. Baumgart-Vogt. 2008. Peroxisomes in mouse and human lung: their involvement in pulmonary lipid metabolism. *Histochem. Cell Biol.* 130: 719–740.
- Baumgart, E., I. Vanhorebeek, M. Grabenbauer, M. Borgers, P. E. Declercq, H. D. Fahimi, and M. Baes. 2001. Mitochondrial alterations caused by defective peroxisomal biogenesis in a mouse model for Zellweger syndrome (PEX5 knockout mouse). *Am. J. Pathol.* 159: 1477–1494.
- Peeters, A., A. B. Shinde, R. Dirx, J. Smet, K. De Bock, M. Espeel, I. Vanhorebeek, A. Vanlander, R. Van Coster, P. Carmeliet, et al. 2015. Mitochondria in peroxisome-deficient hepatocytes exhibit impaired respiration, depleted DNA, and PGC-1 α independent proliferation. *Biochim. Biophys. Acta* 1853: 285–298.
- Khan, M., M. Contreras, and I. Singh. 2000. Endotoxin-induced alterations of lipid and fatty acid compositions in rat liver peroxisomes. *J. Endotoxin Res.* 6: 41–50.
- Contreras, M. A., M. Khan, B. T. Smith, A. M. Cimini, A. G. Gilg, J. Orak, I. Singh, and A. K. Singh. 2000. Endotoxin induces structure-function alterations of rat liver peroxisomes: Kupffer cells released factors as possible modulators. *Hepatology* 31: 446–455.
- Dhausi, G. S., C. D. Hanevold, and I. Singh. 1994. Impairment of peroxisomal beta-oxidation system by endotoxin treatment. *Mol. Cell. Biochem.* 135: 187–193.
- Dixit, E., S. Boulant, Y. Zhang, A. S. Lee, C. Odendall, B. Shum, N. Hacohen, Z. J. Chen, S. P. Whelan, M. Fransen, et al. 2010. Peroxisomes are signaling platforms for antiviral innate immunity. *Cell* 141: 668–681.
- Odendall, C., E. Dixit, F. Stavru, H. Biernie, K. M. Franz, A. F. Durbin, S. Boulant, L. Gehrke, P. Cossart, and J. C. Kagan. 2014. Diverse intracellular pathogens activate type III interferon expression from peroxisomes. *Nat. Immunol.* 15: 717–726.
- Facciotti, F., G. S. Ramanjaneyulu, M. Lepore, S. Sansano, M. Cavallari, M. Kistowska, S. Forss-Petter, G. Ni, A. Colone, A. Singhal, et al. 2012. Peroxisome-derived lipids are self antigens that stimulate invariant natural killer T cells in the thymus. *Nat. Immunol.* 13: 474–480.
- Oruqaj, G., S. Karnati, V. Vijayan, L. K. Kotarkonda, E. Boateng, W. Zhang, C. Ruppert, A. Günther, W. Shi, and E. Baumgart-Vogt. 2015. Compromised peroxisomes in idiopathic pulmonary fibrosis, a vicious cycle inducing a higher fibrotic response via TGF- β signaling. *Proc. Natl. Acad. Sci. USA* 112: E2048–E2057.
- Terlecky, S. R., L. J. Terlecky, and C. R. Giordano. 2012. Peroxisomes, oxidative stress, and inflammation. *World J. Biol. Chem.* 3: 93–97.
- Ahlemeyer, B., M. Gottwald, and E. Baumgart-Vogt. 2012. Deletion of a single allele of the Pex11 β gene is sufficient to cause oxidative stress, delayed differentiation and neuronal death in mouse brain. *Dis. Model. Mech.* 5: 125–140.
- Jedlitschky, G., E. Mayatepek, and D. Keppler. 1993. Peroxisomal leukotriene degradation: biochemical and clinical implications. *Adv. Enzyme Regul.* 33: 181–194.
- Diczfalusy, U., B. F. Kase, S. E. Alexson, and I. Björkhem. 1991. Metabolism of prostaglandin F2 alpha in Zellweger syndrome. Peroxisomal beta-oxidation is a major importance for in vivo degradation of prostaglandins in humans. *J. Clin. Invest.* 88: 978–984.
- Soehnlein, O., and L. Lindbom. 2010. Phagocyte partnership during the onset and resolution of inflammation. *Nat. Rev. Immunol.* 10: 427–439.
- Naidu, S., V. Vijayan, S. Santoso, T. Kietzmann, and S. Immenschuh. 2009. Inhibition and genetic deficiency of p38 MAPK up-regulates heme oxygenase-1 gene expression via Nrf2. *J. Immunol.* 182: 7048–7057.
- Vijayan, V., E. Baumgart-Vogt, S. Naidu, G. Qian, and S. Immenschuh. 2011. Bruton's tyrosine kinase is required for TLR-dependent heme oxygenase-1 gene activation via Nrf2 in macrophages. *J. Immunol.* 187: 817–827.
- Zhang, X., R. Goncalves, and D. M. Mosser. 2008. The isolation and characterization of murine macrophages. *Curr. Protoc. Immunol.* Chapter 14: Unit 14.1.
- Cao, H., L. Xiao, G. Park, X. Wang, A. C. Azim, J. W. Christman, and R. B. van Breemen. 2008. An improved LC-MS/MS method for the quantification of prostaglandins E(2) and D(2) production in biological fluids. *Anal. Biochem.* 372: 41–51.
- Salm, P., P. J. Taylor, and K. Kostner. 2011. Simultaneous quantification of total eicosapentaenoic acid, docosahexaenoic acid and arachidonic acid in plasma by high-performance liquid chromatography-tandem mass spectrometry. *Biomed. Chromatogr.* 25: 652–659.
- Berault, D. R., and G. H. Werstuck. 2013. Detection and quantification of endoplasmic reticulum stress in living cells using the fluorescent compound, Thioflavin T. *Biochim. Biophys. Acta* 1833: 2293–2301.
- Li, X., E. Baumgart, G. X. Dong, J. C. Morrell, G. Jimenez-Sanchez, D. Valle, K. D. Smith, and S. J. Gould. 2002. PEX11alpha is required for peroxisome proliferation in response to 4-phenylbutyrate but is dispensable for peroxisome proliferator-activated receptor alpha-mediated peroxisome proliferation. *Mol. Cell. Biol.* 22: 8226–8240.
- Sexton, J. Z., Q. He, L. J. Forsberg, and J. E. Brenman. 2010. High content screening for non-classical peroxisome proliferators. *Int. J. High Throughput Screen.* 2010: 127–140.
- Grant, P., B. Ahlemeyer, S. Karnati, T. Berg, I. Stelzig, A. Nenicu, K. Kuchelmeister, D. I. Crane, and E. Baumgart-Vogt. 2013. The biogenesis protein PEX14 is an optimal marker for the identification and localization of peroxisomes in different cell types, tissues, and species in morphological studies. *Histochem. Cell Biol.* 140: 423–442.
- Brose, R. D., G. Shin, M. C. McGuinness, T. Schneidereich, S. Purvis, G. X. Dong, J. Keefer, F. Spencer, and K. D. Smith. 2012. Activation of the stress prosensor as a mechanism for small molecule therapeutics. *Hum. Mol. Genet.* 21: 4237–4252.
- Kim, H. J., J. S. Jeong, S. R. Kim, S. Y. Park, H. J. Chae, and Y. C. Lee. 2013. Inhibition of endoplasmic reticulum stress alleviates lipopolysaccharide-induced lung inflammation through modulation of NF- κ B/HIF-1 α signaling pathway. *Sci. Rep.* 3: 1142.
- Maxwell, M., J. Bjorkman, T. Nguyen, P. Sharp, J. Finnie, C. Paterson, I. Tonks, B. C. Paton, G. F. Kay, and D. I. Crane. 2003. Pex13 inactivation in the mouse disrupts peroxisome biogenesis and leads to a Zellweger syndrome phenotype. *Mol. Cell. Biol.* 23: 5947–5957.
- Jeong, J. Y., and D. M. Jue. 1997. Chloroquine inhibits processing of tumor necrosis factor in lipopolysaccharide-stimulated RAW 264.7 macrophages. *J. Immunol.* 158: 4901–4907.
- Fletcher, T. C., A. DiGiandomenico, and J. Hawiger. 2010. Extended anti-inflammatory action of a degradation-resistant mutant of cell-penetrating suppressor of cytokine signaling 3. *J. Biol. Chem.* 285: 18727–18736.
- Ortiz-Lazareno, P. C., G. Hernandez-Flores, J. R. Dominguez-Rodriguez, J. M. Lerma-Diaz, L. F. Jave-Suarez, A. Aguilar-Lemarroy, P. C. Gomez-Contreras, D. Scott-Algara, and A. Bravo-Cuellar. 2008. MG132 proteasome inhibitor modulates proinflammatory cytokines production and expression of their receptors in U937 cells: involvement of nuclear factor-kappaB and activator protein-1. *Immunology* 124: 534–541.
- Wu, Y. T., H. L. Tan, G. Shui, C. Bauvy, Q. Huang, M. R. Wenk, C. N. Ong, P. Codogno, and H. M. Shen. 2010. Dual role of 3-methyladenine in modulation of autophagy via different temporal patterns of inhibition on class I and III phosphoinositide 3-kinase. *J. Biol. Chem.* 285: 10850–10861.
- Mbonye, U. R., C. Yuan, C. E. Harris, R. S. Sidhu, I. Song, T. Arakawa, and W. L. Smith. 2008. Two distinct pathways for cyclooxygenase-2 protein degradation. *J. Biol. Chem.* 283: 8611–8623.
- Lee, T. S., and L. Y. Chau. 2002. Heme oxygenase-1 mediates the anti-inflammatory effect of interleukin-10 in mice. *Nat. Med.* 8: 240–246.
- De Duve, C., and P. Baudhuin. 1966. Peroxisomes (microbodies and related particles). *Physiol. Rev.* 46: 323–357.
- Rigamonti, E., G. Chinetti-Gbaguidi, and B. Staels. 2008. Regulation of macrophage functions by PPAR-alpha, PPAR-gamma, and LXRs in mice and men. *Arterioscler. Thromb. Vasc. Biol.* 28: 1050–1059.
- Wells, C. A., T. Ravasi, and D. A. Hume. 2005. Inflammation suppressor genes: please switch out all the lights. *J. Leukoc. Biol.* 78: 9–13.
- Dai, Y., S. Datta, M. Novotny, and T. A. Hamilton. 2003. TGFbeta inhibits LPS-induced chemokine mRNA stabilization. *Blood* 102: 1178–1185.
- Schott, J., S. Reitter, J. Philipp, K. Haneke, H. Schäfer, and G. Stoecklin. 2014. Translational regulation of specific mRNAs controls feedback inhibition and survival during macrophage activation. *PLoS Genet.* 10: e1004368.
- Vasko, R., and M. S. Goligorsky. 2013. Dysfunctional lysosomal autophagy leads to peroxisomal oxidative burnout and damage during endotoxin-induced stress. *Autophagy* 9: 442–444.
- Seibert, K., Y. Zhang, K. Leahy, S. Hauser, J. Masferrer, and P. Isakson. 1997. Distribution of COX-1 and COX-2 in normal and inflamed tissues. *Adv. Exp. Med. Biol.* 400A: 167–170.
- Wada, M., T. L. Saunders, J. Morrow, G. L. Milne, K. P. Walker, S. K. Dey, T. G. Brock, M. R. Opp, D. M. Aronoff, and W. L. Smith. 2009. Two pathways for cyclooxygenase-2 protein degradation in vivo. *J. Biol. Chem.* 284: 30742–30753.
- Hilliard, M., C. Frohnert, C. Spillner, S. Marcone, A. Nath, T. Lampe, D. J. Fitzgerald, and R. H. Kehlenbach. 2010. The anti-inflammatory prostaglandin 15-deoxy-delta(12,14)-PGJ2 inhibits CRM1-dependent nuclear protein export. *J. Biol. Chem.* 285: 22202–22210.
- Ali, M., K. Heyob, and L. K. Rogers. 2016. DHA suppresses primary macrophage inflammatory responses via Notch 1/Jagged 1 signaling. *Sci. Rep.* 6: 22276.
- Li, X., Y. Yu, and C. D. Funk. 2013. Cyclooxygenase-2 induction in macrophages is modulated by docosahexaenoic acid via interactions with free fatty acid receptor 4 (FFA4). *FASEB J.* 27: 4987–4997.

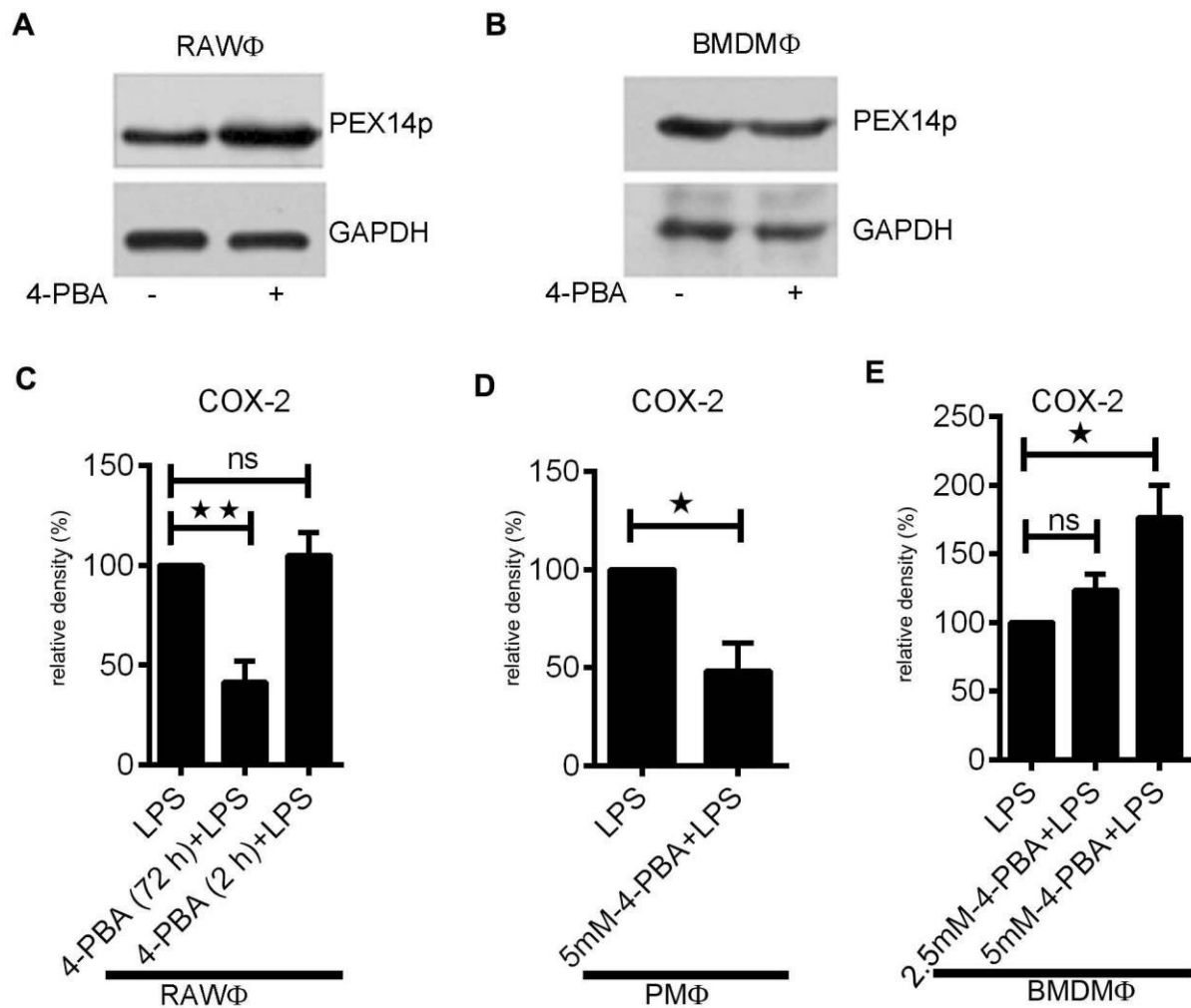


Figure S1: (A) RAW ϕ s or (B) BMDM ϕ s were left untreated or pretreated with 4-PBA, 2.5 mM (A) and 5 mM (B) respectively for 72 h. The isolated proteins were analyzed by Western blot using antibodies against PEX14p and GAPDH. A representative image from three independent experiments is shown. (C-E) Values \pm SEM represent the % densitometric values of COX-2 of the indicated cells left untreated or treated with 4-PBA (2.5 mM or as shown) calculated from Western blot images from three independent experiments. The values were normalized with the densitometric values of the loading control GAPDH. LPS-induced COX-2 values were taken as 100%. * $P \leq 0.05$; ** $P \leq 0.01$; ns, not significant (ANOVA).

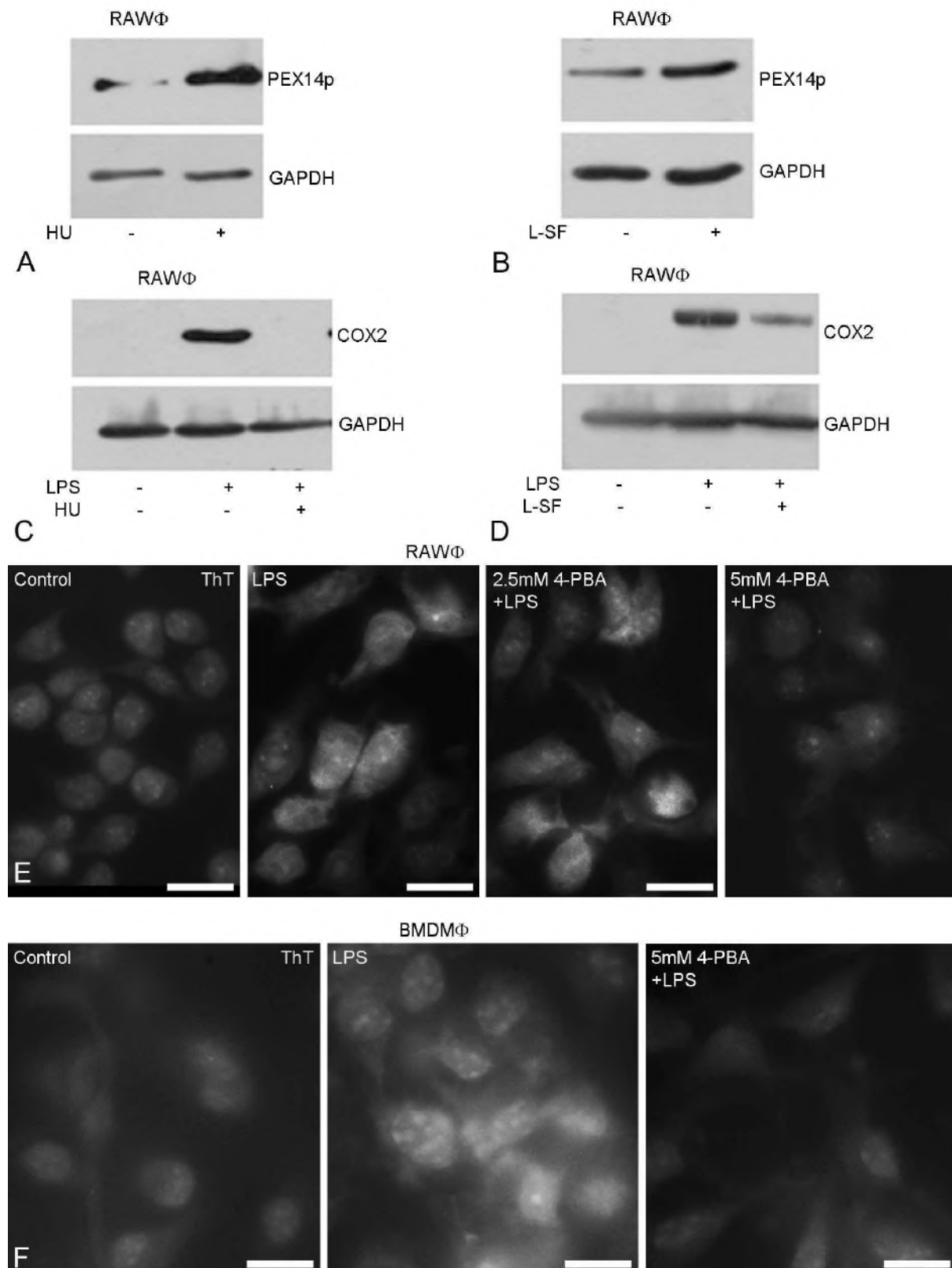


Figure S2: (A-B) RAW ϕ s were left untreated or treated with HU (100 μ M) or L-SF (10 μ M) for 48 h as indicated. The cells were lysed and subjected to Western blot analyses using an

antibody against PEX14p and GAPDH. A representative image of three independent experiments is shown. (C-D) RAW ϕ s were left untreated or treated with HU (100 μ M) or L-SF (10 μ M) as indicated for 48h after which the medium containing LPS (100ng/ml) for 12 h. The cells were lysed and subjected to Western blot analyses using an antibody against COX-2 and GAPDH. A representative image of three independent experiments is shown. (E) RAW ϕ s or (F) BMDM ϕ s were left untreated or treated with 4-PBA at the indicated concentration for 72 h. Medium was replaced with medium containing LPS (100 ng/ml) and incubated for 12 h. The cells were subjected to ThT staining as described in *Materials and Methods*. Bars represent A-B: 20 μ m.

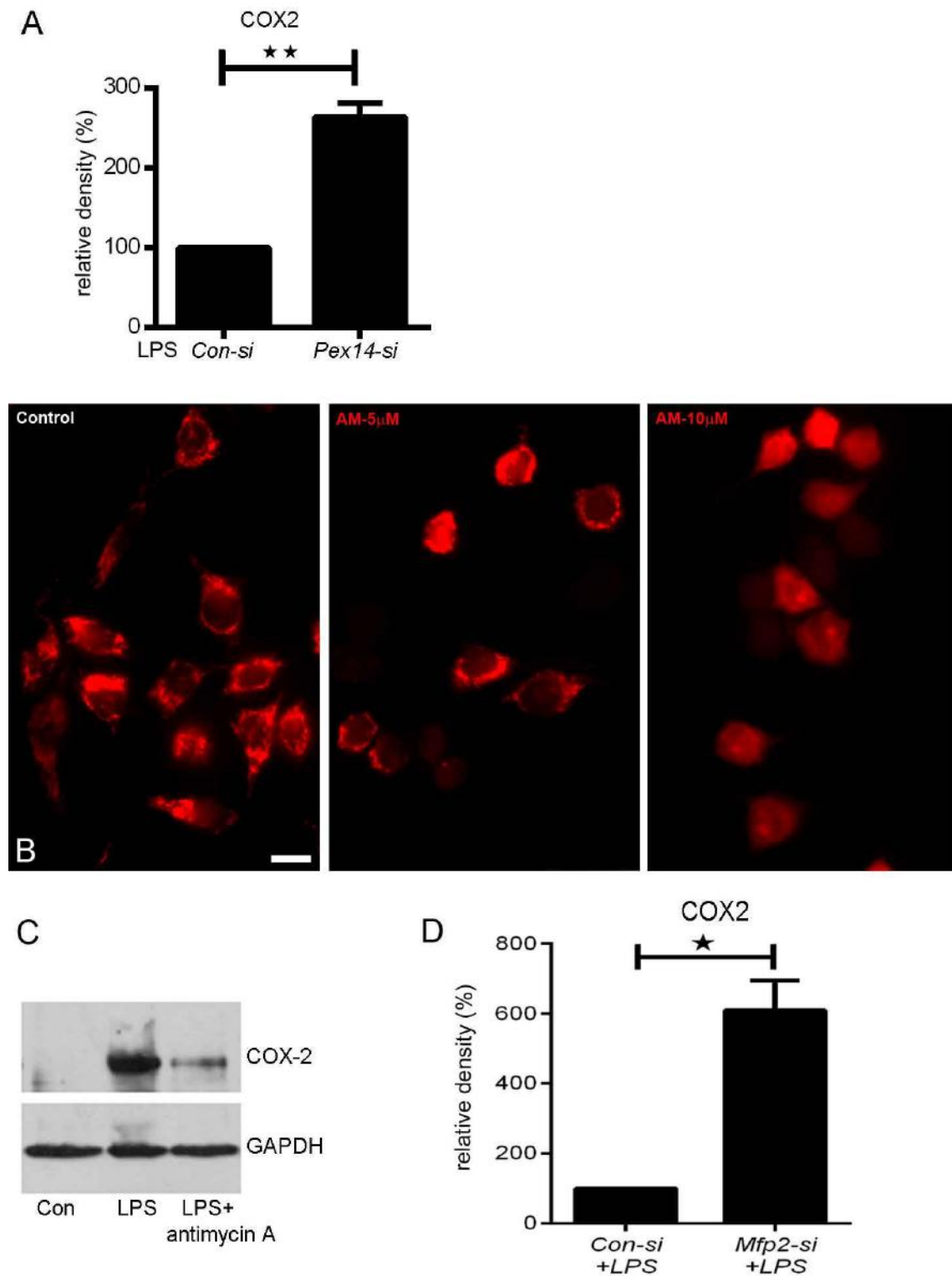


Figure S3: (A) The densitometric values of COX-2 quantified from Western blot images from three independent experiments of RAW ϕ s transfected with control-siRNA or *Pex14*-siRNA and treated with LPS for 12 h. The values were normalized to the respective GAPDH values. Mean values \pm SEM represent relative % density of COX-2 * $P \leq 0.05$; ** $P \leq 0.01$; ns,

not significant (Student's t test). (B) RAW ϕ s were treated with the indicated concentration of antimycin A for 1 h and stained with mitotracker as described in Materials and Methods (n=3). (C) RAW ϕ s pretreated with 10 μ M antimycin A for 1 h followed by LPS (100 ng/ml) stimulation for an additional 12 h was subjected to Western blot analyses using an antibody against COX-2 and GAPDH. A representative image of three independent experiments is shown. (D) Densitometric values of COX-2 quantified from Western blot images from three independent experiments of RAW ϕ s transfected with control-siRNA or *Mfp2*-siRNA and treated with LPS for 12 h. The values were normalized to the respective GAPDH values. Mean values \pm SEM represent relative % density of COX-2. Bars represent B: 25 μ m.

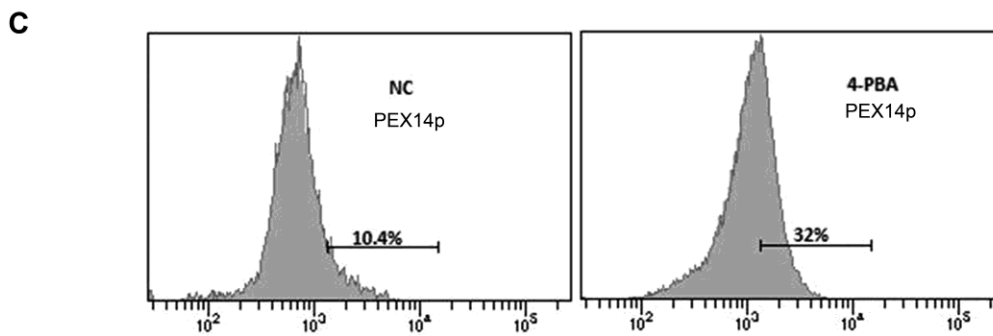
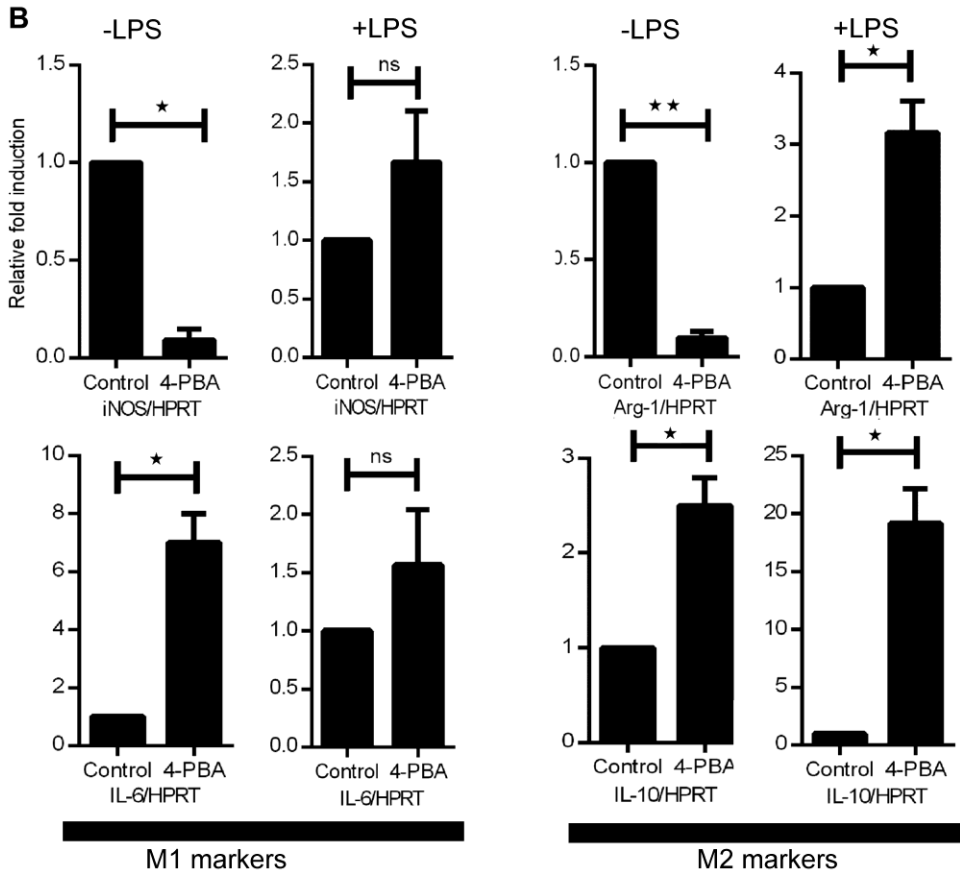
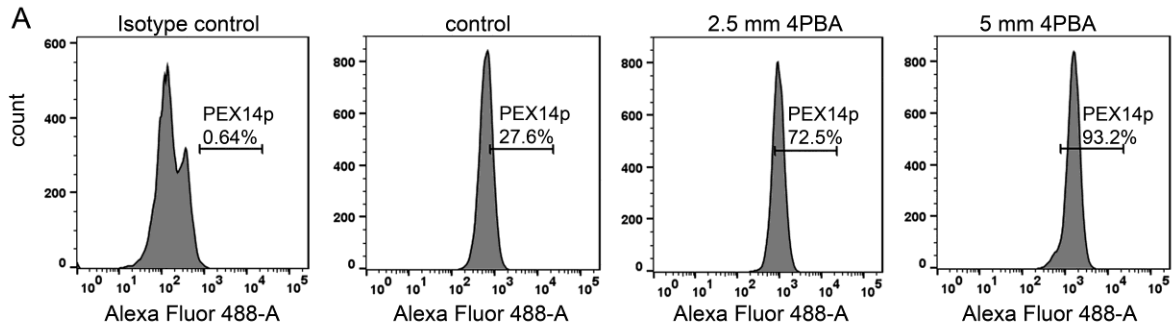


Figure S4: (A) RAW ϕ s were left untreated or treated with 4-PBA at the indicated concentration for 72 h, after which the cells were stained with an anti-PEX14p antibody as indicated and analyzed by FACS. A representative histogram showing % positive cells is shown. (B) RAW ϕ s were treated with 4-PBA (2.5 mM) for 72 h followed by stimulation with LPS for an additional 12 h wherever indicated. The RNA was isolated and analyzed by real-time PCR for M1-markers (iNOS, IL-6) and M2 markers (Arg-1 and IL-10). Values \pm SEM represent relative fold induction of the indicated genes (n=3). *P \leq 0.05; **P \leq 0.01; ns, not significant (Student's t test). (C) MEFs were left untreated (NC) or treated with 4-PBA (4-PBA) 3.5 mM for 5 days, after which the cells were stained with an antiPEX14p antibody as indicated and analyzed by FACS. A representative histogram showing % positive cells is shown.